

**ELECTROFLOTATION: ITS APPLICATION TO
WATER TREATMENT AND MINERAL
PROCESSING**

A thesis submitted for the degree of

DOCTOR OF PHILOSOPHY

By

MD. SHAHJAHAN KAISAR ALAM SARKAR

(MSc Engg.)

Discipline of Chemical Engineering
THE UNIVERSITY OF NEWCASTLE

March 2012

DECLARATION

I hereby certify that the work embodied in this thesis is the result of the original research and has not been submitted for a degree to any University or Institution except for publications.

Md. Shahjahan Kaisar Alam Sarkar

ACKNOWLEDGEMENTS

Firstly, I would like to express my deepest gratitude to my principal supervisor Professor Geoffrey M. Evans, for his continuous guidance, invaluable suggestions, constructive comments, and endless encouragement throughout the research work as well as the preparation of this thesis. I would also like to thank my co supervisor Dr. Scott W. Donne for his suggestions and comments during the research and writing process.

I would like to thank the University of Newcastle for awarding me the International Endeavour Postgraduate Research Scholarship to carry out this study. Special thanks to Geoffrey and Tony for their cordial help at the early stage of my settling in Australia. I am also grateful to Ron, Neil, Darren, Con, John, Jenny, Gillian and Bob for their kind supports in laboratory, technical and other stuffs.

I would like to extend my gratitude to my parents, and brothers (especially Mahbub Alam) for their supports. They sacrificed a lot to ensure the opportunities I required to receive the education that made this journey possible. Finally, I am grateful to my beloved wife Rumi for her unbound care and love, continuous encouragement, and patience throughout the study. It was really become possible for me to keep continuing this lonely and difficult journey due to her loving company with all my joys and sorrows.

TABLE OF CONTENTS

Chapter 1	Introduction.....	1
1.1	Background of the study.....	1
1.2	Definition of the problem.....	3
1.3	Research Objectives.....	4
1.4	Thesis outline.....	4
Chapter 2	Literature Review.....	6
2.1	Introduction.....	6
2.2	Effect of bubble size on flotation.....	6
2.3	Effect of particle size on flotation.....	14
2.4	Effect of surface charge on flotation.....	18
2.5	Effect of hydrophobicity or contact angle on flotation.....	20
2.6	Entrainment in conventional flotation.....	23
2.7	Bubbles sizes in different cells.....	23
2.7.1	Mechanically Agitated Cell.....	23
2.7.2	Column Flotation.....	26
2.7.3	Dissolved Air Flotation.....	28
2.7.4	Gas Aphrons.....	29
2.7.5	Turbulent Microflotation.....	30
2.7.6	Electroflotation Cell.....	30
	<i>Hydrogen bubble size</i>	31
	<i>Oxygen bubble size</i>	34
	<i>Hydrogen and oxygen bubble sizes measured combined without making distinction</i>	35
2.8	Electrolytic bubble formation process.....	38
2.8.1	Bubble Nucleation.....	38
2.8.2	Bubble Growth.....	39
	<i>Region I ($t < 10$ ms)</i>	40
	<i>Region II ($10 \leq t \leq 100$ ms)</i>	41
	<i>Region III ($t > 100$ ms)</i>	41
2.8.3	Bubble Detachment.....	42
2.9	Factors affecting bubble sizes produced in electroflotation.....	42

2.9.1	Electrode material.....	42
2.9.2	Electrode geometry and roughness.....	43
2.9.3	pH.....	44
2.9.4	Current density.....	45
2.9.5	Effect of liquid flow on bubble size.....	46
2.10	Hydrogen transfer from the cathode.....	46
2.11	Depressant effect of inorganic salts on flotation.....	47
2.12	Bubble detachment: contact angle of water on electrode surfaces.....	48
2.13	Application of electroflotation.....	50
2.13.1	Mineral processing.....	50
2.13.2	Water and wastewater treatment.....	51
2.14	Safety precaution in applying electroflotation.....	51
2.15	Advantages of electroflotation.....	51
2.15.1	Production of fine bubbles.....	52
2.15.2	Absence of coalescence of bubbles.....	52
2.15.3	Production of bubbles of desired size and flux.....	52
2.15.4	Higher chance of bubble particle collision.....	53
2.15.5	Activeness.....	53
2.16	Disadvantages of electroflotation.....	54
2.17	Opportunity of research.....	54
2.17.1	Interaction of mineral surface with gas phase.....	54
2.17.2	Depressant effect of electrolyte on flotation.....	55
2.17.3	Bubble size measurement.....	55
2.17.4	Fractional coverage of bubble surface.....	56
2.17.5	Fraction of hydrogen gas results in bubble.....	56
2.17.6	Electroflotation recovery and modelling.....	57
2.17.7	Electroflotation optimization.....	58
Chapter 3	Theoretical Modelling.....	59
3.1	Introduction.....	59
3.2	Electroflotation recovery.....	59
3.3	Bubble loading parameter.....	61
3.4	Particle-bubble attachment rate constant.....	62
3.4.1	Probability of Collection.....	63

<i>Bubble-particle collision</i>	63
<i>Bubble particle attachment/adhesion</i>	70
<i>Bubble particle detachment</i>	73
3.4.2 Particle-bubble collision frequency.....	75
3.5 Bubble particle aggregate velocity.....	76
3.6 Maximum particle size that can be floated by a given size of bubble.....	79
3.6.1 Particle detachment.....	80
3.6.2 Buoyancy.....	81
3.6.3 Calculation of pulp density.....	81
3.7 Effect of maximum floatable particle diameter on flotation recovery.....	82
3.8 Numbers of bubbles produced in electrolysis.....	83
3.9 Bubble size produced in electroflotation.....	85
3.9.1 Bubble detachment diameter.....	85
3.9.2 Bubble diameter in the bulk.....	86
3.10 Estimation of bubble size produced in Denver cell.....	89
3.10.1 Bubble break up and maximum stable bubble size.....	89
3.10.2 Average energy dissipation in Denver cell.....	90
3.10.3 Power input to the cell in the presence of gas.....	91
3.10.4 Sauter mean bubble size.....	92
3.11 Summary.....	92
Chapter 4 Experimental Methodology.....	94
4.1 Introduction.....	94
4.2 Materials.....	96
4.2.1 Silica.....	96
4.2.2 Electrodes.....	96
4.2.3 Reagents.....	96
4.3 Cleaning methods.....	97
4.3.1 Cleaning of glassware.....	97
4.3.2 Cleaning of silica surface.....	97
4.4 Denver cell: comparison of recovery.....	98
4.4.1 Calibration of rotameter.....	98
4.4.2 Methodology.....	101
4.5 Electroflotation cell: bubble size measurement.....	102

4.5.1 Apparatus.....	103
4.5.2 Procedure.....	104
4.5.3 Liquid velocity determination.....	106
4.6 Electroflotation cell: hydrogen gas fraction.....	106
4.6.1 Apparatus.....	107
4.6.2 Methodology.....	108
4.7 Electroflotation cell: silica recovery using stainless steel mesh cathode.....	110
4.7.1 Materials.....	110
4.7.2 Methodology.....	111
4.8 Contact angle measurement.....	115
4.9 Surface tension measurement.....	115
Chapter 5 Results and Discussion.....	117
5.1 Introduction.....	117
5.2 Denver cell: comparison of recovery.....	117
5.2.1 Air only: effect of pH on silica recovery.....	118
5.2.2 Air only: effect of sodium sulphate on silica recovery.....	120
5.2.3 Air and hydrogen: effect of gas flow on silica recovery.....	122
5.2.4 Air and hydrogen: effect of CTAB on silica recovery.....	123
5.2.5 Comparison between air and molecular hydrogen flotation recovery.....	125
<i>Bubble size</i>	125
<i>Induction time</i>	125
5.2.6 Summary on comparison of recovery by air and hydrogen.....	126
5.3 Electroflotation cell: bubble size measurement.....	126
5.3.1 Bubbles experiencing no external fluid flow.....	127
<i>Bubble visualisation</i>	127
<i>Bubble diameter at detachment</i>	129
<i>Bubble nucleation rate</i>	131
<i>Bubble diameter in the bulk</i>	132
5.3.2 Bubbles experiencing external upward fluid flow.....	138
5.3.3 Summary on bubble size measurement.....	141

5.4 Electroflotation cell: hydrogen gas fraction.....	142
5.4.1 Effect of dissolved gases on hydrogen bubble production rate.....	144
5.4.2 Effect of agitation on hydrogen bubble production rate.....	144
5.4.3 Effect of solids concentration on hydrogen bubble production rate.....	145
5.4.4 Summary on gas fraction.....	146
5.5 Electroflotation cell: silica recovery using stainless steel mesh cathode.....	146
5.5.1 Effect of current density on bubble diameter for different wire diameters.....	148
<i>Bubbles produced from 190 μm diameter cathode.....</i>	149
<i>Bubbles produced from 400 μm diameter cathode.....</i>	149
5.5.2 Effect of particle mass fraction on flotation recovery and bubble surface loading.....	150
5.5.3 Effect of particle diameter and gas flow rate on flotation recovery and bubble surface loading.....	155
5.5.4 Summary on silica recovery by electrolytic hydrogen bubbles.....	160
5.6 Conclusions.....	161
Chapter 6 Conclusions and Recommendations.....	163
6.1 Summary.....	163
6.2 Recommendations for future work.....	165
References.....	166
Appendices	
Appendix A: Determination of bubble and particle velocity.....	183
Appendix B: Applying drift flux theory to predict bubble size.....	187
Appendix C: Particle size distributions for different samples.....	191
Appendix D: Flotation recovery in Denver cell.....	196
Appendix E: Contact angle and surface tension measurement.....	206
Appendix F: Bubble size measurement and model prediction.....	210
Appendix G: Gas collection data.....	218
Appendix H: Flotation recovery in electroflotation cell.....	224

ABSTRACT

Flotation of particles of diameter less than 10 μm is important economically yet recovery is very poor in conventional flotation machines where the bubble diameter is typically greater than 600 μm . Many studies have reported that flotation recovery of fine particles increases with decreased bubble size. Electroflotation can create very fine hydrogen and oxygen bubbles and may be a viable option to recover very fine particles. This study aims to develop an increased understanding of the principles of electroflotation and to use this knowledge to float very fine particles.

The interaction between the gas phase with the mineral surface may bring about changes in the surface properties of the mineral, which can be either beneficial or detrimental in improving the flotation recovery. To investigate this interaction, flotation recovery of silica between air and molecular hydrogen was performed in a laboratory Denver, type D12, flotation machine. For both gases, the pH of the suspension, gas flow rate, concentration of collector and frother, solids concentration, particle size and speed of impeller were kept constant. Almost identical recoveries were obtained for both gases, suggesting that gas composition played no significant role in silica flotation.

There is wide variation in the reported measurements of bubble size in electroflotation, and uncertainty with the influence of electrode curvature, surface preparation and current density on bubble size have made it difficult to effectively design an efficient electroflotation system for fine particle recovery. Experiments were performed in a viewing cell that allowed direct visualization of hydrogen bubbles being generated and transported away from platinum wire electrodes of 90, 120 and 190 μm in diameter. It was found that the detached bubble diameter varied between 15-23 μm in diameter, and for each wire diameter, was little influenced by the applied current in the range 150-350 A/m^2 . The measurements were consistent with those predicted from a simple force-balance analysis based on a H_2 -Pt-0.2M Na_2SO_4 contact angle of 0.18° . Interestingly, upon detachment the bubble size increased rapidly, recording up to an 8-fold increase in volume in the first few millimetres of rise, before approaching a steady state diameter of between 30-50 μm in the bulk. This increase in bubble size was found to be mostly due to the transfer of dissolved hydrogen into the growing bubble while moving through the electrolyte that was super-saturated with dissolved hydrogen. The equilibrium bulk

diameter was found to be a function of the rate of hydrogen production, bubble nucleation rate, and dissolved gas concentration field. Consequently, it was concluded that in order to optimise electroflotation performance the cell geometry needed to be designed to optimise the contact between the supersaturated liquid and the rising bubble plume. By doing this, the volumetric flux of bubbles will be maximised leading to improved flotation performance.

The influence of electrolyte flowrate past the electrode surface on resultant bubble size was also investigated. A peristaltic pump was used to create a flow of electrolyte past 90 and 190 μm diameter platinum wire electrodes operating at a constant current density of 354 A/m^2 . The superficial upward liquid velocity ranged from 1.5-7.1 mm/s. It was observed directly that the detachment diameter varied between 8-15 and 15-22 μm for the 90 and 190 μm diameter cathode wires, respectively. The corresponding bubble diameters in the bulk were found to be 14-31 and 30-43 μm , respectively. Both detachment and bulk bubble diameter decreased with increased superficial liquid velocity.

Both bulk bubble size and electroflotation recovery are functions of the fraction of generated hydrogen that results in gas bubbles. Experimentally it was found that approximately 98 percent of the (theoretical) hydrogen produced by the electrolysis resulted in gas bubbles. This is a positive result, in that almost all of the electrical power is being converted to hydrogen (and oxygen) bubbles that can be used for flotation recovery. For a given current density, the rate of hydrogen gas production was largely independent of the concentration of the suspended solids. There was a very small increase in the hydrogen bubble production rate with the introduction of mechanical agitation, while the opposite trend was observed for the degassed electrolyte solution.

Flotation of 3-15 μm diameter silica particles was carried out with electrolytically generated hydrogen bubbles with mean diameters of 30 and 40 μm . Fractional recoveries after two minutes of flotation were found to be 0.82, 0.90, 0.96 and 0.88 for the 3.1, 5.3, 12.3 and 14.7 μm diameter particles, respectively. The relatively high recoveries were directly attributed to the very small bubbles generated by the electrolysis process, which are known to increase flotation recovery for very fine particles.

Finally, a flotation recovery model was developed which included a layered packing structure when estimating the fractional surface coverage of the bubble. Whilst it was not possible to measure surface coverage directly, the observed maximum plateau in flotation recovery appeared to occur when the bubble-particle aggregate projected area, based on a single layer particle packing, approached that of just the bubble. Moreover, flotation recovery was also found to be negatively influenced with a reduction in the bubble rise velocity due to attached particles.

LIST OF FIGURES

Figure 2.1: Comparison of experimental probability of collection (points) versus the probability collision using Equation 2.4 for different bubble and particle sizes, after Yoon and Luttrell (1989).

Figure 2.2: Correlation between contact angle and flotation recovery, after Fuerstenau (1957).

Figure 3.1: Geometry of the bubble-particle aggregate

Figure 3.2: Geometry for bubble on curved electrode surface

Figure 4.1: Size distribution of 60G silica [$d_{50} = 36.7 \mu\text{m}$]

Figure 4.2: Schematic of experimental apparatus for bubble size measurement

Figure 4.3: Photograph of experimental apparatus for bubble size measurement

Figure 4.4: Apparatus used for hydrogen gas collection

Figure 4.5: Size distribution of silica sample ID 1 [$(d_p)_{50}=15.0 \mu\text{m}$]

Figure 4.6: Schematic of experimental apparatus for floating silica by hydrogen bubble of $30 \mu\text{m}$ diameter

Figure 4.7: Size distribution of silica Sample ID 2-5 [$d_{50} = (\bullet) 3.1, (\circ) 5.3, (\blacksquare) 12.3, (\square) 14.7 \mu\text{m}$]

Figure 5.1: Flotation recovery vs. pH [$T_{\text{exp}}= 10 \text{ min}$; gas type=air; gas flow = 8 L/min; CTAB = $8.3 \times 10^{-6} \text{ M}$; $\text{Na}_2\text{SO}_4 = 0.05\text{M}$]

Figure 5.2: Flotation recovery vs. sodium sulphate concentration [gas type = Air; $T_{\text{exp}}= 10 \text{ min}$; pH = 10; gas flow = 8 L/min; CTAB= $6.64 \times 10^{-6} \text{ M}$]

Figure 5.3: Interaction of CTA^+ and Na^+ ions with negatively charged silica surface

Figure 5.4: Flotation recovery vs. gas flow rate [$T_{\text{exp}} = 10$ min; pH = 10: CTAB = 8.3×10^{-6} M; $\text{Na}_2\text{SO}_4 = 0.05$ M; gas type = (●) Air, (○) Hydrogen]

Figure 5.5: Flotation recovery vs. collector concentration [gas type: at 0.05M Na_2SO_4 = (●) Air, (○) Hydrogen; at 0.1M Na_2SO_4 = (■) Air, (□) Hydrogen; $T_{\text{exp}} = 10$ min; pH = 10; gas flow = 8 L/min]

Figure 5.6: Bubble diameter vs. distance from top of electrode [Pt: $D =$ (◆) 90, (■) 120, (●) 190 μm ; $\dot{I} = 354 \text{ A/m}^2$; photograph: $D =$ (a) 90, (b) 120, (c) 190 μm]

Figure 5.7: Bubble detachment diameter vs. current density [Pt: $D =$ (◆) 90, (■) 120, (●) 190 μm ; Platinised: $D =$ (○) 190 μm]

Figure 5.8: Bubble nucleation rate vs current density [Pt: $D =$ (◆) 90, (■) 120, (●) 190 μm ; Platinised: $D =$ (○) 190 μm]

Figure 5.9: Bulk bubble diameter vs current density [Pt: $D =$ (◆) 90, (■) 120, (●) 190 μm ; Platinised: $D =$ (○) 190 μm]

Figure 5.10: Fraction total hydrogen in bubble vs current density [at detachment: Pt: $D =$ (◆) 90, (■) 120, (●) 190 μm ; Platinised: $D =$ (▲) 190 μm ; in bulk: Pt: $D =$ (◇) 90, (◊) 120, (○) 190 μm ; Platinised: $D =$ (Δ) 190 μm]

Figure 5.11: Dissolved hydrogen gas concentration vs time and distance above wire [Pt wire; $\dot{I} = 354 \text{ A/m}^2$; $\psi = 0.79$ ($D = 190 \mu\text{m}$), 0.83 ($D = 90$ and $120 \mu\text{m}$); bubble location and diameter (μm): $D =$ (◆) 90, (■) 120, (●) 190 μm]

Figure 5.12: Measured and predicted bubble diameter vs distance above wire [Pt wire; $\dot{I} = 354 \text{ A/m}^2$; measured: $D =$ (◆) 90, (■) 120, (●) 190 μm]

Figure 5.13(a): Images of Hydrogen produced as a function of liquid flow [$D = 90 \mu\text{m}$; $\dot{I} = 354 \text{ A/m}^2$; liquid velocity = (a) 0.0, (b) 1.56, (c) 3.38, (d) 7.02 mm/s]

Figure 5.13(b): Images of Hydrogen produced as a function of liquid flow [$D = 190 \mu\text{m}$; $\dot{I} = 354 \text{ A/m}^2$; liquid velocity = (a) 0.0, (b) 2.48, (c) 4.0, (d) 7.09 mm/s]

Figure 5.14: Bubble diameter vs liquid velocity [Pt wire; At detachment: $D =$ (●) 90, (■) 190 μm ; In bulk: $D =$ (○) 90, (□) 190 μm]

Figure 5.15: Hydrogen bubble generation vs time [$d_w = 0.400$ mm; with agitation]

Figure 5.16: Hydrogen bubble generation rate vs solids concentration [—eq. 3.88, with $f = 1$; ● normal solution; ○ degassed solution; with agitation]

Figure 5.17: Bubble diameter distribution vs. current density [direct visualization; diameter of steel cathode: $400 \mu\text{m}$]

Figure 5.18: Flotation Recovery and Bubble Surface Coverage vs Solids Concentration [$d_p = 15 \mu\text{m}$; $d_b = 41 \mu\text{m}$; (●) R exptal; (○) ϕ calc]

Figure 5.19: Layered Orientation of Particles on the Bubble Surface

Figure 5.20: Recovery and Bubble Surface Coverage vs Gas Flowrate [● Recovery (exptal); ○ surface coverage (model); $X_S = 0.02$; $d_b = 30 \mu\text{m}$; $f = 1$]

Figure 5.21: Bubble-particle aggregate diameter and rise velocity vs gas flowrate [d_p (μm): 3.1 (●), 5.3 (○), 12.3 (■), 14.7 (□); $X_S = 0.02$; $d_b = 30 \mu\text{m}$; $f = 1$]

LIST OF TABLES

Table 2.1: Summary of the studies focussing the effect of bubble size on flotation

Table 2.2: Summary of the studies focussing the effect of particle size on flotation

Table 2.3: Bubble sizes produced in different flotation cells

Table 2.4: Summary of contact angle from different studies

Table 3.1: Values of B and m of Equation 3.18 under different flow conditions

Table 3.2: $y_1, y_2 = f(\text{Re}_b)$

Table 4.1: Summary of all test performed

Table 4.2: Cleaning methods used in this study

Table 4.3: Calibrated flow of hydrogen gas

Table 4.4: Values of entrainment as a function of gas flow rate

Table 4.5(a): Cathode dimensions and current density values for bubble production experiments from platinum wire without any external fluid flow

Table 4.5(b): Cathode dimensions and current density values for bubble production experiments from platinum wire experiencing external fluid flow

Table 4.6: Current density values used in gas collection experiments

Table 4.7: Particle size distribution

Table 4.8: Solids concentration values for silica flotation experiments using steel mesh of 400 μm wire diameter

Table 4.9: Current density values for silica flotation experiments using steel mesh

Table 4.10: Cathode dimensions and current density values for bubble production from stainless steel wire

Table 5.1: Fitted coefficients for Equation 5.1

Table 5.2: Average experimental and predicted detached bubble diameter

Table 5.3: Hydrogen Gas Generation Rate vs Current Density

Table 5.4: List of parameter discussed in Section 5.5

Table 5.5: Bubble Diameter vs Current Density and SS Wire Cathode Diameter

Table 5.6: Experimental and Model Data for different X_S

Table 5.7: Calculated φ , N_P , v_{b-N_L} , d_{b-N_L} vs N_L and ρ_{pulp}

Table 5.8: Experimental and Model Data for different d_p and Q_G

Table 5.9: Calculated φ , N_P , v_{b-N_L} , d_{b-N_L} vs N_L and $\rho_{pulp}=983 \text{ kg/m}^3$

LIST OF PUBLICATIONS

Journal Papers

1. Sarkar, M. S. K. A., Donne, S. W. and Evans, G. M. Utilization of hydrogen in electroflotation of silica. *Advanced Powder Technology*, 22, 482-492, 2011.
2. Sarkar, M. S. K. A., Evans, G. M. and Donne, S. W. (2010) Bubble size measurement in electroflotation. *Minerals Engineering*, 23, 1058-1065.
3. Sarkar, M. S. K. A., Donne, S. W. and Evans, G. M. (2010) Hydrogen bubble flotation of silica. *Advanced Powder Technology*, 21, 412-418.

Conference Papers

1. Evans, G. M., Mohr, S., Donne, S. W., Sarkar, M. S. K. A. and Machniewski, P. D. (2011) Modelling and measurement bubble formation and growth in electroflotation processes. In proceedings 'GLS10'. 26-29 June, 2011, Braga, Portugal.
2. Sarkar, M. S. K. A., Donne, S. W. and Evans, G. M. (2010) Hydrogen utilization in electroflotation of silica at varying solids concentrations, In proceedings 'Chemeca 2010'. Paper No. 319, 26-29 September, Adelaide, Australia.
3. Sarkar, M. S. K. A., Evans, G. M. and Donne, S. W. (2009) Estimation of bubble size produced in Electroflotation. In proceedings 'Flotation 09'. November 9-12, 2009, Cape Town, South Africa.
4. Sarkar, M. S. K. A., Evans, G. M. and Donne, S. W. (2009) Investigating the flotation recovery of silica by using hydrogen gas. In proceedings 'Chemeca 2009'. Paper No. 176, 27-30 September 2009, Perth, Australia.

NOMENCLATURE

English Alphabet

a	constant in eq. 3.37 (-)
A	cross-sectional area of the cell (m^2)
$A_{b/p}$	projected area of the bubble or particle (m^2)
A_c	area of the cathode surface (m^2)
A_e	actual surface area of electrodes (m^2)
A_{ft}	area of float (m^2)
A_t	area of charge transfer (m^2)
A_p	projected area of particle (m^2)
A_r	Archimedes number (-)
A_1	cross-sectional area of the tube of the rotameter (m^2)
A_2	cross-sectional area of the annulus between the float and the tube (m^2)
A'	effective Haymaker constant (J)
B	parameter that vary with Reynolds numbers (-)
b_m	machine acceleration (m/s^2)
C	coefficient used in eq. 2.25 (-)
C_h	coefficient in the particle-particle pair interaction (-)
C_D	drag coefficient (-)
C_R	coefficient used in eq. 4.1 (-)
C_0	saturation concentration of the dissolved gas in solution (mol/m^3)
C_b	bulk molar concentration of gas in the liquid (mol/m^3)
C^{sat}	saturation molar concentration of gas in the liquid-gas interface (mol/m^3)
C'	concentration of dissolved gas in solution (mol/m^3)
$C(r,t)$	concentration of dissolved gas at radial position, r, and time, t (mol/m^3)
d	distance travel by the bubble (m)
D	diameter of electrode (m)
d_a	diameter of the bubbles stayed on the electrode surface (m)
d_i	equivalent spherical bubble diameter (m)
$d_{b/p}$	diameter of bubble/particle (m)
d_{b-N_p}, d_{b-N_L}	projected diameter of the bubble particle aggregate (m)

d_f	diameter of the bubbles detached from the electrode but stayed in the neighbourhood of the electrode surface (m)
D_I	diameter of impeller (m)
d_{25}	diameter of particle corresponding to 25% particle less than that (m)
d_{50}	diameter of particle corresponding to 50% particle less than that (m)
d_{75}	diameter of particle corresponding to 75% particle less than that (m)
d_b	diameter of bubble (m)
$(d_b)_S$	Sauter mean bubble diameter (m)
$(d_b)_{max}$	maximum stable diameter (m)
d_p	diameter of particle (m)
$d_{b,b}$	bulk diameter of a bubble (m)
$d_{b,d}$	detachment diameter of a bubble (m)
$(d_p)_{av}$	average diameter of particle (m)
$(d_p)_{max,d}$	maximum floatable particle diameter based on detachment criteria (m)
$(d_p)_{max,b}$	maximum floatable particle diameter based on buoyancy criteria (m)
$(d_p)_{max,}$	maximum floatable particle diameter calculated as the minimum of $(d_p)_{max,d}$ and $(d_p)_{max,b}$ (m)
d_e	net distance between electrodes (m)
D'	diffusivity of gas (m^2/s)
D''	diffusion constant of fine particles (m^2/s)
E	constant in eq.3.37 (-)
E_F	energy dissipation from feed flow (W/kg)
E_G	energy dissipation from sparged gas (W/kg)
E_I	energy dissipation from impeller rotation (W/kg)
f	gas fraction results in bubbles (-)
f'	constant used in eq. 3.44 (-)
F	Faraday's constant, 96485.3 (C/mol)
Fo'	Fourier number of mass transport (-)
F_B	force due to buoyancy (N)
$F_{B,A}$	weight of displaced liquid by the bubble-particle aggregate (N)
$F_{B, b}$	buoyancy force of a bubble (N)
$F_{B, p}$	buoyancy force of n particles (N)
F_c	capillary force (N)
F_d	hydrodynamic drag force (N)

$F_{d,b-N_p}$	hydrodynamic drag force of bubble-particle aggregate (N)
F_e	excess force (N)
F_P	pressure force (N)
F_w	force due to gravity (N)
$F_{W,A}$	weight of bubble-particle aggregate (N)
$F_{W,b}$	weight of a bubble (N)
$F_{W,p}$	weight of n particles (N)
F_σ	surface tension force (N)
g	acceleration due to gravity (m/s^2)
G	dimensionless particle gravity (-)
h	vertical distance shown in figure 3.1 and 3.2 (m)
H	height of the cell (m)
I	absolute current (A)
i	current density (A/m^2)
I_0	modified Bessel function of the first kind of order zero (-)
J	homogeneous bubble nucleation rate (nos./s)
Ja	Jackob number of mass transport
J_g	gas superficial velocity (m/s)
J_l	liquid superficial velocity (m/s)
J_T	total volumetric flux (m/s)
J_{gl}	drift flux for gas phase (m/s)
k	flotation rate constant (s^{-1})
k_m	mass transfer coefficient (m/s)
k_p	rate constant (min^{-1})
K	fitting parameter used in eq. 5.1 (-)
K_1	particle-bubble attachment rate constant (m^3/s)
K_2	particle-bubble detachment rate constant (s^{-1})
K_3	mathematical expression used in eq. 3.44-3.45 (-)
K_4	number fraction of particles with diameter greater than $(d_p)_{max}$ (-)
K_5	mathematical expression used in eq. 4.2-4.6 (-)
K'	mathematical expression used in eq. 4.5-4.8 (-)
l	time coefficient (-)
L	mathematical expression used in eq. 3.31 and 3.35 (-)

L_C	length of cathode (m)
m	parameter that vary with Reynolds numbers (-)
\dot{m}	mass flow rate of solids (kg/s)
M	mathematical expression used in eq. 3.31 and 3.35 (-)
M_G	molar mass of gas (kg/mol)
M_o	Morton number
N_p	number of particles (-)
N_e	number of electrodes (-)
n	number of moles (nos.)
n_1	Richardson-Zaki index
N	molar strength of gas (mol/m^2)
N_I	impeller rotational speed (rev/s)
N_L	number of layers particles attached to bubble (-)
\dot{N}	molar strength of gas per sec ($\text{mol/m}^2.\text{s}$)
\dot{n}	molar gas generation rate (mol/s)
\dot{N}_{H_2}	theoretical molar flux rate ($\text{mol/m}^2.\text{s}$)
N_{bT}	total number of bubbles (nos./s)
$(N_P)_{UG}$	Power Number for the ungasged system (-)
$N_{p, f(0)}$	number of free particles in the pulp at time, $t = 0$ s (-)
$N_{p, pulp(0)}$	number of particles in the pulp at time, $t = 0$ s (-)
$N_{p, pulp(t)}$	number of particles in the flotation cell after electroflotation of t s (-)
$N_{p,c}$	number of particles collected in the concentrate (-)
$N_{p,a}$	number of particles attached to the bubbles (-)
p	pressure of the system (N/m^2)
P	probability of collection/ collection efficiency (-)
P_c	collision efficiency (-)
$(P_c)_{Ic}$	interceptional collision efficiency (-)
$(P_c)_G$	gravitational collision efficiency (-)
$(P_c)_{In}$	inertial collision efficiency (-)
P_a	probability of attachment/adhesion (-)
P_d	probability of detachment (-)
P_G	power input to the cell in the presence of gas (W)
P_{UG}	power input to the cell in the absence of gas (W)

P_0	vapour pressure of the pure solvent (N/m^2)
P'	external pressure in liquid (N/m^2)
P''	pressure of dissolved gas inside the bubble (N/m^2)
ΔP	internal excess pressure (N/m^2)
Q_G	volumetric gas flow rate (theoretical) (m^3/s)
Q_L	volumetric liquid flow rate (m^3/s)
$(Q_G)_b$	measured gas flow rate of bubbles (m^3/s)
Q_{Air}	flow rate of air (m^3/s)
Q_{Hydrogen}	flow rate of hydrogen (m^3/s)
R	universal gas constant, 8.31451 (J/mol.K)
Re	Reynolds number (-)
Re_b	Reynolds number of bubble (-)
R'	collision radius (m)
$r(t)$	radius of bubble after time, t (m)
$R(t)$	recovery of particles (kg/kg)
$(R_{\text{exp}})_{\text{corr}}$	corrected fractional flotation recovery (-)
r_b	radius of bubble (m)
r_p	radius of particle (m)
r^*	critical radius of bubble (m)
r_b^*	dimensionless bubble radius
S	ratio of the surface area of bubble to the projected area of a particle (-)
S_b	bubble surface area (m^2)
S_B	bubble surface area flux (s^{-1})
S_c	fractional surface coverage of electrodes (-)
S_t	dimensionless Stokes number (-)
T	temperature of the system (K)
t	time (s)
t_i	induction time (s)
t_{sl}	sliding/contact time (s)
u	velocity of bubble or particle (m/s)
U_{Stokes}	stokes velocity of bubble or particle (m/s)
U_b	electromobilities of bubble ($\mu\text{m/s.V.cm}$)
U_p	electromobilities of particle ($\mu\text{m/s.V.cm}$)

V_{b-N_p}, V_{b-N_L}	rise/fall velocity of the bubble-particle aggregate (m/s)
\bar{u}^2	mean square velocity difference between two points in the turbulent flow acting a distance apart equal to the maximum bubble diameter, $(d_b)_{max}$ (m^2/s^2)
V	volume of the cell (m^3)
V_{THS}	hindered settling velocity (m/s)
V_{TFS}	terminal settling velocity (m/s)
v_b	velocity of bubble (m/s)
$(v_b)_f$	velocity of bubble experiencing external fluid flow (m/s)
$(v_b)_t$	theoretical velocity of bubble experiencing no external fluid flow (m/s)
v_F	final velocity of feed (m/s)
v_G	gas superficial velocity (m/s)
V_{ft}	volume of float (m^3)
v_O	initial velocity of feed (m/s)
v_p	velocity of particle (m/s)
V_{rel}	relative velocity between the bubble and particle (m/s)
v_S^*	dimensionless velocity (-)
We_c	critical Weber number (-)
x	distance from top of electrode surface (m)
$x_{b,d}$	distance below the top of electrode surface (m)
y_1, y_2	constants used in eq. 3.29 (-)
X	mathematical expression used in eq. 3.32-3.33 (-)
X_s	mass fraction of solids (-)
Y	mathematical expression used in eq. 3.31 and 3.33 (-)
z	no. of electron required produce 1 mole gas (-)
Z_1	Particle-bubble collision frequency (m^3/s)

Greek Symbols

α	mathematical expression used in equation 3.40 (-)
β	average bubble loading parameter (-)
γ_1, γ_2	number of atoms per unit volume in two interacting bodies (atm/m^3)
ε	average energy dissipation per unit mass (W/kg)

ϵ_s	volumetric fraction of solid (m^3/m^3)
ϵ_f	volumetric fraction of liquid (m^3/m^3)
ϵ_G	volumetric fraction of gas (m^3/m^3)
θ	angle shown in figure 3.2 (deg)
$\theta_1, \theta_2, \theta_3$	angle shown in figure 3.1 (deg)
θ_a	attachment angle (deg)
$\theta_{a,\text{max}}$	maximum value of the attachment angle (deg)
θ_c	contact angle (deg)
θ_d	critical value of three phase contact angle right before detachment (deg)
θ_s	angular coordinate describing the trajectory of a particle moving past a bubble in streamline flow (deg)
θ_t	angle of tangency (deg)
ω	contact angle of bubble-electrode-liquid interface (deg)
ρ_{Air}	density of air (kg/m^3)
$\rho_{\text{b/p}}$	density of bubble/particle (kg/m^3)
ρ_f	density of fluid (kg/m^3)
ρ_{ft}	density of float (kg/m^3)
ρ_G	density of gas (kg/m^3)
ρ_{Hydrogen}	density of hydrogen (kg/m^3)
ρ_{pulp}	density of pulp (kg/m^3)
ρ_p	density of particle (kg/m^3)
$\Delta\rho$	difference in density between particle and pulp (kg/m^3)
σ	gas-liquid interfacial tension (N/m)
σ_{mg}	mineral-gas interfacial tension (N/m)
σ_{mw}	mineral-water interfacial tension (N/m)
σ_{wg}	water-gas interfacial tension (N/m)
μ	viscosity of liquid ($\text{kg}/\text{m}\cdot\text{s}$)
μ_g	viscosity of gas phase ($\text{kg}/\text{m}\cdot\text{s}$)
μ_{pulp}	absolute viscosity of pulp ($\text{kg}/\text{m}\cdot\text{s}$)
μ_m	mixture dynamic viscosity of gas and liquid phase pulp ($\text{kg}/\text{m}\cdot\text{s}$)
χ	gas holdup (m^3/m^3)
ζ	dielectric constant (-)
λ	dimension less number (-)

λ_0	surface potential (V)
κ	Debye length (m)
κ_c	conductivity of suspension (S/m)
η	coefficient relating to degree of supersaturation
η'	growth coefficient
ϕ	fractional coverage of bubble surface (-)
ϕ	angle shown in figure 3.2 (deg)
ϕ_c	collision angle of the grazing trajectory (deg)
ψ	gas fraction goes into bulk solution (-)
ψ_c	stream function
ψ_c^*	dimensionless stream function (-)
ξ_0^*	surface vorticity (s^{-1})
Γ	Boltzmann's constant (J/K)

Chapter 1

INTRODUCTION

1.1 BACKGROUND OF THE STUDY

Due to the advances in grinding in recent years, the exploitation of low grade mineral deposits has become economically viable, which in turn enhances the importance of fine particle flotation (George et al., 2004). Fine particle has very small inertial force compared to large particle and usually follows the streamlines around the bubble. Hence, it does not readily collide with bubble (Yoon and Luttrell, 1989). This phenomenon makes the flotation of very fine particles (less than 10 μm in diameter) very poor, depending on the bubble size and hydrophobicity of the particle (Trahar and Warren, 1976, Gontijo et al., 2007). The poor recovery is due to the decreased probability of collision between the particle and bubble (Sutherland, 1948, Flint and Howarth, 1971b, Reay and Ratcliff, 1973).

In the past 40 years there have been numerous studies focusing on the flotation of fine mineral particles (e.g., Flint and Howarth (1971b); Reay and Ratcliff (1975); Anfruns and Kitchener (1977); Ahmed and Jameson (1985); Yoon and Luttrell (1989); Dai et al. (1998); Ramirez and Davis (2001); Tao (2004); Nguyen et al. (2006); Miettinen (2007); Waters et al. (2008); Shahbazi et al. (2010); Tran et al. (2010)). For the latest review of the literature on fine particle flotation see Miettinen et al. (2010). Many of the studies listed have reported that the recovery of particles in the diameter range of 1-10 μm is increased with decreasing bubble size, which is largely the result of the increased collision efficiency between the particles and the bubbles (e.g., Anfruns and Kitchener (1977); Diaz-Penafiel and Dobby (1994); Nguyen and Schulze (2004); Sarrot et al. (2007)). Small gas bubbles are being used successfully in both environmental and industrial separation processes (Burns et al., 1997), especially for the flotation of fine particles (DeVivo and Karger, 1970 , Yoon and Luttrell, 1989). Flint and Howarth (1971b) also advised the necessity of small bubbles to maximise collision efficiency which in turn enhances the recovery.

While it is widely acknowledged that the recovery of fine particles is generally enhanced by using fine bubbles, it is also recognized that conventional mechanically agitated and sparged column flotation cells produce bubbles that are too large, i.e. greater than 500 μm , to obtain this benefit. The review by Jameson and Allum (1984) reported that at the time the bubble size in most industrial flotation circuits within Australia was of the order 1000 μm . While there have been improvements in overall cell design since then, the reliance on a mechanical agitator to create the bubbles has meant that the bubble size produced has remained relatively unchanged. As conventional flotation cells have very poor performance for very fine particles of diameter less than 10 μm (Mallikarjunan and Venkatachalam, 1984, Ketkar et al., 1988), alternative flotation methodologies capable of producing bubbles with sizes less than 100 μm have been investigated, namely dissolved air flotation (e.g. Rodrigues and Rubio (2007); Rubio et al.(2007); Englert et al.(2009); Yalcin and Byers (2006)), picobubbles (Tao et al., 2006), colloidal gas aphrons (CGAs) (Waters et al., 2008), turbulent microflotation (Rulyov, 2001) and electroflotation.

The focus of this study is on electroflotation. Electroflotation can create very fine bubbles of diameter in the range of 15-80 μm (Ketkar et al., 1988, Han et al., 2006), and hence can be a promising option for floating fine particles. There have been a number of electroflotation studies involving mineral flotation as well as water and wastewater treatment. Examples include the recovery of chalcopyrite by Raju and Khangaonkar (1984b), quartz by Ketkar et al. (1991), sphalerite by Llerena et al. (1996), kaolin particles by Han et al. (2006) and platinum group minerals by Montes-Atenas et al. (2010). The examples of the studies that engaged in water and wastewater treatment include the separation of oil and low density suspended solids by Manjunath et al. (2000); as well as the treatment of oil-water emulsions by Bande et al. (2008); mining wastewater by Alexandrova et al. (1994); restaurant wastewater by Chen et al. (2000); textile effluent by Merzouk et al. (2010); and urban sewage by Il'in et al. (2002). More examples of studies involving mineral flotation and water and wastewater treatment are reported in Chapter 2 (Section 2.13).

1.2 DEFINITION OF THE PROBLEM

As discussed in the previous section, the recovery of fine particles is inversely related to bubble size and having bubble size smaller than that of conventional flotation device, electroflotation has the viability of being an efficient system for floating fine particle. Hence it is very important to have a clear understanding of the factors that influence the size of bubbles produced by electrolysis of water while designing an electroflotation system. However, the detachment of bubbles from electrodes and their subsequent growth while rising through electrolyte solution supersaturated by dissolved gases are not well understood yet. There is a wide variation in reported measurements of bubble size across the literature. The uncertainty in influences of variables such as electrode curvature, surface preparation, and most importantly current density, on bubble size has made it difficult to effectively design efficient electroflotation systems for fine particle recovery.

The electrolytically-generated gases are in the form of atomic hydrogen and oxygen. Though this atomic state remains active for a very short time, it may be able to alter the surface properties of mineral surface. This change may be either beneficial or detrimental in improving flotation recovery depending on the mineral, i.e., cassiterite and pyrolusite float better by hydrogen gas whereas chalcopyrite and sphalerite float better by oxygen gas; while barite, calcite and chromite are insensitive to the choice of gas (Mallikarjunan and Venkatachalam, 1984).

The fraction of hydrogen that results in gas bubbles is also an important factor in determining the bulk bubble diameter and recovery in electroflotation. Recovery will be maximised if all of the dissolved gases produced as part of the electrolysis process result in the formation of gas bubbles. However, this may not be always the case and a portion of gases remains dissolved in solution and thereby reducing recovery (Vogt, 1984b, Vogt, 1984a, Müller et al., 1989). More comprehensive research is required to understand the transformation mechanism of dissolved gases both at the surface of the electrodes and in the bulk solution.

For effective design of an efficient electroflotation system it is necessary to have a clear understanding of the influence of the bubbles and particle size, buoyancy of bubble-particle aggregate, fractional coverage of bubble surface, contact angle of mineral-

liquid-gas interface, current density, and solids concentration, etc., on recovery. Experimental observations along with theoretical analyses are required to explore these factors. While applying electroflotation commercially, the energy requirement for producing hydrogen and oxygen bubbles from electrolysis of water should also be considered.

1.3 RESEARCH OBJECTIVES

The aim of this study was to develop an increased understanding of the principles of electroflotation and to use this knowledge to optimize its application in water treatment and mineral processing. Specifically, the aims were:

- To compare the flotation recovery of silica using air and hydrogen gas at the same superficial gas velocity and bubble size, and to determine the influence, if any, of gas composition on flotation performance.
- To measure the effect of wire geometry, surface preparation and current density, on (1) size and frequency of detaching bubbles, and (2) growth of these bubbles as they move away from the electrode surface.
- To compare the detachment and bulk bubble size produced by electrolysis of water with theoretical prediction.
- To investigate the influence of solids concentration, introduction of mechanical agitation, and presence of pre-existing dissolved gases on the rate of hydrogen gas generation.
- To determine the influence of gas flow rate, mass fraction, and particle size on the recovery of silica particles by electrolytic hydrogen bubbles.
- To develop theoretical model to predict recovery in an electroflotation cell.
- The study was restricted to the hydrogen bubble only; with the role of oxygen not being considered here.

1.4 THESIS OUTLINE

A critical review of the existing literature relating to fine particle flotation and electroflotation is performed in Chapter 2. The chapter describes different factors

(bubble and particle size, surface charge, contact angle) that affect the flotation recovery. Bubble sizes produced by different types of flotation cells available in the literature are analysed. Electrolytic bubble formation process and the factors affecting bubble size produced by electrolysis of water are then reviewed. Application of electroflotation in mineral processing and water and wastewater treatment is reported. Finally, the gaps in the existing literature are identified and the opportunity of research is discussed.

In chapter 3, a theoretical model is developed that can predict recovery by electrolytically generated bubbles. The model incorporates the effect of bubble and particle size, stability and buoyancy force of bubble-particle aggregate, fractional coverage of bubble surface, contact angle of mineral-liquid-gas interface, current density, superficial gas velocity, gas fraction that results in bubbles, and solids concentration on recovery. Prediction of detachment and bulk bubble size as a function of current density, electrode geometry and surface preparation is also presented. Estimation of bubble size produced by a mechanically agitated Denver cell is also given.

Chapter 4 contains a description of the materials used, the experimental apparatuses and methods applied.

The experimental results are presented and discussed in Chapter 5. The interaction of gas phase (air and molecular hydrogen) with mineral surface (silica) is explored by comparing the recovery of silica in a Denver cell at the same gas superficial velocity, bubble size and cell hydrodynamics. The measurement of hydrogen bubble size, hydrogen gas generation rate, and flotation recovery by electrolytic hydrogen bubbles in an electrochemical cell is also presented. The experimental results are then compared with model predictions. The optimization of the usage of electroflotation in context of energy consumption is then performed which really indicates the window of application of electroflotation.

In chapter 6, overall conclusions drawn from this research work, along with the significance of the study and recommendations for future work, are presented.

Chapter 2

LITERATURE REVIEW

2.1 INTRODUCTION

Flotation is a simple process that floats minerals or pollutants to the surface of a solution by small bubbles. Different types of bubbles may be used in the flotation process; e.g., air, nitrogen, hydrogen or oxygen bubbles. The success of flotation depends on hydrodynamic factors (bubble size, particle size, gas superficial velocity, bubble flux, bubble velocity, particle velocity, pulp density etc.), as well as on surface chemistry (pH of the suspension, surface charge, contact angle and surface tension forces etc.). The flotation of very fine particles (<10 μm in diameter) is very critical, and the recovery is very poor or almost negligible depending on the bubble size applied in flotation, and the hydrophobicity of the particles (Gontijo et al., 2007). This chapter reviews and outlines the effect of bubble and particle size, surface charge, and hydrophobicity or contact angle on flotation performance. It also discusses different studies that measured the size of bubbles produced in different flotation cells (e.g., mechanically agitated cell, flotation column, dissolved air flotation, gas aphanes, turbulent micro-flotation, and electroflotation). Electrolytic bubble formation processes (bubble nucleation, growth and detachment) are also discussed here. In addition this chapter discusses the factors (electrode material, geometry and roughness, pH, current density and external liquid flow) that affect bubble size production in an electroflotation cell. Then the application of electroflotation along with its specific advantages and disadvantages has been summarized. Following these critical analyses, this chapter also outlines the opportunities of future research.

2.2 EFFECT OF BUBBLE SIZE ON FLOTATION

The efficiency of a flotation system can be determined by the term 'probability of collection'. The probability of collection, P , refers to the number of particles that can be successfully transported by bubbles from the pulp phase to froth phase. These transported particles will lead to a successful recovery. Collection of particles is the

consequences of collision, attachment and detachment of particles from bubbles and can be written mathematically as (Yoon, 2000):

$$P = f(P_c, P_a, P_d), \quad (2.1)$$

where P_c , P_a , and P_d are the probability of particle-bubble collision, attachment, and detachment, respectively. The probability of collision, P_c , is the amount of hydrophobic mineral particles that can encounter the bubbles in the pulp phase. The size of bubble has a significant effect on particle bubble collision and consequently on collection of particles in a flotation system. It is well known that the removal efficiency in flotation strongly depends on bubble size. Chen et al. (2002) summarized that in general the removal efficiency increases with an decrease in bubble size. Different studies had been performed to investigate the effect of bubble sizes of different ranges on flotation performance as discussed below.

Flint and Howarth (1971b) studied the hydrodynamics of particle collection by air bubbles and suggested two dimensionless groups to characterize collection efficiency as particle inertia (S_t) and particle gravity (G):

$$S_t = \frac{\rho_p v_b d_p^2}{9\mu d_b}, \quad (2.2)$$

and

$$G = \frac{(\rho_p - \rho_f) d_p^2 g}{18\mu v_b}, \quad (2.3)$$

where ρ_p is the density of particle, ρ_f is the density of liquid, v_b is the velocity of bubble, μ is the viscosity of liquid, g is the acceleration due to gravity, d_p is the diameter of the particle, and d_b is diameter of the bubble. For fine particles (where $S_t < 0.1$) the collision efficiency (P_c) is independent of S_t but strongly dependent on G , i.e., the inertial effects are very small compared to the viscous effects. The collision efficiency, P_c , can be estimated as (Flint and Howarth, 1971b):

$$P_c = \frac{G}{I + G}. \quad (2.4)$$

Since G increases with decreasing bubble size, the collision efficiency for fine particles will increase with decreasing bubble size. This was verified for 6 μm galena particles collected by air bubbles of diameters in the range of 50-100 μm .

Reay and Ratcliff (1973) theoretically studied the effect of bubble size in flotation using very small bubbles typically less than 100 μm in diameter. The major conclusion of this study was that $P \propto d_b^{-2.05}$, where P is the probability of collection. Later these authors (Reay and Ratcliff, 1975) experimentally showed that $P \propto d_b^{-1.9}$ for particles of diameter ranged from 3-9 μm . The flotation experiments were performed using very small bubbles produced from fine and medium frit. The root mean square diameters were 42 and 71 μm for the fine and medium frit, respectively.

Anfruns and Kitchener (1977) studied the effect of bubble size (0.6-1.0 mm in diameter) and concluded that the collection efficiency increased with decreasing bubble size within the particle size range from 10-50 μm . A later analysis done by Jameson et al. (1977) on Anfruns and Kitchener's (1977) data shows that $P_c \propto d_b^{-1.69}$ and $k \propto d_b^{-2.69}$, where k is the flotation rate constant. They also concluded that the effect of bubble size on flotation rate constant became more prominent for $d_b < 100 \mu\text{m}$, and for particle size in the range 4-30 μm as $k \propto d_b^{-3}$.

Later, Ahmed and Jameson (1985) studied the effect of mean bubble size over the range 75-655 μm , and reported that the flotation rate was very strongly affected by the bubble size, there being an increase of up to 100-fold when the bubble size was reduced from 655 μm to 75 μm .

Dobby and Finch (1987) developed a fundamental model of flotation considering particle inertia and particle-bubble collision. Their model results clearly show that collection efficiency increases with decreasing bubble size. This increase in collection efficiency was attributed to increases in both collision and attachment efficiency with decreasing bubble size.

Yoon and Luttrell (1989) concluded that the probability of collision (P_c) between bubbles and particles varied inversely as the square of the bubble diameter (d_b) as shown in Figure 2.1. The solid lines in the figure represent the calculated values of probability of collision (P_c) based on:

$$P_c = \left[\frac{3}{2} + \frac{4 Re_b^{0.72}}{15} \right] \left(\frac{d_p}{d_b} \right)^2, \quad (2.5)$$

where Re_b is the Reynolds number of bubbles. They experimentally measured the collection probability (P) for three different particle sizes as a function of bubble sizes and compared with theoretical estimation of bubble particle collision, as shown as points (triangular, square, and circle) in Figure 2.1. Both the experimental P and calculated P_c values showed a drastic increase with decreasing bubble size. It can be seen that the measured collection probability has been reasonably compared with theoretical estimation of bubble particle collision. As discussed in Equation 2.1, the probability of collection is a function of bubble particle collision, attachment, and detachment. The attachment efficiency of particles with bubbles depends on the hydrophobicity of particles. For high hydrophobic particles, P_a can be assumed as unity. The detachment of particles is negligible for a relatively quiescent condition. In such case the collection probability mostly depends on the collision of particles and can be written as:

$$P \approx P_c \quad (2.6)$$

The construction of Figure 2.1 was verified using coal sample from the Buller seam coal, New Zealand. The coal sample was very hydrophobic in nature, and the probability of adhesion (P_a) was assumed as unity. For such hydrophobic coal samples collection probability (P) can reasonably agree with collision probability (P_c) as shown in Equation 2.6.

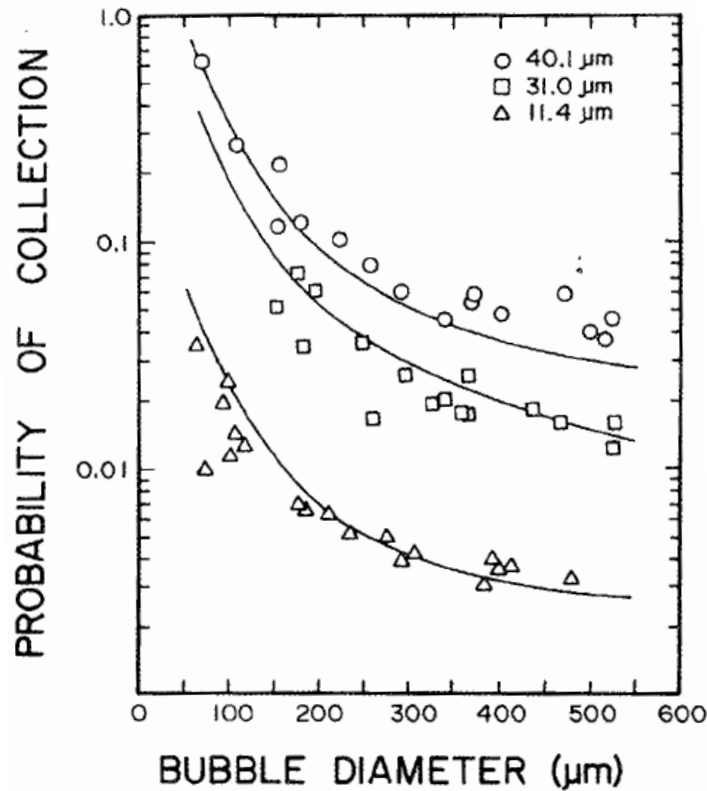


Figure 2.1: Comparison of experimental probability of collection (points) versus the probability collision using Equation 2.5 for different bubble and particle sizes, after Yoon and Luttrell (1989).

Later, Yoon (1993) concluded that the first order flotation rate (k) was inversely proportional to d_b^3 (valid up to the value of d_b 100 μm), which showed a strong incentive for using smaller bubbles. However, the author suggested that as bubble size increased the collision efficiency (P_c) became less dependent on bubble size and k varied as $d_b^{-1.46}$. He also observed that at low agitation speed (100 rpm), the experimental k values were in close agreement with predicted values, particularly with regard to slope. As the agitation speed increased, k became less dependent on d_b . His (Yoon, 1993) finding suggested that the benefits of using small bubbles for flotation are best achievable under quiescent conditions.

Diaz-Penafiel and Dobby (1994) conducted a study on the effect of bubble size on the flotation rate constant and concluded that it is affected by the average bubble size. They reported that the rate constant is an exponential function of the bubble size (bubbles of

diameter 0.8-2.0 mm were investigated). For silica particles it was verified that $k \propto d_b^{-1.54}$ and $P \propto d_b^{-0.54}$.

Hewitt et al. (1995) measured the collection efficiency (P) of single bubbles of three different diameters (750, 1200 and 2000 μm) to float methylated quartz particles of diameters in the range of 5-80 μm over a wide range of particle-water advancing contact angles. From the observed experimental value of P they calculated the attachment efficiency (P_a) and concluded that it was higher for small bubbles for all particle sizes.

Similarly, Dai et al. (1999) measured the capture efficiency of nitrogen bubbles of diameters 770, 1000 and 1520 μm to recover rough, angular quartz particles of diameters ranged from 7.5-70 μm . The attachment efficiency (P_a) was calculated using these capture data together with the Generalized Sutherland collision model. Dai et al. (1999) suggested that attachment efficiency increased with decreasing bubble size and particle size, but with increasing particle contact angle and electrolyte concentration (KCl). Later these authors (Dai et al., 2000) experimentally measured the collision efficiency of hydrophobic quartz particles (advancing contact angle of 74°) with bubble of diameters of 770 and 1520 μm . It was concluded that the collision efficiency was higher with smaller bubbles. The particle diameters used in their experiments were in the range of 5-60 μm .

Ramirez and Davis (2001) performed trajectory analysis considering hydrodynamic interactions and van der Waals attractions, and calculated the kinetic recovery constant of fine but non-Brownian oil droplets (3-20 μm in diameter) by tiny air bubbles (40-80 μm in diameter). It was verified that the theoretical kinetic constant (k) depends on bubble and particle size as $k \propto \chi d_b^{-0.86} d_p^{1.21}$, where χ is the gas holdup. Their experimental findings using a batch flotation cell supported the scaling, but the quantitative predictions for the flotation rate were about three-fold higher than the measured values. It was observed that small bubble has higher collection efficiency due to a higher surface area per volume and weaker hydrodynamic interactions.

Tao (2004) reviewed the fundamentals of flotation including bubble-particle collision, adhesion and detachment processes and summarized that small bubbles increased the probability of bubble-particle collision and adhesion but reduced the probability of detachment, consequently increasing the possibility of collecting particles.

Recently, Han et al. (2006) reported a higher removal efficiency of kaolin particles when the bubble size was similar to particle size.

While all the studies reported above suggest that the collection efficiency or the flotation rate constant directly depends on bubble size, Gorain et al. (1997) stated that the flotation rate constant (k) could not be related to bubble size independently, but could be related in conjunction with gas superficial velocity. The term ‘bubble surface area flux’ (S_B) was used in their analysis and was defined as: $S_B = 6v_G/(d_b)_S$, where v_G is the gas superficial velocity, and $(d_b)_S$ is the Sauter mean bubble diameter. They performed experiments in a portable industrial scale flotation cell (2.8 m³) and proposed a linear relationship between k and S_B through the cell. This k - S_B relationship implies weaker dependence of k on d_b in such a way that k should be inversely proportional to d_b . This weaker dependence of the flotation rate constant on the bubble size was explained by Deglon et al. (1999) as a conflict between the sub processes of bubble particle attachment and detachment in mechanical flotation cells. They concluded that the attachment-detachment model, used in conjunction with the bubble population balance model, represents the origin of the k - S_B relationship and that the weaker dependence of k on d_b predicted by this relationship is due to the effects of particle-bubble detachment.

All the above studies clearly indicate a general decrease in collision and collection efficiency, as well as in flotation rate constant with increased bubble size, which can be expressed by the general equations below:

$$P \propto d_b^{-m_1} \tag{2.7}$$

$$P_c \propto d_b^{-m_2} \tag{2.8}$$

$$k \propto d_b^{-m_3} \tag{2.9}$$

The values of exponents vary in the range of 0.54-2.05, 1.69-2, and 0.86-3.05 for m_1 , m_2 and m_3 , respectively, depending on hydrodynamic characteristics such as bubble and particle size. Table 2.1 summarizes the values of exponent used in different studies above under different hydrodynamic conditions.

Table 2.1: Summary of the studies focussing the effect of bubble size on flotation

Authors	Findings	Conditions
Reay and Ratcliff (1973)	$P \propto d_b^{-2.05}$	$d_b < 100 \mu\text{m}$
Reay and Ratcliff (1975)	$k \propto d_b^{-3.05}$ $P \propto d_b^{-1.9}$	d_b : 42 and 71 μm ; d_p : 7-22 μm (glass beads) d_b : 42 and 71 μm ; d_p : 3-9 μm (polystyrene latex particles)
Jameson et al. (1977)	$k \propto d_b^{-3}$ $P_c \propto d_b^{-1.69}$, $k \propto d_b^{-2.69}$	$d_b < 100 \mu\text{m}$; d_p : 4-30 μm d_b : 600-1000 μm ; d_p : 10-50 μm
Yoon and Luttrell (1989)	$P_c \propto d_b^{-2}$	
Yoon (1993)	$P_c \propto d_b^{-2}$, $k \propto d_b^{-3}$ $k \propto d_b^{-1.46}$	$d_b < 100 \mu\text{m}$ d_b : very large
Diaz-Penafiel and Dobby (1994)	$k \propto d_b^{-1.54}$, $P \propto d_b^{-0.54}$	d_b : 800-2000 μm
Gorain et al. (1997)	$k \propto d_b^{-1}$, $k \propto S_b$	
Ramirez and Davis (2001)	$k \propto \chi d_b^{-0.86} d_p^{1.21}$	d_b : 40-80 μm

2.3 EFFECT OF PARTICLE SIZE ON FLOTATION

Gaudin et al. (1942) performed the first study showing the effect of particle size on flotation. They concluded that for particles up to 4 μm in diameter, the flotation rate was independent of particle size, but in the range of 4-20 μm it was directly proportional to the particle diameter. Other works on the effect of particle size include that of Morris (1952), Bushell (1962), Tomlinson and Fleming (1963), and Flint and Howarth (1971b). Flint and Howarth (1971b) theoretically calculated the collision efficiency of fine particles (6 μm in diameter) and concluded that it is independent of flow types (Stokes and potential flow) for very fine particles (air bubbles of diameter of 50-100 μm were considered).

Later, Reay and Ratcliff (1973) proposed two flotation regimes (collision and diffusion regimes) based on particle size. It was concluded that particles larger than 3 μm in diameter were large enough not to be affected by Brownian motion (fall in the collision regime), and their flotation rate would be directly proportional to the square of the diameter (when the bubbles are small enough to obey Stokes' law). The sub-micron particles become susceptible to Brownian diffusion and fall into diffusion regime, in which case $k \propto \frac{1}{d_p^{2/3}}$ (Reay and Ratcliff, 1973). The bubble size used in Reay and

Ratcliff's analysis was in the range 20-100 μm in diameter. Later, these authors (Reay and Ratcliff, 1975) experimentally observed the flotation of glass beads (diameter 7-22 μm) and polystyrene particles (diameter 3-9 μm) and concluded that for glass spheres $k \propto d_p^{1.5}$, but for polystyrene particles $k \propto d_p^{0.5}$. They suggested that electrical forces, which were not considered in their theory, could have an important effect. The average bubble diameters of in their experiments were 42 and 71 μm produced from fine and medium frit, respectively. In contrast, Collins and Jameson (1976) showed that $k \propto d_p^{1.5}$ for polystyrene latex particles of diameter 4-20 μm . In their experiment, the charge of the particle, which was varied in the range of 30-60 mV, showed a little effect on the exponent.

Trahar and Warren (1976) concluded that the best recoveries were obtained, in general (for a wide range of minerals, reagents and flotation machines), with particles in size from 10-100 μm in diameter. It was also observed that the recovery fell gradually for

particle sizes smaller than 10 μm , while there was no critical size below which particles became non-floatable (particle diameter considered down to 1 μm).

Jameson et al. (1977) analysed the experimental quartz recovery data of Anfruns and Kitchener (1977) and proposed that $P_c \propto d_p^2$ and $k \propto d_p^2$ for particles in the range 10-50 μm . Their analysis also stated that the dependency of flotation rate constant on particle size becomes weaker for smaller particles (4-30 μm); i.e. $k \propto d_p^{1.5}$.

A fundamental flotation model developed by Dobby and Finch (1987) reported a peak in collection efficiency (P) for particle diameter around 30 μm considering constant induction time. The induction time is the time required to capture the thin film separating particle and bubble and to establish contact between bubble and particle. The peak in collection efficiency was due to increase in collision efficiency (P_c) but decrease in attachment efficiency (P_a) with increasing particle size.

Yoon and Luttrell (1989) concluded that the probability of collision between bubbles and particles varied as the square of the particle diameter (d_p). Figure 2.1 also clearly shows that for a constant bubble size, the probability of collection increases with increased particle size. Later, Yoon (2000) reported that $k \propto d_p^2$.

Ketkar et al. (1991) used hydrogen bubbles evolved from a polished stainless steel plate cathode at a current density of 250 A/m² (average bubble diameter 29 μm) to recover quartz particles of average diameter 6.5-65 μm . In contrast to the conventional conception of higher removal efficiency with increased particle size, they reported a decrease in removal efficiency with increased particle size. They also suggested that specific particle sizes float better with specific bubble size. It was observed that the finest particle fraction (+4-10 μm ; average diameter 6.5 μm) floated best with the finest bubble size (diameter ranged from 22-34 μm), while medium particle size fraction (+10-20 μm ; average diameter 14.3 μm) showed best recovery with medium bubble size (diameter ranged from 28-39 μm), and the coarse fraction (+20-30 μm ; average diameter 25.5 μm) showed highest recovery with the largest bubble size (diameter ranged from 30-45 μm).

Dai et al. (1999) measured capture efficiency with nitrogen bubbles of diameters 770, 1000 and 1520 μm to recover rough, angular quartz particles of diameters ranging from 7.5-70 μm , and calculated P_a using these capture data together with the Generalized Sutherland collision model. Their analysis concluded that attachment efficiency increases with decreasing particle size.

By trajectory analysis, Ramirez and Davis (2001) calculated the kinetic constant (k) for the recovery of fine, non-Brownian oil droplets (3-20 μm in diameter) by minute air bubbles (40-80 μm in diameter), and suggested that k was directly proportional to the 1.21 power of d_p . They also found that smaller droplets were captured less efficiently as they easily tended to flow around rising bubbles.

Recently, Nguyen et al. (2006) investigated the collection of nanoparticles by air bubbles. Their theoretical analysis followed by experimental observations proved that the electrical double layer and non-DLVO hydrophobic attractive forces have significant effect on the collection of nanoparticles. The van der Waals and electrical double-layer are the key element of Derjaguin–Landau–Verwey–Overbeek (DLVO) theory. The attractive force between hydrophobic surfaces is one of the non-DLVO forces relevant to the bubble–particle collision interaction. They demonstrated that the collection efficiency becomes a minimum at particle diameter of $\sim 0.1 \mu\text{m}$. With larger particles, the interception and collision mechanism apparently dominates; while the diffusion and colloidal forces control the collection of particles with diameter $< 0.1 \mu\text{m}$. Fine bubbles having an average diameter of $\sim 150 \mu\text{m}$ produced in a small laboratory column cell were used for collecting the particles.

More recently, Gontijo et al. (2007) studied the limits of fine and coarse particle flotation (particle diameter ranging from 0.5-1000 μm) as a function of advancing water contact angle. The maximum floatable particle size of coarse particles was determined by the stability of the bubble particle aggregate, while the flotation limit of fine particles was directed by the energy requirement for rupturing the intervening liquid film between the particle and the bubble. It was also demonstrated that high contact angles with small bubbles made the flotation of very large and very fine particles became possible.

All the above studies, except that of Ketkar et al. (1991), clearly indicate that when particles are large enough not to be affected by Brownian motion, the collection efficiency and flotation rate increase with increasing particle size. The relation between flotation rate constant and particle diameter can be expressed by the general equation:

$$k \propto d_p^n, \quad (2.10)$$

where n is an exponent. The exponent varies in the range 0.5-2.05 depending on hydrodynamic conditions such as bubble and particle size. Table 2.2 summarizes the exponent used in different studies. The decrease in recovery with increasing particle size observed in the study of Ketkar et al. (1991) might be attributed to the insufficient lifting capacity of small bubbles (average diameter 29 μm) compared to particle size (6.5-65 μm in diameter).

Table 2.2: Summary of the studies focussing the effect of particle size on flotation

Study	Findings	Conditions
Reay and Ratcliff (1973)	$k \propto d_p^{2.05}$ $k \propto d_p^{-0.67}$	$d_b < 100 \mu\text{m}$; d_p : 3-15 μm $d_b < 100 \mu\text{m}$; d_p : submicron (<0.2 μm)
Reay and Ratcliff (1975)	$k \propto d_p^{1.5}$ $k \propto d_p^{0.5}$	d_b : 42 and 71 μm ; d_p : 7-22 μm (glass beads) d_b : 42 and 71 μm ; d_p : 3-9 μm (polystyrene latex particles)
Collins and Jameson (1976)	$k \propto d_p^{1.5}$	d_p : 4-20 μm (polystyrene latex particles); zeta potential: 30-60 mV
Jameson et al. (1977)	$k \propto d_p^{1.5}$ $P_c \propto d_p^2$, $k \propto d_p^2$	$d_b < 100 \mu\text{m}$; d_p : 4-30 μm d_b : 600-1000 μm ; d_p : 10-50 μm
Yoon and Luttrell (1989)	$P_c \propto d_p^2$	
Yoon (2000)	$k \propto d_p^2$	
Ramirez and Davis (2001)	$k \propto \chi d_b^{-0.86} d_p^{1.21}$	d_b : 40-80 μm ; d_p : 3-20 μm

2.4 EFFECT OF SURFACE CHARGE ON FLOTATION

The surface charge of both particles and bubbles affects flotation efficiency. Derjaguin and Dukhin (1961) theoretically analysed the various stages of flotation and showed that when the thickness of the liquid film between a bubble and a particle became very thin, the effect of adsorbed ions of the same charge on the two opposite surfaces would tend to keep particle and bubble apart. They proposed a criterion for rapid flotation expressed by:

$$\frac{\zeta \lambda_o^2}{\kappa A'} \ll 1. \quad (2.11)$$

where ζ is the dielectric constant, λ_o is the surface potential, κ is the Debye length, and A' is the effective Hamaker constant. For the interaction of two van der Waals bodies Hamaker constant can be defined as:

$$A' = \pi^2 C_h \gamma_1 \gamma_2, \quad (2.12)$$

where γ_1 and γ_2 are the number of atoms per unit volume in two interacting bodies and C_h is the coefficient in the particle-particle pair interaction (Lee and Sigmund, 2002). Derjaguin and Shukakidse (1961) tested this criterion for floating antimonite particles. They stated that the rate of flotation of antimonite, which is naturally hydrophobic, dropped sharply as the zeta potential of the particles was increased beyond a critical value. Later, Jaycock and Ottewill (1963) investigated the flotation of negatively charged silver iodide particles with a cationic surfactant and reported the highest flotation rate at zero zeta potential of silver iodide. DeVivo and Karger (1970) also found a similar effect on clay particles. However, in both cases, the zeta potential was zero which might lead to coagulation of particles, and if coagulation had occurred, the increase in particle size could have caused an increase in the rate of flotation. Dibbs et al. (1972) investigated the effect of zeta potential of rising bubbles on the flotation of quartz in the presence of dodecylamine hydrochloride and stated the importance of the presence of double layer interactions.

Collins and Jameson (1976) studied the flotation of polystyrene particles (20 μm diameter). A cationic surfactant (CTAB) and sodium sulphate were used to alter the hydrophobicity and charge. The addition of CTAB changed the charge of the polystyrene latex from negative to large positive, and the addition of sodium sulphate reduced the positive charge. By measuring mobility, it was reported that the polystyrene particles had adsorbed the CTAB^+ ion to such an extent that the zeta potential changed from approximately -30 mV to $+60$ mV, and the addition of sodium sulphate reduced the charge to about $+30$ mV. It was assumed that the bubbles carried the adsorbed CTAB and was therefore positively charged. This positive charge was then reduced by the addition of sulphate ions. They summarized that in the presence of a cationic surfactant, both particles and bubbles will be positively charged, which will tend to cause double-layer repulsions that must be overcome by the dispersion forces between the adsorbed layer on both the particle & bubble. Consequently, flotation is encouraged by reducing the charge by the addition of a negative ion such as sulphate (Collins and Jameson, 1976).

Later, these authors (Collins and Jameson, 1977) measured the charge of bubbles and particles in flotation process and confirmed that both the bubbles and the particles (4-20 μm polystyrene beads) were found to carry a positive charge of approximately the same value under the same electrolytic concentrations. Experimentally determined rate constants for flotation were found to depend strongly on the bubble and particle charge, increasing by an order of magnitude as the charge decreased from $+60$ to $+30$ mV. Their results implied that the maximum rate of flotation was achieved when the zeta potential of the particles was zero. As the charge on the particles and the bubbles builds up, coalescence between them is inhibited by double layer repulsion. In the case of floating only one particle, such as suspension of oil or clay from wastewater, it would obviously be advantageous to keep the charge as near to zero as possible to promote coagulation prior to flotation, as well as to help the bubbles and particles to coalesce. However, in the case of selective separation of a particle from two or more species, coagulation of various species would be undesirable. Therefore, in selective flotation, it is necessary to ensure that the particles must carry sufficient charge to prevent coagulation, but not too much to inhibit collision and attachment with bubbles through double layer repulsion. Collins and Jameson (1977) proposed a simple correlation to express the effect of charge on flotation rate constant as:

$$-\ln(k_p / d_p^{1.5}) = 3.9 + 0.116U_p U_b . \quad (2.13)$$

where k_p is the rate constant (min^{-1}), d_p is the particle diameter (μm), U_p is the electromobility of the particle ($\mu\text{m/s.V.cm}$), and U_b is the electromobility of the bubble ($\mu\text{m/s.V.cm}$).

Fukui and Yuu (1980) investigated the collection of submicron particles by electrogenerated bubbles and concluded that the flotation performance varied with the charge of both the particle and the bubble. Later, these authors (Fukui and Yuu, 1985) summarized that the maximum flotation rate would be achieved when the zeta potentials of the gas bubbles and particles had opposite signs. Han et al. (2006) also reported that the removal efficiency was high when the zeta potentials of bubbles and particles had opposite signs, or when both potentials were close to 0 mV. They also demonstrated that bubble and particle zeta potentials were similar under identical conditions.

Shin (2003) suggested that bubbles could be selectively targeted at specific particles by taking their zeta potential into account. Han et al. (2004) performed a study in the presence of calcium and magnesium metal ions to investigate the zeta potential of bubbles and to find factors that can produce positively charged bubbles. It was reported that in the case of calcium, the zeta potential of bubbles was negatively charged over the entire pH range. With magnesium, on the other hand, positively charged bubbles were observed at concentrations of above 0.01 M Mg, especially above pH 9. They (Han et al., 2004) concluded that the zeta potential of bubbles is a function of the type and concentration of metal ions and the pH of the solution, and it may be possible to create solution conditions under which bubbles with positive charges can be formed.

2.5 EFFECT OF HYDROPHOBICITY OR CONTACT ANGLE ON FLOTATION

The ability of mineral particles to attach to bubbles strongly depends on the hydrophobicity of the mineral particles. The degree of hydrophobicity can be described by the contact angle, the angle at the three phase line of contact between the mineral,

the liquid phase and the gaseous phase (Gaudin, 1957). It is well known that the higher the contact angle of a mineral surface, the more readily it is wetted by the gaseous phase, and is thus more hydrophobic (Lucassen-Reynders and Lucassen, 1984, Gaudin, 1957). For flotation to be successful, a mineral-gas interface must be created with the simultaneous destruction of water-gas and mineral-water interfaces of equal area. Hence, the contact angle between bubble and mineral surface must be finite for the attachment of mineral particles to bubbles. Following the Young's equation, the contact angle (θ_c) can be defined as:

$$\theta_c = \cos^{-1} \left(\frac{\sigma_{mg} - \sigma_{mw}}{\sigma_{wg}} \right), \quad (2.14)$$

where σ_{mg} , σ_{mw} , and σ_{wg} are the interfacial energies at the mineral-gas, mineral-water, and water-gas interfaces, respectively.

Fuerstenau (1957) investigated the correlation of contact angles and flotation rate, and concluded that flotation rate increased with an increase in contact angle. Figure 2.2 demonstrates excellent correlation among contact angle, adsorption density, zeta potential and flotation recovery, with an increase in flotation recovery as contact angle increases.

Recently, Gontijo et al. (2007) investigated the flotation behaviour of quartz particles (0.5-1000 μm in diameter) as a function of advancing water contact angle and concluded that flotation of very fine and large particles being possible at high contact angle. It was reported that the advancing water contact angle required for floating very fine quartz particles (0.5-5 μm in diameter) was 55-60° or above. Their study showed that for fine quartz particles, recovery increases rapidly with increased contact angles between 50 and 60°, but plateaus above 60°.

Later, Chipfunhu et al. (2011) examined the effect of contact angle on fine particle flotation. They floated fine quartz particles (0.2-50 μm in diameter) by air bubble of Sauter mean diameter of 420 μm produced in a mechanical cell. It was reported that flotation recovery increased with increased contact angle and particle size.

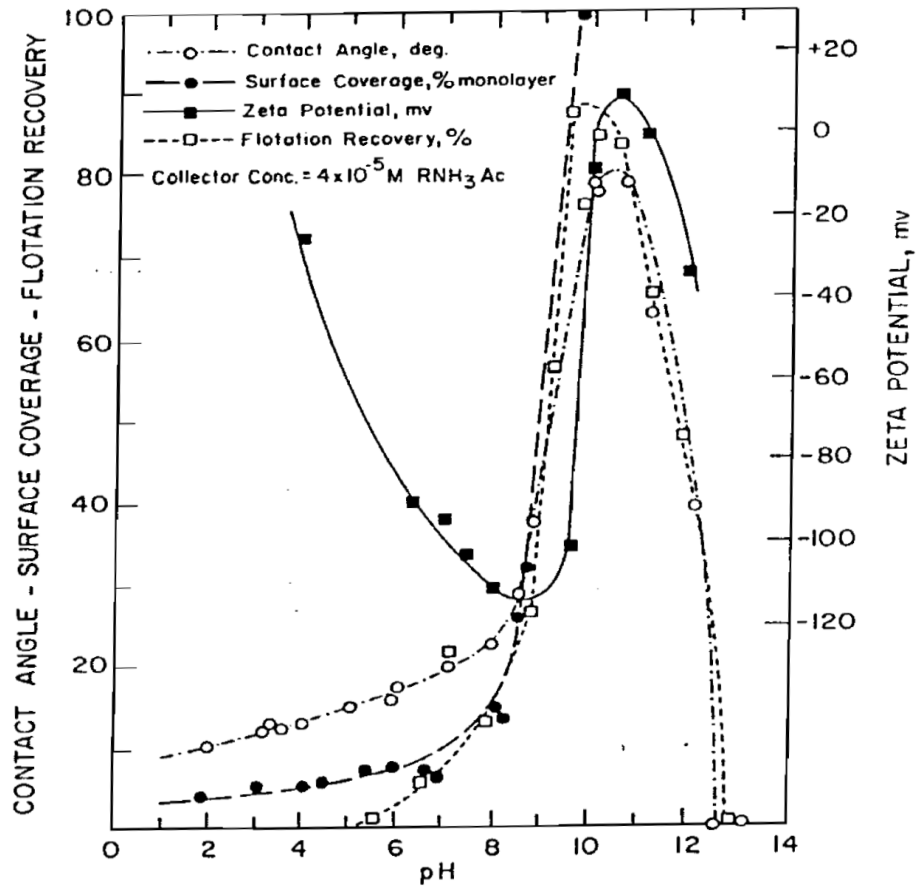


Figure 2.2: Correlation between contact angle and flotation recovery, after Fuerstenau (1957).

Scheludko et al. (1976) first proposed the existence of a critical contact angle, below which the flotation of fine particles usually does not happen. Their theory was based on the concept that to be attached to the bubbles, the kinetic energy of fine particles must be larger than the energy required to replace the intervening liquid film and to form a three-phase contact line. Usually, fine particles do not possess sufficient kinetic energy to displace the intervening liquid layer between the colliding particle and bubble (Hewitt et al., 1995). Following Scheludko et al. (1976), some other studies (e.g., Crawford, 1986, Gontijo et al., 2007, Miettinen, 2007)) also supported the existence of such critical contact angle. Recently, Chipfunhu et al. (2011) validated experimental data with the theory of the existence of a critical contact angle, below which particles became non-floatable. They interpreted the non-floating component as a fraction consisting of particles below the critical contact angle for flotation to be initiated for

that size. The critical contact angle depends on particle size, showing an increase with decreased particle size (Chipfunhu et al., 2011).

2.6 ENTRAINMENT IN CONVENTIONAL FLOTATION

The particles that are dragged from the pulp into the froth in the interstitial liquid can cause entrainment flotation. The capture of particles in the interstitial liquid is non-selective and hence can produce low grade product for a system of mixed species. Hence, entrainment is a major problem for recovering very fine minerals by conventional flotation machines and limits the lower size to which efficient separation can be achieved (Trahar, 1981).

It is well known that the entrained particles can enter the pulp-froth interface by both mechanical and hydraulic entrainment. Mechanical entrainment is formed by pulp agitation while hydraulic entrainment is formed by the bubble wake and bubble swarm effects. In electroflotation experiments, no mechanical agitation was used; hence the contribution of mechanical entrainment could be neglected. The formation of wake behind a rising bubble depends on hydrodynamic conditions. George et al. (2004) numerically showed that wake will only form if the Reynolds number is larger than 20.

2.7 BUBBLES SIZES IN DIFFERENT CELLS

2.7.1 Mechanically Agitated Cell

Mechanically agitated cells are the most common flotation cell in the mineral industry. In this cell, bubbles are produced by the shearing forces generated at the impeller. There have been numerous studies that performed bubble size distribution analysis for both laboratory and industrial flotation cells. Some of them have been as discussed below. Photographic and/or bubble size analyser technique were used in these studies. Bubble sizes were reported either as a mean size or a Sauter mean size. Bubble size distribution performed for both forced aeration and self-aeration flotation cells have been reported here. Bubble sizes measurements had been performed for a wide range of variables including impeller type, impeller speed, air flow rate, frother type and dosages, cell volume & location of measurement.

Jameson and Allum (1984) measured bubble size using photographic technique and reported that the Sauter mean bubble diameter (d_{32}) in most industrial flotation cells within Australia was in the range of 0.5-1.8 mm.

Tucker et al. (1994) used a novel device named as The UCT (University of Cape Town) bubble sampler, in conjunction with the UCT bubble size analyser to investigate the effect of frothers on the bubble size distributions obtained in two phase (gas-liquid) and three phase (gas-liquid-solid) systems, concluding that the frother type was found to have the greatest influence on bubble size. A modified Leeds 3.0 L laboratory flotation cell was used for their investigation. The cell was agitated at 1200 rpm with an air flow of 6 lpm. For the two phase system they observed a general decrease in bubble size as frother dosages increased, reporting a mean bubble size of $\sim 470 \mu\text{m}$ produced by all the frothers tested (methyl isobutyl carbinol, MIBC; di-isobutyl ketone, DIBK; triethoxybutane, TEB; Senfroth 6010; and Senfroth 6010B), at a dosage of 20 ppm. To investigate the effect of solids on bubble size they performed bubble size measurements at different solids concentration, and concluded that the presence of solids greatly influenced the mean bubble size produced in a flotation device. It was observed that without the presence of solids only 5-10 ppm frother was required to produce a mean bubble size $< 1 \text{ mm}$, whereas $> 20 \text{ ppm}$ frother was required to produce the same bubble size at 30% solids concentration. Among the frothers tested (DIBK, MIBC, and TEB), DIBK was the best frother up to 30% solids concentrations; while MIBC performed best above 30% solids concentration and moderately well below (Tucker et al., 1994).

Following the method of Tucker et al. (1994), Gorain et al. (1995) measured bubble size distributions in an industrial scale (2.8 m^3) flotation cell operated in the zinc cleaner circuit at Hellyer Mine in Tasmania, Australia. They measured bubble size at six different locations in the cell and reported the result as a “global mean” bubble size, which was the arithmetic average of bubble sizes obtained at six locations. Four types of impeller i.e., Chille-X, Pipsa, Outokumpu, and Door-Oliver were investigated in their measurement. The impeller speed was varied in the range 105-295 rpm, and the air flow rate was ranged from 16.5-56.7 l/s. The “global mean” bubble sizes were found to vary in the range 0.53-1.75 mm. The “global” mean size was calculated by simple arithmetic averages of the values at six locations. The mean bubble size increased with an increase in air flow rate, and decreased with an increase in impeller speed at various locations in

the cell, for all four impellers. Later, these authors (Gorain et al., 1997) expressed the bubble size distributions of the above 2.8 m³ portable industrial cells as Sauter mean size, (d_b)_S, which ranged from 0.7-1.8 mm. The Sauter mean diameter is defined as:

$$(d_b)_S = \frac{\sum_{i=1}^{i=n} d_i^3}{\sum_{i=1}^{i=n} d_i^2}, \quad (2.15)$$

where d_i is the equivalent spherical bubble diameter and n is the sample size.

After that, Deglon et al. (2000) used the same method for a variety of industrial flotation cells operating on South African Platinum concentrators (approximately 15 different types, and configurations of volumes between 3 and 60 m³) and stated that the (d_b)_S values ranged from 1.2-2.7 mm with an overall average of 1.6 mm. They also reported that bubble sizes produced in a column cell are significantly larger than those in the mechanical cells; i.e., 2.6-2.7 mm vs. 1.2-2.7 mm

A new technique named as HUT (combines some of the features of UCT technique) was used by Grau and Heiskanen (2005) to investigate the bubble size distribution in laboratory scale flotation cells (Outokumpu cylindrical flotation cells of volume 50 and 70 l were analysed). The study concluded that frothers mainly control bubble size in flotation cells by decreasing coalescence and affecting the bubble break-up process. The study also reported that the impeller speed and air flow rate have a strong influence on bubble size, and the Sauter mean bubble size (d_b)_S decreased as the impeller speed increased and the air flow rate decreased. For those laboratory scale flotation cells, (d_b)_S varied over the range of 1.2-2.9 mm. Recently, Grano (2006) measured bubble size in the first three rougher cells in the lead circuit of the Elura concentrator (formerly Pasminco Australia Ltd.) using the UCT bubble size analyser and found (d_b)_S in the range of 1.0-1.2 mm. The 8.5 m³ cells were mechanically aerated at impeller speed of 137-157 rpm.

Schwarz and Alexander (2006) surveyed bubble sizes in a large number of industrial cells, recovering different minerals in different countries. Over 800 cells of different

types (operated as rougher, scavenger, cleaner, mids, retreat, etc.) and sizes (up to 150 m³), manufactured by different companies, were investigated. In most cases, the UCT bubble size analyser was used; otherwise the McGill bubble viewer was used. They observed a wide range of bubble sizes produced in the pulp phase across the cells investigated, ranging from 0.7 to 4.0 mm, with an average size of 1.7 mm. The majority of bubbles were found to vary in the range of 1- 2 mm, with larger cells (greater than 100 m³) producing larger bubbles.

In contrast to a forced air machine, bubble size was found to increase with increasing impeller speed, as measured in the self-aerated 5.5 l laboratory-scale Denver flotation cell by Girgin et al. (2006) using the McGill Bubble Size Analyser (MBSA). This is due to the associated increase in gas rate, which causes an increase in bubble size that more than offsets the effect of increased shear.

The development of the UCT technique made it possible to measure bubble sizes in three phase (gas-liquid-solid) systems, which represents the actual conditions of flotation cells. In general, the measured bubble sizes produced in mechanically agitated cells varied in the range of 0.5-2.9 mm.

2.7.2 Column Flotation

In a flotation column, bubbles are generated either directly, through internal spargers, or after external contacting of gas with water or pulp (Finch and Dobby, 1990).

Yianatos et al. (1988) measured bubble size produced in a flotation column using photographic method. Three different frothers, Dowfroth 250C, triethoxy butane (TEB) and MIBC, were used to produce bubbles. It was observed that at constant gas superficial velocity, bubble size decreased with increased frother concentrations for all frothers, whereas at constant frother concentration, bubble size increased with increased gas superficial velocity. The Sauter mean bubble diameter was found to vary in the range 0.62-1.51 mm for a wide range of frother concentrations and gas superficial velocity.

Huls et al. (1991) studied bubble generation in an industrial flotation column using two sparging systems; i.e., a cloth sparger and an external air water contacting system

originally developed by the U.S. Bureau of Mines. Drift flux approach was applied to estimate the bubble sizes. At constant gas superficial rate (8.6 mm/s), bubble sizes were investigated for three cases; i.e., cloth sparger, external contacting sparger with the contacting chamber in place, and external contacting sparger without the contacting chamber. It was observed that bubble diameters were smaller in case of an external contacting sparger (average diameter 0.76-0.78 mm), compared to a cloth sparger (average diameter 0.86 mm). It was also observed that bubbles of similar sizes were produced by an external sparger with and without a contacting chamber, with a decrease in bubble size at an increased system pressure (i.e., sparger water rate).

Biswal et al. (1994) measured bubble sizes produced in a 100 mm diameter glass column both for air-water and air-water-coal systems. Measurements were performed both in flotation and cleaning zones (froth phase, where wash water was applied to alleviate entrained gangue particles), concluding that the cleaning zone produced larger bubbles than flotation zone. For air-water system, the average diameter ranged from 0.712-0.82 and 1.362-1.437 mm produced in flotation and cleaning zone, respectively. However, for air-water-coal system, the average diameter ranged from 0.695-0.75 and 1.35-1.379 mm produced in flotation and cleaning zone, respectively. The presence of solids (coal) did not have any significant influence on bubble size. It was also reported that a mixture of frothers (pine oil and MIBC) created finer bubbles compared to the individual species. Likewise, Ityokumbul et al. (1995) applied drift flux analysis to predict the bubble sizes produced in a flotation column with the presence of three different frothers; i.e., Dowfroth 250C, MIBC and Triton X-100. It was observed that frother types have a significant effect on bubble size. Triton X-100 produced larger bubbles (approximate diameter 1.85-3.12 mm) than Dowfroth 250C (approximate diameter 0.62-1.5 mm), and MIBC (approximate diameter 0.67-1.24 mm).

From the results of the above studies, it can be concluded that a flotation column produces smaller bubbles than a mechanically agitated cell. In general, the bubble size produced in a flotation column varies in the range 0.6-1.5 mm.

2.7.3 Dissolved Air Flotation

Dissolved air flotation (DAF) is the bubble generation method most commonly used in the treatment of potable water. In this method, gas (normally air) is dissolved in solution by applying pressure (Zabel, 1984). The solution is then released through needle valves to atmospheric pressure. After the pressure is reduced, the air transfers out of the solution, forming bubbles that rise to the surface of the liquid. The reported typical diameter range for bubbles generated using DAF is 10-120 μm , with a mean of 40 μm (Edzwald, 1995, Zabel, 1984).

Takahashi et al. (1979) measured bubble size produced in a DAF cell using a photographic method. Air was dissolved in water at 1-5 kg/cm^2 gauge pressure and flashed to atmospheric pressure through a nozzle. Bubble diameters were found to vary in the range 100-200 μm at a distance about 100 cm above the nozzle tip. It was reported that the mean bubble diameter decreased with an increase in both pressure and liquid flow rate, although at large liquid flow rate the bubble diameter became constant.

De Rijk et al. (1994) studied the distribution of bubble sizes in DAF both on laboratory and industrial cells (sewage treatment plant) using an image analysis method. The effects of pressure, flow rate, the presence of a tube behind the valve, the geometry of tube, etc. were investigated. The bubble size was found to decrease with an increase in pressure and flow rate (at low pressure) with the absence of the tube behind the valve. However, at high pressure the effect of flow rate was not significant. It was also observed that at constant pressure and flow rate, bubble size increased with the presence of the tube behind the valve, while the effect of tube geometry on bubble size was not clear. In general, the bubble diameters were found to vary between 10 and 300 μm .

Rykaart and Haarhoff (1995) used a photographic method to measure bubbles produced in a laboratory scale DAF cell. Median bubble size was reported here instead of mean bubble size. The median diameter of bubbles was found to vary in the range 29.5-76.8 μm depending on nozzle design, saturator pressure and measurement position downstream of the channel exit. A general increase in bubble diameter was reported with a decrease in saturator pressure and an increase in downstream distance.

Burns et al. (1997) measured the bubble size produced from a pilot-scale DAF system using a pressure in the range 414-635 kPa, using image analysis technique. The water flow rate was kept constant at 3.8 l/min, whereas the air flow rate was varied between 0.45 and 0.57 m³/h. The average bubble size ranged from 46.4-57.5 µm. The analysis reported that air pressure forced into solution did not significantly affect the bubble size produced in DAF system, although increasing pressure induced a slight decrease in mean bubble size.

Han et al. (2002) measured bubble size produced in DAF by three different techniques; i.e., image analysis, batch type particle counter, and online particle counter. The pressure was kept constant at 6 atm throughout the DAF experiments. They found the narrowest bubble size distribution by image analysis which was 14-56 µm, with an average value of 32 µm. Wider size distributions of 13-96 µm and 15-85 µm were obtained by batch type and online particle counters, respectively. However, the average sizes observed by batch type and online particle counters were 31 and 28 µm, respectively, which were very close to those found by image analysis.

Englert et al. (2009) used a 7.7 l cylindrical flotation cell as a DAF unit to float quartz particles. Air was dissolved at 300 kPa saturation pressure in a vessel, aiming for the air-saturation of the frother solution to take place within a time of 30 min, and allowed to enter the flotation column at 0.2 l/min. They applied the LTM_BSizer technique to measure bubble size and reported that the Sauter mean and arithmetic mean bubble diameters were 79 and 56 µm, respectively. The arithmetic mean is the simple arithmetic averages of the bubbles measured.

In conclusion, it can be said that the average bubble diameter in DAF varies in the range of 10-300 µm, which is quite smaller than those produced by mechanically agitated cell (diameter 500-2900 µm) or column flotation cell (diameter 600-1500 µm).

2.7.4 Gas Aphrons

Colloidal gas aphrons (CGAs) are surfactant-stabilised micro bubbles having a diameter > 25 µm generated by high stirring (5000-10000 rpm) of surfactant solutions (Sebba, 1987). Recently, Xu et al. (2008) performed a comparative study of microbubble generation by mechanical agitation and sonication. They created microbubbles with two

different surfactant solutions; i.e., 1% sodium dodecyl sulphate (SDS), and 1% L-150A (mixture of 38% sucrose laurate ester, 10% ethanol, and 52% water). For both surfactants, bubbles generated by sonication were smaller than those generated by mechanical agitation. For a 1% SDS solution, the average bubble diameter was 26 ± 12 μm by sonication and 68 ± 27 μm by mechanical agitation. Similarly, for 1% L-150A, the average bubble diameter was 46 ± 12 μm by sonication and 72 ± 28 μm by mechanical agitation (Xu et al., 2008).

2.7.5 Turbulent Microflotation

Turbulent microflotation is performed in a long narrow channel where the treated three phase (water-particles-microbubbles) mixture flows. Turbulent stream flow is maintained by adjusting the flow rate of the mixture to avoid early separation of the phases, and to ensure the accomplishment of all three major sub-processes; i.e., aggregation (flocculation or coagulation) of suspended particles, hetero coagulation of particles (and/ or their aggregates) with bubbles, and aggregation of particles with bubbles attached to them. Based on theoretical analysis and pilot plant experimental findings, Rulyov (2001) concluded that for the effective separation of very fine particles ($d_p < 1\mu\text{m}$), the utilisation of relatively fine bubbles with the initial diameter < 40 μm was necessary. He also concluded that the diameters of particles required to be higher than 7 μm (which was achieved by coagulation or flocculation of fine particles) to ensure hetero coagulation of particles with bubbles.

2.7.6 Electroflotation Cell

Electroflotation is a simple process that floats pollutants or minerals to the surface of a solution by small bubbles of hydrogen and oxygen gases generated from the electrolysis of water. The usage of electricity for treating water was first proposed in 1889 (Strokach, 1975), while Elmore first proposed 'electroflotation' for recovery of valuable minerals from ores in Broken Hill, Australia in 1904 (Elmore, 1905). The process was not successful due to the high requirement of electrical energy, and the absence of adequate technological advantages (Mamakov and Avvakumov, 1968).

In electroflotation experiments hydrogen and oxygen bubbles are produced at the cathode and anode, respectively. There have been several studies dealing with the measurement of bubble sizes produced in electroflotation. Some of them measured

hydrogen bubbles, some measured oxygen bubbles, some measured both, while some measured the bubbles without distinction as to what they were hydrogen or oxygen bubbles.

Hydrogen bubble size

Landolt et al. (1970) measured hydrogen bubble sizes by stop-motion photography at different flow rates. A rectangular flow channel (85 mm length \times 8 mm width \times 0.5 mm high) was used for viewing the bubbles. Its side walls were made of flat glass plates, which provided for the optical observation of the inter-electrode gap. Copper electrodes (3.17 mm long in the flow direction and 0.53 mm wide) were used for bubble production. The centre of the electrode was positioned 10 mm from the downstream end. To investigate the effect of flow rates on bubble sizes, flow rates up to 25,000 mm/s were employed. The major limitations of this study were that bubbles of diameter $< 20 \mu\text{m}$ were below the optical resolution of their aperture and hence not counted; and bubbles close to the cathode surface were usually not individually visible (cloudy), and were therefore, not counted.

Janssen and Hoogland (1970) produced hydrogen bubbles using a platinum foil (0.1 mm thick \times 10 mm wide \times 2 mm high) as cathode at current density ranging from 100-5000 A/m². They measured the bubble sizes by photographic method. The pH of the solution was acidic and pictures were taken from a region about 100 μm above the upper edge of the electrode. Bubble size was independent of current density up to 400 A/m² (average diameter 30 μm), but after that bubble size increased with current density due to coalescence of bubbles.

Later, these same authors (Janssen and Hoogland, 1973) measured hydrogen bubbles produced from a platinum disc of 11.2 mm diameter (geometric surface area of 100 mm²) in both acidic and alkaline medium using current densities in the range 40-1000 A/m². The platinum cathode was mounted vertically in a resin and its flat circular end was exposed horizontally for hydrogen production. Measurements were taken in a region about 200 μm above the electrode surface. The bubbles that stayed on the electrode surface (diameter referred as d_a), as well as bubbles detached from the electrode, but in the neighbourhood of the electrode surface (diameter referred as d_f) were measured. Janssen and Hoogland stated that in an acidic medium the hydrogen

bubble size (d_f) remained constant for current densities up to 100 A/m^2 , and after that bubble size increased with an increase in current density. However, in an alkaline solution the bubble size did not seem to be a function of current density. They observed that at current densities less than 100 A/m^2 , there was no coalescence of bubbles, but as current density increased especially above 300 A/m^2 , the coalescence of bubbles, except for hydrogen bubbles in an alkaline medium, was very usual. In an acidic medium, the average hydrogen bubble diameters were 36 and 85 μm at current densities of 40 and 1000 A/m^2 , respectively. But in an alkaline medium, similar average bubble diameters were observed; i.e., 26 and 28 μm at current densities of 40 and 1000 A/m^2 , respectively.

Ketkar et al. (1988) used stainless steel mesh (wire diameter 50-215 μm) and plate (mirror polished) cathodes to produce hydrogen bubbles at current densities in the range $125\text{-}370 \text{ A/m}^2$, and measured those bubble sizes using a photographic technique. The hydrogen bubbles were produced in alkaline medium (pH of electrolyte 9) and were photographed at the cathode surface. The average bubble diameters were 28-49 and 22-34 μm produced by mesh and plate cathodes, respectively. Hydrogen bubble diameter decreased with increased current density and decreased wire diameter. However, the smallest size of hydrogen bubble (22 μm) was observed with stainless steel plate.

Burns et al. (1997) used flat polished graphite (76 mm x 25 mm x 13 mm) as the electrode to produce hydrogen bubbles at current densities in the range of $20\text{-}100 \text{ A/m}^2$. They videotaped the bubbles by focusing the camera on the electrode surface and measured the diameter of hydrogen bubbles. The average equivalent bubble diameters were found to be in the range 19.3-37.7 μm , and no clear trend of bubble size with respect to current density was observed. Using a photographic method, Setty and Venkatachalam (1997) measured hydrogen bubble sizes produced from polished stainless steel cathodes ($4.52 \times 10^{-4} \text{ m}^2$) in an alkaline medium (pH 10). It was reported that the statistical mean hydrogen bubble diameters were 37 and 30 μm at current density 225 and 400 A/m^2 , respectively.

Lumanauw (2000) characterized hydrogen bubbles produced from nickel screen and plate cathodes in an alkaline solution of 1 M K_2CO_3 . Screen of wire diameter 350 μm (smooth and rough) and a plate of thickness 500 μm (crystalline and amorphous alloy)

were used in this study. An image analysis method was used to measure bubble sizes with no external flow of electrolyte, while a particle size analyser was used to measure bubble sizes with and without external flow of electrolyte. The study reported that the image analysis method could be successfully applied up to current densities of 400 A/m². Above 400 A/m², bubbles nucleated over the entire surface of the electrode making the application of the image analysis difficult. The data obtained by the image analysis method concluded that plate electrodes produced larger bubbles than screen electrodes. It was also reported that the amorphous alloy plate produced bigger bubbles than the crystalline alloy plate. Only the smooth screen was used for bubble size measurements by a particle size analyser without external flow of electrolyte, and a slight increase in bubble size was reported with increased current density in the range 250-1250 A/m². Then electrolysis was performed using all types of cathodes with an external flow of 300-600 mm/s and a current density of 1000-2500 A/m². The study summarized that screen electrodes produced smaller bubble sizes than plate electrodes, and between the screens the smooth screen produced smaller bubble compared to rough screen, while crystalline and amorphous plates produced almost similar bubble sizes. Lumanauw (2000) also reported that mean hydrogen bubble diameters were found to increase with increased current density for smooth screens, and plate electrodes, but decrease for rough screen electrode.

Han et al. (2002) used a flat aluminium (50 mm length × 50 mm width × 0.5 mm thick) electrode to produce hydrogen bubbles from the electrolysis of water (distilled and deionized water mixed with same volume of tap water). An image analysis method and an online particle counter both were used to measure hydrogen bubble sizes. The microscope was focused directly above the cathode and the bubble diameters were found to vary between 5 and 40 μm with an average of 18 μm using image analysis. Sampling for online particle counter was performed by a short straight tube at 100 ml/min. For the online particle counter, the bubble diameters were observed in the range of 15-65 μm, with an average of 22 μm.

Recently, Jiménez et al. (2010) studied hydrogen bubble sizes produced in a laboratory scale electroflotation cell (100 mm length x 20 mm width x 200 mm high) using a stainless steel cathode and very low current densities (10-35 A/m²). A digital camera was used to take still photographs of the hydrogen bubbles produced. However, the

distance of photographs from the bubble production sites was not mentioned. They reported a decrease in bubble size as current density increased before bubble size attained a plateau (mean diameter $\sim 63 \mu\text{m}$) at current density approximately 25 A/m^2 , after that a slight increase in bubble size is also observed.

Analysing all the studies mentioned above, it can be said that the hydrogen bubble size produced at cathode surface during electrolysis of water varies in the range of 5-65 μm . However, the reported bubble size measurements are not consistent with respect to different parameters especially current density. Wide variations of bubble generation methods, measurement techniques, measurement positions, material and geometry of electrodes were observed. This makes it difficult to design an efficient electroflotation system. The discrepancies in reported bubble sizes as a function of current density, pH, as well as electrode material, geometry and roughness are discussed later in this chapter (Section 2.9).

Oxygen bubble size

Janssen and Hoogland (1973) produced oxygen bubbles using a platinum disc of 11.2 mm diameter (geometric surface area of 100 mm^2) in both acidic and alkaline media using current densities in the range $80\text{-}2000 \text{ A/m}^2$ with the bubble sizes measured using photographic method. Measurements were taken in a region about $200 \mu\text{m}$ above the electrode surface. The bubbles that stayed on the electrode surface (diameter referred as d_a), as well as the bubbles that detached from the electrode but stayed in the neighbourhood of the electrode surface (diameter referred as d_f) were measured. The authors concluded that at low current densities (typically $<100 \text{ A/m}^2$) the bubble size did not vary with current density, but at current densities above 100 A/m^2 the average diameter of free oxygen bubbles (d_f) increased with increased current density both in acidic and alkaline media. It was observed that at current densities less than 100 A/m^2 , practically there was no coalescence of bubbles, but as current density increased especially above 300 A/m^2 , the coalescence of bubbles occurred frequently. In acidic media, the diameter increased from 25 to $95 \mu\text{m}$ as the current density was increased from 80 to 2000 A/m^2 . While in an alkaline media the diameter increased from 40 to $210 \mu\text{m}$ as current density was increased from 80 to 2000 A/m^2 .

Later, Ketkar et al. (1988) used a platinum plate and sieve (wire diameter 60 μm) to produce oxygen bubbles using current densities in the range 125-370 A/m^2 , measuring those bubbles by a photographic technique. The oxygen bubbles were produced in an alkaline media (pH of electrolyte 9) and were photographed at the electrode surface. The average diameters were 42-48 and 38-50 μm produced by mesh and plate anodes, respectively, with a decreasing trend with increased current density. The study reported that oxygen bubbles were larger compared to hydrogen bubbles in alkaline media.

Burns et al. (1997) produced oxygen bubbles using flat polished graphite electrode (76 mm \times 25 mm \times 13 mm) at absolute currents ranging from 15-440 A/m^2 . The oxygen bubbles were videotaped by focusing the camera on the anode surface. Later they measured the diameters of those bubbles from the photographs. The equivalent diameters of oxygen bubbles were in the range of 17.1-37.9 μm . The oxygen bubble size was found not to be a function of current density (Burns et al., 1997).

Recently, Phongikaroon et al. (2010) studied the effect of liquid viscosity and current density on oxygen bubble formation. A rectangular vessel (75 mm \times 80 mm \times 195 mm) was used as the electrochemical cell using platinum wire of 1 mm diameter as anode at current densities of 966-4830 A/m^2 . Sodium chloride solution (0.065 M) with kinematic viscosity in the range 0.0091-0.0378 cm^2/s was used as the electrolyte. It was observed that bubble size increased with an increase in viscosity up to 0.017 cm^2/s . Above this viscosity the bubble size became dependent on current density. At a viscosity higher than 0.017 cm^2/s , bubble sizes were found to increase with increased current density.

From the discussion of above studies, it can be concluded that in general the oxygen bubble is larger than the hydrogen bubble produced from electrolysis of water, with the size varying in the range 15-95 μm .

Hydrogen and oxygen bubble sizes measured combined without making distinction

Chen et al. (2002) used a phase-Doppler anemometer to measure bubble sizes (without distinction of hydrogen and oxygen bubbles) produced in an electroflotation cell (170 mm \times 40 mm \times 52 mm). Fork-like electrodes, with an effective surface area of 600 and 900 mm^2 for anode and cathode, respectively, were used in the electroflotation experiments. Titanium was used as cathode, while titanium coated by $\text{IrO}_x\text{-Sb}_2\text{O}_5\text{-SnO}_2$

was used as anode material. They reported that bubble diameters were randomly distributed, with above 90% of the bubbles in the range of 15-45 μm .

Ben Mansour et al. (2007) produced hydrogen and oxygen bubbles in a laboratory scale electroflotation cell (a cylindrical glass vessel of 30 mm diameter and 500 mm height) using titanium coated ruthenium oxide as the anode and a stainless steel screen as the cathode, with current densities ranging from 35-500 A/m^2 . Different aqueous solutions of 0.007M sodium sulphate with glycerine or ethanol were used as the electrolyte. Both the oxygen and hydrogen bubbles were captured by a digital camera focused at a distance approximately 400 mm from the electrode. The bubbles (without distinction of hydrogen and oxygen) were then analysed by a photographic method to obtain their sizes. They concluded that the bubble size increased with an increase in current density, liquid viscosity, and surface tension. A wide range of bubble size (diameter 25-116 μm) was observed at different current densities.

Recently, Montes-Atenas et al. (2010) studied the effect of flotation reagents (collector, frother and depressant) on bubbles produced in electroflotation. A column type cell (250 mm high \times 50 mm diameter) with platinum and stainless steel as the anode and cathode, respectively, was used to produce oxygen and hydrogen bubbles. A mixture of SIBX and Senkol 5 was used as collector, while Dowfroth 200 and guar gum were used as the frother and depressant, respectively. Electrolysis was performed in a column cell at two phase system at identical reagent concentration and stirring conditions (800 rpm). Liquid with hydrogen and oxygen bubbles was pumped from the column cell into a flat glass cell. The flat cell was used for viewing the bubbles which was placed under an optical microscope linked with a camera. The size of the oxygen and hydrogen bubbles (without distinction of oxygen and hydrogen bubbles) was then measured by photographic method. This study reported a decrease in bubble size from 99 ± 40 μm to 45 ± 15 μm in the presence of Dowfroth 200, but a slight increase in size in the presence of both collector and depressant.

While there are a considerable research on getting bubble size information, care should be taken regarding discrepancies in measurements. The discrepancies might be attributed to variations in electrode materials used for bubble production, pH of the electrolyte solution, surface tension and viscosity of the electrolyte solutions, geometry

and surface roughness of the electrodes, cleaning of the electrodes, current density applied for bubble generation, measurement position, detached and free (bulk) bubble size, instrument used (photographic, laser etc.) for measurement, and data analysis techniques.

The average bubble sizes produced by different flotation cells discussed above are summarized in Table 2.3. Finally, it can be concluded that electroflotation has potential for the production of very fine bubbles which may be very effective to recover very fine particles. Besides the small size, electroflotation provides very quiescent hydrodynamic conditions in the flotation cell, which favours the recovery process (Yoon, 1993).

Table 2.3: Bubble sizes produced in different flotation cells

Cell type	Bubble diameter (μm)
Mechanically agitated cell	500-2900
Column flotation	600-1500
Dissolved air flotation	10-300
Electroflotation: Hydrogen bubble	5-65
Electroflotation: Oxygen bubble	15-95

2.8 ELECTROLYTIC BUBBLE FORMATION PROCESS

When an aqueous solution is electrolysed, hydrogen and oxygen are liberated at the cathode and anode, respectively, due to the following redox reactions (Raju and Khangaonkar, 1984a):



At low current densities these gases are dissolved in the electrolyte solution, while at higher current densities gas bubbles are evolved at the electrodes. The physical process of gas evolution from electrodes can be divided into three stages; i.e., nucleation, growth and detachment.

2.8.1 Bubble Nucleation

Bubbles nucleate at the electrode surface from solutions supersaturated with product gas. Bubbles having a radius greater than or equal to the critical radius grow, while bubbles having a radius less than the critical radius tend to decay. The critical radius, r^* is defined by (Lubetkin, 1995):

$$r^* = \frac{2\sigma\Omega}{\kappa T \ln(P''/\dot{P})}, \quad (2.18)$$

where σ is the surface tension of liquid, Ω is the molecular volume, κ is Boltzmann's constant, T is the system temperature, P' is the external pressure in the liquid, and P'' is the pressure of dissolved gas inside the bubble. Now the pressure of dissolved gas inside the bubble can be calculated by (Sides, 1986):

$$P'' = \frac{P'C'}{v_2C_o} + \frac{P_o}{v_1} \left\{ \exp\left[\frac{v_1(P' - P_o)}{\kappa T}\right] \exp(-C') \right\}, \quad (2.19)$$

where C_o is the saturation concentration of the dissolved gas in solution, C' is the concentration of dissolved gas in solution, P_o is the vapour pressure of the pure solvent, and v_1 is the specific volume of the pure solvent, v_1 , v_2 are activity coefficients of

solvents. From Equation 2.17, it can be seen that as the concentration of dissolved gas increases, the gas pressure inside the bubble will increase with all other factors being constant. This increase in the pressure of dissolved gas inside the bubble will then reduce the critical radius.

The rate of homogeneous bubble nucleation, (J) is given by (Sides, 1986):

$$J = Z \exp\left[-\frac{16\pi\sigma^3}{3kT(P'' - P')^2}\right], \quad (2.20)$$

where Z is the pre-exponential frequency factor. Here, it can be seen that keeping the other factors constant, the bubble nucleation rate will increase with an increase in the pressure of dissolved gas inside the bubble. As mentioned above, the pressure of dissolved gas inside the bubble depends on the concentration of dissolved gas in solution. Furthermore, the concentration of dissolved gas depends on current density. Therefore, as current density increases the concentration of dissolved gas will increase, thus increasing the bubble nucleation rate.

Surface inhomogeneities, such as cracks, are generally considered high-energy nucleation sites due to the availability of atomic ledges as high-energy anchorage points. During electrolysis, it is generally agreed that surface inhomogeneities such as pits, fissures, cracks and scratches act as preferred nucleation sites (Glas and Westwater, 1964, Westerheide and Westwater, 1961). Janssen and Hoogland (1970) studied bubble nucleation on a rotating platinum wire and concluded that bubbles nucleate at specific sites that depend on pre-treatment and current density.

2.8.2 Bubble Growth

The nucleated bubbles grow initially from the critical radius as a result of high internal pressure and by mass transfer of dissolved gas into the growing bubble. The bubbles may also grow by coalescence with other bubbles at the electrode (Sides and Tobias, 1985).

Scriven (1959) has provided a general analysis of diffusion controlled bubble growth. According to his analysis, the radius of bubble $r(t)$ after time t since nucleation can be determined by:

$$r(t) = 2\eta(D't)^{0.5}, \quad (2.21)$$

where η is the coefficient relating to the degree of supersaturation, and D' is the diffusivity of gas.

Later, Brandon and Kelsall (1985a) studied the growth of hydrogen bubbles from a platinum electrode with a 25 μm diameter. They observed that a very high current density was required to nucleate and grow bubbles due to the high rate of diffusion of dissolved gas away from such a small electrode. They also observed that an induction time was necessary for bubble nucleation, which was due to the time required to attain the necessary supersaturation of the electrolyte with respect to dissolved gas at the electrode surface. Following previous attempts (e.g., (Glas and Westwater, 1964, Verhaart et al., 1980)), the authors proposed a general expression to define bubble growth kinetics; i.e.,

$$r(t) = \eta' t^l, \quad (2.22)$$

where t is time (ms), η' is the growth coefficient, and l is the time coefficient. According to time of growth, they proposed three regions of growth; e.g., Region I ($t < 10$ ms), Region II ($10 \leq t \leq 100$ ms), and Region III ($t > 100$ ms).

Region I ($t < 10$ ms)

During the initial period, ($t < 10$ ms), bubble growth is controlled by liquid inertia and excess pressure, and the time coefficient, l tends to be unity. Such growth may be described by the Rayleigh (1917) equation as:

$$r(t) = (2\Delta P / 3\rho)^{0.5} t, \quad (2.23)$$

where ρ is the density of the electrolyte (kg/m^3), and ΔP is the internal excess pressure (kN/m^2). The internal excess pressure depends on the bubble radius and the surface tension of the gas-liquid interface. Assuming the bubbles to be spherical, Laplace equation can be used to determine the internal excess pressure as:

$$\Delta P = 2\sigma / r. \quad (2.24)$$

Region II ($10 \leq t \leq 100 \text{ ms}$)

The high initial growth rate creates a rapid decrease in the local supersaturation of gas, and so the diffusion of dissolved gas to the bubble surface becomes rate controlling. Brandon and Kelsall (1985a) reported that after initial growth, for $10 < t < 100 \text{ ms}$, the value of l reduces to about 0.5 and the growth kinetics become similar to that derived by Scriven (1959) for diffusion controlled spherical phase growth in an infinite, incompressible fluid. Bubble growth in this stage is given by (Brandon and Kelsall, 1985a):

$$r(t) = C(D't)^{0.5}, \quad (2.25)$$

where C is a coefficient described by Scriven (1959).

Region III ($t > 100 \text{ ms}$)

After longer growth times ($t > 100 \text{ ms}$) steep dissolved gas concentration gradients exist between the base of the bubble and the electrode, and gas enters almost directly into the bubble with little diffusion to the bulk electrolyte solution with the time coefficient l reduced to 0.33. Bubble growth is then given by (Brandon and Kelsall, 1985a):

$$r(t) = \eta' t^{0.33}, \quad (2.26)$$

where the growth coefficient, (η') depends primarily on the current density and the faradic charge per mole requirement of the gas generated. According to Faraday's and Charles' laws, η' can be expressed by the following empirical relation (Brandon and Kelsall, 1985a):

$$\eta' = \left(\frac{3RTI}{4\pi zFP} \right)^{0.33}, \quad (2.27)$$

where R is the universal gas constant (8.31451 J/mol/K), I is the absolute current (μA), F is Faraday constant (96485.3 C/mol), z is the electron stoichiometric number required to produce gas, and P is the system pressure (kN/m^2).

2.8.3 Bubble Detachment

The last stage of gas evolution in electrolysis is the detachment of growing bubbles. From equilibrium measurements, Kabanov and Frumkin (1933) concluded that the growing bubbles detach when the surface adhesive forces (related to surface tension and bubble contact angle) can no longer restrain them due to increasing buoyancy force. However, Brandon and Kelsall (1985a) stated that forces other than surface tension may act as a holding force. They proposed that electrostatic interaction between the bubble and the electrode double layers controls the bubble departure diameter, and that the two phases are separated by a thin liquid film of electrolyte, though they did not show any experimental evidence to support their claim.

2.9 FACTORS AFFECTING BUBBLE SIZES PRODUCED IN ELECTROFLOTATION

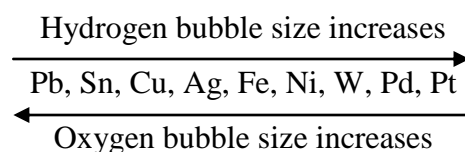
The size of bubbles produced in electroflotation depends on the electrode material, the geometry of electrode, the pH and ionic strength of solution, and the current density.

2.9.1 Electrode Material

The size of bubbles produced in electrolysis of water depends on the electrode material and its position in the electromotive series. Ibl and Venczel (1970) investigated the size of hydrogen bubbles produced by copper and platinum cathodes and summarized that the copper cathode produced smaller hydrogen bubbles compared to those produced by platinum. Venczel (1970) also observed that bubbles produced from platinum were larger than those produced by iron and copper electrodes.

Later, Glembotsky et al. (1973) studied three metals (platinum, tin and copper) as cathodes to investigate the effect of material on hydrogen bubble size. They reported

that in an alkaline medium copper and tin cathodes produced smaller bubbles than those produced by the platinum cathode. It was also reported that the effect of electrode material on bubble size was more pronounced in acidic media than in a neutral media, where there was almost no effect of electrode material on bubble size. Later, Mamakov (1975) established the following series to show the changes in bubble size depending on electrode material:



For smooth platinum electrodes, the decomposition potential of an acidic or alkaline aqueous solution is about 1.5 V. This value differs (mainly increases) if other materials are employed as electrodes. This is due to the over potential for O₂ and H₂ evolution on the different materials, which is related to the activation energy for charge transfer.

Recently, Jiménez et al. (2010) studied hydrogen bubble production using stainless steel and titanium as cathode materials, and concluded that stainless steel can produce smaller bubbles than titanium.

2.9.2 Electrode Geometry and Roughness

At constant current density, the bubble diameter is influenced by the diameter of the electrode wire (Matov and Lazavenko, 1965). The curvature of both cathode and anode surfaces influences the distribution of hydrogen and oxygen bubbles, respectively, around the circumference of the electrode.

Ketkar et al. (1988) studied the production of hydrogen bubbles from stainless steel mesh with different wire diameters, as well as polished plate. They reported that at constant current density and pH, the bubble diameter was found to decrease with decreased wire diameter at the cathode. As the diameters of the wires become small, curvature of the surface is increased, resulting in production of smaller bubbles. It is also stated that, in case of finer sieves, the number of overlapping sites of two wires are more, which produce large number of nucleation sites. These large numbers of

nucleation sites lead to the production of smaller diameter bubbles. In contrast, for the coarser wires, the curvature and the number of overlapping sites of two wires are less that results in production of bigger bubbles. While polished plate is used as an electrode, smallest bubbles are produced due to large number of nucleation sites (Ketkar et al., 1988). Glembotsky et al. (1975) also reported a decrease in possible bubble diameter with the decrease in the diameter of cathode wire.

Lumanauw (2000) investigated the effect of electrode geometry and roughness on hydrogen bubbles produced from a nickel mesh and plate cathode in alkaline solution. Mesh with wire diameter 350 μm (smooth and rough) and plate of thickness 500 μm (crystalline and amorphous alloy) were used. He concluded that mesh electrodes produced smaller bubble than plate electrodes and between the meshes, smooth surfaces produced smaller bubbles compared to rough surface, while crystalline and amorphous plates produced almost similar bubble sizes.

Recently, Jiménez et al. (2010) investigated the effect of roughness of electrode on hydrogen bubble size and reported that roughness plays an important role with larger numbers of smaller bubbles being produced at higher roughness.

2.9.3 pH

The size variation of gas bubbles tends to follow a trend opposite to that of the excess ion; i.e., hydrogen bubbles are smaller in an alkaline media, compared to a neutral or acidic media and oxygen bubbles attain a minimum size in acidic medium with the diameter increasing with increased pH (Glembotsky et al., 1973). Similar findings have also been observed by Janssen and Hoogland (1973); i.e. hydrogen bubbles are being larger when produced in acidic media, while oxygen bubbles are larger in an alkaline medium at constant current density.

Later, Brandon and Kelsall (1985a) reported that in an alkaline media, cathodically evolved hydrogen bubbles was found to have a smaller departure diameter than anodically evolved oxygen bubbles, whilst the converse was observed in an acid medium. In an acidic medium, the attraction between positively charged hydrogen bubbles and the negatively charged platinum electrode increases the restraining forces and thus produces a larger diameter bubble, before buoyancy forces cause bubble

departure. In an alkaline medium, bubbles and electrode are negatively charged, and so their electrostatic repulsion helps to produce very small bubbles. In another study, these same authors (Brandon and Kelsall, 1985b) reported that the bubbles were shown to be charged even under surfactant-free conditions, with a point of zero charge in the range pH 2-3; i.e., they are negatively charged at $\text{pH} > 3$ and positively charged at $\text{pH} < 2$.

In contrast to the above studies, Jiménez et al. (2010) concluded that neutral media (pH 7) produced the smallest mean hydrogen bubble size associated with higher bubble flux, whilst strongly acidic (pH 2) and alkaline (pH 14) media generate larger hydrogen bubbles and lower bubble flux.

2.9.4 Current Density

There have been conflicting studies investigating the influence of current density on bubble size. For example, Landolt et al. (1970), Sides (1986) and Ben Mansour et al. (2007) have all reported a general increase in hydrogen bubble diameter with an increase in current density. They attributed this to bubble coalescence at higher current densities. Conversely, Kabanow and Frumkin (1933), Venczel (1970), Glembotskii et al. (1973) and Ketkar et al., (1988) reported the opposite influence. Janssen and Hoogland (1970) reported that in acidic media hydrogen bubble size was independent of current density up to 400 A/m^2 , but above that, bubble size increased with current density due to coalescence of bubbles. Later, these same authors (Janssen and Hoogland, 1973) stated that in acidic medium the hydrogen bubble size remained constant at current densities up to 100 A/m^2 and above that bubble size increases with current density, while in alkaline solution the bubble size does not seem to be a function of current density. Burns et al. (1997) found no clear trend of bubble diameter as a function of current density with range $40\text{-}210 \text{ A/m}^2$, while Lumanauw (2000) concluded that mean bubble size increased with an increase in current density for a smooth-surface electrode, with the opposite trend observed for rough-surface electrodes.

Recently, Jiménez et al. (2010) investigated the size of bubbles produced at very low current densities ($10\text{-}35 \text{ A/m}^2$) and concluded that a large number of small bubbles (diameter $\sim 65 \text{ }\mu\text{m}$) were observed with increased current density, with an apparent increase in size above current density of 25 A/m^2 .

2.9.5 Effect of Liquid Flow on Bubble Size

Landolt et al. (1970) studied the effect of flow rate on bubble detachment size and observed a reduction in bubble size with increased flow rate and decreased current density. They found the bubble diameters as below 20 μm (the smallest diameter resolved by their optical arrangement) at a flow rate above 8000 mm/s. The median bubble diameters were reported as 99, 69, and 35 μm , at flow rates of 1000, 2000 and 4000 mm/s, respectively.

The reasons for such discrepancies in literature may be due to differences in bubble generation methods, measurement techniques and data analysis. These includes materials used as electrodes, the pH of the electrolyte solution, surface tension and viscosity of the electrolyte solution, geometry and surface roughness of electrodes, cleaning of electrodes, measurement position, i.e., detached and free (bulk) bubble size, instrument used (photographic, laser etc.), differentiation or mix-up of hydrogen and oxygen bubbles, etc.

2.10 HYDROGEN TRANSFER FROM THE CATHODE

The theoretical analyses of Vogt (1984b, 1984a) dealt with the transport of electrochemically evolved hydrogen and chlorine from the electrode surface into the bulk of the solution. Using the experimental data of Glas and Westwater (1964) and Shibata (1976, 1978), Vogt showed that hydrogen produced at cathode is transferred by two ways, i.e., (i) a portion enters into the growing bubbles attached to the cathode, (ii) another portion dissolves into the bulk electrolyte by convective diffusion. It was reported that at low current densities the major portion of the dissolved gas was transferred to the bulk solution by convective diffusion, and this portion was found to decrease with increasing current density.

Later, Müller et al. (1989) measured both fractions; i.e., the portion of hydrogen leaving the electrode surface by convective diffusion, and the portion of hydrogen reaching the electrolyte bulk by gas bubbles, by using a platinum disc electrode of 8 mm diameter. In contrast to Vogt's (1984b, 1984a) findings, they concluded that at low current density (1000 A/m^2) the convective diffusion into the bulk electrolyte was less than 50% and at high current density (3000 A/m^2) the convective diffusion was only 15%. However,

they concluded that at current density higher than 1000 A/m^2 , all the hydrogen produced reached the bulk solution by gas bubbles. This finding postulates the growth of gas bubbles while they move through the electrolyte solution. Therefore, it can be said that more comprehensive research is required to investigate the transfer mechanism of dissolved gases both at the surface of electrode and in bulk solution.

2.11 DEPRESSANT EFFECT OF INORGANIC SALTS ON FLOTATION

For the electroflotation experiments an electrolyte (inorganic salt) is required to make the solution conductive for charge transport. Unfortunately, as discussed below, their presence can have a depressant effect on flotation. The depressant effect of inorganic salts on the flotation of quartz using amine collectors depends upon whether the collector ions are adsorbed through electrostatic attraction as individual counter ions in the double layer, or through van der Waals interactions of hydrocarbon chains (Onoda and Fuerstenau, 1964). In floating quartz, using amine salts as the collector, the ammonium ions act as counter ions in the electrical double layer at the solid-liquid interface.

Onoda and Fuerstenau (1964) investigated the flotation of quartz as a function of collector (dodecyl ammonium acetate) concentration in the presence of inorganic salts (sodium chloride and barium chloride). At low concentrations the adsorption mechanism of both ions was similar, but varied at high concentration. They showed that at low concentrations, both collector and sodium ions were adsorbed only through electrostatic attraction by negative surface charge, and the competition for sites in the double layer occurred between both ions. Consequently, sodium ions depressed the adsorption of collector to the mineral surface. But at high concentrations, the collector was strongly adsorbed through both van der Waals and electrostatic attraction, while inorganic salts were adsorbed only through electrostatic attraction. Once the collector ions are adsorbed at the surface, inorganic ions are not able to depress flotation. This is in agreement with the flotation results obtained by Estefan (1976), who observed that the presence of 10^{-6} mole of Ca^{2+} ions insignificantly affected the rate of flotation of quartz at pH 10 where hemi-micelle formation of CTAB ions was completed. Hence, higher amount of collector is required to overcome the depressant effect of inorganic

electrolyte. Experimental observation seems to be necessary to optimize the collector concentration at which the depressant effect is negligible.

Onoda & Fuerstenau (1964) stated that increasing the number of carbon atoms in the amine salts would make the depression action of inorganic salts even less, but at higher concentrations association of the hydrocarbon chains of the adsorbed ammonium ions give rise to large adsorption potentials, about 33.5 kJ per mole for a 12-carbon collector.

2.12 BUBBLE DETACHMENT: CONTACT ANGLE OF WATER ON ELECTRODE SURFACES

Bewig and Zisman (1965) measured the contact angle of water on platinum and gold surfaces. For cleaning the metal surfaces, they heated the metals until white hot for 3 min, which was followed by quick cooling in a 150-ml/min gas stream. Hydrogen, as well as inert gases such as krypton, neon, argon and nitrogen were used in heating and cooling operations. They observed that platinum and gold specimens exhibit zero water contact angle when the specimens were heated (white-hot) and cooled in a stream of 150-ml/min hydrogen. They reported that if a completely wetting water films were allowed to evaporate in the stream of hydrogen, after 6 minutes the film began to recede as a flat lens from the edges of the metal surfaces. These water lenses showed immeasurably small contact angles ($<1^\circ$). They (Bewig and Zisman, 1965) also obtained similar results (complete wetting and zero contact angles) when they used research grade inert gases such as krypton, neon, argon and nitrogen in heating and cooling operations instead of hydrogen.

Gardner and Woods (1974) measured the contact angle between nitrogen bubbles and platinum and gold electrode surfaces activated by an anodic-cathodic treatment in an electrochemical cell using 1 M Na_2SO_4 and 0.05 M sodium tetraborate solution. The study reported the contact angle of the platinum electrode to be below 10° at all potentials in the available region between hydrogen and oxygen evolution in the electrolyte solution. Similar finding (contact angles below 10°) for a gold electrode in 0.05 M sodium tetraborate alone or in the presence of xanthates was also reported.

Later these authors (Gardner and Woods, 1977) studied the dependency of contact angle on the chemical and electrochemical procedures employed for cleaning noble metal surfaces (platinum and gold). The electrochemical cell used in their previous study (Gardner and Woods, 1974) was also used here with 0.05 M sodium tetraborate as the electrolyte. The metal surface was first repolished with 0.25 μm grade “Hyperz” diamond compound lubricated with water on a “Buehler” nylon cloth. Three different types of chemical treatments, i.e., washed with water only, washed with ethanol and water, as well as washed with ethanol, chromic acid and water, were then applied followed by electrochemical treatment. They reported that among the three chemical treatments only the (ethanol, chromic acid and water) can clean the metal surfaces and zero contact angles was observed. While for the electrochemical treatment a zero contact angle was observed at all potentials between hydrogen and oxygen evolution in borate and sulphate solutions in 100 mV steps between -0.4 and 1.1 V. In summary, they concluded that in the absence of inorganic and organic contaminants, the gold and platinum surfaces are hydrophilic. Removal of impurities, either chemically or electrochemically, yields a hydrophilic gold and platinum surface that exhibits a zero contact angle (Gardner and Woods, 1977).

Brandon and Kelsall (1985a) studied the departure of hydrogen bubbles from a platinum electrode of 25 μm diameter. Sodium sulphate at a concentration 10 mol/m³ was used as the electrolyte. They analysed the contact angle of water on platinum electrode in surfactant free electrolytes and reported no measurable contact angle.

Finally, it can be concluded that the contact angle of water on platinum or gold surfaces can be 0-10° depending on the cleaning method adopted. The small value of contact angle of water with platinum or gold surface will produce minimum value of surface tension, which holds bubble with electrode surface. Table 2.4 provides the summary of the contact angles obtained in different studies.

Table 2.4: Summary of contact angle from different studies

Authors	Contact angle (degree)
Bewig and Zisman (1965)	0
Gardner and Woods (1974)	<10
Gardner and Woods (1977)	0
Brandon and Kelsall (1985a)	~0

2.13 APPLICATION OF ELECTROFLOTATION

2.13.1 Mineral Processing

There have been a number of studies that have used electroflotation involving mineral flotation. Raju and Khangaonkar (1984b) reported a 74-81% recovery of 4 μm chalcopyrite with electrolytically generated hydrogen bubbles using a current density in the range of 490-1470 A/m^2 . Ketkar et al. (1991) reported more than 60% recovery of +4-10 μm quartz with hydrogen bubbles of 22 μm diameter. Llerena et al. (1996) reported an almost 100% recovery of -25 μm sphalerite after 4 minutes of electroflotation with a mean bubble diameter of 16 ± 2 μm generated using a stainless steel screen with a wire diameter of 115 μm and operated at a current density of 500 A/m^2 in a solution of pH of 4. Han et al. (2006) used electroflotation to generate very fine bubbles with 27 μm mean diameter to obtain 98% recovery of 28 μm flocculated kaolin particles.

Recently, Montes-Atenas et al. (2010) applied electroflotation to recover platinum group minerals (PGMs), e.g., Merensky reef and UG2 ores, both belonging to the Bushveld Complex in South Africa. Other previous studies include: Mamakov et al. (1969); Romanov et al. (1973); Glembotskii et al. (1975); Hogan et al. (1979b); Setty and Venkatachalam (1997); Casqueira et al. (2006).

2.13.2 Water and Wastewater Treatment

Electroflotation has mainly been used in mineral processing (Nenno et al., 1988). However, in water and wastewater treatment, flotation is often the most effective process for the separation of oil and low-density suspended solids (Chen and Horan, 1998, Huang and Liu, 1999, Lafrance and Grasso, 1995, Manjunath et al., 2000, Vaughan et al., 2000). Electroflotation is also found effective in treating palm oil mill effluent (Ho and Chan, 1986), oily wastewater or oil–water emulsion (Hosny, 1996, Il'in and Sedashova, 1999, Ibrahim et al., 2001, Balmer and Foulds, 1986, Il'in, 2002, Bande et al., 2008, Nahui et al., 2008), spent cooling lubricant (Prokop'eva et al., 1988), wastewater from coke-production (Aleksandrov et al., 1992), mining wastewater (Alexandrova et al., 1994), groundwater (Poon, 1997), food processing wastewater (Hernlem and Tsai, 2000), fat-containing solutions (Shendrik et al., 1993), restaurant wastewater (Chen et al., 2000) or food industry effluents (Kubritskaya et al., 2000), dairy wastewater (Rabilizirov and Gol'man, 1986), textile effluent (Bouyakoub et al., 2010, Merzouk et al., 2010), urban sewage (Il'in et al., 2002), pit waters (Zolotukhin et al., 1983), clarification of apple juice (Araya-Farias et al., 2008), colloidal particles (Fukui and Yuu, 1985), heavy metal containing effluents (Nenno et al., 1994), and gold and silver recovery from cyanide solution (Llerena et al., 1996, Il'in and Sedashova, 1999, Camilleri, 1985) etc.

2.14 SAFETY PRECAUTION IN APPLYING ELECTROFLOTATION

Applying electroflotation in the laboratory and on an industrial scale, one major concern may be the flammability of hydrogen gas. Lewis and Elbe (1961) reported that at atmospheric pressure, the gas mixture becomes explosive at 560°C, and at a pressure of 13.2 atm the explosion temperature is 430°C within both data referring to a sealed vessel. In designing an electroflotation cell, the pressure exerted by tiny hydrogen bubbles and the temperature evolved by electrolysis reaction should be considered.

2.15 ADVANTAGES OF ELECTROFLOTATION

Electroflotation has the following principal features that differentiate it from conventional flotation, and also constitute its advantages. Electroflotation is also accepted as a fully cost effective means of treating effluents, and many plants are

operating in Europe and the U.K., where they compete strongly with such established processes as dissolved air flotation (Hogan et al., 1979b).

2.15.1 Production of Fine Bubbles

In conventional flotation, air bubbles that are used of longer diameters. They are effective in floating coarser particles. These bubbles are not useful in the flotation of fine particles of diameter less than 20 μm (Ketkar et al., 1988). The process of electroflotation leads to the formation of extremely finely dispersed gas bubbles as shown in Table 2.3. This feature represents a great and undoubted advantage where compared with conventional flotation cells. Electroflotation ensures the generation of large quantities of finely dispersed gas bubbles, whose dimensions vary between 5 to 95 μm , according to the condition of electrolysis.

2.15.2 Absence of Coalescence of Bubbles

In addition to a fine dispersion, these bubbles are homogeneous in size, evenly distributed within the flotation cell, and do not coalesce after separation from the electrodes. Matov (1973) attributed this lack of coalescence of the electrolytic bubbles to the bubble surface charge being the same sign as the electrode charge.

2.15.3 Production of Bubbles of Desired Size and Flux

By varying the current density, it becomes possible to create any gas bubble concentration in the flotation medium as well as to reach flotation chamber saturation, something that is not usually realized in conventional flotation. The number ratio of solids particles and gas bubbles per unit volume of the flotation cell per unit time is an important factor to get optimum recovery as observed in flotation practices as well as in theoretical analyses. This is a difficult problem in conventional flotation. Electroflotation permits the creation of such condition. During the electroflotation, it is possible to obtain a continuous adjustment of bubble dimensions. It is possible to obtain bubbles of electrolytic gases of predetermined sizes by using a suitable wire mesh electrode. By adjusting the pH, choosing different metals with different surface geometries for the electrodes, and by varying the current density and the other medium parameters such as temperature, solution concentration, etc., the required and predetermined bubble size dispersion may be obtained (Glembotskii et al., 1973).

2.15.4 Higher Chance of Bubble Particle Collision

The main influence of the bubble size is in the number of collisions between bubbles and particles. As the buoyancy of larger bubbles is high, they rush to the surface with fewer opportunities for bubble-particle encounters. This also creates turbulence in the frothing zone which can destroy the froth layer that is being built up. In contrast, because of lower buoyancy, the smaller bubbles rise more slowly and hence their residence time in the cell is longer. Consequently, there is a greater chance of small bubbles attaching themselves to the particles. The reverse is the case of conventional flotation. The smaller particles, because of their low mass and inertia, are carried away along the streamlines caused by bigger bubbles and not collide with the bubbles. Hence a much lower amount of fine particles is recovered by big bubbles. In addition to bubble size, reduced bubble flux and total number of bubbles is also responsible for reduction in recovery (Setty and Venkatachalam, 1997).

2.15.5 Activeness

The role of gases formed in the electroflotation process becomes more significant, since hydrogen and oxygen in the nascent state are extremely active. This atomic state is in existence only for an extremely brief period of time and yet adequate to produce significant change in the surface conditions of the minerals, owing to the adsorption of these gases, ion exchange, oxidation and reduction, and other electrochemical reactions. Electrolytic gases cause significant oxidation-reduction reactions on mineral surfaces compared to the molecular gases, particularly on sulphide minerals (Mallikarjunan and Venkatachalam, 1984). Gas bubbles may bring changes on the mineral surfaces and this effect may be useful in improving the flotation recovery. This unique property of electroflotation can be advantageously utilized by the separate use of oxygen and hydrogen bubbles (Raju et al., 1987). Mamakov et al. (1969) and Hogan et al. (1979b) observed that fine hydrogen bubbles improve the recovery of cassiterite. Romanov et al. (1973) studied the electroflotation recovery of manganese minerals, e.g. pyrolusite and psilomelane, and reported 92-95% recovery of manganese with hydrogen bubbles which is greater than in column flotation. Lazarenko (1969) reported that hydrogen is much more effective in the electroflotation of diamond-containing ores. In contrast, Raju and Khangaonkar (1982, Raju and Khangaonkar, 1984b) have observed that oxygen gas bubbles improve the recovery of chalcopyrite fines. Electrolytic oxygen makes the surface of the pyrite and other sulphides (chalcopyrite, sphalerite) particles so

strongly hydrophobic that there was no need to use collectors. Glembotskii et al. (1975) were able to recover pyrite up to 98% without the need of collector with oxygen bubbles. Khosla et al. (1995) also reported that the use of oxygen bubbles at any given gas evolution rate resulted in a higher flotation recovery for alumina.

2.16 DISADVANTAGES OF ELECTROFLOTATION

The main disadvantage of electroflotation is the control of system pH. Since OH^-/H^+ ions are continuously released, to the system, the changes in pH during the process may be difficult to control. The change in the pH of the pulp becomes higher as the current density increases. However, this does not have much effect when the selectivity varies in wide range of pH (Raju and Khangaonkar, 1984a). It is well known that when a neutral solution is electrolysed, a pH gradient is set up, with an alkaline region in the vicinity of the hydrogen-evolving electrode (cathode) and an acid region near the oxygen-evolving electrode (anode). The pH values at different parts of the solution depend on the amount of inter-mixing permitted. Thus, when hydrogen and oxygen gas are separated during electrolysis, a pH-time effect will be obtained, the pulp becoming progressively more alkaline or acidic depending on whether hydrogen or oxygen is being generated. These pH changes may affect many of the flotation parameters, especially collector-mineral interaction and bubble size. Laboratory experiments are, of course, largely batch type. On a plant, with a throughout of feed, pH gradients could be reduced (Hogan et al., 1976).

2.17 OPPORTUNITY OF RESEARCH

2.17.1 Interaction of Mineral Surface with Gas Phase

The gas phase may bring about changes in the hydrophobicity of the mineral surface due to the adsorption of gas, oxidation-reduction reactions, ion exchange and other electrochemical reactions. This change may be beneficial or detrimental in improving flotation recovery. In the literature there are some studies that reported improved flotation recovery using hydrogen and oxygen bubbles formed by electrolysis (e.g., in case of hydrogen bubbles improved recovery of cassiterite (Mamakov et al., 1969, Hogan et al., 1979a) and manganese minerals (Romanov et al., 1973) were reported,

while oxygen bubbles improved the recovery of chalcopyrite fines (Raju and Khangaonkar, 1982) and pyrite fines (Khosla et al., 1995) were observed. However, no direct comparison with air was made in those studies. To date no study has investigated the interaction of the gas phase with the mineral surface (especially for silica) at the same superficial gas velocity, bubble size and cell hydrodynamics. Hence this study aims to investigate the flotation performance of silica at the same gas superficial velocity, bubble size and cell hydrodynamics.

2.17.2 Depressant Effect of Electrolyte on Flotation

In electroflotation, an electrolyte is required to make the suspension conductive enough for charge transfer. Unfortunately, its presence can have a depressant effect on flotation recovery, as discussed in Section 2.11. Hence, it is important to minimize this depressant effect to make the flotation possible, as well as to optimize the recovery. The minimization of this depressant effect and optimization of flotation recovery has not been reported in the literature so far.

2.17.3 Bubble Size Measurement

As discussed in Section 2.7.6 and 2.9, there is wide variety in reported measurements of bubble size across the literature. The forces influencing the detachment of bubbles from electrodes are not well understood. There have been conflicting studies investigating the influence of current density on bubble size. Until now, no study has been performed to investigate the effect of electrode surface preparation on bubble size. Wide variation of bubble generation methods, measurement techniques, measurement position, geometry and surface roughness of electrodes, cleaning of electrodes, differentiation or mix-up of hydrogen and oxygen bubbles are also observed in bubble size measuring experiments reported across the literature. To date, there is no study in the literature that has differentiated between the detachment and bulk size of bubbles. The growth of the bubbles as they move through the electrolyte solution was mentioned in only few studies (e.g.,(Janssen and Hoogland, 1970, Müller et al., 1989)). However, no experimental observation of bubble growth has been reported.

The effect of fluid flow on detachment of bubbles is still a matter of research. This phenomenon has been examined experimentally in a few studies (e.g., Landolt et al. (1970) and Lumanaw (2000)). The study of Landolt et al. (1970) had some major

limitations. Firstly, bubbles of diameter less than 20 μm were below the optical resolution, and hence not counted in their study. Secondly, bubbles close to the cathode surface were usually not individually visible (i.e. the solution was cloudy) and therefore were not counted. Thirdly, the number of measured gas bubbles (27-60) represented only part of the total gas volume, and the differentiation between discernible and non-discernible bubbles was subject to personal interpretation.

The uncertainty in the influence of variables such as electrode curvature, surface preparation, and most importantly current density on bubble size, have made it difficult to effectively design efficient electroflotation systems for fine particle recovery. Hence, this study aims to remove such uncertainty in bubble size measurement.

2.17.4 Fractional Coverage of Bubble Surface

Fractional coverage of the bubble surface, ϕ , is defined as the portion of the surface area of the bubble that can be occupied by the attached silica particles. Hence it is an important parameter for predicting the recovery. Koh and Schwarz (2006) assumed that about half of the total bubble surface can be occupied by the attached particles, and proposed the value of ϕ to be 0.5. Later, these authors (2008) compared the simulated and experimental recovery with results suggesting that the simulated recovery matched well with experimental data in the case of $\phi = 0.2$, compared to the case of $\phi = 0.5$. Both studies were related to a conventional flotation machine (stirred vessel). However, more experimental observations are required to determine the value of ϕ as a function of surface properties of particles, collector and frother chemistry, as well as the geometry and hydrodynamics of the cell.

2.17.5 Fraction of Hydrogen Gas Results in Bubble

Flotation recovery will be maximised if all of the hydrogen produced as part of the electrolysis process results in the formation of bubbles. However, this is not always the case, and a portion of the hydrogen remains dissolved in solution (see Section 2.10). Sometimes this portion can be significant, resulting in reduced flotation efficiency. There are only few studies available in literature that determined the fraction of hydrogen resulted in the gas phase, for example, Shibata (1976, 1978) and Vogt (1984b, 1984a) dealt with the gas fraction at adhering electrodes, whereas Müller et al.

(1989) dealt with gas fraction both at adhering electrodes and in the bulk solution. Their experimental observations were restricted to platinum electrodes only. But the gas fraction was found to vary significantly from a small amount (Vogt, 1984b, Vogt, 1984a) to a large amount (Müller et al., 1989) depending on the electrode material, electrode geometry, surface treatment of the electrode, and current density, etc. Hence it is important to investigate the effect of all parameters discussed above on the gas fraction both at adhering electrodes and in the bulk solution. To the best of our knowledge, no study has been performed to determine the fraction of total hydrogen (theoretical) resulting in gas bubbles in case of other cathode materials. Therefore, it can be said that a more comprehensive study is required to investigate the transfer mechanism of dissolved gases both at the surface of the electrode and in bulk solution.

2.17.6 Electroflotation Recovery and Modelling

The effect of particle size on flotation recovery has been discussed in Section 2.3. The results from this have shown that the effect of particle size on recovery in electroflotation is not clearly understood yet. Ketkar et al. (1991) experimentally observed the flotation recovery of quartz particles by electrolytically generated hydrogen and oxygen bubbles relating a decrease in flotation recovery with increased particle size. Their findings contradicted the other studies available in the literature (Reay and Ratcliff, 1973, Collins and Jameson, 1976, Jameson et al., 1977, Yoon, 2000, Ramirez and Davis, 2001). These studies investigated the effect of particle size on flotation recovery using conventional flotation cell which clearly indicated that when particles are large enough not to be affected by Brownian motion, the collection efficiency and the flotation rate of those particles increase with increased particle size. The particle size was in the range of 6.5 to 65 μm , as used in the study of Ketkar et al. (1991). Therefore, it is important to investigate the effect of particle size on electroflotation, especially for floating very fine particles of diameter less than 10 μm , which is the usual limit of conventional flotation (Trahar and Warren, 1976). It is also important to determine the maximum floatable particle size by analysing bubble-particle aggregate stability and buoyancy force.

Finally, a comprehensive modelling approach that can predict particle recovery considering the effects of bubble size, particle size, stability and buoyancy force of bubble-particle aggregate, fractional coverage of bubble surfaces, the contact angle of

mineral-liquid-gas phase, current density, gas fraction results in bubbles, superficial gas velocity, and solids concentration is deemed to be necessary.

2.17.7 Electroflotation Optimization

While electrolytically generated hydrogen and oxygen bubbles are reported to improve the recovery of fine particle, the high energy consumption may restrict the application of electroflotation on the industrial scale (Hogan et al., 1979a). However, no direct comparison of energy consumption between electroflotation and conventional flotation has been reported to date. Hence, the optimization of the usage of electroflotation with respect to energy consumption is necessary.

Chapter 3

THEORETICAL MODELLING

3.1 INTRODUCTION

In this chapter, a model has been developed which can predict the recovery in an electroflotation cell. The model is based on the approach of Koh and Schwarz (2006), assuming that the particle-bubble detachment rate is negligible. Bubble size seems to be a very important factor in predicting recovery. Consequently, theoretical analyses have been performed to predict the detachment and bulk bubble size produced by electrolysis of water as a function of current density and electrode geometry. This chapter also discusses the estimation of bubble size produced by mechanical agitation of a laboratory Denver cell.

3.2 ELECTROFLOTATION RECOVERY

In an electroflotation cell the recovery of particles, $R(t)$, can be determined by the ratio of the number of particles removed from the cell at any given time after the electroflotation begins to the number of particles initially present in the cell, and can be expressed as:

$$R(t) = \frac{N_{p,pulp}(0) - N_{p,pulp}(t)}{N_{p,pulp}(0)}, \quad (3.1)$$

where $N_{p,pulp}(0)$ is the initial ($t = 0$ s) number concentration of particles in the pulp, and $N_{p,pulp}(t)$ is the number concentration of particles in the pulp after electroflotation of time, t . The bubble produced from electrolysis of water captures particles and transports them to the froth layer where the particles can be scrapped or skimmed off.

The number of particles remaining in the pulp, $N_{p,pulp}(t)$ depends on the number concentration of particles collected in the concentrate, $N_{p,c}$ and can be expressed by:

$$N_{p,pulp}(t) = N_{p,pulp}(0) - N_{p,c}(t), \quad (3.2)$$

Combining Equations 3.1 and 3.2 gives:

$$R(t) = \frac{N_{p,c}(t)}{N_{p,pulp}(0)}. \quad (3.3)$$

While the electroflotation is running, there may be two types of particles; some are already attached with bubbles, while some are still free. Obviously, at time, $t = 0$ s, all the particles in the pulp are free as there are no bubbles in the system yet. In such case:

$$N_{p,f}(0) = N_{p,pulp}(0), \quad (3.4)$$

where $N_{p,f}$ is the number concentration of free particles in the cell.

The recovery of particles can be computed provided $N_{p,c}(t)$ is known. The number of particles collected in the concentrate is a function of the number concentration of attached particles, $N_{p,a}(t)$, in the pulp. To compute the number concentration of attached particles the modelling approach of Koh and Schwarz (2006) can be suitably used.

The rate of change with time of the number concentration of free particles in the suspension ($N_{p,f}$) is given by Koh and Schwarz (2006) as:

$$\frac{dN_{p,f}}{dt} = -K_1 N_{p,f} (1 - \beta) N_{bT} + K_2 \beta N_{bT}, \quad (3.5)$$

where K_1 is particle-bubble attachment rate constant, K_2 is particle-bubble detachment rate constant, β is the normalised bubble loading parameter, defined as the number of particles able to be attached per bubble, and N_{bT} is the total number of bubbles present in the flotation cell per sec.

For flotation of very fine and light particles involving low levels of turbulence, such as in electroflotation, bubble-particle detachment can reasonably be neglected (Yoon and

Luttrell, 1989, Tao, 2004) and so $K_2 \approx 0$. Under these conditions, Equation 3.5 becomes:

$$\frac{dN_{p,f}}{dt} = -K_1 N_{p,f} (1 - \beta) N_{bT}. \quad (3.6)$$

Following integration of Equation 3.6 and rearrangement, the number of particles attached to the bubbles, $N_{p,a}$, is given by:

$$N_{p,a}(t) = \int_0^t K_1 N_{p,f} (1 - \beta) N_{bT} dt, \quad (3.7)$$

Equation 3.7 can be applied to compute the number of particles attached to bubbles at any time, for an initial particle concentration, provided the values of the following parameters are known:

- Bubble loading parameter, β , which depends on fractional surface coverage of bubble, φ .
- Particle-bubble attachment rate constant, K_1 , which depends on probability of collection, P , and particle-bubble collision frequency, Z_1 .
- Number of bubbles in the flotation cell, N_{bT} , which depends on bubble size, d_b and gas fraction results in bubbles, f .

These parameters are discussed in the following sections.

3.3 BUBBLE LOADING PARAMETER (β)

The number of particles attached to bubbles depends on the free surface area of the bubble available for particle attachment. The free surface area of the bubble available for particle attachment depends on the bubble loading parameter, β , with a value of zero (no attached particles) and one (maximum number of particles attached). The bubble loading parameter is defined by Koh and Schwarz (2006) as:

$$\beta = \frac{N_{p,a}}{\varphi S N_{bT}}, \quad (3.8)$$

where S is the ratio of the total surface area of the bubble (πd_b^2) to the projected area of a particle $\left(\frac{\pi d_p^2}{4}\right)$, and ϕ is the fractional coverage of bubble surface. Here, d_b and d_p are the diameter of the bubble and the particle, respectively. Equation 3.8 can be used to predict the bubble loading parameter provided the value of ϕ is known.

The surface properties of the particles, collector and frother chemistry, as well as the geometry and hydrodynamics of the cell may influence the bubble surface coverage (Evans et al., 2008). Due to packing, shape, and other factors, the whole bubble surface may in reality not be covered by particles, and the value of ϕ can reasonably be assumed to be less than one. Koh and Schwarz (2006) assumed that about half of the total bubble surface can be occupied by the attached particles, proposing the value of ϕ to be 0.5. Later, these authors (Koh and Schwarz, 2008) compared the simulated recovery with experimental recovery and suggested that the simulated recovery matched well with experimental data in case of $\phi = 0.2$ better than the case of $\phi = 0.5$.

3.4 PARTICLE-BUBBLE ATTACHMENT RATE CONSTANT (K_1)

The particle-bubble attachment rate constant is given by (Koh and Schwarz, 2006):

$$K_1 = Z_1 P, \quad (3.9)$$

where P is the probability of collection, and Z_1 is the particle-bubble collision frequency.

The bubble particle attachment rate constant can be determined using Equation 3.9 once the value of P and Z_1 is known. The probability of collection (P), can be calculated using appropriate models available in the literature, as discussed in Section 3.4.1.

3.4.1 Probability of Collection (P)

The ultimate success of the flotation process depends on the capture of the hydrophobic mineral particles by bubbles in the pulp phase, and the successful transport of the bubble-particle aggregates to the froth phase. As discussed in Section 2.2, the success of flotation can be described by the term ‘probability of collection’ or ‘chance of recovery’, which is the consequence of three actions:

1. Collision between particles and bubbles,
2. Attachment of the particles to the bubbles, and
3. Detachment or otherwise of particles from bubbles.

Mathematically, the probability of collection, P, can be written as (Yoon, 2000):

$$P = P_c P_a (1 - P_d), \quad (3.10)$$

where P_c , P_a , and P_d are the probability of particle-bubble collision, attachment, and detachment, respectively.

Bubble-particle collision (P_c)

The efficiency of particle-bubble collision depends mainly on the size of the bubbles and the particles, the hydrodynamics in the cell, and on the density of the pulp. To collide with a bubble, a particle must have sufficient momentum to resist the tendency to follow the streamlines around the bubble.

Sutherland (1948) introduced the concept of “collision efficiency”. By assuming a bubble of radius (r_b) rising vertically through the pulp, he proposed the existence of a collision radius, R' , such that all particles within the tube will eventually be captured. The collision radius is related to the bubble radius by (Sutherland, 1948):

$$\frac{R'}{r_b} = \left(\frac{3r_p}{r_b} \right)^{0.5} \quad (3.11)$$

where, r_b , and r_p are the radius of the bubble, and the particle, respectively. Since according to Sutherland’s theory all particles residing within a distance R' from the line

of motion of the bubble will collide with it, the collision efficiency, P_c , may be defined as the ratio of the area of the collision tube (πR^2) to the projected area of the bubble (πr_b^2); i.e.,

$$P_c = \frac{R'^2}{r_b^2}. \quad (3.12)$$

From Equation 3.11 and 3.12 we have:

$$P_c = \frac{3r_p}{r_b} = \frac{3d_p}{d_b}. \quad (3.13)$$

However, Sutherland's model is applicable only when the bubbles are very large and the flotation cell liquid is non-viscous, neither of which is realistic. Consequently, it may not be used to compute collision efficiency precisely. Later, Gaudin (1957) developed a model to compute the collision efficiency of very small bubbles (diameter less than 100 μm) under the Stokes flow condition i.e.,

$$P_c = 1.5 \left(\frac{d_p}{d_b} \right)^2. \quad (3.14)$$

Gaudin's model is valid for bubble diameters up to 100 μm , above which his model significantly underestimates the possibility of collision.

Neither Sutherland's nor Gaudin's model is applicable for intermediate bubble sizes. For the intermediate range of Reynolds numbers of bubbles ($0 < Re_b < 300$), a model to compute interceptional collision efficiency was developed by Weber (1981), and Weber and Paddock (1983a), which is given by:

$$P_c = 1.5 \left[1 + \frac{(3/16)Re_b}{1 + 0.249Re_b^{0.56}} \right] \left(\frac{d_p}{d_b} \right)^2, \quad (3.15)$$

where Re_b is the Reynolds numbers of bubble.

However, for the accurate prediction of P_c , appropriate stream functions for different ranges of bubble sizes were required. To fulfil this demand, Yoon and Luttrell (1989) derived a stream function, ψ_c , for the intermediate Reynolds number range i.e.,

$$\psi_c = v_b r_b^2 \sin^2 \theta_s \left[\frac{1}{2} x^2 - \frac{3}{4} x + \frac{1}{4x} + \frac{Re_b^{0.72}}{15} \left(\frac{1}{x^2} - \frac{1}{x} + x - 1 \right) \right], \quad (3.16)$$

where θ_s is the angular coordinate describing the trajectory of a particle moving past a bubble in streamline flow.

Using this dimensionless stream function, Yoon and Luttrell (1989) then derived the following expression to calculate the collision efficiency of intermediate size bubbles with Reynolds number in the range $0.2 < Re_b < 100$, i.e.,

$$P_c = \left[\frac{3}{2} + \frac{4 Re_b^{0.72}}{15} \right] \left(\frac{d_p}{d_b} \right)^2. \quad (3.17)$$

Yoon and Luttrell's model is applicable for particles smaller than 100 μm and bubbles smaller than 1000 μm in diameter.

Finally, it can be noted that collision efficiency, P_c , increases with the power to the ratio of particle size to bubble size, with the relationship expressed by a general form as:

$$P_c = B \left(\frac{d_p}{d_b} \right)^m \quad (3.18)$$

where B and m are the parameters that vary with Reynolds numbers. Values of B and m are presented in Table 3.1 under different flow regimes.

Table 3.1: Values of B and m of Equation 3.18 under different flow conditions

Flow condition	B	m
Stokes (Equation 3.14)	1.5	2
Intermediate (Equation 3.15)	$1.5 \left[1 + \frac{(3/16)\text{Re}_b}{1 + 0.249\text{Re}_b^{0.56}} \right]$	2
Intermediate (Equation 3.17)	$\left[\frac{3}{2} + \frac{4\text{Re}_b^{0.72}}{15} \right]$	2
Potential (Equation 3.13)	3	1

The Schulze model

All of the models discussed above consider only interception effects and neglect inertial and gravitational effects. To overcome this shortfall, Schulze (1989) proposed a more comprehensive model considering all three effects (e.g., interception, inertial and gravitational). According to Schulze (1989), the overall collision efficiency can be obtained by:

$$P_c = (P_c)_{ic} + (P_c)_G + \left(1 - \frac{(P_c)_{ic}}{(1 + (d_p/d_b))^2} \right) (P_c)_{in}, \quad (3.19)$$

where $(P_c)_{ic}$, $(P_c)_G$, and $(P_c)_{in}$ are the interceptional, gravitational and inertial collision efficiency, respectively.

The interceptional collision efficiency is given by Schulze (1989); i.e.,

$$(P_c)_{ic} = \frac{2\psi_c^*}{1 + v_s^*}, \quad (3.20)$$

where ψ_c^* is the dimensionless stream function, and v_s^* is the dimensionless velocity. ψ_c^* can be predicted by (Schulze, 1989):

$$\psi_c^* = (3/4)(d_p/d_b)^2 \left(1 + \frac{(3/16)Re_b}{1 + 0.249Re_b^{0.56}} \right), \text{ for } (d_p/d_b) \leq (1/\xi_o^*) \quad (3.21)$$

$$\psi_c^* = \exp \left[\ln \psi^*(1/\xi_o^*) + \left\{ \frac{2.6328 - \ln \psi^*(1/\xi_o^*)}{1.4569 - \ln(1/\xi_o^*)} \right\} \{ \ln(d_p/d_b) - \ln(1/\xi_o^*) \} \right],$$

for $(d_p/d_b) > (1/\xi_o^*)$ (3.22)

where ξ_o^* is the surface vorticity given by:

$$\xi_o^* = 1.5 \left[1 + \frac{(3/16)Re_b}{1 + 0.249Re_b^{0.56}} \right] (1/\sin \phi_c), \quad (3.23)$$

where ϕ_c is the collision angle of the grazing trajectory (i.e., the maximum collision angle). Dobby and Finch (1987) fitted collision data to an empirical curve and proposed the following equations to compute ϕ_c :

$$\phi_c = 90.0 - 2.50 \log(100 Re_b) \quad \text{for } 0.1 < Re_b \leq 1, \quad (3.24)$$

$$\phi_c = 98.0 - 12.49 \log(10 Re_b) \quad \text{for } 1 < Re_b \leq 20, \text{ and} \quad (3.25)$$

$$\phi_c = 78.1 - 7.37 \log Re_b \quad \text{for } 20 < Re_b < 400. \quad (3.26)$$

The dimensionless velocity, v_s^* , is defined by (Schulze, 1989):

$$v_s^* = \frac{v_p}{v_b}, \quad (3.27)$$

where v_p and v_b are the particle and bubble velocity, respectively.

According to Weber and Paddock (1983b) the gravitational collision efficiency, $(P_c)_G$, can be determined by:

$$(P_c)_G = \left(1 + \frac{d_p}{d_b}\right)^2 \left(\frac{v_p}{v_p + v_b}\right) \sin^2 \phi_c. \quad (3.28)$$

The inertial collision efficiency is given by Plate (as quoted in (Schulze, 1989)):

$$(P_c)_m = \frac{\left(1 + d_p/d_b\right)^2 \left(\frac{S_t}{S_t + y_1}\right)^{y_2}}{1 + v_s^*}, \quad (3.29)$$

where S_t is the Stokes number, and y_1 and y_2 are constants. S_t can be determined by Equation 2.2. The values of y_1 and y_2 depend on the Reynolds number of bubble and are given in Table 3.2 (Schulze, 1989).

Table 3.2: $y_1, y_2 = f(Re_b)$

Re_b	<5	5-25	25-50	50-100	100-250	250-500	>500
y_1	1.3	2.48	2.06	1.12	0.8	0.6	0.5
y_2	3.7	1.95	2.06	1.84	2	2	2

The Flint-Howarth model

Being aware of the limited applicability of the earlier collision models, Flint and Howarth (1971a) tried to provide a complete analysis for the bubble-particle collision process. In the Stokes number range between 0.001 and 0.1, where inertial forces were neglected, they derived theoretical grazing trajectories for the particles by solving the equations of particle motion for both potential and Stokes flow. It was concluded that as the Stokes number approached zero, the expression for the collision efficiency was the same for both flow regimes. The Flint-Howarth collision efficiency, P_c , can be related to the particle and bubble velocities by:

$$P_c = \frac{v_p}{v_p + v_b}. \quad (3.30)$$

The Nguyen-Van model

By using the following assumptions, Nguyen-Van (1992) developed a collision model using numerical methods (Nguyen et al., 1998); i.e.,

1. The long-range hydrodynamic and gravitational forces are the only forces that control the bubble-particle collision,
2. The distance between the bubble and particle during collision is insignificant compared with the sizes of the bubble and the particle,
3. The bubble acts as a rigid sphere,
4. The particles do not affect the motion of the bubble, and
5. The particles have no inertial forces.

The model can be expressed as:

$$P_c = \frac{2M}{9Y(1 + v_p/v_b)} (d_p/d_b)^2 \left[\left\{ (X + L)^2 + 3Y^2 \right\}^{0.5} + 2(X + L) \right]^2, \quad (3.31)$$

where,

$$X = 1.5 + \frac{9 Re_b}{32 + 9.888 Re_b^{0.694}}, \quad (3.32)$$

$$Y = \frac{3 Re_b}{8 + 1.736 Re_b^{0.518}}, \quad (3.33)$$

$$L = \frac{v_p/v_b}{(d_p/d_b)^2}, \text{ and} \quad (3.34)$$

$$M = \frac{\left\{ (X + L)^2 + 3Y^2 \right\}^{0.5} - X - L}{3Y}. \quad (3.35)$$

Bubble particle attachment/adhesion (P_a)

Not all particles that collide with bubbles can be attached with those. For a successful attachment of particles with bubbles, the contact time must be higher than the induction time. The following mechanisms occur chronologically for bubble particle adhesion:

Step 1: Approach of a particle to a bubble.

Step 2: Thinning of a water film between particle and bubble to rupture thickness.

Step 3: Receding of the residual film to give an air-solid interface.

Among these, Step 2 is the most important since it controls the mechanism of adhesion.

Contact or sliding time is defined as the finite period of time taken by a particle to slide over the surface of the bubble before leaving the bubble after their collision. Dobby and Finch (1986) proposed a model to compute sliding time assuming potential fluid flow around a completely mobile surface. In their model, the time taken by a particle to travel from the point of collision to the point where it leaves bubble surface was referred to as the sliding time. From the model, the sliding time, t_{sl} , was defined as:

$$t_{sl} = \frac{d_p + d_b}{2(v_p + v_b) + v_b \left(\frac{d_b}{d_p + d_b} \right)^3} \ln \left(\tan \frac{\phi_c}{2} \right). \quad (3.36)$$

The minimum time required for thinning, and subsequently rupturing the disjoining film between the bubble and the particle is defined as induction time. From experimental observations, the induction time has been found to increase with increased particle size and decreased hydrophobicity of the particle surface (Glembotskii, 1953, Ye and Miller, 1988). The induction time, t_i , can be correlated with particle size as (Trahar and Warren, 1976, Dai et al., 1999, Jowett, 1980):

$$t_i = E d_p^a, \quad (3.37)$$

where the parameters E and a are constant and independent of particle size. Dai et al. (1999) investigated the particle-bubble interactions of various sizes and concluded that

the parameter α is constant with a value of 0.6 and the parameter E is inversely proportional to the contact angle of the particle.

Based on the above findings, Koh and Schwarz (2006) proposed the following expression to compute the induction time:

$$t_i = \frac{75}{\theta_c} d_p^{0.6}, \quad (3.38)$$

where θ_c is the contact angle (degree) of solid-liquid interface.

Once the induction time is known, the following models can be used to determine the particle-bubble attachment efficiency (P_a).

Using the stream function as described in Equation 3.16, Yoon and Luttrell (1989) derived the following expression for predicting attachment efficiency (P_a); i.e.,

$$P_a = \sin^2 \left[2 \tan^{-1} \exp \left(\frac{-(45 + 8 Re_b^{0.72} v_b t_i)}{15 d_b (1 + d_b/d_p)} \right) \right]. \quad (3.39)$$

Yoon and Luttrell assumed that particle bubble collision occurs uniformly over the entire upper half of the bubble surface, which may not always be the case. Later, Ralston et al. (1999) derived a more general expression for P_a as:

$$P_a = \frac{\sin^2 \left[2 \tan^{-1} \exp \left\{ -t_i \frac{2(v_p + v_b) + (v_p + v_b) \left(\frac{d_b}{d_b + d_p} \right)^3}{d_b + d_p} \right\} \right]}{2\alpha \left((1 + \alpha^2)^{0.5} - \alpha \right)}, \quad (3.40)$$

where $\alpha = \frac{12d_b}{d_p} \times \frac{\rho_f}{\rho_p - \rho_f} \times \frac{1}{Re_b}$, v_p is the settling velocity of the particle, ρ_f is the density of the fluid, and ρ_p is the density of the particle.

However, in case of coarse particles, where bubble surface deformation and consequent particle rebound are significant, neither Equation 3.39 nor Equation 3.40 is accurate for calculating the attachment efficiency. Both Equations 3.39 and 3.40 show that P_a decreases with increasing particle size and decreasing particle hydrophobicity. Yoon and Luttrell (1989) demonstrated that P_a increases with decreasing induction time, particle size and bubble size until the bubble size becomes too small.

Dobby and Finch model

Dobby and Finch (1987) derived a model to determine the bubble-particle attachment efficiency, P_a , based on a kinetic energy approach. The model can be mathematically described as:

$$P_a = \frac{\sin^2 \theta_a}{\sin^2 \theta_{a,max}}, \quad (3.41)$$

where θ_a is the attachment angle, and $\theta_{a,max}$ is the maximum value of the attachment angle. The specific value of the collision angle, ϕ_c , when the sliding time, t_{sl} , equals the induction time, t_i , is referred as attachment angle, θ_a . Mathematically, θ_a can be expressed as:

$$\theta_a = \phi_{c(t_{sl}=t_i)}. \quad (3.42)$$

The value of maximum attachment angle can be found from the literature. Yoon and Luttrell (1989) suggested the value of $\theta_{a,max}$ to be 90° , whereas Dai et al. (1999) referred $\theta_{a,max}$ to be equal to the angle of tangency, θ_t . According to Dukhin (1982), the angle of tangency can be obtained from:

$$\theta_t = \arcsin \left[2\lambda \left\{ (1 + \lambda^2)^{0.5} - \lambda \right\} \right]^{0.5}, \quad (3.43)$$

where λ is a dimension less number given by:

$$\lambda = \frac{2f' \left(\frac{3d_p}{d_b} \right)}{9K_3}. \quad (3.44)$$

K_3 is defined as:

$$K_3 = \frac{S_t (\rho_p - \rho_f)}{\rho_p}, \quad (3.45)$$

where S_t is the Stokes number and can be obtained from Equation 2.2. Dukhin and Rulev (1977) reported the value of f' to be 2.0.

Bubble particle detachment (P_d)

The particles attached to the bubbles are lifted by the buoyancy force and reach the froth phase. However, while rising to froth phase, some of them may be detached from the bubble surface and drop back into the pulp phase. The stability of the bubble-particle aggregate depends on the surface tension and viscosity of the liquid, bubble and particle size, the three phase contact angle, acceleration induced by the bubble generating machine, and the density of the particle and the pulp. To keep the particles attached with the bubble surface, the detachment forces must be counter balanced by the adhesive forces. The balance between these forces determines the maximum size floatable.

The forces acting between a bubble and the attached particle are generally categorized into four types, i.e., capillary force, F_c , excess force, F_e (which is the difference between the excess pressure in the bubble and the hydrostatic force), real weight of the particle in the liquid medium, F_w , and the hydrodynamic drag force, F_d (Tao, 2004). Drzymala (1994) provided the following expressions to compute these forces:

$$F_c = 0.5\pi l_p \sigma (1 - \cos \theta_d), \quad (3.46)$$

$$F_e = 0.25\pi d_p^2 (1 - \cos \theta_d) \left(\frac{2\sigma}{d_b} - \frac{\rho_f g d_b}{2} \right), \quad (3.47)$$

$$F_w = \frac{1}{6} \pi d_p^3 \rho_p (g + b_m) - \frac{1}{8} \pi d_p^3 \rho_f g \left(\frac{2}{3} + \cos\left(\frac{\theta_d}{2}\right) - \frac{1}{3} \cos^3\left(\frac{\theta_d}{2}\right) \right), \quad (3.48)$$

$$F_d = \frac{C_D \rho_f v_p^2 A_p}{2} \quad (3.49)$$

where σ is the liquid surface tension, μ is the dynamic viscosity of fluid, θ_d is the critical value of three phase contact angle right before detachment, b_m is the machine acceleration, C_D is the drag coefficient, and A_p is the projected area of particle. In case of electroflotation, no mechanical agitation is used for bubble production, and hence b_m can be taken as zero.

Fine particle usually falls in the Stokes Regime ($Re < 1$) and in such case the drag coefficient can be estimated as:

$$C_D = \frac{24}{Re} \quad (3.50)$$

By combining Equations 3.49 and 3.50, we can get:

$$F_d = 3\pi d_p \mu v_p, \quad (3.51)$$

Equation 3.51 is only valid for Stokes flow. If the particles are too fine ($< 1\mu\text{m}$ in diameter), then these particles will move erratically-almost appearing to hop around discontinuously. This Brownian motion is due to collision with water molecules, which makes the particles undergo random-walk motion. In such case the drag coefficient, C_D , can be estimated by Einstein–Smoluchowski relation (Ashcroft and Mermin, 1988):

$$C_D = \frac{\Gamma K}{D''} \quad (3.52)$$

where Γ is the Boltzmann's constant, T is the absolute temperature and D'' is the diffusion constant.

By combining Equations 3.49 and 3.52, we can get:

$$F_d = \frac{\Gamma K \rho_f v_p^2 A_p}{2D''} \quad (3.53)$$

Equation 3.53 is only valid for ultra-fine particle (0.1 to 1 μ m in diameter).

It can be summarized that for fine particle (Stokes flow, $Re < 1$) the drag force, F_D , can be determined by using Equation 3.51, whereas Equation 3.53 can be used for ultra-fine particle (0.1 to 1 μ m in diameter). Among these forces, F_c acts as the major adhesive force, F_w and F_d act as detachment forces, while F_e may act as adhesive or detachment force depending on the relative magnitude of the excess pressure in the bubble and the hydrostatic force. When $\frac{2\sigma}{d_b} > \frac{\rho_f g d_b}{2}$ or $d_b < 5.5$ mm, F_e works against detachment. The probability of detachment can be predicted by (Tao, 2004):

$$P_d = \frac{F_d + F_e}{F_c + F_e + F_w + F_d} \quad (3.54)$$

However, most of the models discussed previously have been developed assuming a single bubble-single particle system, which may not represent the real flotation system where a swarm of bubbles is used. The particle-bubble interaction in a real system may be influenced by the gas holdup effect, the interaction between neighbouring bubbles, and the presences of multi-layers of bubbles. All of these interactions tend to straighten the liquid streamlines around a bubble and consequently may enhance the probability of collection.

3.4.2 Particle-Bubble Collision Frequency (Z_1)

For a system with homogenous turbulence, such as in an electroflotation cell without mechanical agitation, the particle-bubble collision frequency, Z_1 can be reasonably approximated by the expression provided by Nguyen and Schulze (2004); i.e.,

$$Z_l = \pi \left(\frac{d_b + d_p}{2} \right)^2 V_{rel}, \quad (3.55)$$

where V_{rel} is the relative velocity between the bubble (v_b), and the particle (v_p). Appendix A describes the determination of bubble and particle velocity in water contaminated by collector and frother.

3.5 BUBBLE-PARTICLE AGGREGATE VELOCITY

The velocities of the bubble and particle in the flotation pulp can be obtained by balancing the buoyancy, F_B , weight, F_W , and drag forces, F_d , where (assuming bubble and particle are spherical in size):

$$F_B = \frac{\pi d_{b/p}^3 \rho_{pulp} g}{6}, \quad (3.56)$$

$$F_W = \frac{\pi d_{b/p}^3 \rho_{b/p} g}{6}, \quad (3.57)$$

$$F_d = \frac{\rho_{pulp} u^2 A_{b/p} C_D}{2}, \quad (3.58)$$

where ρ_{pulp} is the pulp density, $\rho_{b/p}$ is the density of bubble or particle, u is the velocity of bubble or particle, $A_{b/p}$ is the projected area of the bubble or particle ($\pi d_{b/p}^2 / 4$), C_D is the drag coefficient, which for Stokes flow ($Re < 0.1$), is given by:

$$C_D = \frac{24}{Re} = \frac{24 \mu_{pulp}}{\rho_{pulp} u d}, \quad (3.59)$$

where Re is the Reynolds number, and μ_{pulp} is the absolute viscosity of pulp. Substituting $A_{b/p}$ and C_D into Equation 3.58 gives:

$$F_d = 3\pi u d_{b/p} \mu_{pulp}. \quad (3.60)$$

When particles are attached to a bubble, the bubble particle-aggregate may rise to the froth layer or may sink to the bottom of the cell. The above equations (3.56-3.60) can be

applied to a bubble-particle aggregate. For a bubble with radius (r_b), with N_p particles of radius r_p attached to its outer surface, then:

$$F_{B,b} = \frac{\pi}{6} d_b^3 \rho_{pulp} g, \quad (3.61)$$

$$F_{B,p} = \frac{\pi}{6} N_p d_p^3 \rho_{pulp} g, \quad (3.62)$$

$$F_{W,b} = \frac{\pi}{6} d_b^3 \rho_G g, \quad (3.63)$$

$$F_{W,p} = \frac{\pi}{6} N_p d_p^3 \rho_p g, \quad (3.64)$$

$$F_{d,b-N_p} = 3\pi v_{b-N_p} d_{b-N_p} \mu_{pulp}, \quad (3.65)$$

where $F_{B,b}$ is the buoyancy force of a bubble, $F_{B,p}$ is the buoyancy force of N particles, $F_{W,b}$ is the weight of a bubble, $F_{W,p}$ is the weight of N particles, and $F_{d,b-N_p}$ is the hydrodynamic drag force, v_{b-N_p} is the rise/fall velocity of the bubble-particle aggregate, and d_{b-N_p} is the projected diameter of the bubble particle aggregate (see Figure 3.1).

Equating the buoyancy, weight and drag forces leads to the following expression for the rise/fall velocity of the bubble-particle aggregate, v_{b-n_p} :

$$v_{b-N_p} = \frac{g}{18\mu_{pulp} d_{b-N_p}} \left[d_b^3 (\rho_{pulp} - \rho_G) - N_p d_p^3 (\rho_p - \rho_{pulp}) \right]. \quad (3.66)$$

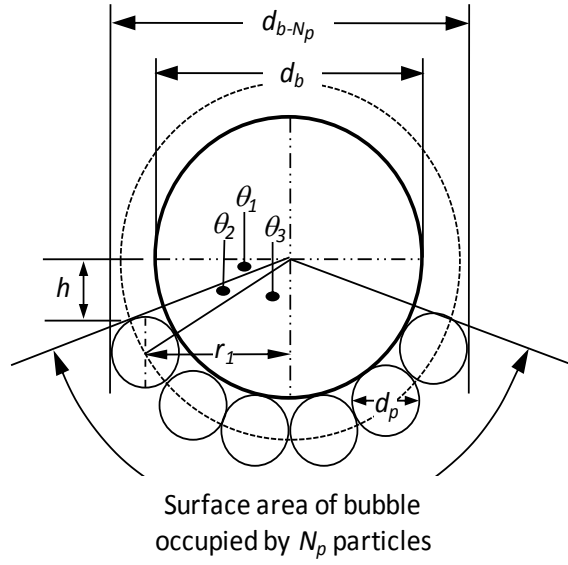


Figure 3.1: Geometry of the bubble-particle aggregate

The projected diameter of the bubble-particle aggregate can be related to the surface coverage, ϕ , of the bubble surface by the particles, where:

$$\phi = \frac{(N_p \pi d_p^2 / 4)}{(4\pi (d_p + d_b)^2 / 4)} = \frac{N_p d_p^2}{4(d_p + d_b)^2}. \quad (3.67)$$

From Figure 3.1, ϕ is also given by:

$$\phi = \frac{\pi(d_p + d_b)[(d_p + d_b) - 2h]}{\pi(d_p + d_b)^2} = \frac{d_p + d_b - 2h}{d_p + d_b}, \quad (3.68)$$

Where h is the vertical distance from the horizontal centreline of the bubble to the top of the attached particle(s). From Equations 3.67 and 3.68:

$$h = \frac{4(d_p + d_b)^2 - N_p d_p^2}{8(d_p + d_b)}. \quad (3.69)$$

From Figure 3.1:

$$\theta_1 = \sin^{-1} \left[\frac{2h}{d_p + d_b} \right]. \quad (3.70)$$

$$\theta_2 = 2 \sin^{-1} \left[\frac{d_p}{2(d_b + d_p)} \right], \quad (3.71)$$

$$\theta_3 = \frac{\pi}{2} - \theta_1 - \theta_2, \quad (3.72)$$

$$r_1 = \frac{(d_b + d_p) \sin[\theta_3]}{2}. \quad (3.73)$$

For a given value of ϕ , the equations above can be solved to obtain r_1 , and from that the diameter of the bubble-particle aggregate, such that:

$$d_{b-N_p} = 2r_1 + d_p = (d_b + d_p) \sin[\theta_3] + d_p, \quad (3.74)$$

By putting the value of d_{b-N_p} in Equation 3.66, the rise/fall velocity of the bubble-particle aggregate, v_{b-n_p} can be estimated as:

$$v_{b-N_p} = \frac{g}{18\mu_{pulp} \left((d_b + d_p) \sin[\theta_3] + d_p \right)} \left[d_b^3 (\rho_{pulp} - \rho_G) - N_p d_p^3 (\rho_p - \rho_{pulp}) \right] \quad (3.75)$$

Equation 3.75 is only valid only for d_{b-N_p} greater than d_b . For d_{b-N_p} less than d_b then the bubble diameter value should be used when calculating the bubble-particle aggregate rise/fall velocity as shown below:

$$v_{b-N_p} = \frac{g}{18\mu_{pulp} d_b} \left[d_b^3 (\rho_{pulp} - \rho_G) - N_p d_p^3 (\rho_p - \rho_{pulp}) \right] \quad (3.76)$$

3.6 MAXIMUM PARTICLE SIZE THAT CAN BE FLOATED BY A GIVEN SIZE OF BUBBLE

Particle detachment and buoyancy are the governing factors for successful particle flotation after being attached with a bubble (Wark, 1933).

3.6.1 Particle Detachment

In flotation there is a maximum floatable particle diameter beyond which the attachment force between the particle and bubble is less than the sum of the detachment forces, which includes the weight force of the particle and the machine acceleration due to agitation in the liquid. The maximum floatable particle diameter, $(d_p)_{max,d}$, for a given bubble size can be determined by (Schulze, 1982):

$$(d_p)_{max,d} = \left[\frac{-6\sigma \sin\left(\pi - \frac{\theta_c}{2}\right) \sin\left(\pi + \frac{\theta_c}{2}\right)}{\{g(\rho_p - \rho_{pulp}) + b_m \rho_p\}} \right]^{\frac{1}{2}} \quad (3.77)$$

where σ is the surface tension, ρ_p is the density of particle, b_m is the machine acceleration for a mechanically agitated flotation cell, and θ_c is the critical three phase contact angle below which the flotation will not take place (Scheludko et al., 1976, Crawford, 1986, Gontijo et al., 2007, Miettinen, 2007). The minimum critical contact angle has been found to increase with decreased particle size (Chipfunhu et al., 2011).

Later, by combining the work of Schulze (1982) and Schubert (1999), Nguyen (2003) proposed the following equation that can be used to compute the maximum floatable particle size, $(d_p)_{max,d}$:

$$(d_p)_{max,d} = \left[\frac{3\sigma(1 - \cos \theta_c)}{(\rho_p - \rho_{pulp})(g + b_m)} \right]^{\frac{1}{2}} \quad (3.78)$$

For systems where machine acceleration is negligible, such as in electroflotation cells, b_m can reasonably be considered to be zero. Using this assumption, Equation 3.78 becomes:

$$(d_p)_{max,d} = \left[\frac{3\sigma(1 - \cos \theta_c)}{g(\rho_p - \rho_{pulp})} \right]^{\frac{1}{2}} \quad (3.79)$$

3.6.2 Buoyancy

Once a particle becomes attached to the bubble the buoyancy of the bubble-particle aggregate is reduced which hinders the ability of the bubble to rise into the froth and report to the concentrate. The extreme case is when the weight of the attached particle(s) results in the bubble-particle aggregate having a zero, or even negative, rise velocity, v_{b-N_p} . Consequently, there will be no flotation product. The conditions under which this will occur can be calculated from Equation 3.66, such that:

$$d_b^3(\rho_{pulp} - \rho_G) = N_p d_p^3(\rho_p - \rho_{pulp}). \quad (3.80)$$

For a single particle ($N_p=1$) attached to a bubble, the maximum particle diameter, $(d_p)_{max,b}$, based on the buoyancy criteria is given by:

$$(d_p)_{max,b} = d_b \left(\frac{\rho_{pulp} - \rho_G}{\rho_p - \rho_{pulp}} \right)^{\frac{1}{3}}. \quad (3.81)$$

The value of $(d_p)_{max,b}$ can be computed once the pulp density of the three phase system in the flotation cell is known. The minimum of $(d_p)_{max,d}$ and $(d_p)_{max,b}$ will be the maximum size of a single particle that can be floated by a single bubble of given size in a flotation cell. For electroflotation systems, where the bubble size is small, the limiting particle diameter able to be floated is determined by the buoyancy criteria. Equation 3.81 is for a single particle attached to a bubble. When more than one particle is attached then Equation 3.80 should be used to determine the maximum floatable diameter.

3.6.3 Calculation of Pulp Density

For a three-phase system in the flotation cell, the pulp density, ρ_{pulp} , can be calculated by:

$$\rho_{pulp} = \varepsilon_s \rho_p + \varepsilon_f \rho_f + \varepsilon_G \rho_G, \quad (3.82)$$

where ε_s , ε_f , and ε_G are the volumetric fraction of solid, liquid and gas, respectively, and ρ_p , ρ_f , and ρ_G are the density of particle, liquid and gas, respectively. The volumetric fraction of gas in a flotation cell is equal to the gas holdup by the cell. According to Nguyen and Schulze (2004), the relation between the volumetric fraction of solids and liquid can be expressed by the ratio of their density as:

$$\varepsilon_s = \frac{X_s \rho_f \varepsilon_f}{\rho_p}, \quad (3.83)$$

where X_s is the mass fraction of solids.

Equation 3.82 can be used to compute the pulp density of the three phase system, provided the value of gas holdup in the cell is known. The gas holdup by the cell can be estimated by drift flux analysis (discussed in Appendix B) for the known size of bubbles produced by the cell.

3.7 EFFECT OF MAXIMUM FLOATABLE PARTICLE DIAMETER ON FLOTATION RECOVERY

Following from Section 3.6, the number of particles with diameter greater than $(d_p)_{\max}$, calculated as the minimum of $(d_p)_{\max,d}$ and $(d_p)_{\max,b}$, needs to be taken into consideration when predicting the fractional flotation recovery. If the fraction of particles with diameter greater than $(d_p)_{\max}$ at time $t = 0$ s is K_4 , then Equation 3.3 becomes:

$$R(t) = \frac{N_{p,c}(t)}{(1 - K_4)N_{p,pulp}(0)}, \quad (3.84)$$

where the numerical value for K_4 is determined from the particle size distribution of the solids in the pulp.

3.8 NUMBER OF BUBBLES PRODUCED IN ELECTROLYSIS

The theoretical volumetric gas flow rate, Q_G , produced by electrolysis of water can be calculated using the ideal gas equation; i.e.,

$$Q_G = \dot{n} \left(\frac{RT}{p} \right), \quad (3.85)$$

where R is gas constant, T is the temperature, p is the pressure, and \dot{n} is the molar flow rate. For electroflotation, the ideal molar generation rate of gas is given by (Nelkon, 1970):

$$\dot{n} = \frac{n}{t} = \frac{I}{zF}, \quad (3.86)$$

where I is the absolute current, z is the number of electrons required to produce 1 mole of gas (for hydrogen, $z = 2$), F is Faraday's constant, n is the number of moles, and t is the time.

The value of \dot{n} has been substituted into Equation 3.85 to produce:

$$Q_G = \frac{IRT}{pzF}. \quad (3.87)$$

Equation 3.87 can be used to calculate the theoretical gas production rate for a given current, which can then be used to calculate the flotation recovery. In practice, however, not all of the gas molecules produced result in gas evolution. The physical process of gas evolution from electrodes can be divided into nucleation, growth and detachment stages. Bubbles nucleate at the electrode surface from solutions supersaturated with product gas. These bubbles then grow either by diffusion of dissolved gas to the bubble surface or by coalescence at the electrode with other bubbles (Paul and Charles, 1985). They detach from the electrode when buoyancy or liquid shearing forces pull the bubbles away by overcoming their binding forces with the electrode. Surface inhomogeneities, such as cracks, are generally considered high-energy nucleation sites due to the availability of atomic ledges as high-energy anchorage points. During

electrolysis, it is generally agreed that the preferred nucleation sites are at surface inhomogeneities, such as fissures, cracks and scratches (Glas and Westwater, 1964). At low current densities, the gases produced by electrolysis are dissolved in the electrolyte, but at higher current densities, gas bubbles are evolved at the electrodes. Under these conditions, a fraction, f , of the total (theoretical) results in gas bubbles, while the remaining portion, $(1-f)$, diffuses into the bulk solution; i.e.,

$$(Q_G)_b = fQ_G, \quad (3.88)$$

where $(Q_G)_b$ is the production rate of hydrogen gas bubbles. The value of f varies between zero (for no bubbles) and one (all of the gas is used to form bubbles).

Relevant to this study is the diffusion of hydrogen molecules from the electrode surface into the bulk solution. Vogt (1984a) found that only a fraction of total hydrogen generated in dissolved form is transformed into gas bubbles adhering to the electrode. Glas and Westwater (1964) and Shibata (1978) also reported that the gas evolved must be transferred from the electrode into the solution to a large extent by convective diffusion. Müller et al. (1989) found that at a current density of 3000 A/m² the quantity of hydrogen leaving the electrode surface by convective diffusion is about 15%.

Once the hydrogen production rate and bubble size produced by electrolysis of water is known, the number of bubbles (N_{bT}) in the electroflotation cell can be calculated. For spherical bubbles, N_{bT} is given by:

$$N_{bT} = \frac{(Q_G)_b}{(\pi d_b^3 / 6)}, \quad (3.89)$$

where d_b is the bubble diameter.

Combining Equations 3.88 and 3.89, we have:

$$N_{bT} = \frac{fQ_G}{(\pi d_b^3 / 6)}. \quad (3.90)$$

The number of bubbles produced in the flotation cell per unit time can be determined by using Equation 3.90 provided the bubble size and the fraction of hydrogen resulted in gas bubbles are known.

3.9 BUBBLE SIZE PRODUCED IN ELECTROFLOTATION

3.9.1 Bubble Detachment Diameter

The detachment diameter, $d_{b,d}$, of a growing bubble from an electrode surface with radius of curvature, $D/2$, has been analysed previously (Ketkar et al., 1988, Lubetkin, 1994). At low growth rates, the drag and inertial forces can be ignored, and detachment take place when the surface tension (attaching) force, F_σ , is equal to the sum of the buoyancy, F_B , and pressure, F_p , (detaching) forces; i.e.,

$$F_\sigma = F_p + F_B. \quad (3.91)$$

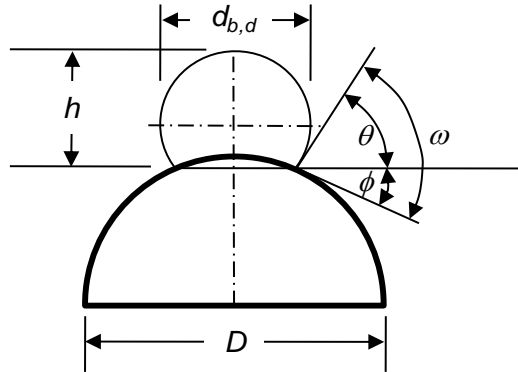


Figure 3.2: Geometry for bubble on curved electrode surface

Briefly, making use of the schematic shown in Figure 3.2, the three forces can be expressed as:

$$F_\sigma = \pi d_{b,d} \sigma \sin^2 \theta, \quad (3.92)$$

$$F_B = g(\rho_f - \rho_G) \left[\frac{\pi d_{b,d}^3 (2 + 3 \cos \theta - \cos^3 \theta)}{24} \right], \quad (3.93)$$

$$F_P = \pi (\sin(\phi D/2))^2 \left\{ (\sigma/d_{b,d}) - (\rho_f - \rho_G)gh \right\}, \quad (3.94)$$

where σ is the liquid surface tension, ρ_f and ρ_G are the density of the liquid and gas, respectively, and h is the height from the top of the detaching bubble to the electrode surface. A possible detachment condition (Boucher and Evans, 1975, Jones et al., 1999a) occurs when $(\sigma/d_{b,d}) = (\rho_f - \rho_G)gh$. If so, then the surface tension and buoyancy forces must be equal. Hence, from Equations 3.92 and 3.93, it can be shown that:

$$d_{b,d} = \sqrt{\frac{24\sigma \sin^2 \theta}{g(\rho_f - \rho_G)(2 + 3 \cos \theta - \cos^3 \theta)}}, \quad (3.95)$$

and

$$\theta = \frac{\omega}{1 + \sin^{-1}(d_{b,d}/D)}, \quad (3.96)$$

where ω is the contact angle. Equations 3.95 and 3.96 can be solved simultaneously to obtain the radius of the detaching bubble for a given electrode radius of curvature, liquid physical properties and contact angle.

3.9.2 Bubble Diameter in the Bulk

In electroflotation, not all of the hydrogen produced at the cathode results in hydrogen bubbles. Instead, a fraction of the hydrogen molecules remain dissolved in the electrolyte solution (Glas and Westwater, 1964, Vogt, 1984a). A portion of the dissolved hydrogen gas, however, is diffused into the detached bubble as it rises through the solution. The rate, n (mol/s), at which the diffusion takes place is given by (Jones et al., 1999b):

$$\frac{dn}{dt} = S_b k_m (C_b - C^{sat}), \quad (3.97)$$

where S_b is the bubble surface area (m^2); k_m is mass transfer coefficient (m/s); C_b is the bulk molar concentration of gas in the liquid (mol/m^3); and C^{sat} is the saturation molar concentration of gas in the liquid-gas interface (mol/m^3), which is a function of the temperature of the liquid and the partial pressure of the hydrogen in the bubble in accordance with Henry's Law. Values for the Henry's Law coefficient for hydrogen gas are given in Lide (2010).

Equation 3.97 can be used to predict the rate of molar diffusion once the value of k_m is known. Vogt (1984a) provides an expression for the mass transfer coefficient; i.e.,

$$k_m = 0.5 \left(\frac{D'}{Fo't} \right)^{0.5} \frac{\rho_G}{M_G (C_b - C^{sat})} \quad (3.98)$$

where D' is the mass diffusivity of gas (m^2/s), Fo' is Fourier number of mass transport, M_G is molar mass of gas (kg/mol), and ρ_G is the density of gas (kg/m^3).

The Fourier number (Fo') used in Equation 3.98, is related with the Jakob number (Ja), of mass transport and can be expressed as (Vogt, 1984a):

$$Fo' = \frac{1}{2C_1 Ja}, \quad (3.99)$$

where C_1 is a numerical constant and has the value of $\ln 2$ for the case of spherical bubbles (Buehl and Westwater, 1966). Therefore, for the spherical bubbles, Equation 3.99 becomes:

$$Fo' = \frac{1}{2 \ln(2) Ja}. \quad (3.100)$$

Now, the Jakob number of mass transport is related to the supersaturation ($C_b - C^{sat}$), and can be written as:

$$Ja = \frac{M_G (C_b - C^{sat})}{\rho_G} \quad (3.101)$$

Substituting Equation 3.101 into Equation 3.100 gives:

$$Fo' = \frac{\rho_G}{2 \ln(2) M_G (C_b - C^{sat})} \quad (3.102)$$

By putting the value of Fourier number in Equation 3.98, we can get the expression of mass transfer, k_m , as:

$$k_m = 0.5 \times \sqrt{\frac{2 \ln(2) D' \rho_G}{t M_G (C_b - C^{sat})}} \quad (3.103)$$

As mentioned in Section 3.8, a fraction, $1 - f = \psi$, of the total hydrogen produced by the electrolysis process is initially dissolved into the liquid and diffuses away from the cathode surface. Consequently, the bulk concentration, C_b , is a function of both time and position. For a cylindrical wire cathode, the modelling by Carslaw and Jaeger (1959) for heat conduction from a line source can be suitably applied. The concentration (mol/m^3) at radial position, r , and time, t , from an instantaneous cylindrical source of diameter, D , and strength, N (mol/m^2), is given by:

$$C(r, t) = \frac{N}{t} \left(\frac{D}{4D'} \right) \exp\left(\frac{-(r^2 + (D/2)^2)}{4D't} \right) I_0\left(\frac{rD}{4D't} \right), \quad (3.104)$$

where I_0 is the modified Bessel function of the first kind of order zero. For a continuous line source, \dot{N} ($\text{mol/m}^2 \cdot \text{s}$), Equation 3.104 can be rewritten as:

$$C(r, t) = \dot{N} \left(\frac{D}{4D'} \right) \int_0^t \exp\left(\frac{-(r^2 + (D/2)^2)}{4D'(t-t')} \right) I_0\left(\frac{rD}{4D'(t-t')} \right) \frac{dt'}{t-t'}. \quad (3.105)$$

For electroflotation:

$$\dot{N} = (1 - f) \dot{N}_{H_2} = \psi \dot{N}_{H_2}, \quad (3.106)$$

where $f + \psi = 1$, \dot{N}_{H_2} is the theoretical molar flux rate (mol/m².s) of molecular hydrogen produced at the cathode surface, and is given by:

$$\dot{N}_{H_2} = \frac{\dot{I}}{zF}, \quad (3.107)$$

where \dot{I} is the current density (A/m²) of electrode surface.

3.10 ESTIMATION OF BUBBLE SIZE PRODUCED IN DENVER CELL

3.10.1 Bubble Break up and Maximum Stable Bubble Size

A bubble experiencing a shearing flow responds to a velocity gradient in the flow, which causes a velocity difference between two opposing apices. The differences in velocity manifest themselves as differences in pressure, which are related to the properties of the turbulent flow field. This pressure difference then tends to stretch the bubble against the restoring forces of surface tension, and the bubble will break into two segments when the stretching forces are high enough. There is a maximum bubble size that can be restrained against the stretching forces for a given flow field.

Hinze (1955) suggested that the bubble would break up if the ratio of the inertial and surface tension forces, in the form of critical Weber number, exceeded a critical value. The critical Weber number, We_c , is given by:

$$We_c = \frac{\rho_{pulp} \bar{u}^2 (d_b)_{max}}{\sigma}, \quad (3.108)$$

where \bar{u}^2 is the mean square velocity difference between two points in the turbulent flow acting a distance apart equal to the maximum bubble diameter, $(d_b)_{max}$, σ is the surface tension, and ρ_{pulp} is the density of suspension.

Based on the critical Weber number and uniform energy dissipation throughout the cell, Evans et al. (1992) proposed a model to predict the maximum stable diameter as:

$$(d_b)_{max} = \left(\frac{We_c \sigma}{2} \right)^{0.6} \rho_{pulp}^{-0.6} \varepsilon^{-0.4}, \quad (3.109)$$

where ε is the energy dissipation rate per unit mass.

Equation 3.109 has been derived assuming that the energy dissipation rate is uniform throughout the vessel and can be used to compute the maximum bubble diameter produced in a Denver cell once the value of critical Weber number and the energy dissipation rate is known. Evans et al. (1992) assumed a critical Weber number of 1.2 based on the average mechanical energy dissipation which was in good agreement with the critical Weber number calculated by Hinze (1955) for bubble break up in viscous shear flow. The predicted maximum bubble diameter has been generally found to agree with measured values to within 20% over a wide range of column operating parameters (a range of column and jet diameters, jet velocities) and liquid physical properties (surface tension, and gas liquid volumetric flow ratio).

3.10.2 Average Energy Dissipation in Denver Cell

In a Denver flotation cell bubbles are produced by mechanical agitation with an impeller. Gas is sparged and broken into bubbles by the shearing forces of the impeller. In such a mechanical cell, feed flow, sparged gas and impeller rotation are the potential sources of energy dissipation. Hence, the average energy dissipation per unit mass, ε , is the sum of all three sources of energy dissipation and can be expressed as:

$$\varepsilon = E_F + E_G + E_I. \quad (3.110)$$

where E_F is the energy dissipation from feed flow, E_G is the energy dissipation from sparged gas, and E_I is the energy dissipation from impeller rotation. Energy dissipation from feed flow, sparged gas and impeller rotation can be obtained from:

$$E_F = \frac{\dot{m}(v_F^2 - v_O^2)}{2V\rho_{pulp}}, \quad (3.111)$$

$$E_G = \frac{gHQ_G}{2V}, \quad (3.112)$$

$$E_I = \frac{P_G}{V\rho_{pulp}}, \quad (3.113)$$

where \dot{m} is the mass flow rate of solids, v_O is the initial velocity of feed, v_F is the final velocity of feed, V is the volume of the cell, H is the height of the cell, Q_G is the gas flow rate, g is the acceleration due to gravity, P_G is the power input to the cell in the presence of gas.

For a semi-batch system (continuous air flow, batch solids input), the energy dissipation from feed flow is zero. Then the value of E_G and E_I has been substituted into Equation 3.110 to find:

$$\varepsilon = \frac{gHQ_G}{2V} + \frac{P_G}{V\rho_{pulp}}. \quad (3.114)$$

Once the value of P_G is known, Equation 3.114 can be used to calculate the energy dissipation rate.

3.10.3 Power Input to the Cell in the Presence of Gas

Following the analysis of Michel & Miller (1962), Vilaça et al. (2000) proposed a correlation for calculating the power consumption for a gassed cell which is mechanically agitated. According to Vilaça et al. (2000), for Newtonian fluids, the power consumption for gassed system, P_G can be predicted by:

$$P_G = 0.937 \left(\frac{P_{UG}^2 N_I D_I^3}{Q_G^{0.56}} \right)^{0.43}, \quad (3.115)$$

where P_{UG} is the power input to the cell in the absence of gas, N_I is the impeller rotational speed (rev/s), and D_I is diameter of impeller.

Now, the power input is a function of power number. In a mechanically agitated cell, the actual power input, P_{UG} , is given by:

$$P_{UG} = (N_p)_{UG} \rho_{pulp} N_I^3 D_I^5, \quad (3.116)$$

where $(N_p)_{UG}$ is the power number for the degassed system, ρ_{pulp} is the density of suspension, and D_I is diameter of impeller. Equation 3.116 can be used to compute the power input to the cell, P_{UG} , once the impeller dimension and rotation, as well as the power number are known. For a mechanically agitated cell (e.g., Denver cell) the power number for an un-gassed system can be estimated from the study of Harris and Mensah-Biney (1977).

3.10.4 Sauter Mean Bubble Size

In flotation studies, the mean bubble size is usually reported as the Sauter mean diameter, $(d_b)_S$. As the maximum bubble size is known, $(d_b)_S$ can be predicted using empirical relations. Many experimental studies (Evans et al., 1992, Calabrese et al., 1986, Zhang et al., 1985) reported the ratio of $(d_b)_S$ and $(d_b)_{max}$ to be in the range 0.6-0.62. So the Sauter mean bubble diameter can be predicted by (Evans et al., 1992):

$$(d_b)_S = 0.61(d_b)_{max} \quad (3.117)$$

From Equations 3.109 and 3.117 we have:

$$(d_b)_S = 0.61 \left(\frac{We_c \sigma}{2} \right)^{0.6} \rho_{pulp}^{-0.6} \mathcal{E}^{-0.4}. \quad (3.118)$$

3.11 SUMMARY

The flotation recovery model can predict recovery provided the bubble surface coverage, attachment rate constant, bubble size, fraction of total hydrogen resulted in gas bubbles are known. The maximum floatable particle size has also an influence on predicting the recovery. To account for this factor, a new parameter K_4 has been

introduced to predict the recovery. The bubble-particle aggregate stability and buoyancy force to lift this bubble-particle aggregate to the froth layer both are considered to compute this maximum floatable particle size. Once this maximum floatable particle size is known, the factor K_3 can be computed from the feed size distribution.

The analysis described in Section 3.9.1 can be used to determine the detachment diameter as a function of electrode curvature, contact angle, interfacial tension and liquid density. For a given fraction of the total rate of hydrogen production at a given current density, the rate of bubble production can be obtained, along with the dissolved hydrogen concentration gradient in the bulk. From this information the growth and eventual equilibrium bubble diameter can be determined.

The hydrogen fraction resulting in gas bubbles is an important factor in electroflotation. The prediction of both recovery and bulk bubble size depends on this hydrogen fraction. Hence experiments were performed to determine this gas fraction. The experimental observations have been discussed in Chapter 5.

The maximum bubble size and Sauter mean bubble size produced by the mechanically agitated Denver cell can be estimated using Equations 3.109 and 3.118 provided the energy dissipation, power number critical Weber number, and impeller dimension and rotation are known.

Chapter 4

EXPERIMENTAL METHODOLOGY

4.1 INTRODUCTION

In this chapter the materials and methods used in the experimental observations are reported in such a way that any of the experiments can be reproduced. The experimental program involved two types of cells, i.e., a Denver cell and an electrochemical cell. The recovery of silica using sparged air and hydrogen was determined by Denver cell experiments, while the recovery of silica using electrolytically generated hydrogen bubble was carried out by electrochemical cell experiment. The hydrogen bubble size and hydrogen gas generation rate were also measured by electrochemical cell experiment. Table 4.1 outlines a brief description (type of test, cell used, parameters measured and purpose of the test) of the experiments performed as a part of this study.

Table 4.1 Summary of all test performed

Types of test	Cell used	Parameter to be measured	Specific purpose of the test
Recovery of silica using sparged air bubbles by a conventional flotation cell	Denver flotation cell (Type D12)	Mass of floated water and silica, flotation time	Interaction of silica with air bubbles
Recovery of silica using sparged hydrogen bubbles by a conventional flotation cell	Denver flotation cell (Type D12)	Mass of floated water and silica, flotation time	Interaction of silica with hydrogen bubbles
Visualization and measurement of hydrogen bubbles produced by electrolysis of water without any influence of external flow	Electrochemical cell (a rectangular glass cell, platinum cathode and anode)	Bubble diameter, and number of bubble	Determination of detached and bulk diameter of bubble without any external liquid flow
Visualization and measurement of hydrogen bubbles produced by electrolysis of water with the influence of external liquid flow	Electrochemical cell (a rectangular glass cell, platinum cathode and anode)	Bubble diameter, and liquid flow	Determination of detached and bulk diameter with external liquid flow
Production and capture of hydrogen gas from electrolysis of water	Electrochemical cell (a cylindrical Perspex cell, stainless steel mesh cathode, carbon anode)	Volume of hydrogen gas, electrolysis time	Determination of hydrogen bubble production rate
Recovery of silica as a function of mass fraction by electrolytically generated hydrogen bubbles	Electrochemical cell (a glass beaker, stainless steel mesh cathode, carbon anode)	Mass of floated silica, solids concentration, time of flotation	Effect of particle mass fraction on flotation recovery and bubble surface loading
Recovery of silica as a function of current density and particle size by electrolytically generated hydrogen bubbles	Electrochemical cell (a rectangular Perspex cell, stainless steel mesh cathode, platinum anode)	Mass of floated silica, time of flotation, particle size, current density	Effect of particle diameter and gas flow rate on flotation recovery and bubble surface loading
Sessile drop measurement	Perspex rectangular cell	Contact angle	Measurement of contact angle of air-water-silica and hydrogen-water-silica
Pendant drop measurement	Perspex rectangular cell	Surface tension	Measurement of surface tension of gas-liquid interface

4.2 MATERIALS

4.2.1 Silica

Silica (supplied by Unimin, Australia) of brand name 60G and 400G was used as feed mineral in flotation and gas collection experiments. The size distribution of 60G and 400G silica was very wide. Hence, a combination of Cyclosizing (Warman, SY300-M6), wet sieving (passing through sieve of 20 and 15 μm opening), and particle settling was applied to the 400G silica material to obtain different silica samples with narrower size distributions.

4.2.2 Electrodes

Platinum (99.99% purity) and stainless steel wire bought from Sigma Aldrich of different diameters were used as electrodes in the bubble size measurement experiments. Stainless steel mesh and carbon rod were used as the cathode and anode, respectively, in both electroflotation recovery and gas collection experiments.

4.2.3 Reagents

Cetyl trimethyl ammonium bromide (CTAB; Sigma Aldrich, $\geq 98\%$ pure) and methyl isobutyl carbinol (MIBC; 4-methyl-2-pentanol; Merck, Germany, 98% pure) were used as collector and frother, respectively. The water (Milli-Q) used was produced by a Millipore filtration system, with an internal specific resistance of 18.2 $\text{M}\Omega/\text{cm}$.

For the electroflotation experiments an electrolyte (inorganic salt) was required to make the solution conductive enough for charge transfer. Unfortunately, its presence can have a depressant effect on flotation which depends on the adsorption mechanism of inorganic salts onto the mineral surface. Divalent cations such as Ca^{2+} , Mg^{2+} or Ba^{2+} are specifically adsorbed and can lead to a positive surface charge (Clark and Cooke, 1968). Hopstock et al. (1968) investigated the depressant effects of sodium, calcium and magnesium ions on the flotation of quartz using amine salts as the collector. They concluded that monovalent Na^+ ions have much less effect compared to divalent Ca^{2+} and Mg^{2+} ions, as Na^+ merely acts as a counter ion and is not specifically adsorbed. Onoda and Fuerstenau (1964) also showed that as barium is divalent and specifically adsorbed, lower concentration of barium salts are required to depress flotation of quartz as compared to sodium salts. For quartz, the adsorption of divalent cations onto the

solid surface is four times higher than that for sodium (Clark and Cooke, 1968). For this reason, sodium sulphate (A.C.S. Reagent grade; Sigma Aldrich) was used as the electrolyte.

Ammonium hydroxide (ammonia content 28-30% by weight; A.C.S. Reagent grade; Sigma-Aldrich), hydrogen peroxide (30% by weight; analytical reagent grade; Chem Supply), and hydrochloric acid (analytical reagent grade; Ajax Finechem) were used for cleaning the silica surface.

Analytical reagent grade sodium hydroxide and nitric acid bought from Sigma Aldrich were used for controlling the pH of the suspension.

4.3 CLEANING METHODS

4.3.1 Cleaning of Glassware

All the glassware was first immersed in concentrated sodium hydroxide solution of pH above 12 in a sonication bath for at least 30 min to remove any organic contamination. The glassware was then thoroughly rinsed with ultrapure water (produced from Millipore filtration system with an internal resistance of 18.2 M Ω /cm). Following this the glassware was immersed in 1 M nitric acid solution overnight to remove any metal complexes, and then rinsed thoroughly with Millipore water. Finally, the glassware was dried overnight in a clean oven at 105°C.

4.3.2 Cleaning of the Silica Surface

The surface of silica may be contaminated by organic contaminants and/or metal complexes. Since, these organic contaminants or metal complexes may interfere with the flotation process, cleaning of the silica surface was essential before its use in flotation experiments. There are various methods available in the literature that can be used to clean the surface of silica (e.g., (Kern and Puotinen, 1970, Dai et al., 1998, Laskowski and Kitchener, 1969)). In this study, acidic and basic hydrogen peroxide solution was used for the cleaning of silica surfaces. Hydrogen peroxide solution at high pH is particularly effective for removing organic contaminants by oxidation; while at

low pH it is effective for desorbing metal contaminants primarily by complexing (Kern and Puotinen, 1970). These two sequential cleaning solutions ($\text{NH}_4\text{OH}-\text{H}_2\text{O}_2-\text{H}_2\text{O}$) and ($\text{HCl}-\text{H}_2\text{O}_2-\text{H}_2\text{O}$) was devised for cleaning of silica surfaces and reported in Table 4.2.

Table 4.2: Cleaning methods used in this study

Method	Steps
1	30 min incubation in 1:1:5 $\text{NH}_4\text{OH}:\text{H}_2\text{O}_2(30\%):\text{H}_2\text{O}$ at 80°C , Rinse in water
2	Method 1+additional incubation (30 min) in 1:1:5 $\text{HCl}:\text{H}_2\text{O}_2(30\%):\text{H}_2\text{O}$ at 80°C , Rinse in water

4.4 DENVER CELL: COMPARISON OF RECOVERY

In order to investigate the interaction of the gas phase (air and hydrogen) with the mineral surface, an experiment was designed to recover silica using air and hydrogen as the gas inputs. To facilitate the use of the same superficial gas velocity and bubble size, a conventional bubble generation machine (mechanically agitated Laboratory Denver cell, Type D12) was used with air and molecular hydrogen as the gas inputs. To maintain the similarity, all the experimental parameters except the choice of gas were kept the same in both sets of experiments. However, it should be noted that molecular hydrogen gas was used here, but in electroflotation, electrolytic hydrogen gas was produced. Electrolytic gases may cause significant oxidation-reduction reactions on mineral surfaces compared to the molecular gases, particularly on the sulphide minerals (Mallikarjunan and Venkatachalam, 1984). Volumetric flow rate of gas was measured using a rotameter, and corrected for the density of gas, as discussed below.

4.4.1 Calibration of Rotameter

As the rotameter is designed and calibrated for measuring the flow of air, it should be calibrated before being used for hydrogen. In a rotameter, mass rate, G (kg/s) is expressed as (Coulson et al., 1990):

$$\dot{m} = C_R A_2 \sqrt{\frac{2g(\rho_{ft} - \rho_G)\rho_G V_{ft}}{A_{ft} \left\{ 1 - \left(\frac{A_2}{A_1} \right)^2 \right\}}}, \quad (4.1)$$

where C_R is a constant, ρ_{ft} is the density of the float, ρ_G is the gas density, V_{ft} is the float volume, A_{ft} is the float area, A_1 is the cross-sectional area of the tube, and A_2 is the cross-sectional area of the annulus between the float and the tube.

Equation 4.1 can be re-written as:

$$Q_G \rho_G = K_5 \sqrt{(\rho_{ft} - \rho_G)\rho_G}, \quad (4.2)$$

where

$$K_5 = C_R A_2 \sqrt{\frac{2gV_{ft}}{A_{ft} \left\{ 1 - \left(\frac{A_2}{A_1} \right)^2 \right\}}}. \quad (4.3)$$

For the same rotameter K_5 is constant. As $\rho_{ft} \gg \rho_G$, $\rho_{ft} - \rho_G \approx \rho_{ft}$, putting this value in Equation 4.2 we have:

$$Q_G = K_5 \sqrt{\frac{\rho_{ft}}{\rho_G}}. \quad (4.4)$$

As ρ_{ft} is constant, Equation 4.4 can be re-written as:

$$Q_G = \frac{K'}{\sqrt{\rho_G}}, \quad (4.5)$$

where

$$K' = K_5 \sqrt{\rho_{ft}} . \quad (4.6)$$

For airflow and hydrogen flow Equation (4.5) becomes:

$$Q_{Air} = \frac{K'}{\sqrt{\rho_{Air}}} , \quad (4.7)$$

$$Q_{Hydrogen} = \frac{K'}{\sqrt{\rho_{Hydrogen}}} . \quad (4.8)$$

From these equations we can get:

$$Q_{Hydrogen} = Q_{Air} \sqrt{\frac{\rho_{Air}}{\rho_{Hydrogen}}} . \quad (4.9)$$

Using the molecular weight of air (29) and hydrogen (2), ρ_{air} and $\rho_{Hydrogen}$ can be computed as 1.29 kg/m^3 and 0.089 kg/m^3 , respectively. Putting these values in Equation 4.9 we have:

$$Q_{Hydrogen} = 3.80715 Q_{Air} . \quad (4.10)$$

By using Equation 4.10, the actual flow of hydrogen can be calibrated from the flow shown by the rotameter. The calibrated values are presented in Table 4.3.

Table 4.3: Calibrated flow of hydrogen gas

Rotameter reading (lpm)	Actual flow of hydrogen (lpm)
1.1	4
1.6	6
2.1	8
2.6	10

4.4.2 Methodology

A 2.4 L laboratory flotation machine (Denver, Type D12) was used to float 60G silica (mean particle diameter, d_{50} , of $36.7 \mu\text{m}$ as determined by a Malvern Mastersizer). The size distribution is shown in Figure 4.1. Two sets of experiments were carried out using sparged air and hydrogen. To maintain similarity, all the experimental parameters except the choice of gas (including flow rate) were kept the same for both sets of experiments. In all the tests, the initial solids concentration and the frother (MIBC) concentration were fixed at 2.0% (w/w) and 29 ppm, respectively. The collector concentration (CTAB) was varied between $4.4\text{-}27.4 \times 10^{-6}$ M. Electrolyte concentration (Na_2SO_4) was varied between 0.0052-0.1M. The pH of the suspension was varied from 9 to 10.5. The Milli-Q water was used for making all the solutions, while reverse osmosis water was used for making the suspension in the flotation cell. The silica surface was cleaned by the method mentioned in Section 4.3.2.

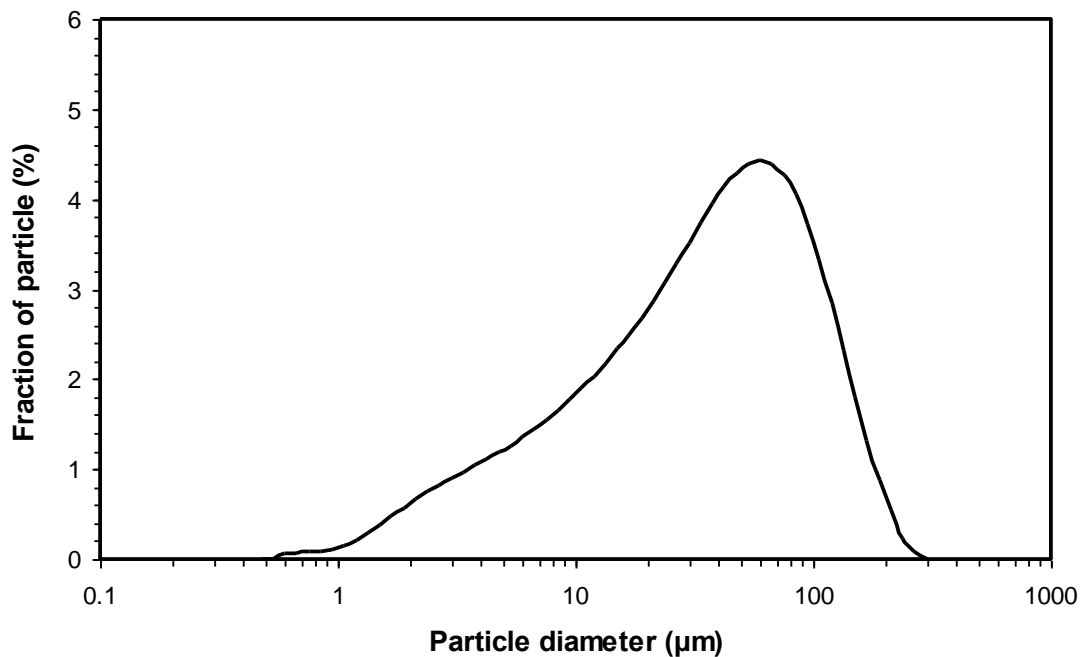


Figure 4.1: Size distribution of 60G silica
[$d_{50} = 36.7 \mu\text{m}$]

The Volumetric flow rate of gas was measured using a rotameter, and corrected for the density of the gas as shown in Table 4.3. The cell was mechanically agitated at a constant impeller speed of 630 rpm. A known amount of silica was transferred to the cell and was conditioned for 2 min, after which collector was added. Electrolyte and frother were added after a total of 5 and 6 minutes of conditioning, respectively. The total conditioning time was 7 minutes. During the conditioning process the pH of the suspension was adjusted using either NaOH or HNO₃. Compressed gas was then introduced with gradual increment of flow for 1 minute in order to produce a stable froth. The average froth height was 25 mm. Each flotation experiment lasted for 10 min. Make-up water, with the same concentration of collector, frother, electrolyte, and pH was added to the cell during the flotation to keep the water level constant in the cell. Blank experiments were conducted at different gas flow rates, and without addition of the collector to estimate flotation recovery due to entrainment. Typically, this amount was less than 3 % of the total recovery, as reported in Table 4.4. The entrained component was later subtracted from experimental recoveries to obtain the true flotation recovery. The flotation experiments were repeated at least twice, with the average and standard deviations reported.

Table 4.4: Values of entrainment as a function of gas flow rate

Gas flow (lpm)	4	6	8	10
Entrainment (%) (w/w)	0.6	1.4	1.7	2.2

4.5 ELECTROFLOTATION CELL: BUBBLE SIZE MEASUREMENTS

The experimental program was designed to investigate the size and flux (number of bubbles produced per unit surface area of cathode per unit time) of hydrogen bubbles produced by electrolysis of water as a function of current density, electrode geometry, surface preparation, as well as flow of electrolyte. The experimental program was also devised to investigate the wide variation in reported bubble sizes across the literature and to remove such variation. An electrochemical cell was used for bubble production. The growth of the bubbles as they moved away from the electrode surface was also measured.

4.5.1 Apparatus

A schematic of the experimental apparatus is shown in Figure 4.2, whereas a photograph is shown in Figure 4.3. It consisted of an open-top Pyrex glass cell with dimensions 50 mm wide \times 50 mm deep \times 15 mm high, which housed the electrolyte solution and electrodes. The platinum anode (oxygen producing electrode) was placed at the rear corner of the cell, while the platinum cathode (hydrogen producing electrode; $D = 90, 120$ and $190 \mu\text{m}$) was placed in the front of the cell to allow viewing of the bubble formation process. The viewing surface of the cathode, where the bubble formation process was observed, comprised a horizontal length, L_c , of approximately 5 mm. The remainder of the cathode was coated in clear lacquer to insulate it from the solution. An isosceles right-angled triangular prism, microscope (ZEISS Stemi 2000-C) with magnification 100X, high speed video (Phantom V 4.0) arrangement, as shown in Figure 4.2, were used to observe the formation, detachment and rise of individual bubbles.

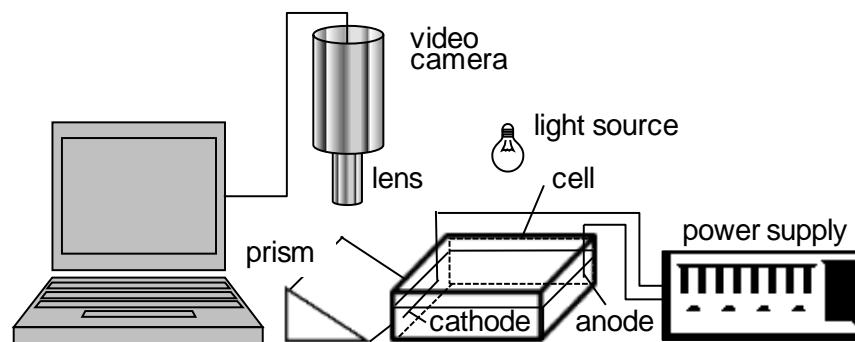


Figure 4.2: Schematic of experimental apparatus for bubble size measurement

In Figure 4.2 the microscope was placed in vertical position and the prism was placed under the objective of the microscope. The hypotenuse side of the prism had a mirror surface and was supported by a stage in such a way that the prism produced a horizontal image of the vertical plane through the axis of the wire. The cell was illuminated using a double lens optical fibre light source. A peristaltic pump was used for creating a flow of electrolyte in the cell.

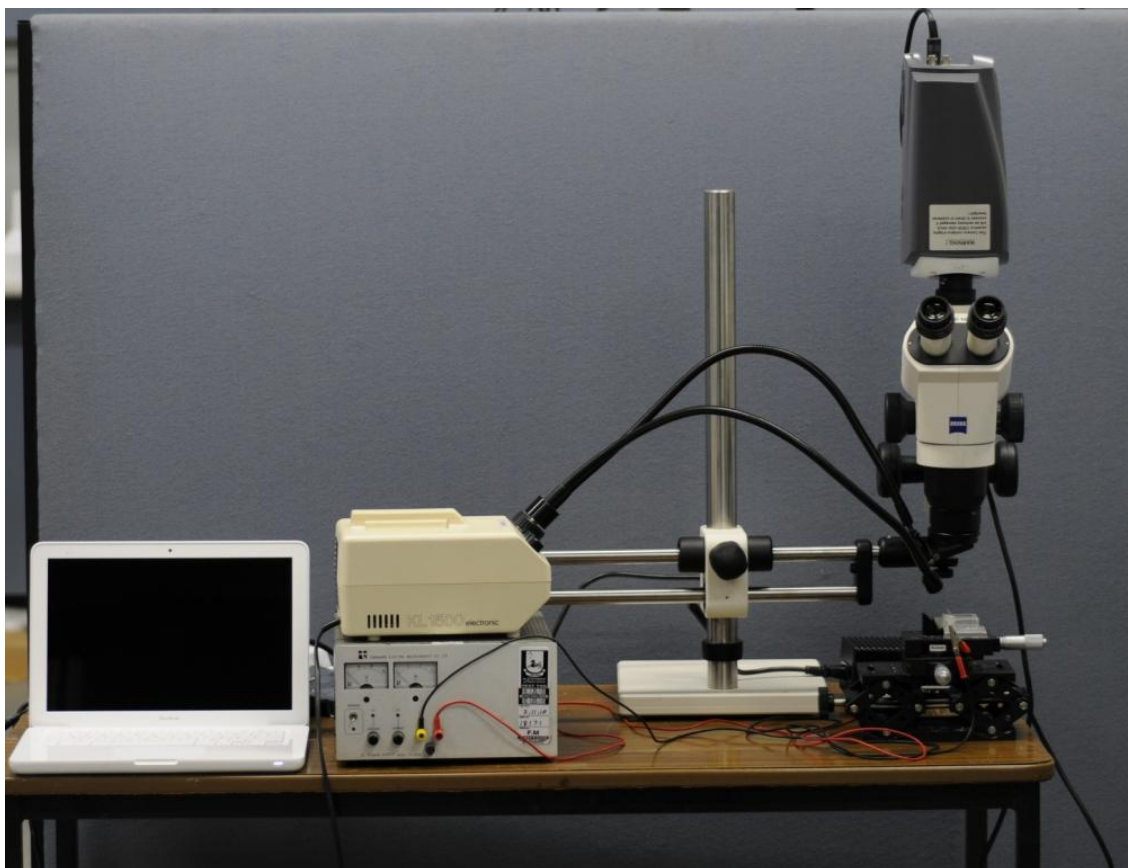


Figure 4.3: Photograph of experimental apparatus for bubble size measurement

4.5.2 Procedure

The platinum wire was cleaned mechanically by rubbing with a soft and clean cloth before being immersed in aqua regia (1 HNO_3 : 3 HCl) for 2 minutes. After rinsing thoroughly with Milli-Q water, the wire was placed in the cell. The cell was then filled with 0.1 M HNO_3 and electrolysis was carried out with changing polarity for 3 minutes. The cathodic polarity was aimed at reducing any oxides, while the anodic polarity was aimed at oxidizing any organics present. The procedure was carried out twice. Experiments were also conducted using a platinised wire. Platinisation was carried out using a 3% chloroplatinic acid (+ 0.2% lead acetate) solution at a current density of 350 A/m^2 for 5 minutes. The electrode was then rinsed and stored in Millipore water prior to use.

Hydrogen bubbles were also produced in the presence of an upward liquid flow along the circumference of the cathode. A peristaltic pump was used for generating the flow of electrolyte in the cell. The tube creating inflow into the cell was placed below the

cathode, while another tube for outflow from the cell was placed at the rear end of the cell. First, the peristaltic pump was switched on to create a flow of electrolyte. When a steady flow of electrolyte was established, the current was turned on to commence the bubble production experiment. The inflow tube below the cathode created an upward flow of electrolyte solution along the circumference of the cathode.

Prior to the commencement of an experiment the cell was rinsed thoroughly with Milli-Q water. It was then filled with 0.2 M Na₂SO₄ electrolyte and adjusted to pH 9.5 using either 0.1 M nitric acid or 0.1 M sodium hydroxide. A home-made power source was used to supply a stable DC current density between 150-360 A/m² of exposed cathode surface. A summary of the cathode current conditions is given in Table 4.5.

Table 4.5(a): Cathode dimensions and current density values for bubble production experiments from platinum wire without any external fluid flow

D (μm)	L _C (μm)	\dot{i}					
		μA	A/m ²	μA	A/m ²	μA	A/m ²
90	5300	228	152	379	253	530	354
120	5250	300	152	500	252	700	354
190	5500	497	151	829	253	1161	354

Table 4.5(b): Cathode dimensions and current density values for bubble production experiments from platinum wire experiencing external fluid flow

D (μm)	L _C (μm)	\dot{i}	
		μA	A/m ²
90	5300	530	354
190	5250	1110	354

At the instant the current was applied the experiment was deemed to have commenced; i.e., $t = 0$ s. At $t = 30$ s, the Phantom V4.0 high speed video camera was used to capture images of the hydrogen bubbles at 1000 fps as they were generated and transported away from the cathode surface. Still images from the video recordings were later analysed using OPTIMAS 6.5 software to obtain bubble diameter as a function of time and position relative to the top of the wire.

4.5.3 Liquid Velocity Determination

The bubbles moving upward were used as tracers for determining the velocity of fluid. The upward velocity of electrolyte solution was measured by measuring the velocity of individual moving bubble. The velocity of the bubble in an external fluid flow, $(v_b)_f$, was measured by:

$$(v_b)_f = \frac{d}{t}, \quad (4.11)$$

where d is the distance travelled by the bubble experiencing external fluid flow and t is the time of travel. In a surfactant free solution, bubbles have internal circulation which reduces the drag force that opposes the velocity. Hence, for a surfactant free solution, the theoretical velocity of the bubble without experiencing any external fluid flow, $(v_b)_t$, was determined using the Hadamard-Rybczynski equation (Clift et al., 1978); i.e.,

$$(v_b)_t = \frac{d_b^2 (\rho_{pulp} - \rho_G) g}{12\mu}, \quad (4.12)$$

The velocity of the fluid, v_f , then can be obtained by:

$$v_f = (v_b)_f - (v_b)_t. \quad (4.13)$$

4.6 ELECTROFLOTATION CELL: HYDROGEN GAS FRACTION

The experimental program described the measurement of hydrogen gas generation rate produced by electrolysis of water. The gas generation rate was investigated as a

function of solids concentration, mechanical agitation, presence of pre-existing dissolved gases and current density.

4.6.1 Apparatus

The experimental apparatus used to measure the rate of hydrogen gas production is shown in Figure 4.4. It consisted of a cylindrical Perspex® tube with 60 mm inner diameter and 75 mm high. A stainless steel screen 33 mm × 29 mm with wire diameter 0.400 mm and total surface area of 1548 mm² was used as the cathode, while a carbon rod was used as the anode. The cathode was placed horizontally 15 mm above the bottom of the cell. An air-tight PVC cap was placed at the top of the cell. A cylindrical hole was made at one corner of the cap for placing a glass tube inside the hole. The glass tube was lowered to the bottom of the cell preventing the hydrogen gas produced at the cathode entering into the glass tube. The anode was placed inside the glass tube and positioned 25 mm above the bottom. This also prevented the oxygen produced at the anode from being involved in the collection process. A graduated burette was used for collecting the hydrogen gas. The burette was filled with water and placed in a water beaker keeping the open end downward. A plastic tube was inserted inside the open end of the burette. The other end of the plastic tube was inserted in a hole at the middle of the cap of the electrochemical cell. The inside surface of the cap was tapered so that the hydrogen bubbles were channelled directly into the outlet tube. A magnetic stirrer was used to homogenize the solution.

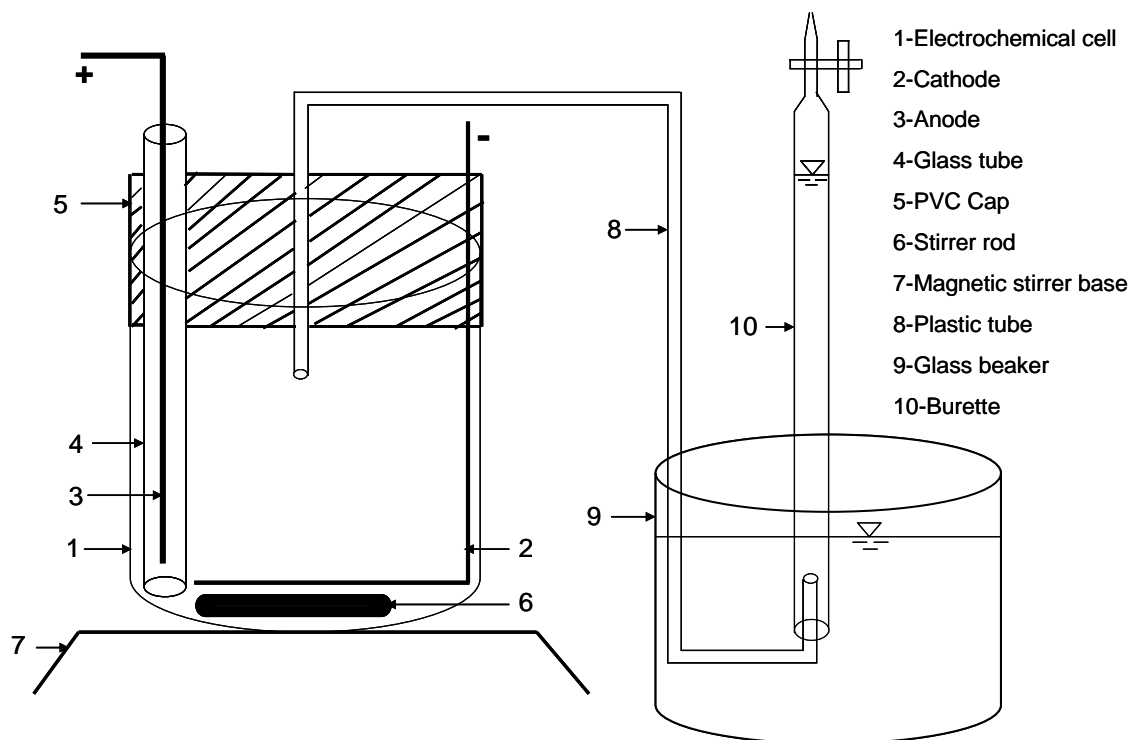


Figure 4.4: Apparatus used for hydrogen gas collection

4.6.2 Methodology

The steel wire was first cleaned mechanically by a soft, clean cloth. The assembled cell was then filled with 0.1 M HNO_3 and the steel wire cathodically electrolysed for 2-3 minutes to remove any oxides. The cell was then emptied and rinsed thoroughly with Millipore water. The anode and cathode were connected to a DC power supply and when switched on the evolving hydrogen gas was captured by the burette as a function of time. Experiments were carried out at current densities, \dot{I} , of 129 and 258 A/m^2 (see Table 4.6) of wire surface for the following conditions:

Table 4.6: Current density values used in gas collection experiments

Wire diameter (mm)	Cathode area (mm^2)	Absolute current, I (A)	Current density, \dot{I} (A/m^2)
0.4	1548	0.2	129
		0.4	258

1. With and without dissolved gases present: Electrolyte solution prepared from Millipore water will normally already contain levels of dissolved oxygen and nitrogen. Degassed electrolyte solution was prepared by heating to 100°C for a period of 30 minutes and then quickly transferred to an airtight container and allowed to cool prior to use.
2. With and without mechanical agitation: To observe the effect, if any, of dissolved gas concentration gradient in the vicinity of the cathode.
3. With non-floatable solids present: To observe the effect, if any, of the presence of non-floating solids (non-floatable, without using a collector) concentration in the electrolyte solution. Gas collection was also performed as a function of solids (non-floatable, without using collector) concentration in the electrolyte solution. The silica used for these experiments was Sample ID 1 (see Table 4.7; the size distribution is shown in Figure 4.5).

Table 4.7: Particle size distribution

Sample ID	Size range ¹ (μm)	(d_p) ₅₀ (μm)	Used for studying:
1	-39.9+0.1	15.0	Effect of solids concentration on: (1) hydrogen gas production; (2) flotation recovery and bubble surface coverage
2	-14.2+0.8	3.1	Effect of particle diameter and gas flow rate on flotation recovery and bubble surface coverage.
3	-25.2+1.1	5.3	
4	-39.9+2.8	12.3	
5	-50.2+5.6	14.7	

¹ See Appendix C for volume fractions for each size interval

Each experiment was repeated at least twice, with the average value and standard deviation reported.

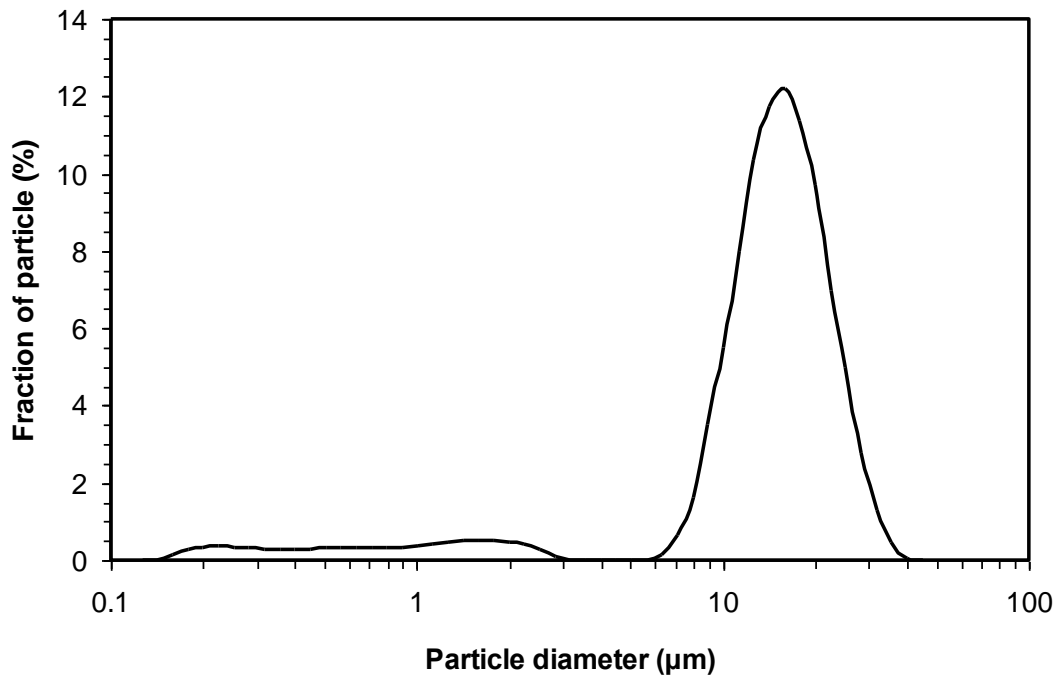


Figure 4.5: Size distribution of silica sample ID 1
 $[(d_p)_{50}=15.0 \mu\text{m}]$

4.7 ELECTROFLOTATION CELL: SILICA RECOVERY USING STAINLESS STEEL MESH CATHODE

An experimental program was devised to investigate the flotation recovery of silica by electrolytically generated hydrogen bubbles of different diameters. The recovery was investigated as a function of current density, solids concentration and particle size. The measured flotation recovery was also compared with model predictions. For model predictions, the sizes of hydrogen bubbles were required to be known. Therefore, the experimental program included the measurement of hydrogen bubble sizes produced from stainless steel wire cathode as a function of current density and electrode geometry.

4.7.1 Materials

Silica of different size fractions as listed in Table 4.7 was used for electroflotation experiments. Before using in flotation experiments the silica surface was cleaned by the method mentioned in Section 4.3.2. The Milli-Q water was used for making all the solutions, and the suspension in the flotation cell. For all experiments carried out in this

study the following reagent conditions were applied: (1) a pH of 10 was maintained using a combination of 0.1 M NaOH or HNO₃; (2) the collector [CTAB] concentration was fixed at 4.46×10⁻⁵ M; (3) frother [MIBC] concentration was fixed at 30 ppm; and (4) the sodium sulphate concentration was fixed at 0.2 M.

For the flotation experiments at varying solids loadings a stainless steel screen 33 mm ×29 mm with wire diameter of 0.400 mm and total surface area of 1548 mm² was used as the cathode, while a carbon rod was used as the anode. For the flotation experiments using varying current densities and particle sizes a stainless steel screen 23 mm ×20 mm with wire diameter of 0.190 mm and total surface area of 409 mm² was used as the cathode; while a platinum wire of 0.190 mm diameter was used as the anode. For both types of cathode the steel wire was first cleaned mechanically by a soft, clean cloth. The assembled cell was then filled with 0.1 M HNO₃ and the steel wire cathodically electrolysed for 2-3 minutes to remove any oxides. The cell was then emptied and rinsed thoroughly with Millipore water. For the bubble size measurement experiment a steel wire of 0.190 mm diameter was used as the cathode while a platinum wire was used as anode.

4.7.2 Methodology

Flotation experiments at varying solids concentrations: A 250 mL glass beaker was used for the electroflotation of silica as a function of solids concentration. A magnetic stirrer bar was placed in the bottom of the beaker. Approximately 285 mL of silica (sample ID 1, see Table 4.7) solution, at solids concentrations of 2-20% by weight (see Table 4.8), was transferred to the beaker and conditioned for 5 minutes, after which time the collector was added. Electrolyte and frother were added after 10 and 11 minutes, respectively, with a further 1 minute of agitation giving a total conditioning time of 12 minutes. Electroflotation experiments were carried out over a two minute period at a constant current density of 775 A/m². During this time the froth height was maintained at 5 mm with the concentrate being regularly collected. The concentrate was then dried and weighed to determine the fractional mass recovery after two minutes of flotation. Each experiment was repeated at least twice, with the average value and percentage of error reported.

**Table 4.8: Solids concentration values for silica flotation experiments
using steel mesh of 400 μm wire diameter**

Wt. of solids (gm)	Wt. of liquid in the cell (gm)	Total wt. of solids +liquid (gm)	Solids (%)
5.9	286.0	291.9	2
10.3	283.6	293.9	3.5
14.8	280.0	294.8	5
22.9	278.0	300.9	7.6
30.8	277.0	307.8	10
47.7	270.0	317.7	15
65.9	263.3	329.2	20

Flotation experiments at varying current density and particle size: A rectangular electrochemical cell (23L×20W×50H mm³) as shown in Figure 4.6 was used for electroflotation experiments as a function of current density and particle size. No stirring of solids was performed in this case. The cathode was placed horizontally at the bottom of the cell, while the anode was confined within a vertical glass tube which prevented the oxygen bubbles from interacting with the suspended particles. The size distributions for the silica used in this experiment (sample ID 2-5; see Table 4.7) are shown in Figure 4.7. The 2% w/w silica solution was conditioned in an ultrasonic bath for 15 minutes to prevent aggregation from taking place. The collector, electrolyte and frother were added after 8, 13, and 14 minutes of conditioning, respectively. Electroflotation experiments were performed over a two minute period for four different particle sizes while current density ranged from 122-685 A/m² (see Table 4.9). Experiments were repeated at least twice and the average taken.

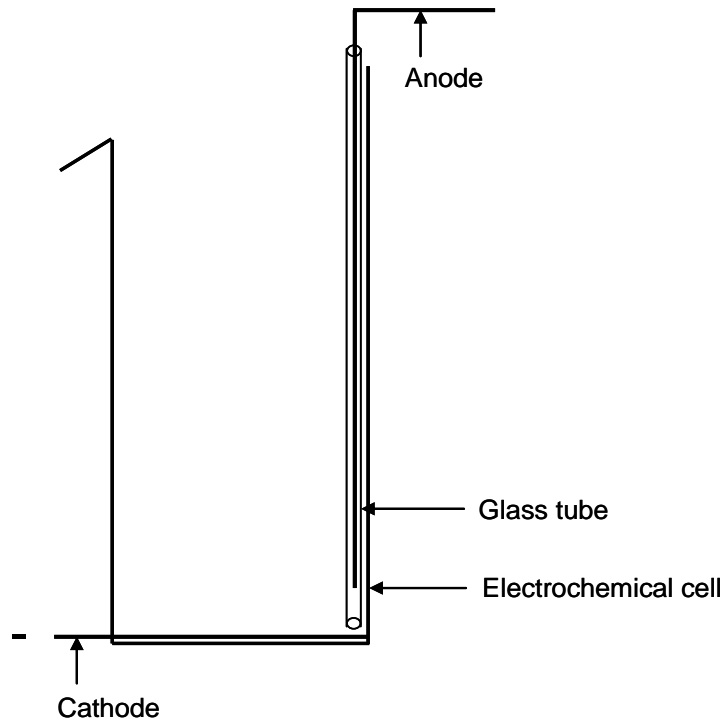


Figure 4.6: Schematic of experimental apparatus for floating silica by hydrogen bubble of 30 μm diameter

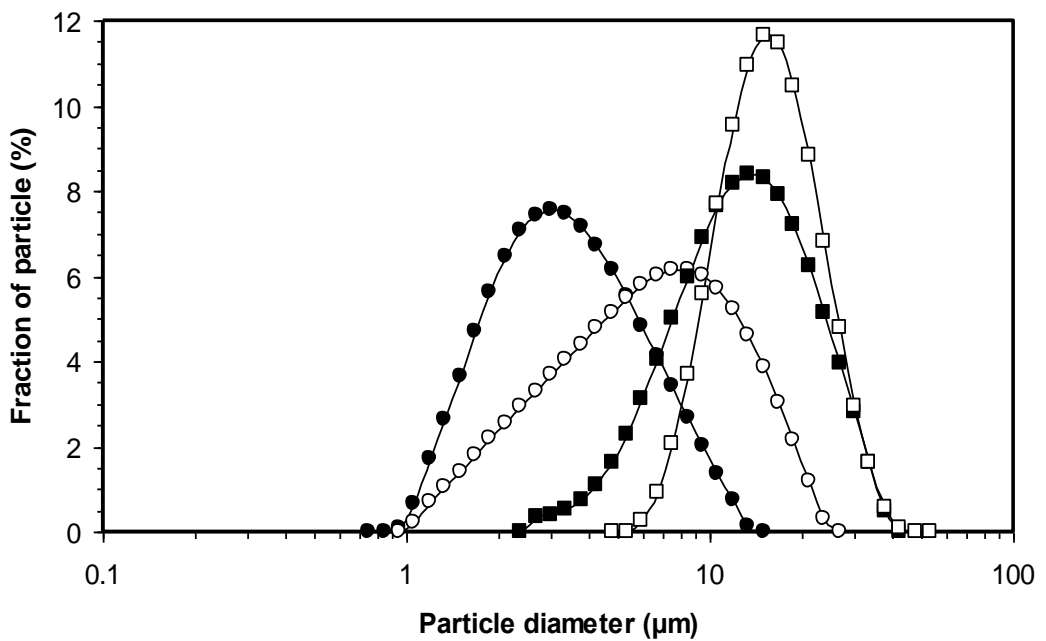


Figure 4.7: Size distribution of silica Sample ID 2-5
 $[d_{50} = (\bullet) 3.1, (\circ) 5.3, (\blacksquare) 12.3, (\square) 14.7 \mu\text{m}]$

Table 4.9: Current density values for silica flotation experiments using steel mesh

Wire diameter (mm)	Cathode area (mm ²)	Absolute current, I (A)	Current density, \dot{I} (A/m ²)
0.19	409	0.05	122
		0.08	196
		0.11	269
		0.14	342
		0.17	416
		0.2	489
		0.24	587

Bubble size measurement: For floating silica, hydrogen bubbles were produced from stainless steel mesh of wire diameters 190 and 400 μm . An experiment was devised to measure these hydrogen bubbles. In this experiment, stainless steel wire of diameters 190 and 400 μm were used as cathodes, whereas platinum wire of diameter of 190 μm was used as anode for electrolysis reactions. The bubble size measurement was performed with the apparatus described in Section 4.5.1. At first, steel wire was cleaned mechanically by a soft and clean cloth or tissue. The cell was then filled with 0.1 M HNO_3 and electrolysis was carried out for 2-3 minutes to reduce any oxides from steel cathode. The cell was then rinsed thoroughly with Milli-Q water. The procedure was repeated at least twice. Prior to the commencement of an experiment the cell was rinsed thoroughly with Milli-Q water. It was then filled with 0.1 M Na_2SO_4 electrolyte and adjusted to pH 10 with the help of 0.1 M HNO_3 or 0.1 M NaOH . A home-made power source was used to supply a stable DC current density between 122-775 A/m^2 of exposed cathode wire surface. A summary of the cathode current conditions is given in Table 4.10. The bubbles were captured and analysed by the method described in Section 4.5.2.

Table 4.10: Cathode dimensions and current density values for bubble production from stainless steel wire

Wire diameter (μm)	Wire length, L_c (μm)	Absolute current, I (μA)	Current density, \bar{I} (A/m^2)
190	4500	328	122
		525	196
		722	269
		919	342
		1117	416
		1314	489
		1576	587
400	5400	1753	258
		2630	388
		3945	581
		5260	775

4.8 CONTACT ANGLE MEASUREMENT

A computer-controlled apparatus (OCA 20 from Data Physics, Germany) was used to determine the contact angle of the air-silica-water and hydrogen-silica-water interfaces. A Perspex cell was filled with surfactant solution and placed in the path of a collimated light beam. A cleaned glass slide was placed over the cell. The glass slide was allowed to soak for 7 minutes in the same surfactant solution that used in the Denver cell experiments. A gas-tight micro syringe was then operated to form a gas bubble on the end of an inverted needle immersed in the solution. The bubble was allowed to attach to the glass slide. The recorded image was analysed to determine the contact angle. The contact angle was measured as a function of the concentration of CTAB, MIBC, and Na_2SO_4 in the flotation cell.

4.9 SURFACE TENSION MEASUREMENT

The pendant drop method was used here to measure the surface tension of the gas-liquid interface. A computer-controlled apparatus (OCA 20 from Data Physics, Germany) was

used for this purpose. A drop of the test liquid was formed out at the lower end of the dosing needle and the image of the drop was recorded. Later, the shape of the drop was analysed and fitted to the Young-Laplace equation by the software (SCA 20) to obtain the interfacial tensions. The interfacial tension was measured as a function of the concentration of CTAB, MIBC, and Na_2SO_4 in the flotation cell.

Chapter 5

RESULTS AND DISCUSSION

5.1 INTRODUCTION

This chapter outlines the results from experimental observations along with the model comparisons. Two types of cells e.g., Denver cell and electrochemical cell were used for the experimental observations. Denver cell was used for the comparison of flotation recovery of silica particles using air and molecular hydrogen as gas input. Electrochemical cell was used to 1) measure hydrogen bubble size produced from electrolysis of water, 2) measure hydrogen gas production rate and 3) determine flotation recovery of fine silica particles using electrolytic hydrogen bubbles. Model predictions for bubble size measurement, determination of gas fraction and flotation recovery have also been discussed.

5.2 DENVER CELL: COMPARISON OF RECOVERY

The surface chemistry of a particle suspension system may influence the flotation performance by altering the contact angle and induction time. The pH of the suspension and the adsorption of a collector on the particle surface, as well as the surface characteristics of the particle may affect its hydrophobicity. Due to the interaction with the gas phase, the surfaces of the mineral may experience changes in hydrophobicity, which may be beneficial or detrimental in improving the flotation recovery. In the literature there are studies that report improved flotation recovery using hydrogen and oxygen bubbles formed by electrolysis. Examples of improved recovery include that for cassiterite by hydrogen bubbles (Hogan et al., 1979a, Mamakov et al., 1969). For the recovery of manganese minerals (e.g., pyrolusite and psilomelane), electroflotation with hydrogen bubbles (92 to 95% recovery) is better than column flotation (Romanov et al., 1973). On the other hand, oxygen gas bubbles improve the recovery of chalcopyrite fines (Raju and Khangaonkar, 1982); pyrite fines (Glembotskii et al., 1975); and alumina (Khosla et al., 1995). Electrolytic oxygen makes the surface of the pyrite and other sulphide particles (chalcopyrite, sphalerite) so strongly hydrophobic that there is no need to use collectors.

The main reasons for the improved flotation, especially for fine particles (Mallikarjunan and Venkatachalam, 1984), include: (i) beneficial redox processes between the gas and mineral surfaces, and (ii) the very small (less than 50 μm diameter) bubble sizes known to be produced in electroflotation cells (Ketkar et al., 1988). Hence, it is important to investigate the interaction of mineral (silica; used in this study) surface with gas phase. However, the interaction of silica surface with oxygen bubble has not been studied in this study and only the interaction with hydrogen bubble has been studied here.

The flotation recovery of silica using air and hydrogen gases has been compared in this section. A laboratory-scale Denver cell was used to compare the flotation performance of sparged air and hydrogen gas at the same superficial gas velocity and bubble size to determine the influence, if any, of gas composition only. The effect of bubble size on flotation has not been considered here. The depressing effect of inorganic salt (sodium sulphate) on flotation was also investigated and the optimization of collector concentration was performed to minimize this depressant effect.

The flotation recoveries obtained at varying pH, gas flow rate, sodium sulphate and collector concentration are reported in Appendix D.

5.2.1 Air Only: Effect of pH on Silica Recovery

Figure 5.1 shows the recovery of silica at different pH values. All the experiments were conducted with constant values of collector (8.3×10^{-6} M, CTAB), electrolyte (0.05 M, Na_2SO_4) and gas (8 L/min). Air was chosen here as gas input. From Figure 5.1, it can be seen that optimum recovery occurs between pH 9.5 to 10, which is consistent with the theories of zeta potential, and contact angle as a function of pH. Gaudin and Fuerstenau (1955) reported that pH controls the extent of dissociation of silica, and the z.p.c of quartz lies between pH 2 to 3.7. However, Parks (1965) advised that the z.p.c of quartz lies at about pH 2 ± 0.2 . At lower pH values, the quartz surface exhibits a net positive charge and above pH 2.5 a net negative surface charge is furnished which increases with increased pH value. Since CTAB exhibits a positive ion (CTA^+) in hydrolysis, the maximum adsorption of CTAB will occur at a maximum negative surface charge of quartz. Estefan (1976) reported that maximum negative surface charge of quartz occurred at pH 10. Fuerstenau (1957) studied the contact angle of quartz in solutions containing dodecyl ammonium acetate as a function of pH and summarized that, from

pH 2 to 8, the contact angle increases slightly with increased pH, but a further increase in pH causes a sharp rise in contact angle to a maximum of about 80°; while at pH values above 11.6 the contact angle drops sharply reaching zero by pH 12.6. As pH of the solution controls the total double layer potential of quartz, the adsorption of all other ions by quartz are affected by pH (Gaudin and Fuerstenau, 1955).

The experimental result obtained in this study is also consistent with Estefan's investigation who reported a rapid flotation of quartz at pH 10. Other experimental observations (e.g., (Fuerstenau, 1957, Scott, 1983)) also reported that maximum flotation recovery occurred at pH near about 10. Therefore, the subsequent experiments were carried out at pH 10.

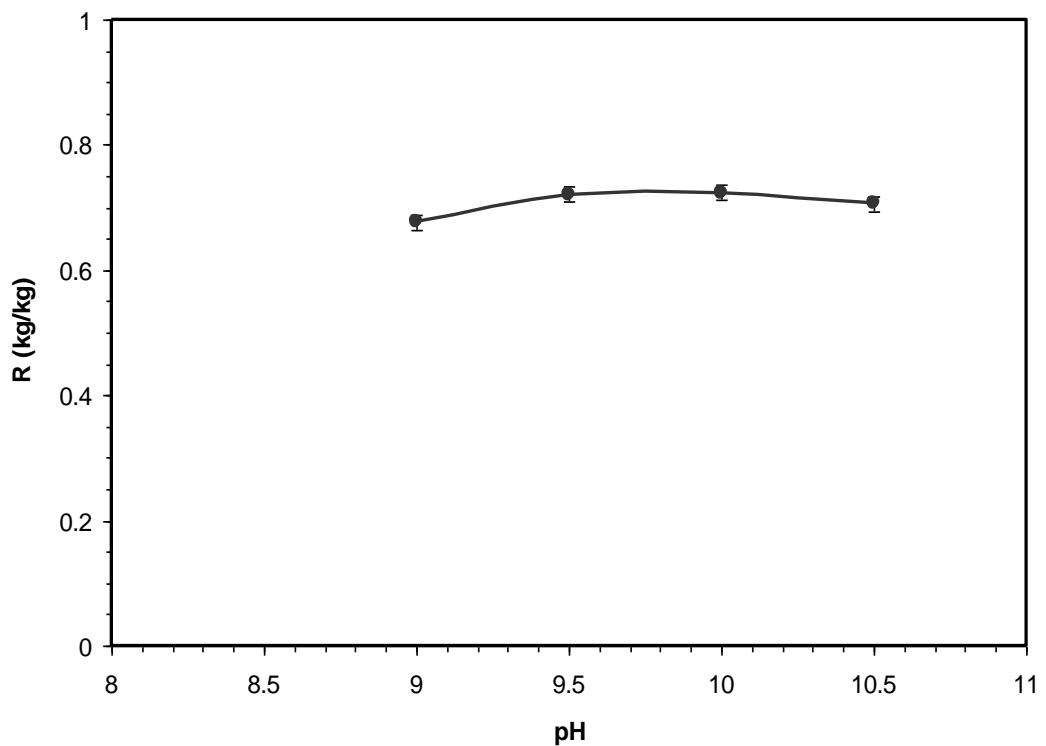


Figure 5.1: Flotation recovery vs. pH
[$T_{\text{exp}} = 10$ min; gas type=air; gas flow = 8 L/min;
CTAB = 8.3×10^{-6} M; $\text{Na}_2\text{SO}_4 = 0.05\text{M}$]

5.2.2 Air Only: Effect of Sodium Sulphate on Silica Recovery

Sodium sulphate was used as electrolyte in electroflotation. Unfortunately, its presence can have a depressant effect on flotation. Therefore, the depression effect of sodium sulphate to float silica particle was investigated here. Figure 5.2 illustrates the effect of sodium sulphate on the recovery of silica using air at a constant concentration of collector (6.64×10^{-6} M, CTAB), pH (10) and gas rate (8 L/min). It can be seen that the flotation recovery of silica was found to decrease linearly with increased concentration of Na_2SO_4 . This is consistent with the findings of Hopstock et al. (1968) who observed a reduction in recovery of quartz using dodecylamine collector with increased concentration of electrolyte (sodium chloride). In the flotation of quartz with amine salts as collector, the CTA^+ ion functions as counter ion in the electrical double layer at the solid-liquid interface. At a low concentration of collector, both positive ions (CTA^+ and Na^+) act as counter ions and are adsorbed only by electrostatic forces onto silica surfaces. This is consistent with the study of Onoda and Fuerstenau (1964), who investigated the flotation performance of quartz as a function of collector (dodecyl ammonium acetate) concentration in the presence of inorganic salts (sodium chloride and barium chloride). They concluded that at low concentrations, the adsorption mechanism of both ions seems to be similar, but must vary at high concentration. Due to ionic competition of CTA^+ and Na^+ ions, less CTA^+ ion were adsorbed on the silica surface to render it hydrophobic, and hence flotation of silica depressed at low collector concentration. The interaction of CTA^+ and Na^+ ions with the negatively charged silica surface is shown in Figure 5.3.

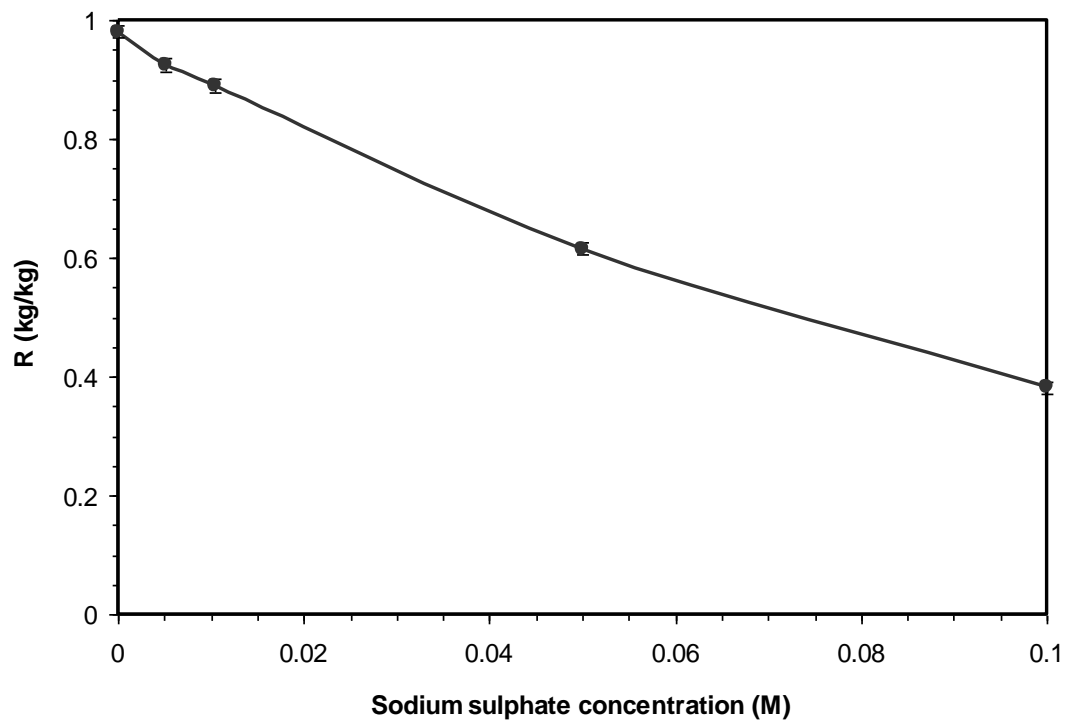


Figure 5.2: Flotation recovery vs. sodium sulphate concentration
[gas type = Air; $T_{\text{exp}} = 10$ min; pH = 10; gas flow = 8 L/min; CTAB = 6.64×10^{-6} M]

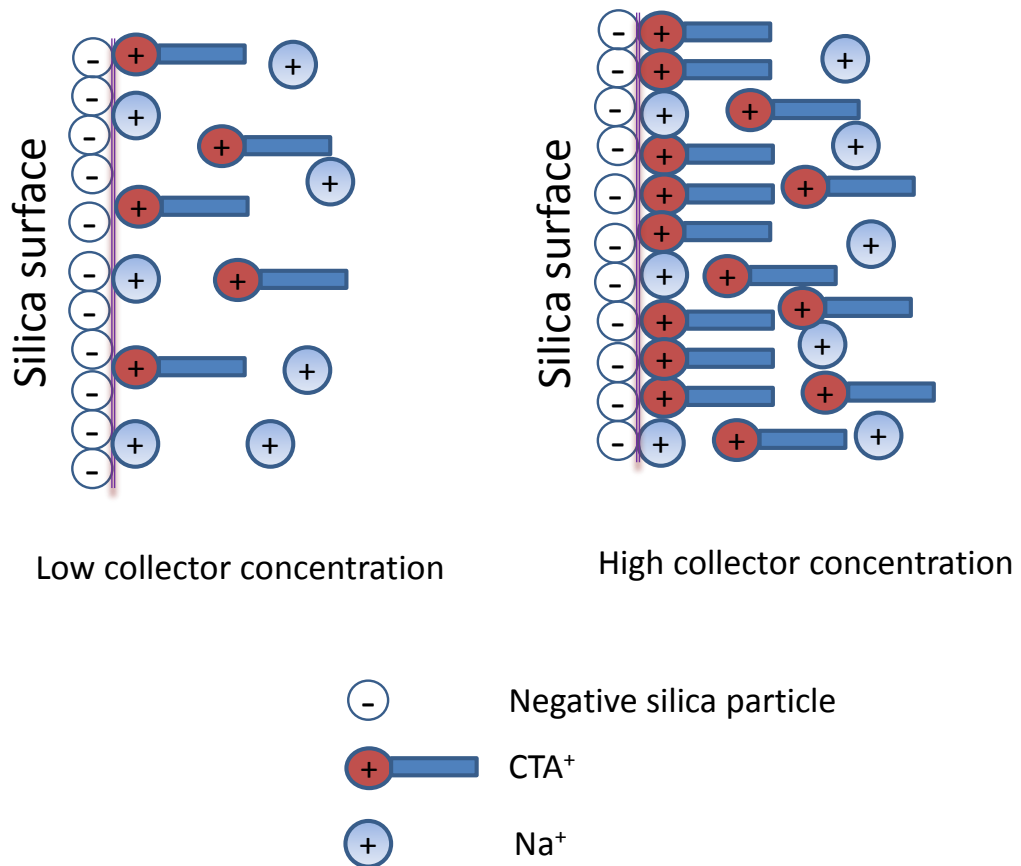


Figure 5.3: Interaction of CTA⁺ and Na⁺ ions with negatively charged silica surface

5.2.3 Air and Hydrogen: Effect of Gas Flow on Silica Recovery

Figure 5.4 shows the flotation recovery of silica at different gas flow rates using air and hydrogen. All the experiments were conducted with constant values of collector (8.3×10^{-6} M, CTAB), electrolyte (0.05 M, Na₂SO₄) and pH (10). It was found that flotation recovery increased with increased gas flow rate for both gases. The flotation rate constant increased linearly with increased superficial gas velocity, which was expected. There was essentially no difference between the flotation recoveries for both gases.

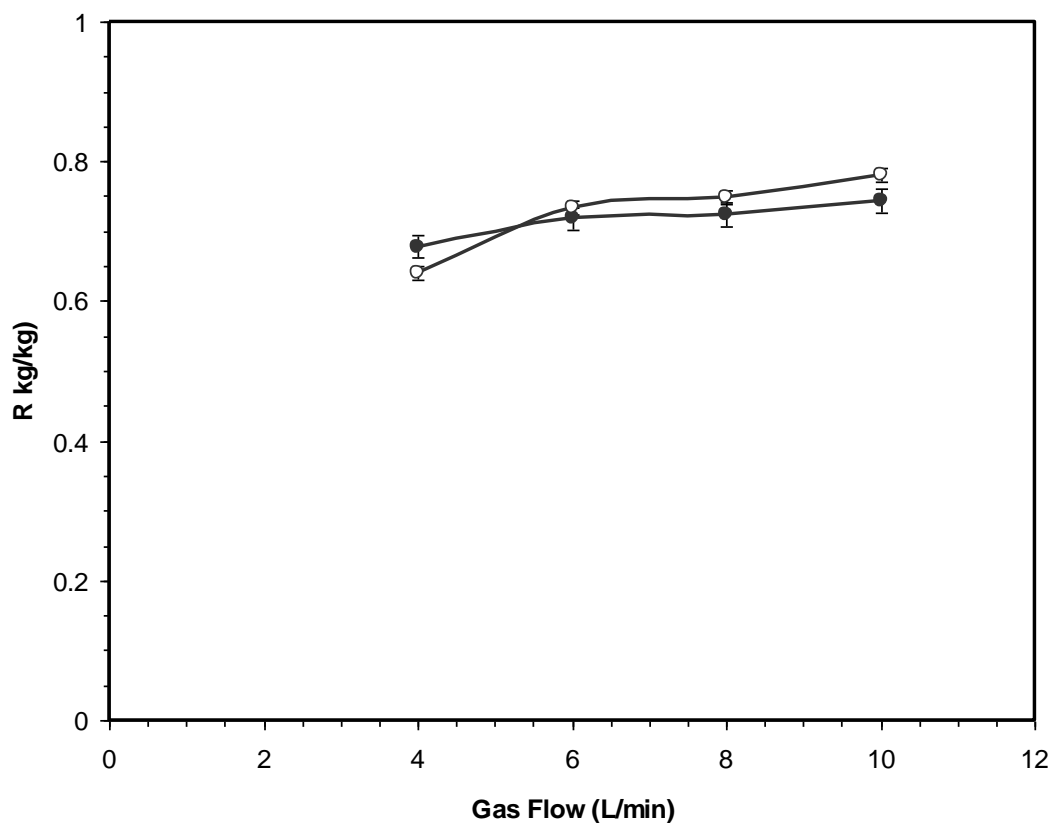


Figure 5.4: Flotation recovery vs. gas flow rate

[$T_{\text{exp}} = 10 \text{ min}$; $\text{pH} = 10$; $\text{CTAB} = 8.3 \times 10^{-6} \text{ M}$; $\text{Na}_2\text{SO}_4 = 0.05 \text{ M}$;
 gas type= (●) Air, (○) Hydrogen]

5.2.4 Air and Hydrogen: Effect of CTAB on Silica Recovery

Figure 5.5 compares the flotation recovery of silica as a function of collector concentration in the presence of 0.05 and 0.1 M sodium sulphate. Here experiments were carried out with constant pH (10) and gas flow rate (8 L/min). The recovery of silica remained the same at different collector concentration using both gases. For both gases, flotation recovery of silica increased with increasing the collector concentration. It was found that with the same concentration of collector, lower recovery of silica was observed with increased sodium sulphate while using both gases. However, as the concentration of collector was increased, the difference in recovery decreased for both gases. The depressant effect of inorganic salts on the flotation of quartz with amine collectors depends upon whether the collector ions are adsorbed as individual counter ions in the double layer through electrostatic attraction, or whether they have associated through van der Waals interactions of hydrocarbon chains. At lower concentration, the

adsorption mechanisms of collector ions and sodium ions seem to be similar (both collector and sodium ions are adsorbed only through electrostatic attraction by negative surface charge, and the competition for sites in the double layer occurs between both ions), but at higher concentration, the adsorption mechanism must differ (the collector is strongly adsorbed through both hydrocarbon chain interaction and electrostatic attraction; while inorganic salts are adsorbed only through electrostatic attraction) (Onoda and Fuerstenau, 1964).

It was also observed that the depressing effects of inorganic electrolyte remained the same for both gases. At higher concentrations, the collector was strongly adsorbed through hydrocarbon chain interaction; hence inorganic salts had little effect on flotation. This is in agreement with the flotation results obtained by Estefan (1976), who observed that the presence of 10^{-6} mole of Ca^{2+} ions insignificantly affected the rate of flotation of quartz at pH 10 where hemi-micelle formation of CTAB ions was completed.

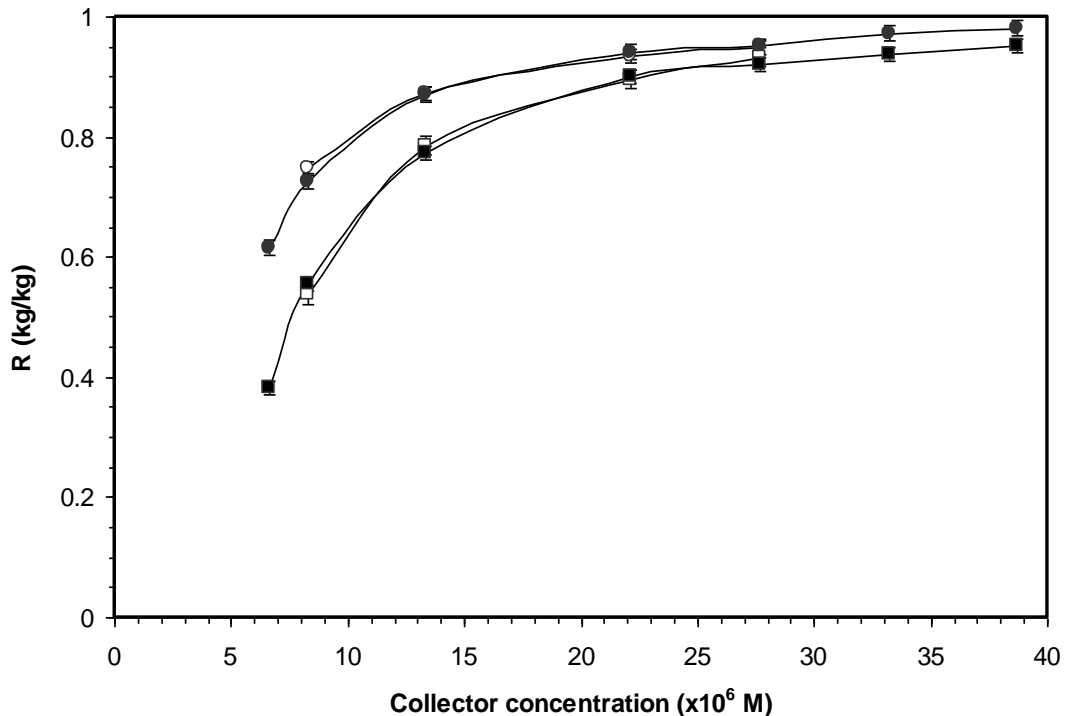


Figure 5.5: Flotation recovery vs. collector concentration

[gas type: at 0.05M Na_2SO_4 = (●) Air, (○) Hydrogen: at 0.1M Na_2SO_4 = (■) Air, (□) Hydrogen; $T_{\text{exp}} = 10$ min; pH = 10; gas flow = 8 L/min]

5.2.5 Comparison between Air and Molecular Hydrogen Flotation Recovery

The results in Figures 5.4 and 5.5 highlight the similarity in recovery for air and molecular hydrogen. It appears that for silica at least, gas composition has no influence on the flotation process. There is the possibility, however, that “competing” effects might somehow be cancelling each other out. Two possibilities for these competing effects are bubble size and induction time.

Bubble size

The Sauter mean diameter, $(d_b)_s$, in the Denver cell can be estimated using Equation 3.118. In the Denver flotation cell the energy dissipation is a function of gas flow rate, impeller geometry and rotational speed. In Equation 3.118, the only input for influence of gas type is the gas-liquid interfacial tension. Pendant drop measurements, using the 27.7×10^{-6} M CTAB:29 ppm MIBC:0.1M Na_2SO_4 solution, yielded a value of 0.065 N/m for both gases (see Appendix E). Therefore, the bubble size would be expected to be the same for both the air and molecular hydrogen. While the bubble size was not measured directly, application of drift-flux analysis to gas holdup measurements implied that the bubble size was the same for both sets of experiments (see Appendix B). Applying Equation 3.118 to the experimental conditions, $(d_b)_s$ was approximately 840 μm , which is consistent with those from other studies (Deglon et al., 2000, Gorain et al., 1997, Jameson and Allum, 1984, Girgin et al., 2006, Grau and Heiskanen, 2005, Tucker et al., 1994).

Induction time

Equation 3.38 can be used to compute the induction time, t_i , provided the value of contact angle, θ_c , of the three phase line is known. Sessile drop measurements for the air-water-silica and hydrogen-water-silica systems yielded values of 58.1° and 58.6° , respectively (see Appendix E). The close similarity between the two measurements would indicate that for a given particle size the induction time would be the same for both gases. For a d_p of 36.7 μm , t_i is about 2.8 ms for both gases, which is consistent with Glembotsky et al. (1971).

5.2.6 Summary on Comparison of Recovery by Air and Hydrogen

It was found that there was no measurable difference between molecular hydrogen and air in the flotation recovery of silica. This implied that there was no interaction between the gas phase and the solids surface, which was supported by very similar contact angle measurements for the two systems.

It was also observed that the depressant effect of sodium sulphate was minimized by using higher amount of collector. Hence sodium sulphate in conjunction with higher concentration of collector can be used as electrolyte in electroflotation studies without sacrificing flotation recovery.

5.3 ELECTROFLOTATION CELL: BUBBLE SIZE MEASUREMENT

The size of bubbles produced by electroflotation is influenced by a number of factors. Firstly, it depends on the type of electrode material and its position in the electromotive series (Glembotskii et al., 1973). Secondly, it is a function of pH, with hydrogen bubbles being larger in an acidic medium compared to a neutral or alkaline medium. Similarly, oxygen bubbles attain a minimum size in acidic medium and increase in diameter with increased pH (Brandon and Kelsall, 1985a). The detachment size of bubble also depends on the curvature of the electrode surface (Matov and Lazavenko, 1965). For a constant current density and pH, detached bubble diameter has been reported to decrease with decreasing wire (electrode) diameter (Ben Mansour et al., 2007, Glembotskii et al., 1975, Ketkar et al., 1988). There have been conflicting studies investigating the influence of current density on bubble size as discussed in Section 2.9.4.

The uncertainty in influences of variables such as electrode curvature, surface preparation, and most importantly current density, have made it difficult to effectively design efficient electroflotation systems for fine particle recovery. This study was aimed at reducing the uncertainty by investigating the size and flux of hydrogen bubbles produced from wire electrodes as part of the electroflotation process. The effect of wire geometry, surface preparation and current density, on (1) size and frequency of detaching bubbles, and (2) growth of these bubbles as they moved away from the electrode surface was measured experimentally and compared with model predictions. Finally, the results are discussed briefly in context of industrial flotation systems.

Two sets of bubble size measurement experiments were performed; first set without any external flow while the second set with upward liquid flow. The upward liquid flow was generated by a peristaltic pump; with the tube creating inflow into the cell being placed at the bottom of the hydrogen bubble producing electrode. The tube for outflow from the cell placed at the other end of the cell. Before producing bubble, the peristaltic pump was switched on to establish a circulating flow of liquid in the bubble producing cell. For the inflow into the cell produced by the peristaltic pump, the cathode experienced an upward flow of liquid along its circumference.

The first set of bubble size measurement was performed with platinum wire having diameter of 90, 120 and 190 μm at current density ranged from 151-354 A/m^2 . While the second set of bubble size measurement was performed with platinum wires having diameter of 90 and 190 μm at current density 354 A/m^2 . The upward liquid velocity varied in the range of 1.5-7.1 mm/s. The bubble size measurement data are presented in Appendix F.

5.3.1 Bubbles Experiencing No External Fluid Flow

Bubble visualisation

Sample images of the hydrogen bubble generation process are shown in Figure 5.6. It can be seen that once the bubble detached from the cathode surface (shown as solid symbols) it grew rapidly in size as it rose through the electrolyte. An 8-fold increase in volume in the first few millimetres of rise was observed. This was due to a combination of both hydrostatic pressure variation and mass transfer of supersaturated hydrogen gas, water vapour and other dissolved gases (oxygen, nitrogen) into the bubble. Also shown (as open symbols), are the diameters of the bubbles at the point of detachments, $d_{b,d}$, which are projected to have nucleated at distance, $x_{b,d}$, below the top of the electrode surface ($x = 0$ m). The projection was required as many of the generation sites were below the top of the electrode and it was only possible to view the bubbles once they had risen into the field of view of the camera. Consequently, the following expression:

$$d_b(x) = d_{b,d} + d_{b,d} \left\{ 1 - e^{-K(x+x_{b,d})/d_{b,d}} \right\}, \quad (5.1)$$

was fitted to the experimental rising bubble diameter measurements to obtain average values for the detachment diameter for each wire diameter and range of current densities. The fitted values, including K and $x_{b,d}$ are given in Table 5.1.

Table 5.1: Fitted coefficients for Equation 5.1

i (A/m ²)	D (μm)	Coefficient					
		K	St. dev.	$d_{b,d}$ (μm)	St. dev.	$x_{b,d}$ (μm)	St. dev.
152	90	0.10	0.03	15.1	1.6	72	56
	120	0.25	0.07	18.8	3.9	9	12
	190	0.23	0.07	22.8	3.7	69	70
	190 (Plat)	0.15	0.08	22.6	5.9	46	46
253	90	0.10	0.04	15.1	2.2	68	51
	120	0.14	0.03	18.9	3.6	25	27
	190	0.26	0.06	23.4	3.8	52	43
	190 (Plat)	0.10	0.04	20.2	4.3	39	57
354	90	0.14	0.09	15.4	1.9	54	56
	120	0.10	0.06	17.3	2.6	36	38
	190	0.17	0.05	21.8	3.4	51	41
	190 (Plat)	0.07	0.02	19.2	2.3	10	14

It can be seen from Table 5.1 that $x_{b,d}$ varied between experiments, reflecting the fact that bubbles can nucleate anywhere on the electrode surface. Similarly, the exponent, K , values varied from 0.07-0.26, resulting in a range of growth rates for the bubbles once they have detached from the wire. Reasons for the variation are given later in this chapter. While $x_{b,d}$ and K might have varied between different nucleation sites the projected detachment diameter values were quite consistent.

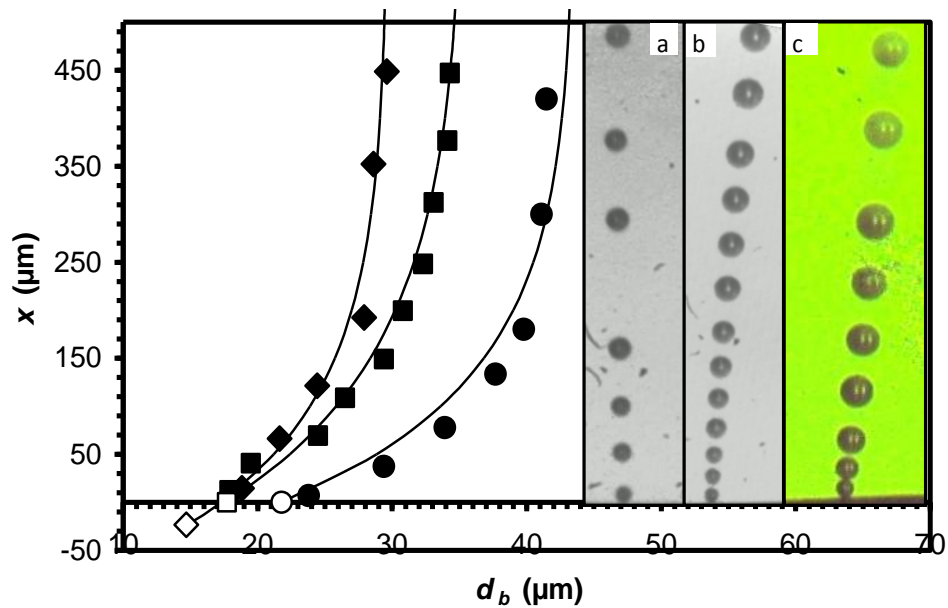


Figure 5.6: Bubble diameter vs distance from top of electrode
 [Pt: $D = (\blacklozenge) 90, (\blacksquare) 120, (\bullet) 190 \mu\text{m}$; $\dot{I} = 354 \text{ A/m}^2$; photograph:
 $D = (\text{a}) 90, (\text{b}) 120, (\text{c}) 190 \mu\text{m}$]

Bubble diameter at detachment

The $d_{b,d}$ values reported in Table 5.1 are plotted as a function of current density in Figure 5.7. It can be seen that for each wire diameter the detachment diameter of the bubble remained relatively constant over the current density range investigated. Similarly, platinisation of the wire surface made little difference to the detachment diameter. However, for a given current density the detachment diameter increased with increasing wire diameter.

Equations 3.95-3.96 were applied, using a fitted contact angle, to predict the diameter of the bubble at the point of detachment. The comparison is given in Table 5.2, where it can be seen that predictions were within ± 20 percent of the experimental values over the range investigated. The predictions were based on a single fitted contact angle, ω , of 0.18 degrees for all four wires. This value was consistent with those from other studies, which ranged from zero (Bewig and Zisman, 1965, Gardner and Woods, 1977, Brandon and Kelsall, 1985a) to ten (Gardner and Woods, 1974) degrees, depending on the cleaning procedure of the platinum surface. Also given in Table 5.2 is the predicted $d_{b,d}$ of 21 μm for a flat surface. Again, this value is consistent with Janssen and Hoogland

(1973) who reported a hydrogen bubble size of 26 μm produced from a platinum disc electrode of 11.2 mm diameter at a current density of 40 A/m^2 . Similarly, Han et al. (2002) reported hydrogen bubbles of 15-65 μm produced from a flat aluminium electrode with average diameter of 22 μm .

Table 5.2: Average experimental and predicted detached bubble diameter

D (μm)	$d_{b,d}$ (μm)		Difference (%)
	Eqs. 3.95-3.96 ¹	Experimental ²	
90	18.0	15.2 \pm 1.4	18
120	18.2	18.3 \pm 2.5	-1
190 ³	18.9	21.7 \pm 2.9	-13
∞ ⁴	21.0		

¹ using fitted contact angle of 0.18 deg, which is the average of 0.15, 0.18, 0.21 deg for 90, 120, 190 μm wires.

² taken as the average value for the three current densities given in Table 2 (\pm values are for 95% confidence interval)

³ average of both platinum and platinised 190 μm wires.

⁴ equivalent to a flat surface.

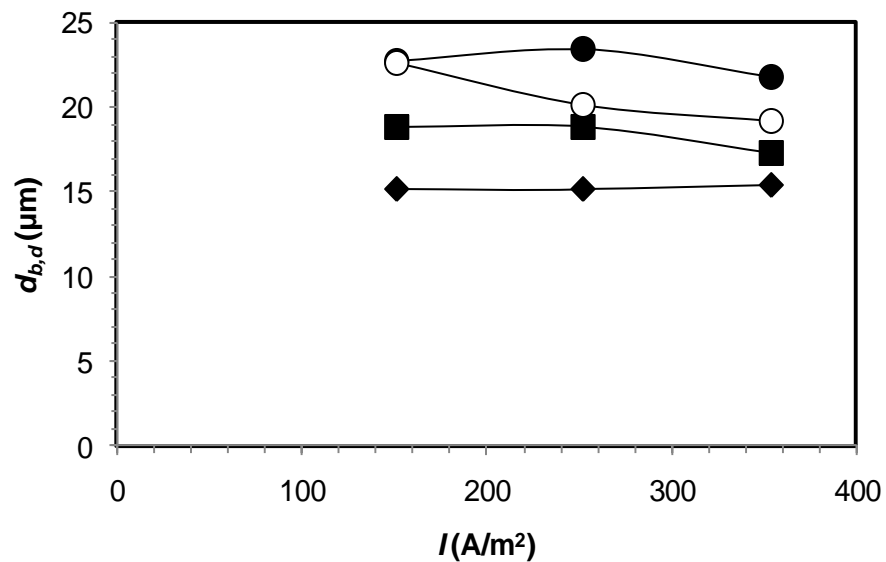


Figure 5.7: Bubble detachment diameter vs current density

[Pt: D= (◆) 90, (■) 120, (●) 190 μm ; Platinised: D= (○) 190 μm]

Bubble nucleation rate

Hydrogen bubble nucleation rate on the cathode surface is shown in Figure 5.8 as a function of current density for both the Pt and platinised wires. It can be seen that bubble nucleation rate (per m^2 of surface area) increased with increasing current density for all of the wire diameters. This is not surprising, given the increase in hydrogen formation with increasing current while the bubble detachment diameter remained relatively constant. Moreover, the bubble flux will depend on number of nucleation sites, and in accordance with Murakawa (1957), more nucleation sites are expected to become active at higher current density as the solution adjacent to the electrode surface becomes more supersaturated. The intent of investigating the platinised surface was the expectation of an increase in nucleation rate as a result of increased nucleation sites created by the platinising process. The results in Figure 5.8 support this supposition, with a marked increase in nucleation rates for the platinised surface. The increase in the rate of bubble production would be of benefit for flotation processes.

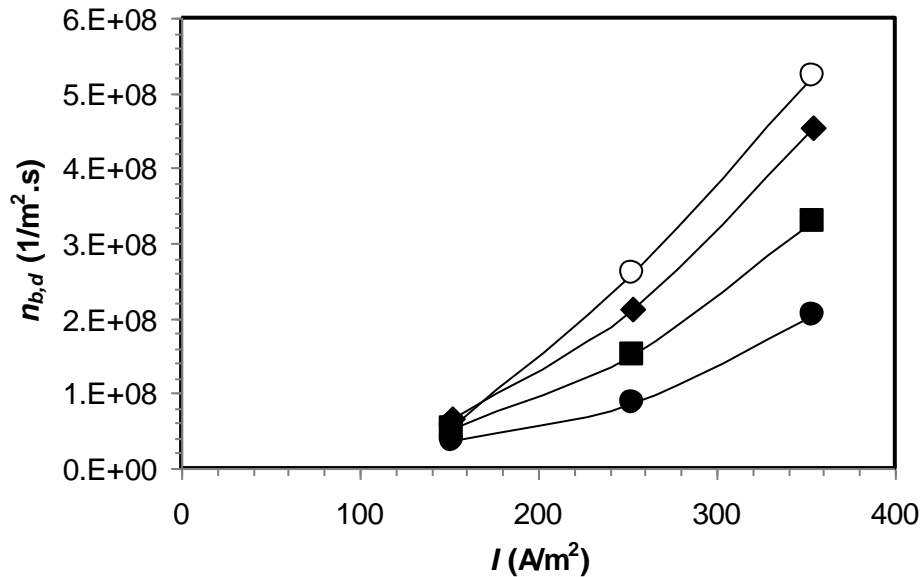


Figure 5.8: Bubble nucleation rate vs current density

[Pt: $D=(\blacklozenge)$ 90, (\blacksquare) 120, (\bullet) 190 μm ; Platinised: $D=(\circ)$ 190 μm]

It can also be seen that bubble nucleation rate increased with decreased wire diameter. This was thought due to smaller detachment diameter of bubble with decreased wire

diameter. This smaller diameter bubble (15.1 μm) detached faster than larger diameter bubble (23.4 μm) and took less amount of dissolved hydrogen before detachment. As detachment time is less, more nucleation sites are expected in the case of smaller wire diameter. Also, the less amount of hydrogen required for forming the smaller hydrogen bubbles, will leave the cathode surfaces more saturated by dissolved hydrogen compared to larger wire diameter cathode.

Bubble diameter in the bulk

As illustrated in Figure 5.6, the detached hydrogen bubble rapidly increases in diameter as it rises in the bulk liquid. At some distance, typically in the range 500-1000 μm , from the cathode surface the bubble diameter becomes relatively constant, which we define as the bulk diameter, $d_{b,b}$. The average bulk bubble diameter, obtained from Equation 5.1 and using the corresponding coefficient values given in Table 5.1, has been plotted as a function of current density for both the platinum and platinised wires in Figure 5.9. The trends are similar to that for the detachment diameter (see Figure 5.7) with $d_{b,b}$: (1) remaining relatively constant over the current density range investigated; (2) decreasing with decreasing wire diameter; and (3) the platinised wire resulting in smaller bubbles than for the untreated platinum surface.

The bulk diameter measurements reported in Figure 5.9 represent almost an order of magnitude increase in the detached bubble volume. The change in bubble diameter is due to three reasons. Firstly, the external pressure experienced by the bubble is decreased as it rises through the liquid, and in accordance with the Laplace equation will result in expansion of the bubble. For the change in liquid height during the bubble rise this effect will be small, resulting in only a few percent increases in volume. Secondly, the bubble will immediately become saturated with water vapour; but will again be very small. Thirdly, a portion of the remaining hydrogen that was originally produced at the cathode and dissolved directly into the liquid will diffuse into the rising bubble. The high level of supersaturation of dissolved hydrogen (Müller et al., 1989) is a strong driving force, and will lead to significant diffusion of dissolved gas into the bubble and large increase in its volume.

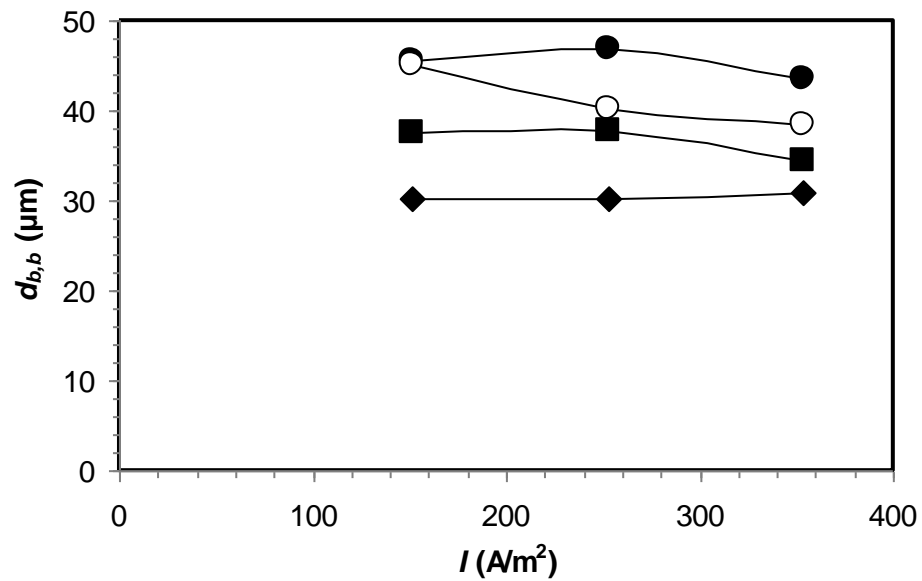


Figure 5.9: Bulk bubble diameter vs current density

[Pt: D= (\blacklozenge) 90, (\blacksquare) 120, (\bullet) 190 μm ; Platinised: D= (\circ) 190 μm]

In electroflotation, a fraction, f , of the hydrogen produced is present as bubbles. The fraction will change as a function of distance from the top of the cathode wire due to diffusion of the dissolved hydrogen into the rising bubbles. It can be easily calculated as the product of the bubble production frequency times the bubble volume. The results are given in Figure 5.10 for the detached and bulk bubble diameters for both the platinum and platinised wires at current densities in the range of 152-354 A/m^2 . It can be seen that at detachment less than 5% of the total hydrogen produced resulted in the formation of hydrogen gas in the form of bubbles. However, in the bulk, where the bubbles had reached a steady size, the gas bubble fraction had increased by between 6-35%.

The gas bubble fraction increased with increased current density and increased wire diameter. It can also be seen that in the bulk the fraction of hydrogen utilised as bubbles was higher for the platinised wire. Given that the platinised wire also produced smaller bubbles (see Figure 5.9), and at higher frequency (see Figure 5.8), it would seem to be a significant advantage in electroflotation to operate with a platinised-surface cathode.

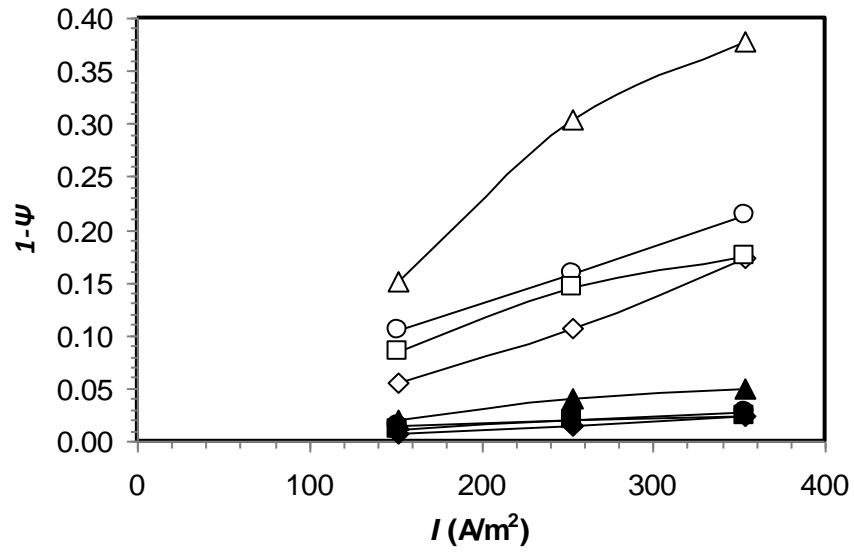


Figure 5.10: Fraction total hydrogen in bubble vs current density
[at detachment: Pt: D= (\blacklozenge)90, (\blacksquare)120, (\bullet)190 μm ; Platinised: D= (\blacktriangle)190 μm ;
in bulk: Pt: D= (\diamond)90, (\square)120, (\circ)190 μm ; Platinised: D= (\triangle)190 μm]

The bubble diameter in the bulk can be predicted from Equations. 3.97-3.107 provided the dissolved gas concentration profile is known. From Figure 5.10, it was shown that the fraction, ψ , of hydrogen remaining in solution was 0.79 (190 μm Pt wire), and 0.83 (90 and 120 μm Pt wires). Assuming these values, the concentration profile of dissolved hydrogen gas, calculated from Equation 3.105, for the Pt wires (90, 120 and 190 μm diameter) and current density of 354 A/m^2 ($\dot{N} = 1.833 \text{ mMol}/m^2 \cdot s$) is shown in Figure 5.11.

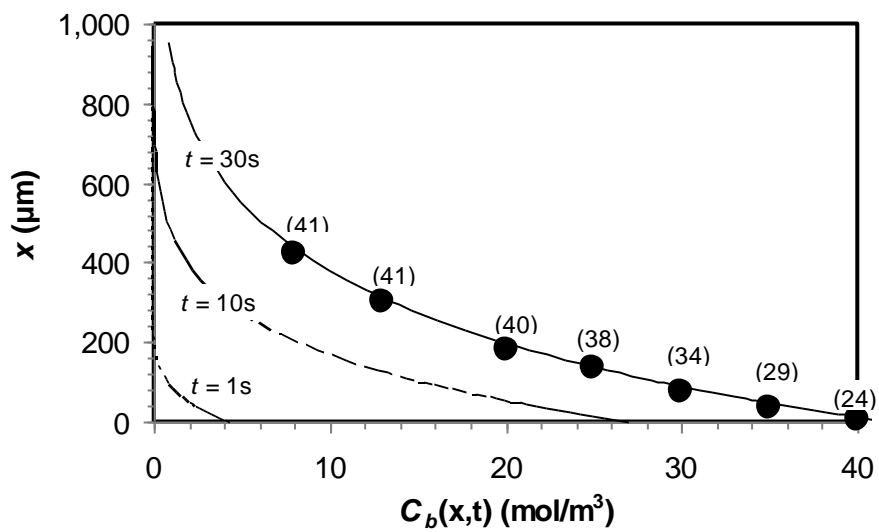
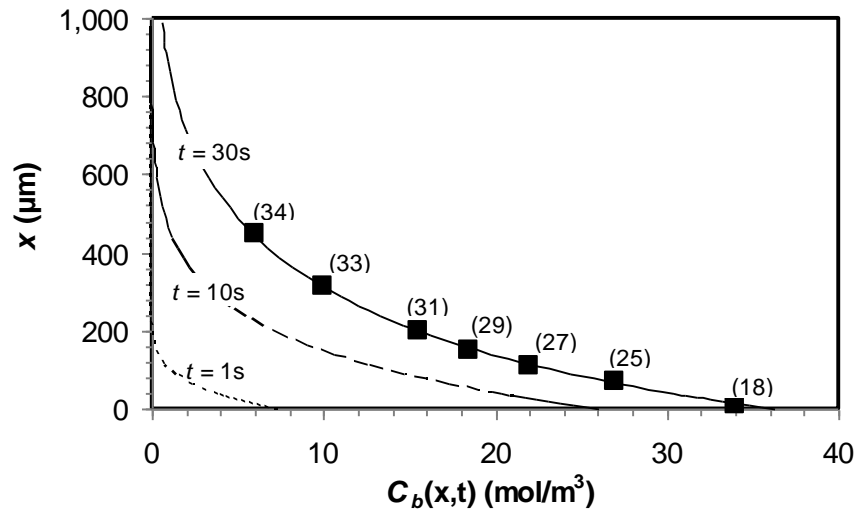
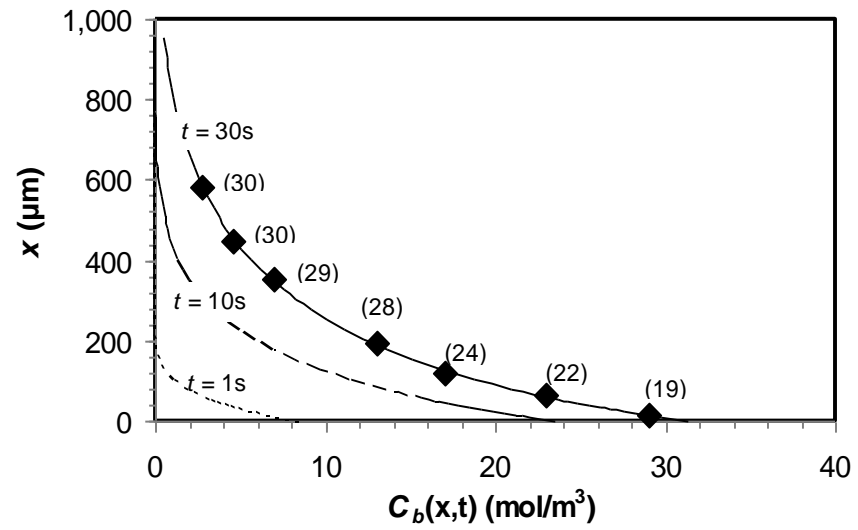


Figure 5.11: Dissolved hydrogen gas concentration vs time and distance above wire [Pt wire; $\dot{I} = 354 \text{ A}/\text{m}^2$; $\psi = 0.79$ ($D=190 \mu\text{m}$), 0.83 ($D=90$ and $120 \mu\text{m}$); bubble location and diameter (μm): $D = (\blacklozenge)$ 90, (\blacksquare) 120, (\bullet) 190 μm]

There was no external flow or mixing of liquid in the cell. The only flow of liquid was due to the displacement of liquid by the rising bubbles. From Figure 5.11, in accordance with unsteady diffusion theory for a constant flux source, the concentration increases with increasing time at the surface, and decreases with increasing distance away from it. Given that the saturation concentration of hydrogen gas at atmospheric pressure is 0.78 mol/m^3 , the normalised (C/C^{sat}) corresponding supersaturation values in the figure are: 5, 33 and 52 at the surface ($x = 0 \text{ }\mu\text{m}$), at times 1, 10 and 30s, respectively; and 0, 1 and 7 for the same times at $x = 550 \text{ }\mu\text{m}$ (for $190 \text{ }\mu\text{m}$ Pt wire). These levels of supersaturation are consistent with the study by Shibata (1978). Also shown in the figure is the position of the bubble overlaid onto the dissolved gas concentration gradient, generated at $t = 30 \text{ s}$ after the current source was switched on. The bracketed values are the diameter measurements as the bubble rises away from the wire surface; whereby the increase in diameter is largely to the high levels of supersaturation in the surrounding liquid.

Knowing the dissolved hydrogen gas concentration profile the model equations can be solved simultaneously to obtain the bubble diameter as a function of distance from the top surface of the electrode. The experimental measurements are compared with predicted bubble diameter values in Figure 5.12 for the Pt wires at a current density of 354 A/m^2 .

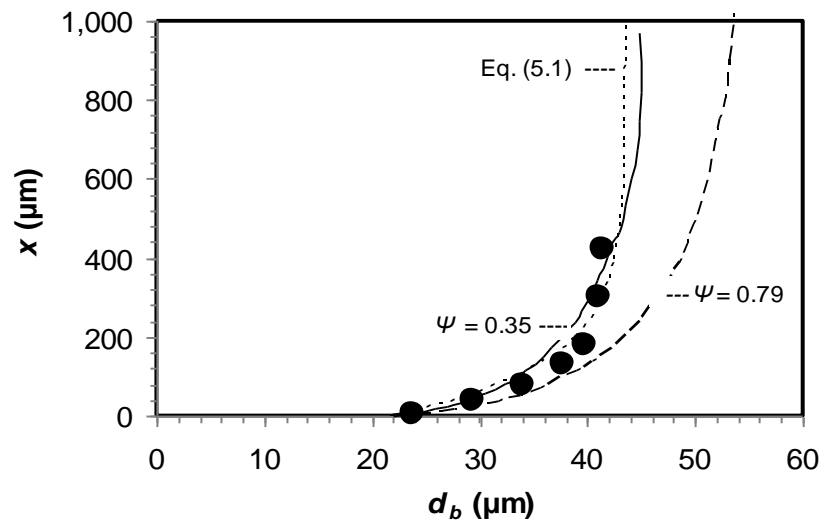
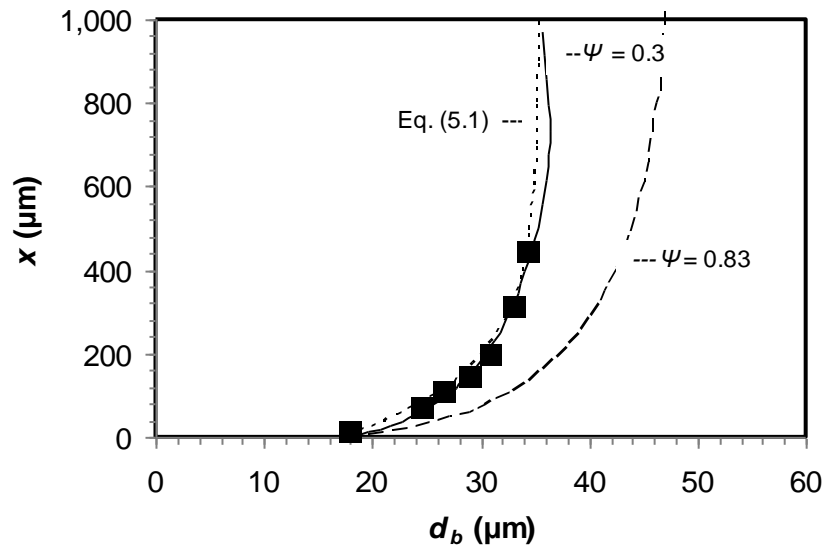
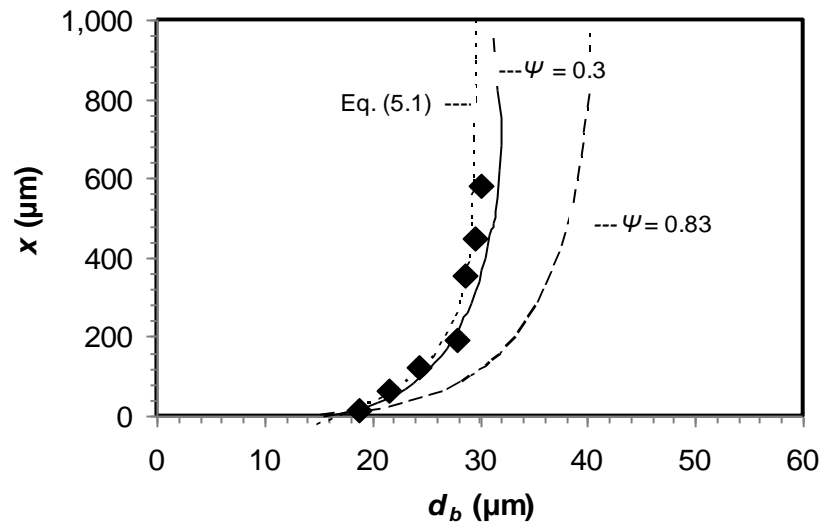


Figure 5.12: Measured and predicted bubble diameter vs distance above wire [Pt wire; $\dot{I} = 354 \text{A/m}^2$; measured: $D = (\blacklozenge) 90, (\blacksquare) 120, (\bullet) 190 \mu\text{m}$]

In Figure 5.12 there are three predictive curves illustrated: Firstly, the prediction using Equation 5.1 shows good agreement with the measurements, which is hardly surprising given the equation parameters K , $x_{b,d}$, and $d_{b,d}$ are fitted to the experimental data. Secondly, the prediction from solution of Equations 3.97-3.107, and using $\psi = 0.79$ (190 μm Pt wire), and 0.83 (90 and 120 μm Pt wires) for the dissolved gas concentration profile as shown in Figure 5.11, leads to an over-prediction of bubble diameter with increasing distance from the top of the wire. The reason for the discrepancy is thought to be the result of the diffusion of the dissolved hydrogen taking place radially in all directions from the electrode wire surface, whereas the bubbles move only in the upward direction. Consequently, the rising bubbles are in contact with the dissolved hydrogen that is in the liquid above the wire and the dissolved hydrogen below the wire will remain in the liquid. As a consequence, the actual concentration of dissolved hydrogen above the wire will be less than the overall value reported in Figure 5.11, resulting in a decrease in the expected rate of bubble growth.

Thirdly, for the reason mentioned in the previous paragraph a lower dissolved gas fraction was assumed, and it was found that $\psi = 0.3$ (90 and 120 μm Pt wires), and 0.35 (190 μm Pt wire) produced good agreement with the experimental measurements. An interesting observation is that the model predicts a peak in the diameter of the bubble as it changes position within the liquid. This is due to the liquid near the surface of the electrode rapidly becoming supersaturated with hydrogen which then diffuses into the bubble, causing it to increase in diameter. The level of supersaturation decreases rapidly with increasing distance from the electrode, however, such that as the bubble rises into this liquid the concentration driving force will result in the hydrogen inside the bubble being dissolved back into the liquid. Hence, the bubble size will decrease. The peak in bubble size occurred at around 1000 μm from the electrode surface for bubbles produced 30 seconds after the commencement of the electric current. The location of the peak will vary with the time from which the current is applied to the electrode.

5.3.2 Bubbles Experiencing External Upward Fluid Flow

Sample images of hydrogen bubble forming on the surface of platinum cathode surface as a function of liquid flow from two different cathode diameters are shown in Figure 5.13.

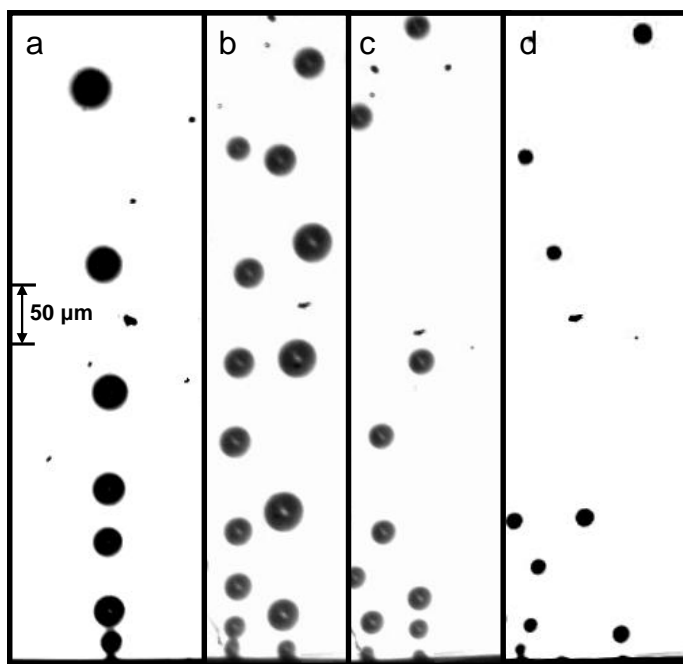


Figure 5.13(a): Images of Hydrogen produced as a function of liquid flow
 [$D=90\ \mu\text{m}$; $\dot{I} = 354\ \text{A}/\text{m}^2$; liquid velocity = (a) 0.0, (b) 1.56, (c) 3.38, (d) 7.02 mm/s]

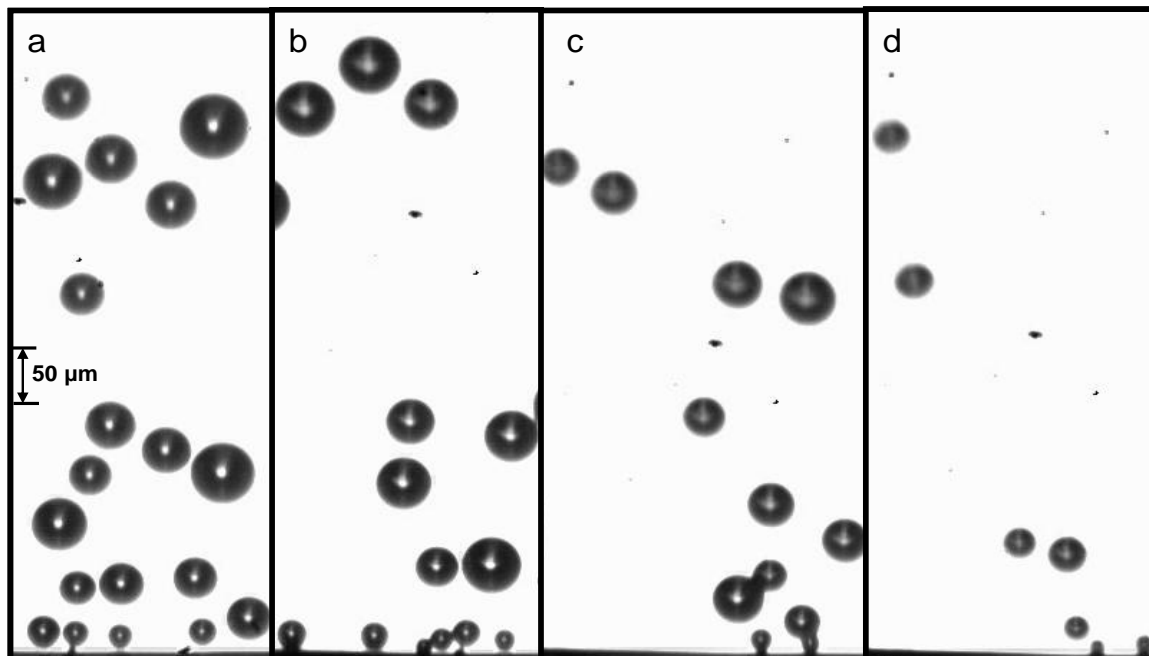


Figure 5.13(b): Images of Hydrogen produced as a function of liquid flow
 [$D=190\ \mu\text{m}$; $\dot{I} = 354\ \text{A}/\text{m}^2$; liquid velocity = (a) 0.0, (b) 2.48, (c) 4.0, (d) 7.09 mm/s]

In Figure 5.13 it can be seen that the bubble diameter decreased with increased flow of liquid for both wires. Similar to the bubbles produced without experiencing any external fluid flow, the detached bubbles grew rapidly as they rose through the electrolyte. The detachment diameter, $d_{b,d}$, was computed by fitting the measured data in Equation 5.1. The diameters of the bubbles were also measured at a distance around 500 μm above the cathode where they became relatively constant in size and reported as bulk diameter, $d_{b,b}$.

The average of the detachment and bulk diameter produced from both cathodes as a function of external liquid flow are shown in Figure 5.14. It can be seen that the detachment diameter of the bubble decreased with increased upward liquid velocity in case of both wires. This was thought to be due to the increase in detaching force with increased upward flow velocity. The finding is consistent with the studies of Landolt et al. (1970) and Lumanauw (2000) who reported a decrease in mean bubble size with increased electrolyte flow.

Similarly, the bulk diameter produced from each cathode was found to decrease as liquid velocity increased. This was thought to be due to three reasons. Firstly, the bulk diameter was found to be a function of detachment diameter as discussed in Section 5.3.1. As discussed above, the detachment diameter was observed to decrease as liquid velocity increased. Being a function of detachment diameter, this smaller bubble at increased liquid velocity remained smaller in bulk solution as well. Secondly, the liquid flow cause a decrease in dissolved hydrogen gas concentration by sweeping the dissolved hydrogen gas away. As the liquid velocity increased, the more likely the concentration of dissolved hydrogen in bulk solution decreased causing a slower growth of bubble. Thirdly, the detached bubble was carried away quickly by the upward flowing liquid and stayed less time in the supersaturated dissolved hydrogen gas region to grow by molecular diffusion of dissolved hydrogen gas. Increase in liquid velocity carried away the detached bubble more quickly. However, in depth analytical analyses regarding this matter may be performed in the future research.

The bulk diameters were also found to increase by almost an order of magnitude for both wires. From Figure 5.14, it can also be seen that both the detachment and bulk diameters increased with increased wire diameter. This is consistent with the findings

observed for bubbles produced without experiencing any external flow as discussed in Section 5.3.1.

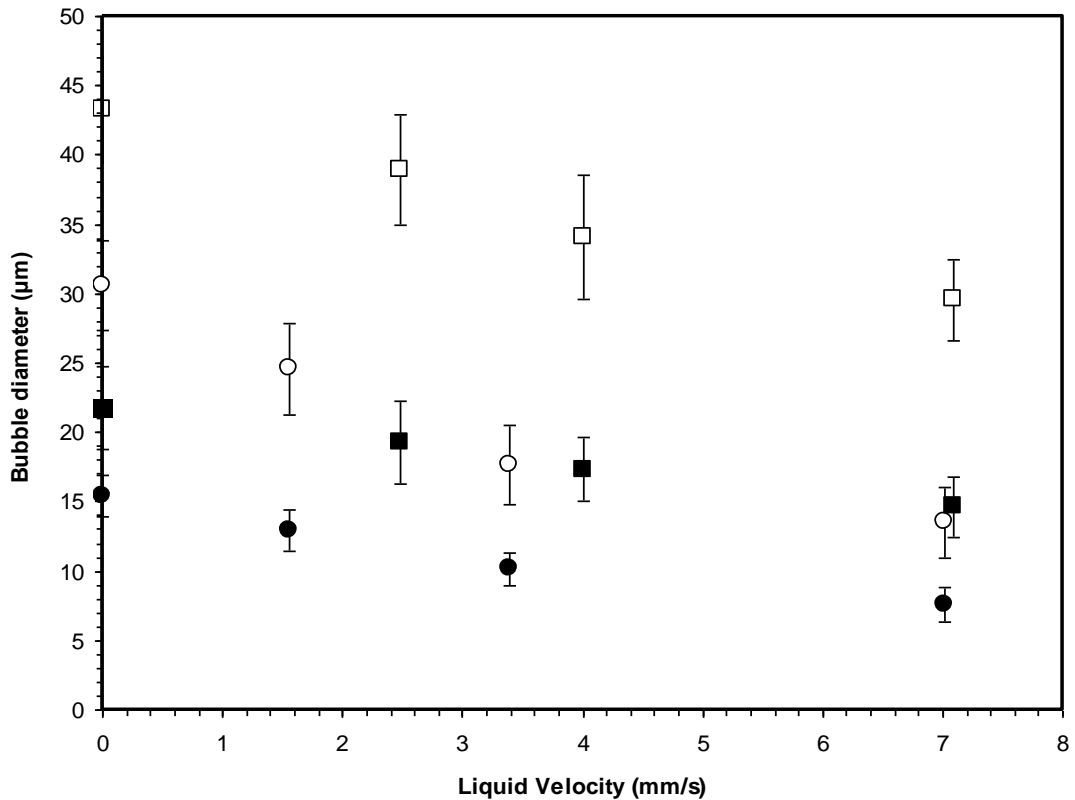


Figure 5.14: Bubble diameter vs liquid velocity

[Pt wire; At detachment: $D = (\bullet)$ 90, (\blacksquare) 190 μm ; In bulk: $D = (\circ)$ 90, (\square) 190 μm]

5.3.3 Summary on Bubble Size Measurement

It has been found that a simple balance including buoyancy and surface tension forces will provide a reasonable estimation of the detachment diameter for hydrogen bubbles produced at a cathode surface. The detachment diameter is strongly influenced by the three phase contact angle, and to a much lesser degree by the diameter of the wire electrode. Conversely, current density seems to have almost no influence on the detachment diameter. As expected, the nucleation rate increased with increasing current density as well as treatment (platinisation) of the electrode surface. It was found that the detached bubbles increased in volume as they moved away from the electrode surface. This was due to absorption of dissolved hydrogen from the surrounding liquid, with the

ratio of dissolved-to-gaseous hydrogen formation being a function of bubble nucleation rate and the time from when the current was applied. It was found that only about 6-35 percent of the total hydrogen produced entered the bubbles for the single wire geometry. This was due to hydrogen diffusion occurring in all radial directions from the wire surface whereas the bubbles rose only in the vertical direction. Consequently, the hydrogen present in the liquid below the wire was not able to be absorbed into the bubbles. For any industrial design it would be necessary to ensure a liquid up-flow so that contact between the bubbles and the remaining dissolved gas is maximised. Both the detachment and bulk diameter seem to be a function of external liquid flow with a decrease in size as liquid flow increases. For effective electroflotation of fine particles, the system should be designed to maximize the amount of the hydrogen produced from the cathode resulting in the formation of bubbles. This can be achieved by increasing the bubble nucleation frequency and having a small detachment diameter. Nucleation frequency was shown to be enhanced by platinisation of the cathode surface, and smaller bubbles were produced with reducing the cathode wire diameter. Finally, the observation that bubble diameter was a function of position, time, dissolved gas concentration profile and electrode surface treatment, helped to explain why there is such a wide variation in reported measurements across the literature.

5.4 ELECTROFLOTATION CELL: HYDROGEN GAS FRACTION

In typical electroflotation operations it is the hydrogen bubbles produced at the cathode surface that are utilised in the collection of the valuable mineral. Bubble nucleates from preferred nucleation sites which depends on surface inhomogeneities (Glas and Westwater, 1964), as well as surface treatment and current density (Janssen and Hoogland, 1970, Sarkar et al., 2010b). The hydrogen either enters into the growing bubbles attached to the cathode or diffuses directly into the bulk electrolyte (Vogt, 1984b). The portion that enters into the growing bubble can vary depending on electrode material, electrode geometry, surface treatment of electrode, and current density etc. The hydrogen that has diffused directly into the bulk solution results in supersaturated conditions close to the cathode surface (Müller et al., 1989). Consequently, dissolved hydrogen diffuses into the detached hydrogen bubbles resulting in an increase in size as they rise through the electrolyte (Sarkar et al., 2010b).

Hence, the amount of produced hydrogen that goes into the bubbles is a combination of the bubble nucleation, growth and detachment processes, as well as diffusion in the bulk as the bubbles rise through regions of varying levels of saturation.

Flotation recovery will be maximised if all of the electrolytically generated hydrogen results in the formation of bubbles. However, the fraction of the total amount that enters the bubbles can vary (e.g., (Sarkar et al., 2010b, Vogt, 1984b, Vogt, 1984a, Müller et al., 1989)). Müller et al. (1989), using an 8 mm diameter platinum disc cathode at current densities higher than 1000 A/m², found that all of the hydrogen gas entered the bubbles. Conversely, Sarkar et al. (2010b) reported that only about 35 percent of the hydrogen generated from a single 0.190 mm diameter platinum wire operating at a current density of 354 A/m² actually entered the bubbles. The conclusions from these and other studies are that utilisation of the hydrogen produced by the electrolysis process for flotation is therefore a function of the nucleation process, which depends on the cathode surface properties (Glas and Westwater, 1964) and current density (Janssen and Hoogland, 1970, Sarkar et al., 2010b), as well as the dissolved gas concentration gradient, especially near the cathode surface and to a lesser extent on the bulk electrolyte.

In electroflotation the complexity of the nucleation process, both at the cathode surface and in the bulk, is increased due to the presence of solids which themselves can act as nucleation sites. Moreover, in flotation cells agitation is almost always applied to suspend the solids. The increased motion will introduce a convective element to the transport of the dissolved hydrogen gas. All of these factors need to be better understood before it will be possible to design effective electroflotation cells. Therefore, this study was aimed at determining the influence of solids concentration, mechanical agitation, and presence of pre-existing dissolved gases on the rate of hydrogen gas generation. An experimental setup was designed to capture the hydrogen gas produced from the electrolysis of water to investigate the influences of the factors discussed above. The details of the experimental setup and methodology are discussed in Section 4.6 in Chapter 4. The data of collected gas rates are reported in Appendix G.

5.4.1 Effect of Dissolved Gases on Hydrogen Bubble Production Rate

The volume of collected hydrogen gas versus time is shown in Figure 5.15 for both normal and degassed electrolyte with mechanical agitation and a current density of 129 A/m^2 . The standard deviation of collected gas at every data point was 0.06 (not shown in the figure due to very small number compared to the total collected volume of gas).

Also shown in Figure 5.15 is the predicted volume from Equation 3.88 assuming that all of the hydrogen generated goes into the bubbles ($f=1$). It can be seen that for all three cases volume increased linearly with time, indicating a constant volumetric flow rate. This was to be expected given current density was held constant. The time lag of approximately 1 minute for the normal electrolyte solution was the time taken for the hydrogen gas to rise through the system and into the inverted burette. The time lag for the degassed solution was higher at just under two minutes. The additional time for the degassed electrolyte was thought to be due to the initial dissolution of all of the hydrogen prior to the formation of the gas bubbles. This notion is supported by the gradual increase in the slope of the degassed curve, corresponding to an increase in the dissolved (hydrogen) gas concentration approaching that for the normal solution.

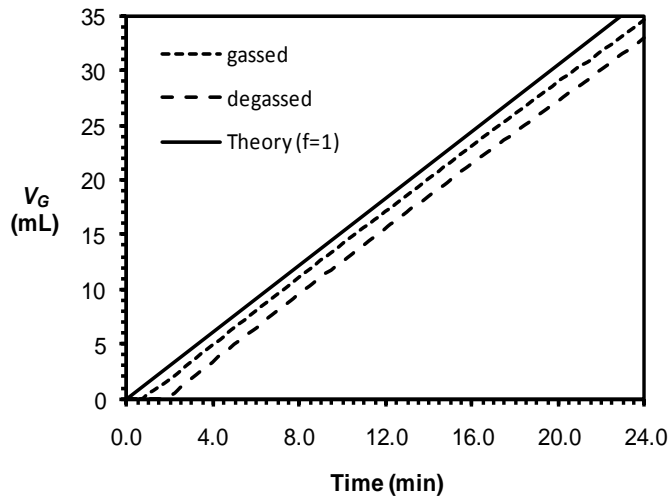


Figure 5.15: Hydrogen bubble generation vs time
[$d_w = 0.400 \text{ mm}$; with agitation]

5.4.2 Effect of Agitation on Hydrogen Bubble Production Rate

The hydrogen gas generation rate, determined from the collected gas experiments (with R^2 typically around 0.99), is reported in Table 5.3 as a function of stirring for normal

and degassed electrolyte solutions, and at different current densities. It can be seen that for both current densities, in general, stirring resulted in a slight increase in the rate of hydrogen gas production. Similarly, over the 24 minute duration of the experiment the degassed solution resulted in a slightly lower gas production rate.

Table 5.3: Hydrogen Gas Generation Rate vs Current Density

i (A/m ²)	Electrolyte solution (mL/min)		Electrolyte solution (degassed) (mL/min)	
	Stirred	Non-stirred	Stirred	Non-stirred
	129	1.56 (0.04 ¹)	1.51 (0.02)	1.51 (0.04)
258	3.20 (0.05)	2.98 (0.04)	3.03 (0.05)	3.03 (0.05)

¹Standard deviation shown as bracketed values

5.4.3 Effect of Solids Concentration on Hydrogen Bubble Production Rate

The influence of (non-floating) silica particle concentration on the average hydrogen gas generation rate over a 24 minute period is shown in Figure 5.16 for both the normal and degassed electrolyte solution, with stirring, and a current density of 129 A/m². It can be seen that the presence of solids had little influence on the gas generation rate. For the degassed solution, the average gas collection rate was 98% of the total (theoretical) hydrogen production rate, which is consistent with Müller et al. (1989) who reported a value of 97% for a platinum disc electrode at a current density of 500 A/m². Such a high gas generation percentage is desirable as it will increase flotation recovery.

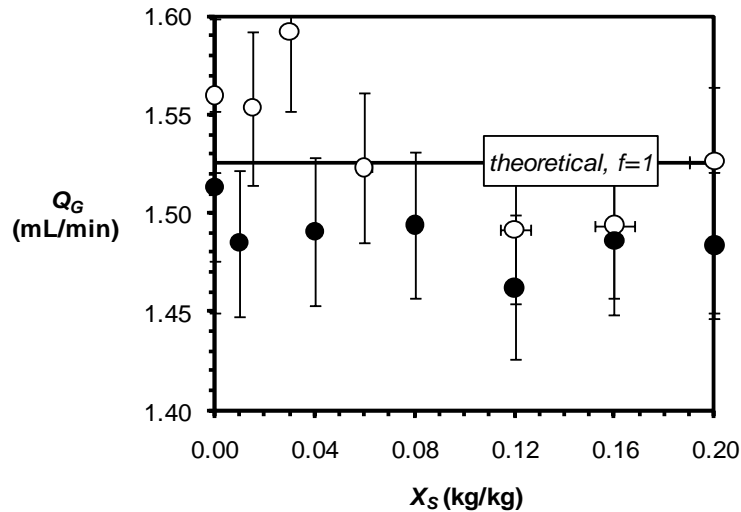


Figure 5.16: Hydrogen bubble generation rate vs solids concentration

[—eq. 3.88, with $f = 1$; ● normal solution; ○ degassed solution; with agitation]

5.4.4 Summary on Gas Fraction

From the experimental measurements it was found that ~ 98% of the (theoretical) hydrogen produced by the electrolysis process resulted in gas phase. This is a positive result, in that almost all of the electrical energy is being converted to hydrogen bubbles that can be used for recovery of valuable minerals. For a given current density, the rate of hydrogen gas production was largely independent of solids loading. Mechanical agitation slightly increased the gas production rate. Conversely, gas production rate decreased a little for degassed electrolyte solution, although this effect is expected to disappear once the dissolved gas(es) concentration reaches a steady state.

5.5 ELECTROFLOTATION CELL: SILICA RECOVERY USING STAINLESS STEEL MESH CATHODE

The flotation of fine particle usually increases with decreased bubble size. This statement has been supported by many experimental (Anfruns and Kitchener, 1977, Ahmed and Jameson, 1985, Yoon and Luttrell, 1989, Sarrot et al., 2007) and theoretical (Yoon, 1993, Dai et al., 2000, Tao, 2004, Miettinen et al., 2010) studies. Hence the performance of small bubble (as produced in electroflotation) to recover fine particle

needs to be understood clearly. Flotation recovery also depends on particle size, though generally in the opposite manner to that of bubble size. Numerous studies (e.g., (Reay and Ratcliff, 1973, Collins and Jameson, 1976, Jameson et al., 1977, Yoon, 2000, Ramirez and Davis, 2001)) clearly indicate that when particles are large enough not to be affected by Brownian motion, the collection efficiency and the flotation rate of those particles increase with increased particle size. However, there are some studies that have reported the opposite trend. For example, Ketkar et al. (1991) reported a decrease in flotation recovery with increased particle size when floating quartz particles by electrolytic hydrogen and oxygen bubbles. These electrolytic bubbles, with an average diameter of 29 μm , were smaller in size than those used in other studies, and it is most likely that the lifting capacity of such small bubbles was insufficient for the particle size (6.5-65 μm) being floated, especially the larger particles. The work of Ketkar et al. (1991) highlights the importance of understanding the relationship between the flotation capability of very fine bubbles and particle size .

Therefore, this study was aimed at determining the influence of solids concentration, particle size, bubble size and current density (gas flow rate) on flotation recovery. To do this, batch-wise electroflotation, where only the hydrogen was utilised, was undertaken using hydrophobised silica particles; with the flotation recovery measurements being compared with model predictions. The flotation recovery obtained by electrolytically generated hydrogen bubbles as a function of gas flow rate, solids concentration, and particle size is reported in Appendix H. Table 5.4 lists the parameters discussed in this section and also describes whether the parameters are measured, or calculated.

Table 5.4: List of parameter discussed in Section 5.5

Parameter	Measured/ calculated
D	Measured
i	Measured
Q_G	Measured
d_p	Measured
d_b	Measured
ε_G	Calculated
ρ_{pulp}	Calculated
$(d_p)_{max}$	Calculated
K_4	Measured
$(R_{exp})_{corr}$	Measured
φ	Calculated
d_{b-Np}	Calculated
v_{b-Np}	Calculated
[CTAB]	Calculated
X_S	Measured
N_P	Calculated
N_L	Calculated
d_{b-N_L}	Calculated
v_{b-N_L}	Calculated

5.5.1 Effect of Current Density on Bubble Diameter for Different Wire Diameters

Stainless steel meshes of wire diameters of 190 and 400 μm were used to obtain the flotation recovery by electrolytically generated hydrogen bubbles. To evaluate the influence of bubble size on flotation recovery, it is important to know the size of the bubbles produced from the electrolysis reactions. To measure these bubble sizes, stainless steel wires of same diameters (190 and 400 μm) as used in electroflotation experiments were used for producing hydrogen bubbles.

Bubbles produced from 190 μm diameter cathode

Hydrogen bubble sizes produced from steel cathode of 190 μm diameter at different current densities are presented in Table 5.5 (the mean diameter of at least 500 bubbles is reported). It can be seen that current density seems to have almost no effect on mean bubble diameter.

**Table 5.5: Bubble Diameter vs Current Density
and SS Wire Cathode Diameter**

D (mm)	i (A/m ²)	Q _G (mL/min)	d _b (μm)	(d _b) _{av} (μm)	St. Dev. (μm)
0.190	122	0.380	32.5		
	196	0.608	32.5		
	269	0.836	31.9		
	342	1.064	31.5	30.0	2
	416	1.293	27.7		
	489	1.521	27.1		
	587	1.825	29.0		
0.400	258	3.037	39.1		
	388	4.567	40.2	41.0	1
	581	6.838	40.9		
	775	9.124	41.4		

Bubbles produced from 400 μm diameter cathode

The mean diameters taken from approximately 500 bubbles are shown in Table 5.5 and Figure 5.17. The observed average diameters of the hydrogen bubble are consistent with Setty and Venkatachalam (1997) who reported 37.1 μm as the mean diameter of hydrogen bubble produced from a stainless steel cathode at a current density of 225A/m². Figure 5.17 also shows the bubble size distributions produced at different current densities. The bubble size distributions are consistent with the study of Chen et al. (2002) who reported that over 90 percent of the bubbles generated by electroflotation were in the range of 15-45 μm . Bubbles produced from 400 μm diameter wire are reported in Sarkar et al. (2010a).

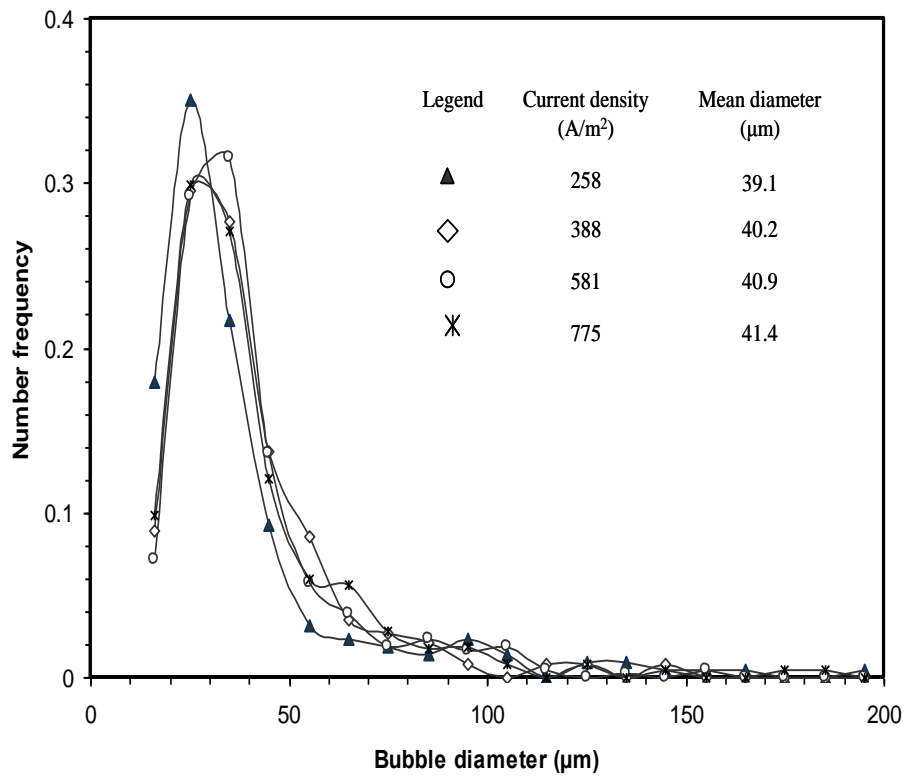


Figure 5.17: Bubble diameter distribution vs. current density
[direct visualization; diameter of steel cathode: 400 μm]

It can be seen from Figure 5.17 and Table 5.5 that the bubble diameters are relatively constant produced at different current densities, while smaller bubbles are produced from the smaller diameter wire. This is consistent with the findings of bubble size measurement produced from platinum cathode as discussed in Section 5.3 and in the study of Sarkar et al. (2010b).

5.5.2 Effect of Particle Mass Fraction on Flotation Recovery and Bubble Surface Loading

Table 5.6 contains the corrected¹ measured fractional recovery and calculated model parameter values for the experiments investigating the effect of solids mass fraction (0.02-0.20) on flotation recovery after 2 minutes of electrolysis at a constant volumetric gas flowrate of 9.12 mL/min.

¹ Recovery is based on the mass of floatable silica only, i.e. (1-K_d).

Table 5.6: Experimental and Model Data for different X_s

		$X_s(\text{kg particles/kg pulp})$						
		0.020	0.035	0.050	0.076	0.100	0.150	0.200
d_p	μm	15.0	15.0	15.0	15.0	15.0	15.0	15.0
d_b	μm	41.0	41.0	41.0	41.0	41.0	41.0	41.0
ε_G	-	0.055	0.055	0.055	0.055	0.055	0.055	0.055
ρ_{pulp}	kg/m^3	957	965	974	989	1002	1029	1055
$(d_p)_{\text{max}}$	μm	33.9	34.0	34.2	34.5	34.7	35.2	35.7
K_4	-	0.006	0.006	0.006	0.006	0.005	0.004	0.004
$(R_{\text{exp}})_{\text{corr}}$	-	0.930	0.873	0.789	0.677	0.555	0.334	0.242
φ	-	0.09	0.14	0.18	0.21	0.23	0.23	0.23
d_{b-Np}	μm	33.7	41.8	47.0	50.4	52.4	52.4	52.4
v_{b-Np}	mm/s	0.67	0.56	0.42	0.36	0.32	0.35	0.37
[CTAB]	$\text{m}^2/\text{m}^2\text{p}$	1.83	1.04	0.72	0.46	0.35	0.22	0.16

Flotation recovery and calculated bubble surface coverage are plotted in Figure 5.18. It can be seen that the measured fractional recovery decreased with increased solids loading. The observation is consistent with that of Ketkar et al. (1991) for solids concentrations higher than 2.5%.

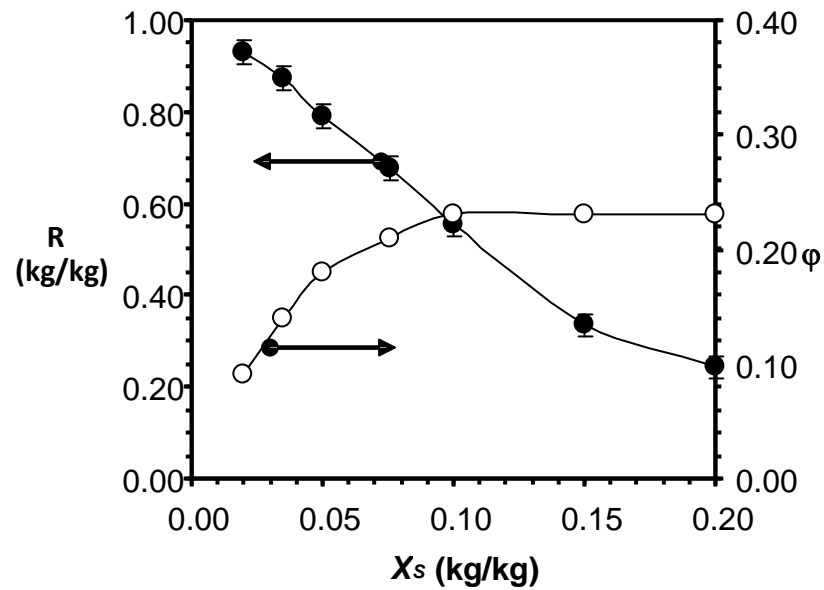


Figure 5.18: Flotation Recovery and Bubble Surface Coverage vs Solids Concentration [$d_p = 15 \mu\text{m}$; $d_b = 41 \mu\text{m}$; (\bullet) R exptl; (\circ) ϕ calc]

It can also be seen from Figure 5.18 that the corresponding calculated bubble surface coverage was 0.09 for a solids fraction loading of 0.02 and increased steadily before reach a steady value of 0.23 above $X_s = 0.1$. This trend is perhaps unexpected given that the collector loading actually decreased with increased solids concentration (see Table 5.6), which one would expect to cause a reduction in the hydrophobicity of the silica particles. If so, then there should be a decrease in the surface loading of particles. Given that the opposite trend in fractional surface coverage has occurred it can be assumed that the reduction in collector surface concentration is not a limiting factor in our flotation experiments.

The following explanation for the observed trend in the calculated bubble surface loading is proposed. Suppose that collected particles are arranged as “layers” around the surface of the bubble as shown in Figure 5.19.

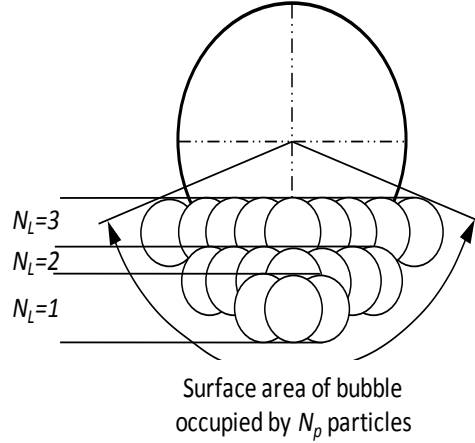


Figure 5.19: Layered Orientation of Particles on the Bubble Surface

Following the same analysis applied to Figure 3.1, the following equations can be derived in terms of the number of layers, N_L , of N_p attached particles:

$$\varphi = \frac{1}{2} \left(1 - \cos \left[\frac{2N_L d_p}{d_p + d_b} \right] \right), \quad (5.2)$$

$$N_p = 2 \left(\frac{d_p + d_b}{d_p} \right)^2 \left(1 - \cos \left[\frac{2N_L d_p}{d_p + d_b} \right] \right), \quad (5.3)$$

$$d_{b-N_L} = (d_p + d_b) \sin \left[\frac{2N_L d_p}{d_p + d_b} \right], \quad (5.4)$$

$$v_{b-N_L} = \frac{g}{18\mu_{pulp} d_{b-N_p}} \left[d_b^3 (\rho_{pulp} - \rho_G) + 2d_p (d_p + d_b)^2 (\rho_{pulp} - \rho_p) \left\{ 1 - \cos \left[\frac{2N_L d_p}{d_p + d_b} \right] \right\} \right]. \quad (5.5)$$

Equations 5.2-5.5 can be used to calculate the fractional coverage of the bubble and the bubble-particle aggregate diameter and rise/fall velocity for different numbers of particle layers. The results are given in Table 5.7.

It can be seen that for a single layer of particles the surface coverage is 0.07 and the rise velocity of the bubble-particle aggregate is positive and will therefore float to the

surface. However, if a second layer of particles is added ($N_L=2$) the rise velocity is negative and the bubble will no longer be able to recover the particles. It would seem therefore that a calculated surface coverage of 0.07 for a solids loading of 0.02, is the result of a single layer comprising of particles being present on the bubble surface. This is the limit for flotation adding another layer will cause the bubble to sink.

Table 5.7: Calculated ϕ , N_P , v_{b-N_L} , d_{b-N_L} vs N_L and ρ_{pulp}

ρ_{pulp} (kg/m^3)	N_L	ϕ	N_P (μm)	v_{b-N_L} (mm/min)	d_{b-N_L} (μm)
957	1	0.07	4	0.579	28.6
	2	0.26	15	-0.211	49.2
Critical conditions ($v_{b-N_L} = 0$)					
957	1.8	0.21	11	0.000	45.2
1055	1.9	0.24	13	0.000	47.7

Also listed in Table 5.7 is the critical number of layers corresponding to a zero rise velocity for the bubble-particle aggregate. For the system with a pulp density of 957 kg/m^3 the critical number of layers is 1.8 (or 11.4 particles). The corresponding surface loading is 0.26, which is close to the experimentally-calculated plateau value of 0.23. The critical surface loading for the highest observed pulp density of 1055 kg/m^3 is also reported in Table 5.7. It can be seen that the increase in pulp density results in an increase in the critical surface coverage, which would explain the observed increase in ϕ . Finally, from Table 5.7, the diameter of the bubble-aggregate is greater than the bubble diameter when there is more than a single layer of particles. The protrusion of the particles beyond the projected area of the bubble would result in increased drag on the attached particles, thereby increasing the likelihood that they would be dragged off the bubbles. This could also be another limiting factor on the number of particles that can remain attached to the bubble.

5.5.3 Effect of Particle Diameter and Gas Flowrate on Flotation Recovery and Bubble Surface Loading

The effect of particle diameter and hydrogen gas flowrate on the corrected flotation recovery fraction, $(R_{\text{exp}})_{\text{corr}}$, is shown in Figure 5.20. The corresponding data used in constructing the figure are summarised in Table 5.8. It can be seen that recovery (solid circles) increased with increased gas flowrate due to the increased number of bubbles (for collecting the particles) in the system. It can also be seen that for each particle size a maximum recovery was reached which remained steady when more gas was introduced into the cell. The maximum recoveries, after 2 minutes of flotation, were found to be 0.82, 0.90, 0.96 and 0.88 for the 3.1, 5.3, 12.3 and 14.7 μm diameter particles, respectively. The peak in the recovery of silica for the 12.3 μm diameter particles is similar to the peak in collection efficiency observed by Dobby and Finch (1987), who attributed it to an optimisation of collision and attachment efficiencies. The observation that there was a decrease in flotation for the 14.7 μm diameter particles is consistent with the findings of Ketkar et al. (1991) who reported a decrease in removal efficiency with increased particle size in the range of 6.5-65 μm . Greater than 90 percent recovery for the 5.3-12.3 μm diameter particles is encouraging given that this particle size range is below the usual limit for conventional flotation devices (Trahar and Warren, 1976).

Also shown in Figure 5.20 are the corresponding fractional coverage of the bubble surface area, ϕ , values that have been calculated from fractional recovery measurements and the model equations presented in this study. The relevant model parameters are listed in Table 5.8, including calculated values of the non-floating component, K_4 , obtained by applying the maximum floatable particle diameter criteria to the particle size distributions listed in Appendix C. It can be seen that for the 3.1 μm diameter particles ϕ remained steady between 0.35-1.6 mL/min, and beyond that range monotonically decreased with further increases in gas flowrate. For the three other particle sizes, ϕ monotonically decreased over the entire range of gas flowrates investigated. There was also the general trend that ϕ decreased with increasing particle diameter, with average ϕ values of 0.32, 0.14, 0.05 and 0.03 being observed for the 3.1, 5.3, 12.3 and 14.7 μm diameter particles, respectively.

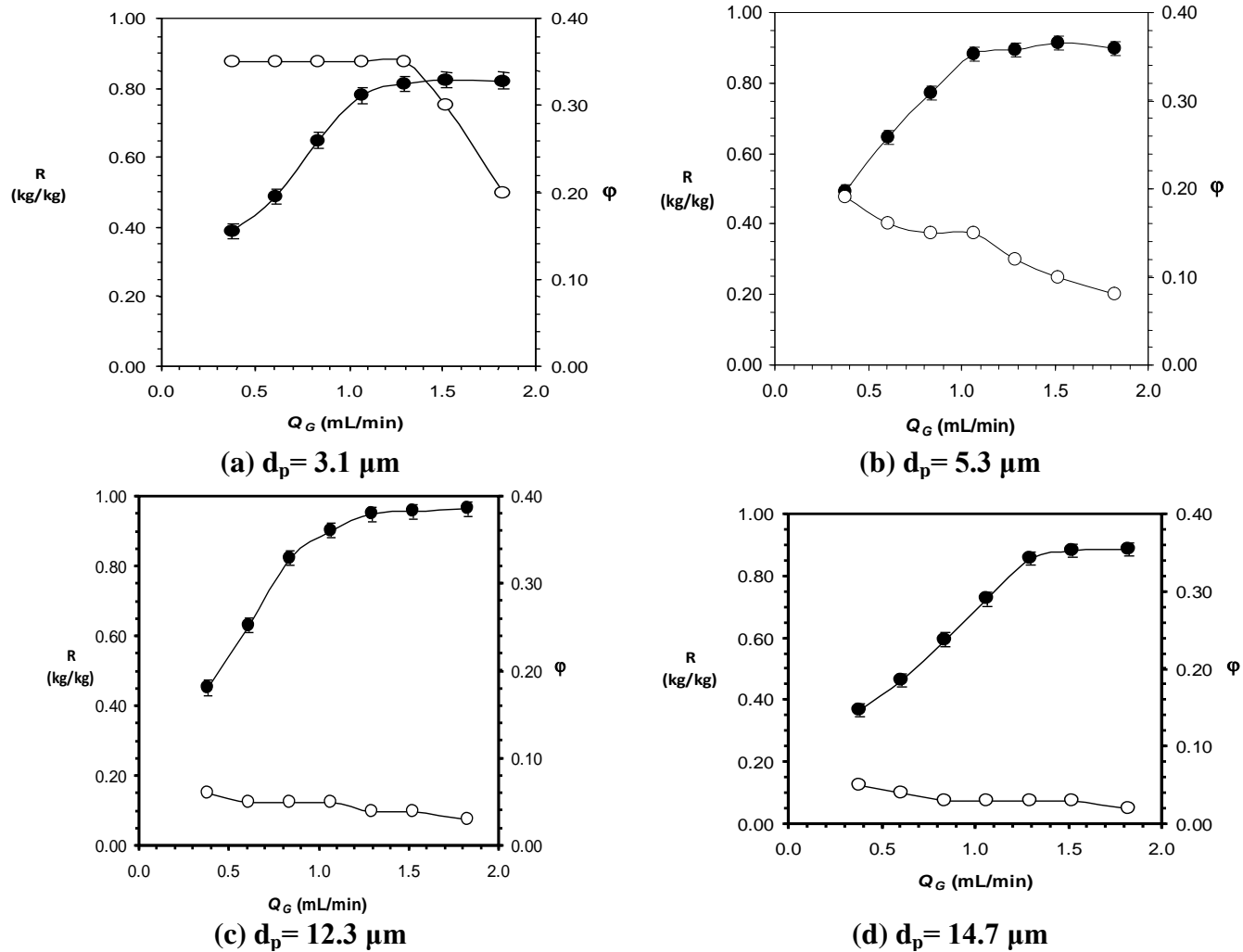


Figure 5.20: Recovery and Bubble Surface Coverage vs Gas Flowrate

[● Recovery (exptl); ○ surface coverage (model); X_S=0.02; d_b=30 μm; f=1]

Table 5.8: Experimental and Model Data for different d_p and Q_G

		0.380	0.608	0.836	1.064	1.293	1.521	1.825
d_p	μm	3.1	3.1	3.1	3.1	3.1	3.1	3.1
X_S	-	0.02	0.02	0.02	0.02	0.02	0.02	0.02
ε_G	-	0.03	0.05	0.07	0.09	0.12	0.15	0.21
ρ_{pulp}	kg/m^3	983	964	944	919	893	861	803
$(d_p)_{\text{max}}$	μm	25.1	24.9	24.6	24.3	23.9	23.5	22.7
K_4	-	0.000	0.000	0.000	0.000	0.000	0.000	0.000
$(R_{\text{exp}})_{\text{corr}}$	-	0.389	0.488	0.650	0.778	0.814	0.823	0.822
φ	-	0.35	0.35	0.35	0.35	0.35	0.30	0.20
d_{b-N_p}	μm	33.6	33.6	33.6	33.6	33.6	32.1	27.6
v_{b-N_p}	mm/s	0.32	0.31	0.30	0.29	0.28	0.29	0.32
d_p	μm	5.3	5.3	5.3	5.3	5.3	5.3	5.3
X_S	-	0.02	0.02	0.02	0.02	0.02	0.02	0.02
ε_G	-	0.03	0.05	0.07	0.09	0.12	0.15	0.21
ρ_{pulp}	kg/m^3	983	964	944	919	893	861	803
$(d_p)_{\text{max}}$	μm	25.1	24.9	24.6	24.3	23.9	23.5	22.7
K_4	-	0.000	0.000	0.000	0.000	0.000	0.000	0.000
$(R_{\text{exp}})_{\text{corr}}$	-	0.491	0.646	0.773	0.881	0.892	0.913	0.896
φ	-	0.19	0.16	0.15	0.15	0.12	0.10	0.08
d_{b-N_p}	μm	29.4	27.3	26.5	26.5	24.0	22.0	19.8
v_{b-N_p}	mm/s	0.37	0.38	0.37	0.36	0.36	0.36	0.34
d_p	μm	12.3	12.3	12.3	12.3	12.3	12.3	12.3
X_S	-	0.02	0.02	0.02	0.02	0.02	0.02	0.02
ε_G	-	0.03	0.05	0.07	0.09	0.12	0.15	0.21
ρ_{pulp}	kg/m^3	983	964	944	919	893	861	803
$(d_p)_{\text{max}}$	μm	25.1	24.9	24.6	24.3	23.9	23.5	22.7
K_4	-	0.071	0.074	0.078	0.082	0.088	0.095	0.111
$(R_{\text{exp}})_{\text{corr}}$	-	0.455	0.636	0.830	0.910	0.955	0.964	0.973
φ	-	0.06	0.05	0.05	0.05	0.04	0.04	0.03
d_{b-N_p}	μm	20.8	19.0	19.0	19.0	17.0	17.0	14.7
v_{b-N_p}	mm/s	0.40	0.40	0.39	0.38	0.38	0.36	0.35
d_p	μm	14.7	14.7	14.7	14.7	14.7	14.7	14.7
X_S	-	0.02	0.02	0.02	0.02	0.02	0.02	0.02
ε_G	-	0.03	0.05	0.07	0.09	0.12	0.15	0.21
ρ_{pulp}	kg/m^3	983	964	944	919	893	861	803
$(d_p)_{\text{max}}$	μm	25.1	24.9	24.6	24.3	23.9	23.5	22.7
K_4	-	0.079	0.082	0.087	0.099	0.102	0.108	0.119
$(R_{\text{exp}})_{\text{corr}}$	-	0.371	0.470	0.601	0.733	0.863	0.891	0.897
φ	-	0.05	0.04	0.03	0.03	0.03	0.03	0.02
d_{b-N_p}	μm	20.1	17.9	15.5	15.5	15.5	15.5	12.6
v_{b-N_p}	mm/s	0.40	0.41	0.41	0.40	0.39	0.37	0.36

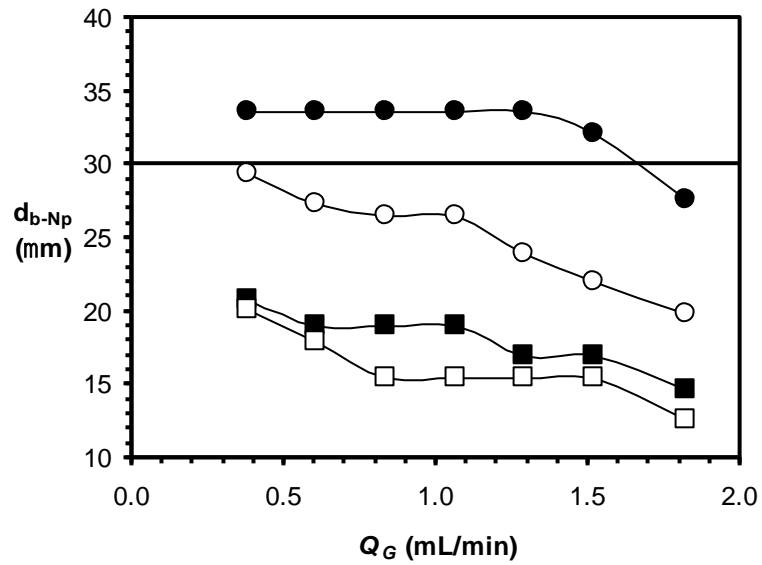
The reason for the variation in the fractional coverage of the bubble, for both gas flow rate and particle size is not immediately apparent. The collector concentration of [CTAB]= 4.46×10^{-5} M was constant for all experiments and corresponded to monolayer surface coatings on the particles of 1.14, 1.84, 4.29 and 5.68 m^2/m^2 for the 3.1, 5.3, 12.3 and 14.7 μm diameter particles, respectively. Surface coatings of greater than unity ensured that there was sufficient collector to maintain a constant hydrophobicity over the entire size range of particles. All four particle systems were operated at the same solids mass fraction so that for a given gas flow rate the number of attached particles per bubble was expected to increase with decreasing particle diameter. Similarly, as more bubbles were introduced by increasing the gas flow rate the surface coverage was expected to decrease. Both of these trends were successfully calculated by the model.

In an effort to understand the variation in the surface coverage of the bubble for the different particle sizes the computed diameter of the bubble-particle aggregate, d_{b-Np} , calculated in accordance with Equation 3.74, has been plotted in Figure 5.21(a) for each particle size and as a function of the gas flowrate. Also shown (as a horizontal solid line) is the corresponding bubble diameter of 30 μm . It can be seen that it was only for the smallest particle diameter of 3.1 μm (●) that the aggregate diameter was greater than that of the bubble. Also shown in Figure 5.21(b) are the corresponding bubble-particle aggregate rise velocities. It can be seen that for all particle sizes the rise velocity was well above zero, so the aggregates were readily able to be floated.

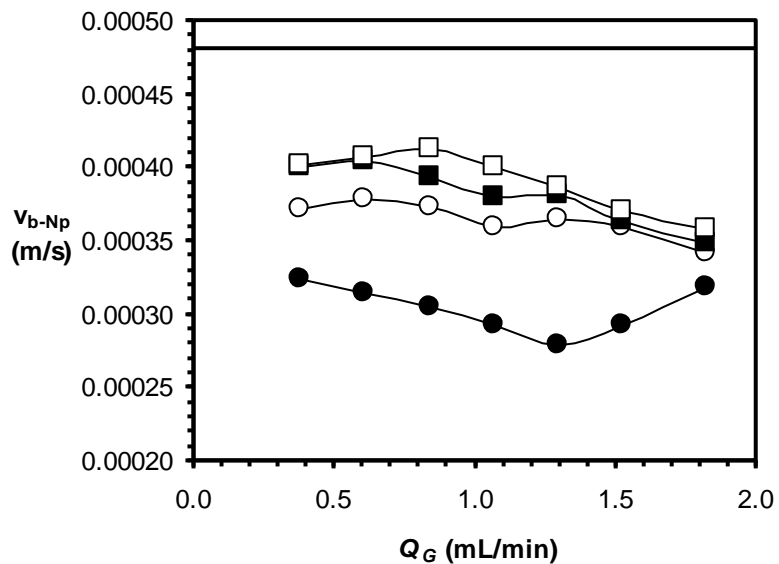
Following the same approach that leads to the development of Equations 5.2-5.5, for the 3.1 μm diameter particles. The analysis showed that the bubble-particle aggregate would still float, i.e. has a positive rise velocity, with 100² percent surface coverage of particles. The analysis also showed that a total of 7 layers (comprising 171 particles) of particles were able to be deposited onto the bubble surface before the bubble-particle aggregate diameter became greater than the bubble size. The corresponding surface coverage was 0.35, which is in close agreement with the 0.33 obtained from the experimental measurements. It would seem, therefore, that the upper limit of attached particles was limited by extra drag they would experience if their surface was extended beyond the original diameter of the bubble. Hence the plateau in the bubble surface

²Falls to 90 percent at the highest gas flowrate due to the decreased density of the pulp.

loading at low gas flow rates. A point is reached at higher gas flow rates where the number of bubbles is increased to such a level that the surface loading is reduced due to an insufficient number of particles.



a) Aggregate diameter



b) Aggregate rise velocity

Figure 5.21: Bubble-Particle Aggregate Diameter and Rise Velocity vs Gas Flowrate [d_p (μm): 3.1 (●), 5.3 (○), 12.3 (■), 14.7 (□) ; $X_s = 0.02$; $d_b = 30 \mu\text{m}$; $f = 1$]

The analysis for particle sizes greater than 3.1 μm diameter is shown in Table 5.9. For the 5.3 μm diameter particles the analysis (not given here) showed that a bubble surface coverage of approximately 0.6 was required before the rise velocity became negative. However, a bubble surface coverage greater than 0.24 was needed before the diameter of the bubble-particle aggregate became greater than the bubble diameter. Consequently, applying a critical condition that $d_{b-N_L} = d_b$ then the bubble would only be able to accommodate 3 layers of particles, with a corresponding bubble surface coverage of 0.18, which is in good agreement with the experimentally-obtained value of 0.19. Applying the same condition to the other two particle sizes gave values of 0.08 and 0.10 for the 12.3 and 14.7 μm diameter particles, respectively, which are in relatively good agreement with the observed values of 0.06 and 0.05. For both the 12.3 and 14.7 μm diameter particles there seems also to be buoyancy limitations, i.e. negative rise velocities, if more than one layer of particles are added to the bubbles.

Table 5.9: Calculated ϕ , N_P , v_{b-N_L} , d_{b-N_L} vs N_L and $\rho_{\text{pulp}}=983 \text{ kg/m}^3$

d_p (μm)	N_L	ϕ	N_P (μm)	v_{b-N_L} (mm/min)	d_{b-N_L} (μm)
5.3	3	0.18	34	0.367	27.9
	4	0.30	57	0.243	33.4
12.3	1	0.08	3.9	0.302	23.3
	2	0.29	14.4	-0.232	39.3
14.7	1	0.10	3.9	0.155	31.0
	2	0.36	13.9	-0.604	43.9
Critical conditions ($d_{b-N_L} = d_b$)					
5.3	3.5	0.24	45	0.318	31.0
12.3	1.4	0.15	7.5	0.106	31.0
14.7	1.2	0.13	5.1	0.037	31.0

5.5.4 Summary on Silica Recovery by Electrolytic Hydrogen Bubbles

It was found that recoveries greater than 85 percent could be achieved by electrolytically produced hydrogen bubbles for the particles in the size range 3-15 μm

diameter. It is encouraging given that this particle size range is below the usual limit for conventional flotation devices (Trahar and Warren, 1976). Application of the model developed in this study highlighted the significance of bubble surface loading when predicting flotation recovery. Unfortunately, it is almost impossible to measure the bubble surface loading directly for actual flotation experiments, and estimates have to be obtained indirectly. The model developed as part of this study was utilised to compute the bubble surface loading. It was found that it varied between experiments and was a function of gas flowrate, bubble and particle size, and solids concentration. Further analysis, based on a layered packing of the particles around the bubble perimeter, indicated that flotation recovery was controlled by either the bubble-particle aggregate rise velocity being greater than zero or the bubble-particle aggregate projected area being less than that of just the bubble. The simple analysis presented in this study highlighted that much more research is needed into how particles are assembled on and detached from the bubble surface.

5.6 CONCLUSIONS

The experimental observations and model analyses helped to remove some of the lacking in the existing literatures of electroflotation study. These include:

From Denver cell experiment of silica recovery, it was found that there was no measurable difference in the flotation recovery using molecular hydrogen and air. This confirmed that there was no interaction between the gas phase (air and molecular hydrogen) and the solids surface (silica).

The electroflotation bubble size measurement experiment explained and tried to remove the uncertainty in the existing literature about hydrogen bubble size produced from cathode through electrolysis of water. It may be concluded that a simple balance including buoyancy and surface tension forces will provide a reasonable estimation of the detachment diameter for hydrogen bubbles. The detachment diameter is strongly influenced by the three phase contact angle, and to a much lesser degree by the diameter of the wire electrode. Conversely, current density seems to have almost no effect on the detachment diameter. The nucleation rate increased with increasing current density as well as treatment (platinisation) of the electrode surface. The detachment and bulk

diameter both seem to be a function of external liquid flow with a decrease in size as liquid flow increases. Finally, the observation that bubble diameter was a function of position, time, dissolved gas concentration profile and electrode surface treatment, has helped to explain why there is such a wide variation in reported measurements across the literature.

From the experimental measurements of gas rate produced from steel mesh cathode, it was observed that almost all of the (theoretical) hydrogen produced by the electrolysis process resulted in gas phase and that the rate of production of hydrogen gas was only slightly influenced by presence of solids, dissolved gas and mechanical agitation. These findings are desirable in terms of flotation since recovery is directly related to the amount (and size) of bubbles inputted into the cell.

Flotation experiments of hydrophobised silica particles utilizing electrolytically-produced hydrogen gave flotation recovery greater than 85 percent for the particles in the size range 3-15 μm diameter which is the usual size limit for conventional flotation. This higher recovery can be directly attributed to the generation of very small bubbles which are known to increase flotation recovery, especially for the fine particles of diameter less than 15 μm used here. The experimental results were inputted into a recovery model, based largely on the work of Koh and Schwarz (2006), that was applied to gain insight into the factors that influence the fractional coverage of the bubble surface by the particles. From the analysis it was found that, for this study at least, flotation recovery was controlled by either the bubble-particle aggregate rise velocity being greater than zero or the bubble-particle aggregate projected area being less than that of just the bubble.

Finally, it can be said that all of the above findings will help to efficiently design efficient electroflotation systems to recover very fine particles.

Chapter 6

CONCLUSIONS AND RECOMMENDATIONS

6.1 SUMMARY

This study was aimed at developing an increased understanding of the principles of electroflotation and to use this knowledge to optimize its application in water treatment and mineral processing. The experimental observations and model analyses have helped to clarify the use of electroflotation in the following areas.

To investigate the interaction between the gas phase with the mineral surface, the flotation of silica was performed in a laboratory scale Denver cell, type D12. From experimental observations it was found that there was no measurable difference in the flotation recovery using molecular hydrogen and air. This confirmed that there was no interaction between the gas phase (air and molecular hydrogen) and the mineral surface (silica). Very similar contact angle measurement for the silica-air-water and silica-hydrogen-water systems also supported this notion.

The electroflotation bubble size measurement experiments explained and tried to remove the uncertainty in the existing literature about hydrogen bubble size produced from the electrolysis of water. Experiments were performed in a transparent cell that allowed direct visualization of hydrogen bubbles being generated and transported away from platinum wire electrodes of 90, 120 and 190 μm in diameter. It may be concluded that a simple force balance including buoyancy and surface tension forces will provide a reasonable estimation of the detachment diameter for hydrogen bubbles. The detachment diameter is strongly influenced by the three phase contact angle, and to a much lesser degree by the diameter of the wire electrode. Conversely, current density seems to have almost no effect on the detachment diameter. The nucleation rate increased with increasing current density, as well as treatment (platinisation) of the electrode surface, which was expected. The detached bubbles were found to increase in volume up to 8-fold as they moved away from the electrode surface and rose through the electrolyte solution. This increase in bubble size was found to be mostly due to the

transfer of dissolved hydrogen into growing bubble while moving through the electrolyte super saturated by dissolved hydrogen gas. Bubble size measurement experiments were also performed with a flow of electrolyte. With the assistance of a peristaltic pump, a flow electrolyte was generated in the cell. The detachment and bulk diameter both were found to be a function of external liquid flow and were found to decrease in size with increased liquid flow. Finally, the observation that bubble diameter was a function of position, time, dissolved gas concentration profile and electrode surface treatment has helped to explain why there is such wide variation in reported measurements across the literature.

In order to investigate the influence of current density, solids concentration, mechanical agitation and pre-existing dissolved gases on hydrogen gas generation rate, experiments were performed to measure hydrogen gas produced from a steel mesh cathode. Experimental observations confirmed that ~ 98% of the (theoretical) hydrogen produced by the electrolysis process resulted in gas phase (bubbles). Almost all of the electrical power is being converted to hydrogen (and oxygen) bubbles that can be used for flotation recovery, which is a very positive finding. For a given current density, the rate of hydrogen gas production was largely independent of solids concentration, while mechanical agitation slightly increased the gas production rate. Conversely, gas production rate decreased slightly for previously degassed electrolyte solution.

Batchwise flotation experiments were performed to investigate the effect of solids concentration, particle size, bubble size and gas flowrate. Very fine silica particles of mean diameter in the range 3-15 μm were floated by electrolytically produced hydrogen bubbles of mean diameter 30 and 40 μm . It was found that recoveries greater than 85 % could be achieved by electrolytically produced hydrogen bubbles for the particles in the size range 3-15 μm diameter. This higher recovery can be directly attributed to the generation of very small bubbles (<40 μm in diameter) which are known to increase flotation recovery, especially for fine particles of diameter <15 μm used in this study. It is encouraging given that this particle size range is below the usual limit for conventional flotation devices (Trahar and Warren, 1976). Application of the model developed in this study highlighted the significance of bubble surface loading when predicting flotation recovery. Unfortunately, it is almost impossible to measure the bubble surface loading directly for actual flotation experiments, and estimates have to

be obtained indirectly. The model developed as part of this study was utilised to compute the bubble surface loading. It was found that it varied between experiments and was a function of gas flowrate, bubble and particle size, and solids concentration. Further analysis, based on a layered packing of the particles around the bubble perimeter, indicated that for this study, at least, flotation recovery was controlled by either the bubble-particle aggregate rise velocity being greater than zero or the bubble-particle aggregate projected area being less than that of just the bubble.

Finally, it can be said that all of the above findings will help to design efficient electroflotation systems to recover very fine particles.

6.2 RECOMMENDATIONS FOR FUTURE WORK

This study has identified the following areas that require further investigation:

- Experimental verification of the interaction between the gas phase with different mineral surfaces.
- Bubble size measurement produced from other cathode conditions (geometry and materials).
- Experimental verification of the effect of liquid flow on bubble size using other cathode conditions (geometry and materials).
- Theoretical analysis of the effect of liquid flow on detachment of bubbles from the electrodes and their subsequent growth.
- Further research to determine the bubble surface loading for a wide range of experimental conditions such as uniformity of particle size (mono size or wide range size), surface properties of particles (shape, roughness), mode of operation (batchwise or continuous), solids loading, gas flowrate, and flotation time.
- Further research to investigate how particles are assembled on and detached from the bubble surface.
- Further research on the effect of bubble-particle aggregate velocity on flotation recovery.
- This research was restricted to the study of hydrogen bubble only. Further research may be performed involving oxygen bubbles as well.

REFERENCES

- Ahmed, N. & Jameson, G. J. (1985) The effect of bubble size on the rate of flotation of fine particles. *International Journal of Mineral Processing*, 14, 195-215.
- Aleksandrov, I. V., Rodyushkin, O. I. & Ibraev, K. S. (1992) Electroflotation treatment of wastewaters from by-product coke production to remove tars and oils. *Koks I Khimiya*, 7, 41-44.
- Alexandrova, L., Nedialkova, T. & Nishkov, I. (1994) Electroflotation of metal ions in wastewater. *International Journal of Mineral Processing*, 41, 285–294.
- Anfruns, J. F. & Kitchener, J. A. (1977) Rate of capture of small particles in flotation. *Transactions of the Institution of Mining and Metallurgy, Section C: Mineral Processing and Extractive Metallurgy*, 86, 9-15.
- Araya-Farias, M., Mondor, M., Lamarche, F., Tajchakavit, S. & Makhlouf, J. (2008) Clarification of apple juice by electroflotation. *Innovative Food Science & Emerging Technologies*, 9, 320-327.
- Ashcroft, N. W. & Mermin, N. D. 1988. *Solid State Physics*, New York, Holt, Rinehart and Winston.
- Balmer, L. M. & Foulds, A. W. (1986) Separation of oil from oil-in-water emulsions by electroflocculation/electroflotation. *Fil. Sep.*, 23, 366–369.
- Bande, R. M., Prasad, B., Mishra, I. M. & Wasewar, K. L. (2008) Oil field effluent water treatment for safe disposal by electroflotation. *Chemical Engineering Journal*, 137, 503-509.
- Ben Mansour, L., Chalbi, S. & Kesentini, I. (2007) Experimental study of hydrodynamic and bubble size distributions in electroflotation process. *Indian Journal of Chemical Technology*, 14, 253-257.
- Bewig, K. W. & Zisman, W. A. (1965) The wetting of gold and platinum by water. *The Journal of Physical Chemistry*, 69, 4238-4242.
- Biswal, S. K., Reddy, P. S. R. & Bhaumik, S. K. (1994) Bubble size distribution in a flotation column. *The Canadian Journal of Chemical Engineering*, 72, 148-152.
- Boucher, E. A. & Evans, M. J. B. (1975) Pendant drop profiles and related capillary phenomena. *Proc. R. Soc. Lond. A*.

- Bouyakoub, A. Z., Kacha, S., Ouhib, R., Bellebia, S. & Lartiges, B. (2010) Combined treatment of a textile effluent containing reactive dyes by coagulation-flocculation and electroflotation. *Revue Des Sciences De L'eau* 23, 89-103.
- Brandon, N. P. & Kelsall, G. H. (1985a) Growth kinetics of bubbles electrogenerated at microelectrodes. *Journal of Applied Electrochemistry*, 15, 475-484.
- Brandon, N. P. & Kelsall, G. H. (1985b) Interfacial electrical properties of electrogenerated bubbles. *Journal of Applied Electrochemistry*, 15, 485-493.
- Buehl, W. M. & Westwater, J. W. (1966) Bubble growth by dissolution: influence of contact angle. *AIChE Journal* 12, 571-576.
- Burns, S. E., Yiacoumi, S. & Tsouris, C. (1997) Microbubble generation for environmental and industrial separations. *Separation and Purification Technology*, 11, 221-232.
- Bushell, C. H. G. (1962) Kinetics of flotation. *Transactions of the American Institute of Mining, Metallurgical and Petroleum Engineers*, 223, 266-278.
- Calabrese, R. V., Chang, T. P. K. & Dang, P. T. (1986) Drop breakup in turbulent stirred-tank contactors. part I: effect of dispersed-phase viscosity. *AIChE Journal*, 32, 657-666.
- Camilleri, C. (1985) Electroflotation et flotation al'air disous. *Industrie Mineral, Les Techniques*, 67, 25-30.
- Carslaw, H. S. & Jaeger, J. C. (1959) *Conduction of heat in solids*, Oxford.
- Casqueira, R. G., Torem, M. L. & Kohler, H. M. (2006) The removal of zinc from liquid streams by electroflotation. *Minerals Engineering*, 19, 1388-1392.
- Chen, G., Chen, X. & Yue, P. L. (2000) Electrocoagulation and electroflotation of restaurant wastewater. *Journal of Environmental Engineering*, 126, 858-863.
- Chen, W. & Horan, N. J. (1998) The treatment of a high strength pulp and paper mill effluent for wastewater re-use-III. Tertiary treatment options for pulp and paper mill wastewater to achieve effluent recycle. *Environ. Technol.*, 19, 173-182.
- Chen, X., Chen, G. & Yue, P. L. (2002) Novel electrode system for electroflotation of wastewater. *Environmental Science and Technology*, 36, 778-783.
- Chipfunhu, D., Zanin, M. & Grano, S. (2011) The dependency of the critical contact angle for flotation on particle size - modelling the limits of fine particle flotation. *Minerals Engineering*, 24, 50-57.

- Clark, S. W. & Cooke, S. R. B. (1968) Adsorption of calcium, magnesium, and sodium ion by quartz. *Transactions of the Society of Mining Engineers of AIME*, 241, 334-341.
- Clift, R., Grace, B. J. & Weber, M. E. (1978) *Bubbles, drops, and particles*, New York, Academic Press.
- Collins, G. L. & Jameson, G. J. (1976) Experiments on the flotation of fine particles: the influence of particle size and charge. *Chemical Engineering Science*, 31, 985-991.
- Collins, G. L. & Jameson, G. J. (1977) Double-layer effects in the flotation of fine particles. *Chemical Engineering Science*, 32, 239-246.
- Coulson, J. M., Richardson, J. F., Backhurst, J. R. & Harker, J. H. (1990) *Chemical Engineering. Volume 1: Fluid Flow, Heat Transfer and Mass Transfer*, Oxford, Pergamon Press.
- Crawford, R. J. (1986) Particle size, hydrophobicity and flotation response. *Department of Applied Chemistry*. Swinburne Institute of Technology.
- Dai, Z., Dukhin, S., Fornasiero, D. & Ralston, J. (1998) The inertial hydrodynamic interaction of particles and rising bubbles with mobile surfaces. *Journal of Colloid and Interface Science*, 197, 275-292.
- Dai, Z., Fornasiero, D. & Ralston, J. (1999) Particle-bubble attachment in mineral flotation. *Journal of Colloid and Interface Science*, 217, 70-76.
- Dai, Z., Fornasiero, D. & Ralston, J. (2000) Particle-bubble collision models -a review. *Advances in Colloid and Interface Science*, 85, 231-256.
- De Rijk, S. E., Jaap H.J.M. Aivan Der, G. & Den Blanken, J. G. (1994) Bubble size in flotation thickening. *Water Research*, 28, 465-473.
- Deglon, D. A., Egya-Mensah, D. & Franzidis, J. P. (2000) Review of hydrodynamics and gas dispersion in flotation cells on south African platinum concentrators. *Minerals Engineering*, 13, 235-244.
- Deglon, D. A., Sawyerr, F. & O'connor, C. T. (1999) A model to relate the flotation rate constant and the bubble surface area flux in mechanical flotation cells. *Minerals Engineering*, 12, 599-608.
- Derjaguin, B. V. & Dukhin, S. S. (1961) Theory of flotation of small bubbles and medium sized particles. *Transactions of the Institute of Mining and Metallurgy*, 70, 221-246.

- Derjaguin, B. V. & Shukakidse, N. D. (1961) Dependence of the floatability of antimonite on the value of zeta-potential. *Transactions of the Institute Mining and Metallurgy*, 70, 569-574.
- Devivo, D. G. & Karger, B. L. (1970) Flotation of colloidal particulates: the effects of aggregation in the flotation process. *Separation Science*, 5, 145-167
- Diaz-Penafiel, P. & Dobby, G. S. (1994) Kinetic studies in flotation columns: bubble size effect. *Minerals Engineering*, 7, 465-478.
- Dibbs, H. P., Sirois, L. L. & Brendin, R. (1972) *Research Reoport*. Ottawa, Canada, Department of Energy, Mines and Resources, Mines Branch.
- Dobby, G. S. & Finch, J. A. (1986) A model of particle sliding time for flotation size bubbles. *Journal of Colloid and Interface Science*, 109, 493-498.
- Dobby, G. S. & Finch, J. A. (1987) Particle size dependence in flotation derived from a fundamental model of the capture process. *International Journal of Mineral Processing*, 21, 241-260.
- Drzymala, J. (1994) Characterization of materials by hallimond tube flotation, part 2: maximum size of floating particles and contact angles. *International Journal of Mineral Processing*, 42, 153-167.
- Dukhin, S. S. (1982) Role of inertial forces in flotation of small particles. *Kolloidnyi Zhurnal* 44, 431-441.
- Dukhin, S. S. & Rulev, N. N. (1977) Hydrodynamic interaction of a solid spherical particle with a bubble in an elementary flotation act. *Kolloidnyi Zhurnal*, 39, 270-275.
- Edzwald, J. K. (1995) Principles and applications of dissolved air flotation. *Water Science and Technology*, 31, 1-23.
- Elmore, F. E. (1905) A process for separating certain constituents of subdivided ores and like substances and apparatus therefor. Br. Patent, 13,578.
- Englert, A. H., Rodrigues, R. T. & Rubio, J. (2009) Dissolved air flotation (DAF) of fine quartz particles using an amine as collector. *International Journal of Mineral Processing*, 90, 27-34.
- Estefan, S. F. (1976) Adsorption and desorption of cetyl trimethyl ammonium bromide in cationic flotation of quartz. *Tenside Detergents*, 13, 34-37.
- Evans, G. M., Doroodchi, E., Lane, G. L., Koh, P. T. L. & Schwarz, M. P. (2008) Mixing and gas dispersion in mineral flotation cells. *Chemical Engineering Research and Design*, 86, 1350-1362.

- Evans, G. M., Jameson, G. J. & Atkinson, B. W. (1992) Prediction of the bubble size generated by a plunging liquid jet bubble column. *Chemical Engineering Science*, 47, 3265-3272.
- Finch, J. A. & Dobby, G. S. (1990) *Column Flotation*, Oxford, Pergamon Press.
- Flint, L. R. & Howarth, W. J. (1971) The collision efficiency of small particles with spherical air bubbles. *Chemical Engineering Science*, 26, 1155-1168.
- Fuerstenau, D. W. (1957) Correlation of contact angles, adsorption density, zeta potentials and flotation rate. *Trans. AIME*, 208, 1365-1367.
- Fukui, Y. & Yuu, S. (1980) Collection of submicron particles in electro-flotation. *Chemical Engineering Science*, 35, 1097-1105.
- Fukui, Y. & Yuu, S. (1985) Removal of colloidal particles in electroflotation. *AIChE Journal*, 31, 201-208.
- Gardner, J. R. & Woods, R. (1974) An electrochemical investigation of contact angle and of flotation in the presence of alkylxanthates-I. Platinum and gold Surfaces. *Australian Journal of Chemistry*, 27, 2139-2148.
- Gardner, J. R. & Woods, R. (1977) The hydrophilic nature of gold and platinum. *Journal of Electroanalytical Chemistry*, 81, 285-290.
- Gaudin, A. M. (1957) *Flotation*, New York, McGraw-Hill.
- Gaudin, A. M. & Fuerstenau, D. W. (1955) Quartz flotation with anionic collectors. *Transactions of the American Institute of Mining, Metallurgical and Petroleum Engineers*, 202 (Tech. Pub. 3964b), 66-72.
- Gaudin, A. M., Schuhmann, R. & Schlechten, A. W. (1942) Flotation kinetics. II. the effect of size on the behaviour of galena particles. *Journal of Physical Chemistry*, 46, 902-910.
- George, P., Nguyen, A. V. & Jameson, G. J. (2004) Assessment of true flotation and entrainment in the flotation of submicron particles by fine bubbles. *Minerals Engineering*, 17, 847-853.
- Girgin, E. H., Do, S., Gomez, C. O. & Finch, J. A. (2006) Bubble size as a function of impeller speed in a self-aeration laboratory flotation cell. *Minerals Engineering*, 19, 201-203.
- Glas, J. P. & Westwater, J. W. (1964) Measurements of the growth of electrolytic bubbles. *International Journal of Heat and Mass Transfer*, 7, 1427-1430.

- Glembotskii, V. A. (1953) Rate of adhesion of air-bubbles to mineral particles during flotation, and methods for its measurement. *Izvestiya Akademii Nauk Sssr, Otdelenie Tekhnicheskikh Nauk* 1524-1531.
- Glembotskii, V. A., Mamakov, A. A., Ramanov, A. M. & Nenno, V. E. (1975) Selective separation of fine minerals slimes using the method of electroflotation. *Eleventh International Minerals Processing Congress, Cagliari*.
- Glembotskii, V. A., Mamakov, A. A. & Sorokina, V. N. (1973) Size of gas bubbles formed under electroflotation conditions. *Elektronnaya Obrabotka Materialov*, 5, 66-68.
- Glembotsky, V. A., Mamakov, A. A. & Sorokina, V. N. (1971) Influence of electrolytic gases on the flotation of barite. *Elektronnaya Obrabotka Materialov*, 5, 41.
- Gontijo, C. D. F., Fornasiero, D. & Ralston, J. (2007) The limits of fine and coarse particle flotation. *The Canadian Journal of Chemical Engineering*, 85, 739-747.
- Gorain, B. K., Franzidis, J. P. & Manlapig, E. V. (1995) Studies on impeller type, impeller speed and air flow rate in an industrial scale flotation cell-part 1: effect on bubble size distribution. *Minerals Engineering*, 8, 615-635.
- Gorain, B. K., Franzidis, J. P. & Manlapig, E. V. (1997) Studies on impeller type, impeller speed and air flow rate in an industrial scale flotation cell, part 4: effect of bubble surface area flux on flotation performance. *Minerals Engineering*, 10, 367-379.
- Grano, S. (2006) Effect of impeller rotational speed on the size dependent flotation rate of galena in full scale plant cells. *Minerals Engineering*, 19, 1307-1318.
- Grau, R. A. & Heiskanen, K. (2005) Bubble size distribution in laboratory scale flotation cells. *Minerals Engineering*, 18, 1164-1172.
- Han, M. Y., Ahn, H. J., Shin, M. S. & Kim, S. R. (2004) The effect of divalent metal ion on the zeta potential of bubbles. *Water Science & Technology*, 50, 49-56.
- Han, M. Y., Kim, M. K. & Ahn, H. J. (2006) Effects of surface charge, micro-bubble size and particle size on removal efficiency of electro-flotation. *Water Science and Technology*, 53, 127-132.
- Han, M. Y., Park, Y. H. & Yu, T. J. (2002) Development of a new method of measuring bubble size. *Water Supply*, 2, 77-83.
- Harris, C. C. & Mensah-Biney, R. K. (1977) Aeration characteristics of laboratory flotation machine impellers. *International Journal of Mineral Processing*, 4, 51-67.

- Hernlem, B. J. & Tsai, L. S. (2000) Chlorine generation and disinfection by electroflotation. *J. Food Sci.*, 65, 834–837.
- Hewitt, D., Fornasiero, D. & Ralston, J. (1995) Bubble-particle attachment. *J. Chem. Soc., Faraday Trans.*, 91, 1997-2001.
- Hinze, J. O. (1955) Fundamentals of the hydrodynamic mechanism of splitting in dispersion processes. *AIChE Journal*, 1, 289-295.
- Ho, C. C. & Chan, C. Y. (1986) The application of lead dioxide-coated titanium anode in the electroflotation of palm oil mill effluent. *Water Res.*, 20, 1523–1527.
- Hogan, P., Kuhn, A. T. & Turner, J. F. (1979) Electroflotation studies based on cassiterite ores. *Transactions of the Institution of Mining and Metallurgy, Section C: Mineral Processing and Extractive Metallurgy*, 88, C83-C87.
- Hogan, P., Kuhn, A. T. & Wills, B. A. (1976) Electroflotation-review and future prospects in mineral separations. *Camborne School of Mines Journal*, 76, 48-54.
- Hopstock, M., D. & Agar, G. E. (1968) Effect of cations on the amine flotation of quartz. *Transactions of the Society of Mining Engineers of AIME*, 241, 466-470.
- Hosny, A. Y. (1996) Separating oil from oil–water emulsions by electroflotation technique. *Separation and Purification Technology*, 6, 9-17.
- Huang, C. J. & Liu, J. C. (1999) Precipitate flotation of fluoride containing wastewater from a semiconductor manufacturer. *Water Res.*, 33, 3403–3412.
- Huls, B. J., Lachance, C. D. & Dobby, G. S. (1991) Bubble generation assessment for an industrial flotation column. *Minerals Engineering*, 4, 37-42.
- Ibl, N. & Venczel, J. (1970) Mass transport at gas-generating electrodes. *Metalloberflaeche*, 24, 365-374.
- Ibrahim, M. Y., Mostafa, S. R., Fahmy, M. F. M. & Hafez, A. I. (2001) Utilization of electroflotation in remediation of oily wastewater. *Sep. Sci. Technol.*, 36, 3749–3762.
- Il'in, V. I. (2002) Unit for sewage cleaning from petroleum products. *Khimicheskoe I Neftyanoe Mashinostroenie*, 5, 41-42.
- Il'in, V. I., Kolesnikov, V. A. & Parshina, Y. I. (2002) Purification of highly concentrated industrial sewage from the porcelain and faience industry by the electric flotation method. *Glass Ceram.*, 59, 242–244.
- Il'in, V. I. & Sedashova, O. N. (1999) An electroflotation method and plant for removing oil products from effluents. *Chemical & Petroleum Engineering*, 35, 480-481.

- Ityokumbul, M. T., Salama, A. I. A. & Al Taweel, A. M. (1995) Estimation of bubble size in flotation columns. *Minerals Engineering*, 8, 77-89.
- Jameson, G. & Allum, P. (1984) A survey of bubble sizes in industrial flotation cells. A report prepared for AMIRA Limited.
- Jameson, G. J., Nam, S. & Moo Young, M. (1977) Physical factors affecting recovery rates in flotation. *Miner Sci Eng*, 9, 103-118.
- Janssen, L. J. J. & Hoogland, J. G. (1970) The effect of electrolytically evolved gas bubbles on the thickness of the diffusion layer. *Electrochimica Acta*, 15, 1013-1023.
- Janssen, L. J. J. & Hoogland, J. G. (1973) The effect of electrolytically evolved gas bubbles on the thickness of the diffusion layer-ii. *Electrochimica Acta*, 18, 543-550.
- Jaycock, M. J. & Ottewill, R. H. (1963) Adsorption of ionic surface-active agents by charged solids. *Bulletin - Institution of Mining and Metallurgy* No. 677, 497-506.
- Jime'nez, C., Talavera, B., Sa'ez, C., Can'izares, P. & Rodrigo, M. A. (2010) Study of the production of hydrogen bubbles at low current densities for electroflotation processes. *Journal of Chemical Technology and Biotechnology*, 85, 1368-1373.
- Jones, S. F., Evans, G. M. & Galvin, K. P. (1999a) Bubble nucleation from gas cavities -a review. *Advances in Colloid and Interface Science*, 80, 27-50.
- Jones, S. F., Evans, G. M. & Galvin, K. P. (1999b) The cycle of bubble production from a gas cavity in a supersaturated solution. *Advances in Colloid and Interface Science*, 80, 51-84.
- Jowett, A. (1980) Formation and disruption of particle bubble aggregates in flotation. In Somasundaran, P. (Ed.) *Fine Particles Processings*. New York, AIME.
- Kabanov, B. & Frumkin, A. (1933) The size of electrolytically generated gas bubbles. *Z. Physik. Chem.*, A166 316-317.
- Karamanev, D. G. 1994. Rise of gas bubbles in quiescent liquids. *AIChE Journal*, 40, 1418-1421.
- Karamanev, D. G. & Nikolov, L. N. 1992. Bed expansion of liquid-solid inverse fluidization. *AIChE Journal*, 38, 1916-1922.
- Kern, W. & Puotinen, D. A. (1970) Cleaning solution based on hydrogen peroxide for use in silicon semiconductor technology. *RCA Review*, 31, 187-206.

- Ketkar, D. R., Mallikarjunan, R. & Venkatachalam, S. (1988) Size determination of electrogenerated gas bubbles. *Journal of the Electrochemical Society of India*, 37, 313-318.
- Ketkar, D. R., Mallikarjunan, R. & Venkatachalam, S. (1991) Electroflotation of quartz fines. *International Journal of Mineral Processing*, 31, 127-138.
- Khosla, K., Khosla, N. K., Venkatachalam, S. & Somasundaran, P. (1995) Flotation of alumina with electrogenerated gas bubbles. *Minerals & Metallurgical Processing*, 12, 132-137.
- Koh, P. T. L. & Schwarz, M. P. (2006) CFD modelling of bubble-particle attachments in flotation cells. *Minerals Engineering*, 19, 619-626.
- Koh, P. T. L. & Schwarz, M. P. (2008) Modelling attachment rates of multi-sized bubbles with particles in a flotation cell. *Minerals Engineering*, 21, 989-993.
- Kubritskaya, T. D., Drako, I. V., Sorokina, V. N. & Drondina, R. V. (2000) Use of electrochemical methods to purify the waste water from the production of concentrates in the food industry. *Surf. Eng. Appl. Electrochem.*, 6, 62-68.
- Lafrance, P. & Grasso, D. (1995) Trajectory modelling of non-brownian particle flotation using an extended Derjaguin–Landau–Verwey–Overbeek approach. *Environ. Sci. Technol.*, 29, 1346–1352.
- Landolt, D., Acosta, R., Muller, R. H. & Tobais, C. W. (1970) An optical study of cathodic hydrogen evolution in high rate electrolysis. *Journal of the Electrochemical Society*, 117, 839-845.
- Laskowski, J. & Kitchener, J. A. (1969) The hydrophilic--hydrophobic transition on silica. *Journal of Colloid and Interface Science*, 29, 670-679.
- Lazarenko, B. R., Glembotskii, V. A., Mamakov, A. A. & Avvakumov, M. I. (1969) Intensification of the extraction of small diamonds by electric flotation. *Elektronnaya Obrabotka Materialov*, 6, 50-54.
- Lee, S.-W. & Sigmund, W. M. (2002) AFM study of repulsive van der Waals forces between Teflon AF(TM) thin film and silica or alumina. *Colloids and Surfaces A: Physicochemical and Engineering Aspects*, 204, 43-50.
- Lewis, B. & Elbe, G. V. (1961) *Combustion of flames and explosions of gases*, NY, London, Academic Press Inc.
- Lide, D. R. (Ed.) (2010) *CRC handbook of chemistry and physics (90th Edition)*, CRC Press, Inc., Boca Raton, FL.

- Llerena, C., Ho, J. C. K. & Piron, D. L. (1996) Effect of pH on electroflotation of sphalerite. *Chem. Eng. Commun*, 155, 217–228.
- Lubetkin, S. D. (1994) Bubble nucleation and growth, controlled particle, droplet and bubble formation. In Wedlock, D. J. (Ed.). Butterworth Heinemann, Oxford.
- Lubetkin, S. D. (1995) The fundamentals of bubble evolution. *Chemical Society Reviews*, 24, 243-250.
- Lucassen-Reynders, E. H. & Lucassen, J. (Eds.) (1984) *The scientific basis of flotation*, The Hague, Martinus Nijhoff.
- Lumanauw, D. (2000) Hydrogen bubble characterization in alkaline water electrolysis. *MSc Thesis, Department of Metallurgy and Materials Science*. University of Toronto, Canada.
- Mallikarjunan, R. & Venkatachalam, S. (1984) Electroflotation - a review. *Proceedings - Electrochemical Society*, 84, 233-256.
- Mamakov, A. A. & Avvakumov, M. I. (1968) Flotation of minerals by electrolytic action (review). *Electroannaya Obrabotka Materialov*, 5, 54-59.
- Mamakov, A. A., Sorokina, V. N. & Avvakumov, M. I. (1969) Electroflotability of cassiterite. *Electroannaya Obrabotka Materialov*, 28, 46-49.
- Manjunath, N. T., Mehrotra, I. & Mathur, R. P. (2000) Treatment of wastewater from slaughter-house by DAF-UASB system. *Water Res.*, 34, 1930–1936.
- Matov, B. M. (1973) Electrical charge of gas bubbles evolved on a wire electrode. *Electroannaya Obrabotka Materialov*, 5, 71-74.
- Matov, B. M. & Lazavenko, B. R. (1965) Size distribution of hydrogen bubbles evolved during electrolysis at a wire cathode. *Electroannaya Obrabotka Materialov*, 2, 201-206.
- Merzouk, B., Madani, K. & Sekki, A. (2010) Using electrocoagulation-electroflotation technology to treat synthetic solution and textile wastewater, two case studies. *Desalination*, 250, 573-577.
- Michel, B. J. & Miller, S. A. (1962) Power requirements of gas-liquid agitated systems. *AIChE Journal*, 8, 262-266.
- Miettinen, T. (2007) Fine Particle Flotation. *PhD thesis, Minerals and Materials*. IAN Wark Research Institute, University of South Australia.
- Miettinen, T., Ralston, J. & Fornasiero, D. (2010) The limits of fine particle flotation. *Minerals Engineering*, 23, 420-437.

- Montes-Atenas, G., Garcia-Garcia, F. J., Mermillod-Blondin, R. & Montes, S. (2010) Effect of suspension chemistry onto voltage drop: application to electro-flotation. *Powder Technology*, 204, 1-10.
- Morris, T. M. (1952) Measurement and evaluation of the rate of flotation as a function of particle size. *Transaction of the American Institute of Mining, Metallurgical and Petroleum Engineers*, 193, 794-798.
- Müller, L., Krenz, M. & Rübner, K. (1989) On the relation between the transport of electrochemically evolved Cl_2 And H_2 into the electrolyte bulk by convective diffusion and by gas bubbles. *Electrochimica Acta*, 34, 305-308.
- Murakawa, T. (1957) Points on the electrode surface where gas bubbles are most frequently formed during electrolysis of water. *Denki Kagaku* 25, 280-283.
- Nahui, F. N. B., Nascimento, M. R., Cavalcanti, E. B. & Vilar, E. O. (2008) Electroflotation of emulsified oil in industrial wastes evaluated with a full factorial design. *Brazilian Journal of Chemical Engineering*, 25, 435-442.
- Nelkon, M. (1970) *Electricity*, London, Edward Arnold.
- Nenno, V. E., Zelentsov, V. I., Datsko, T. Y., Dvornikova, E. E. & Radzilevich, T. M. (1994) Gold and silver sorption from cyanide solutions by activated coal and metal isolation by electroflotation. *Electronnaya Obrabotka Materialov*, 3, 42-44.
- Nenno, V. E., Zelentsov, V. I., Mel' nichuk, E. V., Romanov, A. M., Datsko, T. Y. & Radzilevich, T. M. (1988) Experience in operating a device for concentration of mineral raw material combining electroflotation and separation in a froth layer. *Electronnaya Obrabotka Materialov*, 6, 77-79.
- Nguyen, A. V. (2003) New method and equations for determining attachment tenacity and particle size limit in flotation. *International Journal of Mineral Processing*, 68, 167-182.
- Nguyen, A. V., George, P. & Jameson, G. J. (2006) Demonstration of a minimum in the recovery of nanoparticles by flotation: theory and experiment. *Chemical Engineering Science*, 61, 2494-2509.
- Nguyen, A. V., Ralston, J. & Schulze, H. J. (1998) On modelling of bubble-particle attachment probability in flotation. *International Journal of Mineral Processing*, 53, 225-249.
- Nguyen, A. V. & Schulze, H. J. (Eds.) (2004) *Colloidal Science of Flotation*, New York. Basel, Marcel Dekker, Inc.

- Nguyen Van, A. & Kmet, S. (1992) Collision efficiency for fine mineral particles with single bubble in a counter current flow regime. *International Journal of Mineral Processing*, 35, 205-223.
- Onoda, G. Y. & Fuerstenau, D. W. (1964) Amine flotation of quartz in the presence of inorganic electrolytes. *7th International Mineral Processing Congress*. New York, Gordon And Breach Science Publishers.
- Parks, G. A. (1965) The isoelectric points of solid oxides, solid hydroxides, and aqueous hydroxo complex systems. *Chemical Reviews*, 65, 177-198.
- Paul, J. S. & Charles, W. T. (1985) A close view of gas evolution from the back side of a transparent electrode. *Journal of the Electrochemical Society*, 132, 583-587.
- Phongikaroon, S., Hoover, R. O. & Barker, E. C. (2010) Measurement and analysis of gas bubble evolution from an anode in electrolytic cells. *Industrial & Engineering Chemistry Research*, 49, 2926-2931.
- Poon, C. P. C. (1997) Electroflotation for groundwater decontamination. *Journal of Hazardous Materials*, 55, 159-170.
- Prokop'eva, M. F., Tkacheva, V. N. & Kirshina, E. Y. (1988) A gas chromatographic investigation of the composition of spent cooling lubricants and the products formed during their electroflotation-coagulation treatment. *Khimiya I Tekhnologiya Vody*, 10, 335-337.
- Rabilizirov, M. N. & Gol'man, A. M. (1986) Treatment of dairy waste waters by foam electroflotation-separation. *Khimiya I Tekhnologiya Vody*, 8, 87-88.
- Raju, G. B. & Khangaonkar, P. R. (1982) Electro-flotation of chalcopryrite fines. *International Journal of Mineral Processing*, 9, 133-143.
- Raju, G. B. & Khangaonkar, P. R. (1984a) Electroflotation - a critical review. *Transactions of the Indian Institute of Metals*, 37, 59-66.
- Raju, G. B. & Khangaonkar, P. R. (1984b) Electroflotation of chalcopryrite fines with sodium diethyldithiocarbamate as collector. *International Journal of Mineral Processing*, 13, 211-221.
- Raju, G. B., Prabhakar, S. & Khangaonkar, P. R. (1987) Separation of minerals by electroflotation. *Bulletin of Electrochemistry*, 3, 37-40.
- Ralston, J., Fornasiero, D. & Hayes, R. (1999) Bubble-particle attachment and detachment in flotation. *International Journal of Mineral Processing*, 56, 133-164.

- Ramirez, J. A. & Davis, R. H. (2001) Microflotation of fine oil droplets by small air bubbles: experiment and theory. *Separation Science and Technology*, 36, 1-15.
- Rayleigh, L. (1917) Methods for detecting small optical retardations, and the theory of foucault's test. *Philosophical Magazine*, 33, 161-178.
- Reay, D. & Ratcliff, G. A. (1973) Removal of fine particles from water by dispersed air flotation: effects of bubble size and particle size on collision efficiency. *The Canadian Journal of Chemical Engineering*, 51, 178-185.
- Reay, D. & Ratcliff, G. A. (1975) Experimental testing of the hydrodynamic collision model of the fine particle flotation. *The Canadian Journal of Chemical Engineering*, 53, 481-486.
- Rodrigues, R. T. & Rubio, J. (2007) DAF-dissolved air flotation: potential applications in the mining and mineral processing industry. *International Journal of Mineral Processing*, 82, 1-13.
- Romanov, A. M., Nenno, E. S., Nenno, V. E. & Mamakov, A. A. (1973) Extraction of manganese from ores by electroflotation. *Electroannaya Obrabotka Materialov*, 1, 54-56.
- Rubio, J., Carissimi, E. & Rosa, J. J. (2007) Flotation in water and wastewater treatment and reuse: recent trends in Brazil. *International Journal of Environment and Pollution* 30, 197 - 212
- Rulyov, N. N. (2001) Turbulent microflotation: theory and experiment. *Colloids and Surfaces A: Physicochemical and Engineering Aspects*, 192, 73-91.
- Rykaart, E. M. & Haarhoff, J. (1995) Behaviour of air injection nozzles in dissolved air flotation. *Water Science and Technology*, 31, 25-35.
- Sarkar, M. S. K. A., Donne, S. W. & Evans, G. M. (2010a) Hydrogen bubble flotation of silica. *Advanced Powder Technology*, 21, 412-418.
- Sarkar, M. S. K. A., Evans, G. M. & Donne, S. W. (2010b) Bubble size measurement in electroflotation. *Minerals Engineering*, 23, 1058-1065.
- Sarrot, V., Huang, Z., Legendre, D. & Guiraud, P. (2007) Experimental determination of particles capture efficiency in flotation. *Chemical Engineering Science*, 62, 7359-7369.
- Scheludko, A., Toshev, B. V. & Bojadjev, D. T. (1976) Attachment of particles to a liquid surface (capillary theory of flotation). *Journal of the Chemical Society, Faraday Transactions 1: Physical Chemistry in Condensed Phases*, 72, 2815.

- Schubert, H. (1999) On the turbulence-controlled micro processes in flotation machines. *International Journal of Mineral Processing*, 56, 257-276.
- Schulze, H. J. (1982) Dimensionless number and approximate calculation of the upper particle size of floatability in flotation machines. *International Journal of Mineral Processing*, 9, 321-328.
- Schulze, H. J. (1989) Hydrodynamics of bubble-mineral particle collisions. *Mineral Processing and Extractive Metallurgy Review*, 5, 43-76.
- Schwarz, S. & Alexander, D. (2006) Gas dispersion measurements in industrial flotation cells. *Minerals Engineering*, 19, 554-560.
- Scott, J. L. (1983) The effects of pre-treatment conditions, ionic strength, collector type, chain length and temperature on the cationic flotation of oxide minerals. Reno, University of Nevada.
- Scriven, L. E. (1959) On the dynamics of phase growth. *Chemical Engineering Science*, 10, 1-13.
- Sebba, F. (1987) *Foams and bilyquid foams-aphrons*, Chichester, John Willey & Sons.
- Setty, G. S. & Venkatachalam, S. (1997) Electro and conventional flotation studies on quartz. *Transactions of the Indian Institute of Metals*, 50, 377-381.
- Shahbazi, B., Rezai, B. & Javad Koleini, S. M. (2010) Bubble-particle collision and attachment probability on fine particles flotation. *Chemical Engineering and Processing: Process Intensification*, 49, 622-627.
- Shendrik, O. R., Andreeva, E. E., Ponomareva, M. I. & Ivanenko, I. B. (1993) Electroflotation treatment of fat-containing solutions. *Khimiya I Tekhnologiya Vody*, 15, 54-56.
- Shibata, S. (1976) Super solubility of hydrogen in acidic solution in the vicinity of hydrogen-evolving platinum cathodes having various surface states. *Denki Kagaku*, 44, 709-712.
- Shibata, S. (1978) Supersaturation of oxygen in acidic solution in the vicinity of an oxygen-evolving platinum anode. *Electrochimica Acta*, 23, 619-623.
- Shin, M. S. (2003) The effect of metal ion on the zeta potential of bubbles in electroflotation. *The School of Civil, Urban and Geosystem Engineering*. Seoul National University.
- Sides, P. J. (Ed.) (1986) *Phenomena and effects of electrolytic gas evolution*, New York, NY, Plenum Press.

- Sides, P. J. & Tobias, C. W. (1985) A close view of gas evolution from the back side of a transparent electrode. *Journal of the Electrochemical Society*, 132, 583-587.
- Strokach, P. P. (1975) Electrochem. Ind. Process. *Bio.*, 55, 375.
- Sutherland, K. L. (1948) Kinetics of the flotation process. *The Journal of Physical and Colloid Chemistry*, 52, 394-425.
- Takahashi, T., Miyahara, T. & Mochizuki, H. (1979) Fundamental study of bubble formation in dissolved air pressure flotation. *Journal of Chemical Engineering of Japan*, 12, 275-280.
- Tao, D. (2004) Role of bubble size in flotation of coarse and fine particles-a review. *Separation Science & Technology*, 39, 741-760.
- Tao, Y., Liu, J., Yu, S. & Tao, D. (2006) Picobubble enhanced fine coal flotation. *Separation Science and Technology*, 41, 3597 - 3607.
- Tomlinson, H. S. & Fleming, M. G. (1963) Flotation rate studies in mineral processing. In Roberts, A. (Ed.) *Sixth International Congress*. Cannes, Pergamon Press, London.
- Trahar, W. J. (1981) A rational interpretation of the role of particle size in flotation. *International Journal of Mineral Processing*, 8, 289-327.
- Trahar, W. J. & Warren, L. J. (1976) The floatability of very fine particles - a review. *International Journal of Mineral Processing*, 3, 103-131.
- Tran, D. N. H., Whitby, C. P., Fornasiero, D. & Ralston, J. (2010) Selective separation of very fine particles at a planar air-water interface. *International Journal of Mineral Processing*, 94, 35-42.
- Tucker, J. P., Deglon, D. A., Franzidis, J. P., Harris, M. C. & O'connor, C. T. (1994) An evaluation of a direct method of bubble size distribution measurement in a laboratory batch flotation cell. *Minerals Engineering*, 7, 667-680.
- Vaughan, R. L., Reed, B. E., Roark, G. W. & Masciola, D. A. (2000) Pilot-scale investigation of chemical addition-dissolved air flotation for the treatment of an oily wastewater. *Environ. Eng. Sci.*, 17, 267-277.
- Venczel, J. (1970) Über den gasblasen bei elektrochemischen prozessen. *Electrochimica Acta*, 15, 1909-1920.
- Verhaart, H. F. A., De Jonge, R. M. & Van Stralen, S. J. D. (1980) Growth rate of a gas bubble during electrolysis in supersaturated liquid. *International Journal of Heat and Mass Transfer*, 23, 293-299.

- Vilaça, P. R., Badino Jr., A. C., Facciotti, M. C. R. & Schmidell, W. (2000) Determination of power consumption and volumetric oxygen transfer coefficient in bioreactors. *Bioprocess Engineering*, 22, 261-265.
- Vogt, H. (1984a) The rate of gas evolution at electrodes-ii. an estimate of the efficiency of gas evolution on the basis of bubble growth data. *Electrochimica Acta*, 29, 175-180.
- Vogt, H. (1984b) The rate of gas evolution of electrodes-I. an estimate of the efficiency of gas evolution from the supersaturation of electrolyte adjacent to a gas-evolving electrode. *Electrochimica Acta*, 29, 167-173.
- Wark, I. W. (1933) The physical chemistry of flotation. I. the significance of contact angle in flotation. *The Journal of Physical Chemistry*, 37, 623 - 644.
- Waters, K. E., Hadler, K. & Cilliers, J. J. (2008) The flotation of fine particles using charged microbubbles. *Minerals Engineering*, 21, 918-923.
- Weber, M. E. (1981) Collision efficiencies for small particles with a spherical collector at intermediate Reynolds numbers. *Separation Processes Technology*, 2, 29-33.
- Weber, M. E. & Paddock, D. (1983) Interceptional and gravitational collision efficiencies for single collectors at intermediate Reynolds numbers. *Journal of Colloid Interface Science*, 94, 328-335.
- Westerheide, D. E. & Westwater, J. W. (1961) Isothermal growth of hydrogen bubbles during electrolysis. *AIChE Journal*, 7, 357-362.
- Wills, B. A. (1997) *Mineral Processing Technology*, Oxford, Butterworth-Heinemann.
- Xu, Q., Nakajima, M., Ichikawa, S., Nakamura, N. & Shiina, T. (2008) A comparative study of microbubble generation by mechanical agitation and sonication. *Innovative Food Science and Emerging Technologies*, 9, 489-494.
- Yalcin, T. & Byers, A. (2006) Dissolved gas flotation in mineral processing. *Mineral Processing & Extractive Metallurgy Review*, 27, 87-97.
- Ye, Y. & Miller, J. D. (1988) Bubble/particle contact time in the analysis of coal flotation *coal preparation (London, United Kingdom)* 5, 147-166.
- Yianatos, J. B., Finch, J. A., Dobby, G. S. & Xu, M. (1988) Bubble size estimation in a bubble swarm. *Journal of Colloid and Interface Science*, 126, 37-44.
- Yoon, R.-H. (1993) Microbubble Flotation. *Minerals Engineering*, 6, 619-630.
- Yoon, R.-H. (2000) The role of hydrodynamic and surface forces in bubble-particle interaction. *International Journal of Mineral Processing*, 58, 129-143.

- Yoon, R. H. & Luttrell, G. H. (1989) The effect of bubble size on fine particle flotation. *Mineral Processing and Extractive Metallurgy Review*, 5, 101-122.
- Zabel, T. (1984) Flotation in water treatment. *NATO Asi Series, Series E: Applied Sciences*, 75 (Sci. Basis Flotation), 349-377.
- Zhang, S. H., Yu, S. C., Zhou, Y. C. & Su, Y. F. (1985) A model for liquid-liquid extraction column performance - the influence of drop size distribution extraction efficiency. *Canadian Journal of Chemical Engineering*, 63, 212-226.
- Zolotukhin, I. A., Vasev, V. A. & Lukin, A. L. (1983) Electroflotation purification of the pit waters of the kuzbass. *Khimiya Itekhnologiya Vody*, 5, 252-255.

Appendix A

DETERMINATION OF BUBBLE AND PARTICLE VELOCITY

1. INTRODUCTION

In this appendix the theoretical determination of bubble and particle velocities at Stokes and intermediate flow regimes is described.

2. BUBBLE RISE VELOCITY

Bubble rise velocity is a complicated function of the bubble geometry, the physical properties of the medium and the physicochemical properties of the gas-liquid interface. The drag force on small bubbles may be equal to the drag force on equivalent solid particles. The bubble surface may become mobile, in which case, the bubbles have, in contrast to solid particles, non-vanishing tangential velocities at the gas liquid interface. The gas circulation inside a bubble also reduces the drag on it.

2.1 Rise Velocity of Small Bubble in Contaminated Water

Small bubble (diameter < 0.2 mm) behaves like rigid surface due to adsorbed surface surfactants and have no internal circulation. In Stokes region the bubble terminal velocity can be estimated by Stokes law as:

$$U_{stokes} = \frac{d_b^2 (\rho_f - \rho_G) g}{18\mu}, \quad (\text{A.1})$$

where U_{Stokes} is the bubble stokes velocity, d_b is the diameter of the bubble, ρ_f and ρ_G are the density of liquid and gas, μ is the viscosity of liquid and g is the acceleration due to gravity. Stokes law is applicable for Reynolds number up to 1.92 and Archimedes number up to 2. In the intermediate range of Reynolds number, bubble rise velocity can be calculated by (Nguyen and Schulze, 2004):

$$v_b = \frac{U_{stokes}}{\left(1 + \frac{\frac{Ar}{96}}{(1 + 0.079Ar^{0.749})^{0.755}}\right)} \quad (A.2)$$

where v_b is the velocity of bubble and Ar is the Archimedes Number. Equation A.2 is valid for Archimedes Number in the range of 2-12,332. Archimedes Number can be estimated by:

$$Ar = \frac{d_b^3 \rho_f (\rho_f - \rho_G) g}{\mu^2} \quad (A.3)$$

2.2 Rise Velocity of Large Bubble in Contaminated Water

Large bubble (diameter >1 mm) becomes non-spherical and their shape may oscillate. Usually at Reynolds Number greater than 130, bubbles become non-spherical and their velocity can be determined by (Nguyen and Schulze, 2004):

$$v_b = 18U_{stokes} \left\{ \frac{4a_1^2 Ar^{2b-1} M_o^{0.46b}}{3k_1} \right\}^{\frac{1}{2-2b}} \quad (A.4)$$

where M_o is the Morton number, and a_1 , b , k_1 are the constants. If the shape factor is considered, the drag coefficient of the bubble rise in contaminated water is found to be almost constant, $C_d = k_1$, which takes the value of $k_1 = 0.95$ (Karamanev and Nikolov, 1992) and (Karamanev, 1994). The values of constant a_1 , and b are listed in Table A.1, whereas Morton Number can be estimated by:

$$M_o = \frac{g\mu^4}{\rho_{Pulp}\sigma^3} \quad (A.5)$$

Table A.1: Conditions for Equations A.1, A.2 and A.4 (Nguyen and Schulze, 2004)

Equation	Conditions	a ₁	b
Equation A.1	Ar ≤ 2	-	-
Equation A.2	2 < Ar ≤ 12,332	-	-
Equation A.4	12,332 ≤ 3.158Mo ^{-0.46}	1	0
	3.158Mo ^{-0.46} ≤ Ar ≤ 29.654Mo ^{-0.46}	1.14	-0.176
	29.654Mo ^{-0.46} ≤ Ar ≤ 506.719Mo ^{-0.46}	1.36	-0.28
	506.719Mo ^{-0.46} ≤ Ar	0.62	0

3. PARTICLE SETTLING VELOCITY

Due to gravity, particle tends to settle to the bottom of the flotation cell. When a particle is dropped in water, there is a brief transient period as the particle experiences the acceleration due to gravity. After that transient period, the particle falls with a constant terminal velocity termed as settling velocity.

3.1 Settling Velocity of Single Sphere by Stokes' Law

For spherical particle at Stokes regime (applicable for Archimedes Number, Ar ≤ 2), the settling velocity can be determined by:

$$U_{stokes} = \frac{d_p^2 (\rho_p - \rho_f) g}{18\mu}, \quad (A.6)$$

where ρ_p is the density of particle.

3.2 Settling Velocity at Intermediate Range of Archimedes Number

At the Archimedes number of the intermediate range, the settling velocity can be predicted using the Equation A.2 (applicable for a wide range of Archimedes numbers up to 10⁶). This range of Archimedes number satisfies the particle size and density commonly encountered in flotation.

3.3 Two Phase Liquid-Solid Suspensions

There are a number of correlations reported in the literature for estimating hindered settling velocity from terminal settling velocity in a two phase liquid-solid system. Among those Richardson and Zaki is the most accepted:

$$V_{THS} = V_{TFS} \varepsilon_f^{n_1}, \quad (A.7)$$

where V_{THS} is the hindered settling velocity, V_{TFS} is the terminal settling velocity, ε_f is the liquid volume fraction, and n_1 is the Richardson-Zaki index.

The Richardson-Zaki index is a function of Reynolds number of single particle and can be estimated by:

$$n_1 = \frac{1.791 + 0.133 \times Re^{0.456}}{0.359 + 0.093 \times Re^{0.456}} \quad (A.8)$$

Appendix B

APPLYING DRIFT FLUX THEORY TO PREDICT BUBBLE SIZE

In this appendix drift flux theory to predict bubble size for given gas volumetric fraction and bubble rise velocity are presented.

Wallis' (1969) one dimensional drift flux model relates gas void fraction to bubble size and liquid superficial velocities in gas-liquid flow. The model assumes that the system variables are independent of time and position and that the velocities of gas and liquid phases are constant across the flow area by neglecting the shear stress at the column wall. Here the total volumetric flux (J_T) of the two-phase flow is given by:

$$J_T = J_g + J_l = \frac{Q_G + Q_L}{A}, \quad (\text{B.1})$$

where J_g and J_l are the gas and liquid superficial velocities, Q_G and Q_L are the gas and liquid volumetric flow rates, respectively, and A is the cross sectional flow area of the column. A drift flux for the gas phase (J_{gl}) can be defined in terms of the gas and liquid superficial velocities and the volumetric fraction of gas (ε_G) as:

$$J_{gl} = (1 - \varepsilon_G)J_g - \varepsilon_G J_l. \quad (\text{B.2})$$

Wallis (1969) also proposed an alternative expression for the gas drift flux, based on the volumetric fraction of gas and the terminal rise velocity of a single bubble in an infinite fluid (v_b) as expressed:

$$J_{gl} = (1 - \varepsilon_G)\varepsilon_G v_b f(\varepsilon_G), \quad (\text{B.3})$$

where Ishii and Zuber (1979) defined $f(\varepsilon_G)$ as:

$$f(\varepsilon_G) = g(\varepsilon_G)(1 - \varepsilon_G)^{0.5} \left[\frac{1 + h(r_b^*)}{1 + h(r_b^*) \{g(\varepsilon_G)\}^{6/7}} \right] \quad , \quad (\text{B.4})$$

$$\text{where } g(\varepsilon_G) = (1 - \varepsilon_G)^{0.5} \left(\frac{\mu}{\mu_m} \right) \quad (\text{B.5})$$

In Eq. B.5, μ_m is the mixture viscosity, and can be estimated by dynamic viscosities of the gas and liquid phases, μ_g and μ as expressed by:

$$\mu_m = \mu (1 - \varepsilon_G)^{-5 \times \frac{\mu_g + 0.4\mu}{2(\mu_g + \mu)}} \quad (\text{B.6})$$

and $h(r_b^*)$ can be expressed as:

$$h(r_b^*) = 0.55 \left\{ (1 + 0.08 r_b^3)^{4/7} - 1 \right\}^{3/4} \quad , \quad (\text{B.7})$$

where r_b^* is the dimensionless bubble radius based on the actual bubble radius r_b as

$$r_b^* = r_b \left\{ \frac{\rho_f g (\rho_f - \rho_g)}{\mu^2} \right\}^{1/3} \quad , \quad (\text{B.8})$$

where ρ_f and ρ_g are the liquid and gas phase densities, respectively.

By using Equations B.3-B.8 and with the known values of bubble size and bubble rise velocities corresponding gas volumetric fraction can be calculated. The bubble rise velocity can be estimated using generalised correlation by Wallis (1974).

Application of drift flux analysis (Equations B.3-B.8) for the estimation of bubble diameter produced in a Denver cell (D12) using air and hydrogen as gas input.

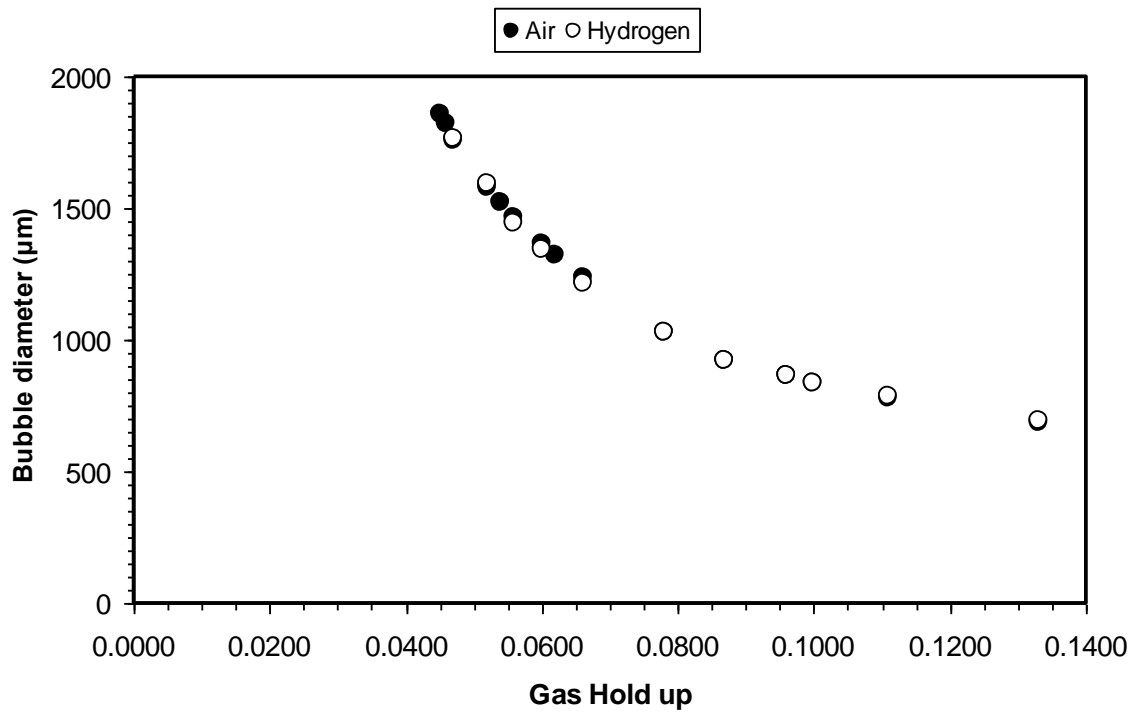


Figure B.1: Bubble diameter as a function of gas holdup in the Denver laboratory cell using air and hydrogen as gas input

Calculation of gas holdup (using Equations A.3-A.8) and pulp density (using Equation 3.82)

Table B.1: Hydrogen bubble produced at stainless steel wire of 190 μm diameter

Solids concentration: 2 % (w/w)

Bubble diameter: 30 μm

Cross sectional area of cell: $4.69 \times 10^{-4} \text{ m}^2$

Current density (A/m^2)	Gas flow rate (mL/min)	Gas superficial velocity (m/s)	Calculated gas holdup, ϵ_G	Pulp density (kg/m^3)
122	0.380	1.35×10^{-5}	0.03	983
196	0.608	2.16×10^{-5}	0.05	964
269	0.836	2.97×10^{-5}	0.07	944
342	1.064	3.78×10^{-5}	0.09	919
416	1.293	4.59×10^{-5}	0.12	893
489	1.521	5.40×10^{-5}	0.15	861
587	1.825	6.48×10^{-5}	0.21	803

Table B.2: Hydrogen bubble produced at stainless steel wire of 400 μm diameter

Current density: 775 A/m^2

Bubble diameter: 41 μm

Cross sectional area of cell: $35.77 \times 10^{-4} \text{ m}^2$

Gas flow rate (mL/min)	Calculated gas holdup, ϵ_G	Gas superficial velocity (m/s)	Solids (%) (w/w)	Pulp density (kg/m^3)
9.12	0.055	4.25×10^{-5}	0.020	957
			0.035	965
			0.050	974
			0.076	989
			0.100	1002
			0.150	1029
			0.200	1055

Appendix C

PARTICLE SIZE DISTRIBUTIONS FOR DIFFERENT SAMPLES

In this appendix particle size distributions for different samples used in electroflotation experiments are listed.

Table C.1: Particle size distribution of SAMPLE ID 1

d_p (μm)			Volume Fraction		d_p (μm)			Volume Fraction	
min	max	mean	(%)	Cum.	min	max	mean	(%)	Cum.
0.13	0.14	0.13	0.00	0.00	2.52	2.83	2.67	0.27	0.09
0.14	0.16	0.15	0.00	0.00	2.83	3.17	3.00	0.09	0.09
0.16	0.18	0.17	0.12	0.00	3.17	3.56	3.36	0.00	0.09
0.18	0.20	0.19	0.29	0.00	3.56	3.99	3.77	0.00	0.09
0.20	0.22	0.21	0.33	0.01	3.99	4.48	4.23	0.00	0.09
0.22	0.25	0.24	0.36	0.01	4.48	5.02	4.75	0.00	0.09
0.25	0.28	0.27	0.34	0.01	5.02	5.64	5.33	0.00	0.09
0.28	0.32	0.30	0.31	0.02	5.64	6.32	5.98	0.00	0.09
0.32	0.36	0.34	0.28	0.02	6.32	7.10	6.71	0.12	0.09
0.36	0.40	0.38	0.26	0.02	7.10	7.96	7.53	0.65	0.10
0.40	0.45	0.42	0.27	0.03	7.96	8.93	8.45	1.63	0.11
0.45	0.50	0.48	0.29	0.03	8.93	10.02	9.48	3.51	0.15
0.50	0.56	0.53	0.30	0.03	10.02	11.25	10.64	5.48	0.20
0.56	0.63	0.60	0.32	0.03	11.25	12.62	11.93	8.01	0.28
0.63	0.71	0.67	0.32	0.04	12.62	14.16	13.39	10.36	0.38
0.71	0.80	0.75	0.31	0.04	14.16	15.89	15.02	11.74	0.50
0.80	0.89	0.84	0.31	0.04	15.89	17.83	16.86	12.18	0.62
0.89	1.00	0.95	0.32	0.05	17.83	20.00	18.91	11.36	0.74
1.00	1.12	1.06	0.35	0.05	20.00	22.44	21.22	9.70	0.83
1.12	1.26	1.19	0.40	0.05	22.44	25.18	23.81	6.96	0.90
1.26	1.42	1.34	0.46	0.06	25.18	28.25	26.71	4.98	0.95
1.42	1.59	1.50	0.50	0.06	28.25	31.70	29.97	2.76	0.98
1.59	1.78	1.69	0.53	0.07	31.70	35.57	33.63	1.29	0.99
1.78	2.00	1.89	0.53	0.07	35.57	39.91	37.74	0.47	1.00
2.00	2.24	2.12	0.48	0.08	39.91	44.77	42.34	0.07	1.00
2.24	2.52	2.38	0.40	0.08	44.77	50.24	47.51	0.00	1.00
$(d_p)_{av}$				15.0			μm		
SA/mass				0.483			(m^2/g)		

Table C.2: Particle size distribution of SAMPLE ID 2

d_p (μm)			Volume Fraction		d_p (μm)			Volume Fraction		
min	max	mean	(%)	Cum.	min	max	mean	(%)	Cum.	
0.71	0.80	0.75	0.00	0.00	3.56	3.99	3.77	7.17	0.62	
0.80	0.89	0.84	0.00	0.00	3.99	4.48	4.23	6.73	0.69	
0.89	1.00	0.95	0.07	0.00	4.48	5.02	4.75	6.17	0.75	
1.00	1.12	1.06	0.65	0.01	5.02	5.64	5.33	5.53	0.81	
1.12	1.26	1.19	1.74	0.02	5.64	6.32	5.98	4.84	0.86	
1.26	1.42	1.34	2.64	0.05	6.32	7.10	6.71	4.13	0.90	
1.42	1.59	1.50	3.67	0.09	7.10	7.96	7.53	3.41	0.93	
1.59	1.78	1.69	4.70	0.13	7.96	8.93	8.45	2.70	0.96	
1.78	2.00	1.89	5.64	0.19	8.93	10.02	9.48	2.01	0.98	
2.00	2.24	2.12	6.45	0.26	10.02	11.25	10.64	1.34	0.99	
2.24	2.52	2.38	7.06	0.33	11.25	12.62	11.93	0.73	1.00	
2.52	2.83	2.67	7.43	0.40	12.62	14.16	13.39	0.14	1.00	
2.83	3.17	3.00	7.56	0.48	14.16	15.89	15.02	0.00	1.00	
3.17	3.56	3.36	7.47	0.55						
$(d_p)_{av}$				3.1			μm			
SA/mass				0.777			(m^2/g)			

Table C.3: Particle size distribution of SAMPLE ID 3

d_p (μm)			Volume Fraction		d_p (μm)			Volume Fraction		
min	max	mean	(%)	Cum.	min	max	mean	(%)	Cum.	
0.89	1.00	0.95	0.00	0.00	5.02	5.64	5.33	5.49	0.44	
1.00	1.12	1.06	0.21	0.00	5.64	6.32	5.98	5.80	0.50	
1.12	1.26	1.19	0.69	0.01	6.32	7.10	6.71	6.03	0.56	
1.26	1.42	1.34	1.04	0.02	7.10	7.96	7.53	6.16	0.62	
1.42	1.59	1.50	1.42	0.03	7.96	8.93	8.45	6.16	0.68	
1.59	1.78	1.69	1.81	0.05	8.93	10.02	9.48	6.01	0.74	
1.78	2.00	1.89	2.19	0.07	10.02	11.25	10.64	5.70	0.80	
2.00	2.24	2.12	2.57	0.10	11.25	12.62	11.93	5.24	0.85	
2.24	2.52	2.38	2.94	0.13	12.62	14.16	13.39	4.62	0.89	
2.52	2.83	2.67	3.31	0.16	14.16	15.89	15.02	3.88	0.93	
2.83	3.17	3.00	3.68	0.20	15.89	17.83	16.86	3.04	0.96	
3.17	3.56	3.36	4.04	0.24	17.83	20.00	18.91	2.14	0.98	
3.56	3.99	3.77	4.41	0.28	20.00	22.44	21.22	1.20	1.00	
3.99	4.48	4.23	4.77	0.33	22.44	25.18	23.81	0.32	1.00	
4.48	5.02	4.75	5.14	0.38	25.18	28.25	26.71	0.00	1.00	
$(d_p)_{av}$				5.3			μm			
SA/mass				0.481			(m^2/g)			

Table C.4: Particle size distribution of SAMPLE ID 4

d_p (μm)			Volume Fraction		d_p (μm)			Volume Fraction	
min	max	mean	(%)	Cum.	min	max	mean	(%)	Cum.
2.24	2.52	2.38	0.00	0.00	10.02	11.25	10.64	7.64	0.40
2.52	2.83	2.67	0.35	0.00	11.25	12.62	11.93	8.17	0.48
2.83	3.17	3.00	0.38	0.01	12.62	14.16	13.39	8.41	0.56
3.17	3.56	3.36	0.51	0.01	14.16	15.89	15.02	8.33	0.65
3.56	3.99	3.77	0.75	0.02	15.89	17.83	16.86	7.92	0.73
3.99	4.48	4.23	1.11	0.03	17.83	20.00	18.91	7.20	0.80
4.48	5.02	4.75	1.63	0.05	20.00	22.44	21.22	6.26	0.86
5.02	5.64	5.33	2.30	0.07	22.44	25.18	23.81	5.14	0.91
5.64	6.32	5.98	3.11	0.10	25.18	28.25	26.71	3.97	0.95
6.32	7.10	6.71	4.03	0.14	28.25	31.70	29.97	2.79	0.98
7.10	7.96	7.53	5.01	0.19	31.70	35.57	33.63	1.65	1.00
7.96	8.93	8.45	5.99	0.25	35.57	39.91	37.74	0.47	1.00
8.93	10.02	9.48	6.89	0.32	39.91	44.77	42.34	0.00	1.00
$(d_p)_{av}$				12.3			μm		
SA/mass				0.206			(m^2/g)		

Table C.5: Particle size distribution of SAMPLE ID 5

d_p (μm)			Volume Fraction		d_p (μm)			Volume Fraction	
min	max	mean	(%)	Cum.	min	max	mean	(%)	Cum.
4.48	5.02	4.75	0.00	0.00	15.89	17.83	16.86	11.47	0.64
5.02	5.64	5.33	0.02	0.00	17.83	20.00	18.91	10.46	0.74
5.64	6.32	5.98	0.25	0.00	20.00	22.44	21.22	8.83	0.83
6.32	7.10	6.71	0.94	0.01	22.44	25.18	23.81	6.82	0.90
7.10	7.96	7.53	2.08	0.03	25.18	28.25	26.71	4.79	0.95
7.96	8.93	8.45	3.68	0.07	28.25	31.70	29.97	2.96	0.98
8.93	10.02	9.48	5.60	0.13	31.70	35.57	33.63	1.62	0.99
10.02	11.25	10.64	7.67	0.20	35.57	39.91	37.74	0.57	1.00
11.25	12.62	11.93	9.55	0.30	39.91	44.77	42.34	0.08	1.00
12.62	14.16	13.39	10.96	0.41	44.77	50.24	47.51	0.00	1.00
14.16	15.89	15.02	11.64	0.52	50.24	56.37	53.30	0.00	1.00
$(d_p)_{av}$				14.7			μm		
SA/mass				0.156			(m^2/g)		

Appendix D

FLOTATION RECOVERY IN DENVER CELL

Flotation recovery obtained using a laboratory Denver cell (D12) as a function of pH, gas flow rate, as well as sodium sulphate and collector concentration is described in this appendix.

Table D.1: Entrainment as a function of gas flow rate (using air as gas input)

Experimental condition:

pH: 10
Na₂SO₄: 0.05 M
CTAB: 0 M
MIBC: 29 ppm
Flotation time: 10 min

Gas flow (L/min)	Input of silica to Denver cell (gm)	Weight of floated silica (gm)	Recovery (%)
4	50	0.31	0.62
6	50	0.68	1.37
8	50	0.86	1.71
10	50	1.12	2.23

Table D.2: Entrainment as a function of gas flow rate (using hydrogen as gas input)

Experimental condition:

pH: 10
Na₂SO₄: 0.05 M
CTAB: 0 M
MIBC: 29 ppm
Flotation time: 10 min

Gas flow (L/min)	Input of silica to Denver cell (gm)	Weight of floated silica (gm)	Recovery (%)
4	50	0.53	1.07
6	50	0.66	1.32
8	50	0.98	1.96
10	50	0.97	1.95

Table D.3: Flotation recovery as a function of pH

Experimental condition:

Gas type: Air
 Gas flow: 8 L/min
 Na₂SO₄: 0.05 M
 CTAB: 8.3×10⁻⁶ M
 MIBC: 29 ppm
 Flotation time: 10 min

pH	Run No.	Apparent recovery (%)	Entrainment (%)	True recovery (3)-(4) (%)	Average recovery (%)
1	2	3	4	5	6
9	1	68.20	1.71	66.49	67.65
	2	69.78	1.71	68.07	
	3	70.10	1.71	68.39	
9.5	1	73.82	1.71	72.11	72.13
	2	73.72	1.71	72.01	
	3	73.98	1.71	72.27	
10	1	74.64	1.71	72.93	72.43
	2	73.87	1.71	72.16	
	3	73.91	1.71	72.2	
10.5	1	71.63	1.71	69.92	70.69
	2	72.70	1.71	70.99	
	3	72.86	1.71	71.15	

Table D.4: Flotation recovery as a function of sodium sulphate concentration

Experimental condition:

Gas type: Air
 Gas flow: 8 L/min
 pH: 10
 CTAB: 6.64×10^{-6} M
 MIBC: 29 ppm
 Flotation time: 10 min

Sodium sulphate (M)	Run No.	Apparent recovery (%)	Entrainment (%)	True recovery (3)-(4) (%)	Average recovery (%)
1	2	3	4	5	6
0	1	99.9	1.71	98.19	98.09
	2	99.7	1.71	97.99	
0.005	1	93.42	1.71	91.71	92.45
	2	94.9	1.71	93.19	
0.010	1	89.97	1.71	88.26	89.02
	2	91.49	1.71	89.78	
0.050	1	63.98	1.71	62.27	61.565
	2	62.57	1.71	60.86	
0.100	1	39.19	1.71	37.48	38.13
	2	40.49	1.71	38.78	

Table D.5: Flotation recovery as a function of gas flow rate (using air as gas input)

Experimental condition:

Na_2SO_4 : 0.05 M
 pH: 10
 CTAB: 8.3×10^{-6} M
 MIBC: 29 ppm
 Flotation time: 10 min

Gas flow (L/min)	Run No.	Apparent recovery (%)	Entrainment (%)	True recovery (3)-(4) (%)	Average recovery (%)
1	2	3	4	5	6
4	1	66.57	0.61	65.96	67.80
	2	69.78	0.61	69.17	
	3	68.89	0.61	68.28	
6	1	73.72	1.37	72.36	71.83
	2	72.05	1.37	70.68	
	3	73.81	1.37	72.44	
8	1	74.64	1.71	72.93	72.43
	2	73.87	1.71	72.16	
	3	73.91	1.71	72.20	
10	1	75.32	2.23	73.09	73.05
	2	77.92	2.23	75.69	
	3	76.61	2.23	74.38	

Table D.6: Flotation recovery as a function of gas flow rate (using hydrogen as gas input)

Experimental condition:

Na₂SO₄: 0.05 M
 pH: 10
 CTAB: 8.3×10⁻⁶ M
 MIBC: 29 ppm
 Flotation time: 10 min

Gas flow (L/min)	Run No.	Apparent recovery (%)	Entrainment (%)	True recovery (3)-(4) (%)	Average recovery (%)
1	2	3	4	5	6
4	1	65.78	1.07	64.71	63.97
	2	63.30	1.07	62.23	
	3	66.05	1.07	64.98	
6	1	73.45	1.32	72.14	73.42
	2	75.30	1.32	73.99	
	3	75.45	1.32	74.14	
8	1	77.66	1.92	75.74	74.77
	2	76.80	1.92	74.88	
	3	75.60	1.92	73.68	
10	1	79.20	1.95	77.25	78.14
	2	81.15	1.95	79.20	
	3	79.90	1.95	77.95	

Table D.7: Flotation recovery as a function of collector concentration (Gas type: air; Na₂SO₄: 0.05 M)

Experimental condition:

Gas flow: 8 L/min

pH: 10

MIBC: 29 ppm

Flotation time: 10 min

CTAB 10 ⁻⁶ M	Run No.	Apparent recovery (%)	Entrainment (%)	True recovery (3)-(4) (%)	Average recovery (%)
	1	2	3	4	5
	2	3	4	5	6
4.43	1	43.70	1.71	41.99	42.89
	2	45.50	1.71	43.79	
6.64	1	63.98	1.71	62.27	61.57
	2	62.57	1.71	60.86	
8.30	1	74.64	1.71	72.93	72.57
	2	73.91	1.71	72.20	
13.30	1	88.10	1.71	86.39	87.05
	2	89.42	1.71	87.71	
16.60	1	90.59	1.71	88.88	89.59
	2	92.01	1.71	90.30	
22.10	1	95.10	1.71	93.39	94.09
	2	96.50	1.71	94.79	
27.70	1	97.20	1.71	95.49	95.12
	2	96.45	1.71	94.74	
33.20	1	98.48	1.71	96.77	97.22
	2	99.38	1.71	97.67	
38.70	1	99.98	1.71	98.27	98.10
	2	99.63	1.71	97.92	

Table D.8: Flotation recovery as a function of collector concentration (Gas type: Air; Na₂SO₄: 0.1 M)

Experimental condition:

Gas flow: 8 L/min

pH: 10

MIBC: 29 ppm

Flotation time: 10 min

CTAB 10 ⁻⁶ M	Run No.	Apparent recovery (%)	Entrainment (%)	True recovery (3)-(4) (%)	Average recovery (%)
1	2	3	4	5	6
6.64	1	39.19	1.71	37.48	38.13
	2	40.49	1.71	38.78	
8.3	1	56.56	1.71	54.85	55.65
	2	58.16	1.71	56.45	
13.3	1	78.26	1.71	76.55	77.27
	2	79.7	1.71	77.99	
16.6	1	84.6	1.71	82.89	82.19
	2	83.2	1.71	81.49	
22.1	1	92.4	1.71	90.69	90
	2	91.02	1.71	89.31	
27.7	1	92.99	1.71	91.28	91.94
	2	94.31	1.71	92.6	
32.2	1	95.9	1.71	94.19	93.84
	2	95.2	1.71	93.49	
38.7	1	96.3	1.71	94.59	95.19
	2	97.5	1.71	95.79	
44.3	1	98.6	1.71	96.89	96.49
	2	97.8	1.71	96.09	
49.8	1	99.8	1.71	98.09	97.59
	2	98.8	1.71	97.09	

Table D.9: Flotation recovery as a function of collector concentration (Gas type: Hydrogen; Na₂SO₄: 0.05 M)

Experimental condition:

Gas flow: 8 L/min

pH: 10

MIBC: 29 ppm

Flotation time: 10 min

CTAB 10 ⁻⁶ M	Run No.	Apparent recovery (%)	Entrainment (%)	True recovery (3)-(4) (%)	Average recovery (%)
	1	2	3	4	5
	1	2	3	4	5
8.3	1	77.66	1.92	75.74	74.77
	2	76.80	1.92	74.88	
	3	75.60	1.92	73.68	
13.3	1	89.85	1.92	87.93	87.26
	2	88.50	1.92	86.58	
22.1	1	94.70	1.92	92.78	93.59
	2	96.32	1.92	94.40	
27.7	1	97.29	1.92	94.53	94.95
	2	96.45	1.92	95.37	

Table D.10: Flotation recovery as a function of collector concentration (Gas type: Hydrogen; Na₂SO₄: 0.1 M)

Experimental condition:

Gas flow: 8 L/min

pH: 10

MIBC: 29 ppm

Flotation time: 10 min

CTAB 10 ⁻⁶ M	Run No.	Apparent recovery (%)	Entrainment (%)	True recovery (3)-(4) (%)	Average recovery (%)
1	2	3	4	5	6
8.3	1	54.85	1.96	52.89	53.79
	2	56.65	1.96	54.69	
13.3	1	81.40	1.96	79.44	78.53
	2	79.57	1.96	77.61	
22.1	1	92.40	1.96	90.44	89.58
	2	90.68	1.96	88.72	
27.7	1	94.12	1.96	92.16	93.25
	2	96.30	1.96	94.34	

Appendix E

CONTACT ANGLE AND SURFACE TENSION MEASUREMENT

In this appendix the measured contact angle and surface tension are reported. Both contact angle and surface tension are measured at different concentration of collector (CTAB). The experimental condition for both contact angle and surface tension measurement was the same as described below:

Experimental condition:

Na₂SO₄: 0.1 M

MIBC: 29 ppm

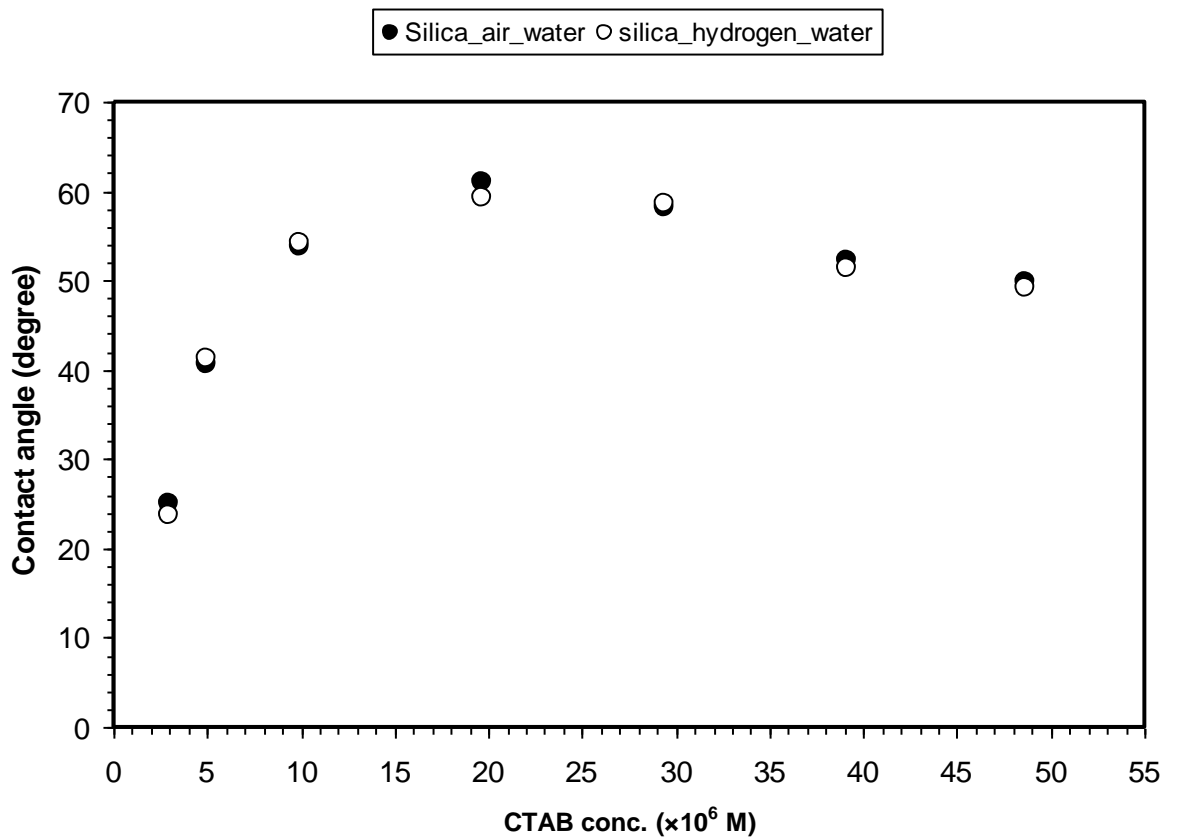


Figure E.1: Contact angle vs. Collector concentration

Table E.1: Contact angle measurement by sessile drop method

CTAB (M)	Run No.	Water-air-silica interface		Water-hydrogen-silica interface	
		Contact angle (degree)	Average contact angle (degree)	Contact angle (degree)	Average contact angle (degree)
2.98×10^{-06}	1	23.35	25.13	23.35	23.82
	2	26.45		22.6	
	3	25.6		25.5	
4.96×10^{-06}	1	40.6	40.53	40.85	41.18
	2	38.5		39.2	
	3	42.5		43.5	
9.89×10^{-06}	1	54.2	53.80	54.1	54.20
	2	55.7		55.7	
	3	51.5		52.8	
19.71×10^{-06}	1	60.9	60.87	61	59.16
	2	58.9		56.52	
	3	62.8		59.95	
29.44×10^{-06}	1	56.9	58.07	57.12	58.59
	2	59.8		60.85	
	3	57.5		57.8	
39.1×10^{-06}	1	52.6	52.33	52.3	51.37
	2	55.5		53.2	
	3	48.9		48.6	
48.68×10^{-06}	1	51.1	49.82	50.95	49.17
	2	48.15		46.9	
	3	50.2		49.65	

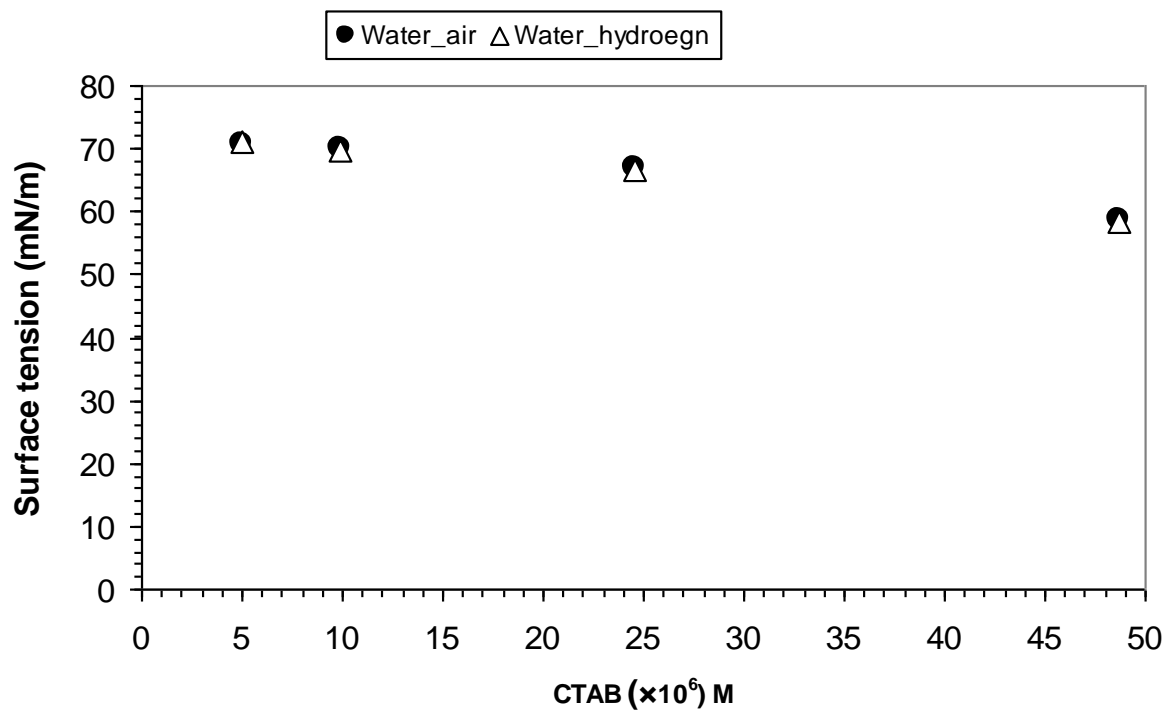


Figure E.2: Surface tension vs. collector concentration

Table E.2: Surface tension measurement by pendant drop method

CTAB (M)	Run No.	Water-air interface		Water-hydrogen interface	
		Surface tension (mN/m)	Average surface tension (mN/m)	Surface tension (mN/m)	Average surface tension (mN/m)
4.95×10^{-06}	1	70.27	70.87	72.12	71.01
	2	69.28		70.25	
	3	71.62		71.62	
	4	72.32		70.05	
9.89×10^{-06}	1	70.12	70.03	69.85	69.82
	2	69.78		70.45	
	3	70.65		68.75	
	4	69.56		70.23	
24.58×10^{-06}	1	66.12	66.86	65.45	66.70
	2	67.12		66.55	
	3	66.58		67.85	
	4	67.6		66.95	
48.68×10^{-06}	1	59.8	58.78	58.65	58.30
	2	58.9		59.78	
	3	58.9		58.65	
	4	57.5		56.12	

Appendix F

BUBBLE SIZE MEASUREMENT AND MODEL PREDICTION

In this appendix the data of bubble size measurement as a function of current density are presented. Also included in this appendix are model predictions for detached and bulk bubble diameter. Dissolved hydrogen gas concentration at bulk electrolyte solution is also predicted.

Bubble measurement data

Data of bubble size measurement produced from 90, 120 and 190 μm diameter platinum wire different at different current densities are presented in the attached CD (see folder titled as Appendix F). Bubbles produced from 90 and 190 μm diameter platinum wire experiencing an external liquid flow were also measured and presented in the CD.

Model Calculation

The concentration of dissolved hydrogen gas (C_b) at a radial distance (r) from the centre of the cylindrical wire can be calculated using Equation 3.105. Sample results of dissolved gas concentration are given in Table F.1-F.3. Detached and bulk bubble sizes are also predicted by solving Equation 3.97-3.107 (sample results are presented in Table F.4-F.6).

Current density, $\dot{I} = 354 \text{ A/m}^2$

Diffusivity of hydrogen, $D' = 4.8 \times 10^{-9} \text{ m}^2/\text{s}$

Distance from top of wire, $x = r - \frac{D}{2}$

Table F.1: Dissolved hydrogen concentration as a function of time of electrolysis at different distances from top of wire (platinum wire diameter, D: 90 μm)

Gas fraction goes into bulk solution, $\psi = 0.83$

x (μm)	$C_b(x,t)$ (mol/m^3)			x (μm)	$C_b(x,t)$ (mol/m^3)		
	1s	10s	30s		1s	10s	30s
0	8.50	23.55	31.28	380	0	1.72	6.17
5	7.88	22.78	30.50	405	0	1.42	5.60
10	7.29	22.02	29.72	430	0	1.17	5.07
15	6.71	21.27	28.96	455	0	0.96	4.59
20	6.17	20.54	28.22	480	0	0.78	4.16
25	5.66	19.84	27.50	505	0	0.64	3.76
30	5.18	19.15	26.79	530	0	0.52	3.40
35	4.74	18.49	26.12	555	0	0.42	3.07
40	4.32	17.86	25.46	580	0	0.33	2.77
45	3.93	17.24	24.83	605	0	0.27	2.49
50	3.58	16.66	24.21	630	0	0.21	2.24
55	3.25	16.09	23.62	655	0	0.17	2.02
80	1.95	13.56	20.96	680	0	0.13	1.81
105	1.13	11.45	18.69	705	0	0.10	1.62
130	0.63	9.70	16.75	730	0	0.08	1.45
155	0.33	8.21	15.07	755	0	0.06	1.30
180	0.17	6.96	13.59	780	0	0.05	1.16
205	0.08	5.89	12.28	805	0	0.04	1.04
230	0.04	4.98	11.11	830	0	0.03	0.92
255	0.02	4.20	10.06	855	0	0.02	0.82
280	0.01	3.53	9.12	880	0	0.02	0.73
305	0.00	2.96	8.27	905	0	0.01	0.65
330	0.00	2.48	7.51	930	0	0.01	0.57
355	0.00	2.07	6.81	955	0	0.01	0.51

Table F.2: Dissolved hydrogen concentration as a function of time of electrolysis at different distances from top of wire (platinum wire diameter, D: 120 μm)

Gas fraction goes into bulk solution, $\psi = 0.83$

x (μm)	$C_b(x,t)$ (mol/m^3)			x (μm)	$C_b(x,t)$ (mol/m^3)		
	1s	10s	30s		1s	10s	30s
0	7.35	26.09	36.29	415	0	1.55	6.73
5	6.83	25.33	35.51	440	0	1.28	6.10
10	6.34	24.58	34.74	465	0	1.05	5.52
15	5.86	23.84	33.97	490	0	0.85	4.99
20	5.41	23.11	33.22	515	0	0.69	4.51
25	4.98	22.40	32.48	540	0	0.56	4.08
30	4.58	21.70	31.75	565	0	0.45	3.68
35	4.20	21.02	31.05	590	0	0.36	3.31
40	3.85	20.36	30.35	615	0	0.29	2.98
65	2.41	17.35	27.16	640	0	0.23	2.68
90	1.45	14.77	24.36	665	0	0.18	2.41
115	0.83	12.57	21.92	690	0	0.14	2.16
140	0.46	10.69	19.77	715	0	0.11	1.94
165	0.24	9.08	17.86	740	0	0.08	1.73
190	0.12	7.71	16.17	765	0	0.07	1.55
215	0.06	6.53	14.65	790	0	0.05	1.38
240	0.03	5.52	13.29	815	0	0.04	1.23
265	0.01	4.65	12.06	840	0	0.03	1.09
290	0.00	3.91	10.94	865	0	0.02	0.97
315	0.00	3.27	9.93	890	0	0.02	0.86
340	0.00	2.73	9.01	915	0	0.01	0.76
365	0.00	2.27	8.18	940	0	0.01	0.68
390	0.00	1.88	7.42	990	0	0.01	0.53

Table F.3: Dissolved hydrogen concentration as a function of time of electrolysis at different distances from top of wire (platinum wire diameter, D: 190 μm)

Gas fraction goes into bulk solution, $\psi = 0.79$

x (μm)	$C_b(x,t)$ (mol/m^3)			x (μm)	$C_b(x,t)$ (mol/m^3)		
	1s	10s	30s		1s	10s	30s
0	4	27	42	305	0	4	13
5	4	26	41	330	0	3	12
10	4	26	40	355	0	3	11
15	4	25	40	380	0	2	10
20	3	24	39	405	0	2	9
25	3	24	38	430	0	2	8
30	3	23	38	455	0	1	7
35	3	22	37	480	0	1	7
40	2	22	36	505	0	1	6
45	2	21	35	530	0	1	5
50	2	21	35	555	0	1	5
55	2	20	34	580	0	0	4
65	2	19	33	605	0	0	4
75	1	18	32	630	0	0	4
85	1	17	30	655	0	0	3
95	1	16	29	680	0	0	3
105	1	15	28	705	0	0	3
130	0	13	26	730	0	0	2
155	0	11	23	755	0	0	2
180	0	9	21	780	0	0	2
205	0	8	19	805	0	0	2
230	0	7	18	830	0	0	1
255	0	6	16	855	0	0	1
280	0	5	15	880	0	0	1

Table F.4: Detached and bulk bubble size prediction by solving Equation 3.97-3.107 (platinum wire diameter, D : 90 μm ; Current density, $i = 354 \text{ A/m}^2$)

x (μm)	$C_b(x,t)$ (mol/m^3)			x (μm)	$C_b(x,t)$ (mol/m^3)		
	1s	10s	30s		1s	10s	30s
0	15.40	0	15.32	262	28.74	539	38.76
5	16.49	5	17.48	288	29.13	596	39.19
10	17.55	11	19.56	314	29.49	655	39.55
17	18.56	20	21.54	342	29.82	715	39.84
25	19.52	32	23.43	370	30.12	777	40.08
34	20.44	47	25.21	399	30.40	839	40.25
44	21.32	65	26.88	428	30.65	902	40.35
56	22.16	86	28.43	459	30.87	966	40.30
68	22.95	111	29.88	490	31.25	1030	40.07
82	23.70	139	31.21	554	31.59	1154	39.79
97	24.41	171	32.43	619	31.85	1277	39.47
114	25.08	206	33.55	687	31.99	1397	39.13
132	25.71	245	34.57	755	31.87	1514	38.78
150	26.30	287	35.48	822	31.67	1629	38.43
171	26.86	332	36.31	889	31.45	1740	38.08
192	27.38	380	37.04	954	31.20	1849	37.74
214	27.86	431	37.69	1017	30.92	1956	37.41
238	28.32	484	38.26	1079	30.64	2060	37.08

Table F.5: Detached and bulk bubble size prediction by solving Equation 3.97-3.107 (platinum wire diameter, D : 120 μm ; Current density, $i = 354 \text{ A/m}^2$)

x (μm)	$C_b(x,t)$ (mol/m^3)			x (μm)	$C_b(x,t)$ (mol/m^3)		
	1s	10s	30s		1s	10s	30s
0	17.27	0	17.46	276	32.15	495	43.95
6	18.43	6	19.75	299	32.57	540	44.47
13	19.55	14	21.97	323	32.97	586	44.94
21	20.63	24	24.08	347	33.34	634	45.34
30	21.65	37	26.08	397	33.99	731	45.99
40	22.64	51	27.98	423	34.28	781	46.24
50	23.57	69	29.77	450	34.80	831	46.63
62	24.47	88	31.45	504	35.26	934	46.92
75	25.32	110	33.02	561	35.67	1038	47.05
89	26.12	134	34.48	618	35.98	1143	46.84
103	26.89	161	35.83	677	36.21	1247	46.55
119	27.62	190	37.09	737	36.33	1349	46.24
136	28.31	222	38.24	797	36.22	1450	45.92
153	28.96	255	39.31	856	36.03	1549	45.59
172	29.58	291	40.28	915	35.81	1647	45.26
191	30.16	328	41.17	973	35.56	1743	44.94
211	30.70	367	41.97	1030	35.30	1838	44.62
232	31.22	408	42.70	1087	35.03	1932	44.30
253	31.70	451	43.36	1142	34.76	2024	43.99

Table F.6: Detached and bulk bubble size prediction by solving Equation 3.97-3.107 (platinum wire diameter, D : 190 μm ; Current density, $i = 354 \text{ A/m}^2$)

x (μm)	$C_b(x,t)$ (mol/m^3)			x (μm)	$C_b(x,t)$ (mol/m^3)		
	1s	10s	30s		1s	10s	30s
0	22	0	22	172	37	286	46
5	23	5	24	194	37	326	47
11	25	12	26	216	38	369	48
18	26	21	29	240	39	415	49
26	27	31	31	265	39	462	50
35	28	45	33	291	40	512	50
46	29	60	35	318	40	563	51
57	30	78	36	346	41	616	51
70	31	100	38	375	41	671	52
84	32	123	40	405	42	726	52
99	33	150	41	436	42	783	53
116	34	180	43	467	43	901	53
133	35	212	44	533	44	1021	54
152	36	248	45	602	44	1144	54

Table F.7: Bubbles experiencing external upward liquid flow (platinum wire: 90 μm diameter; Current density: 354 A/m^2)

Upward liquid velocity (mm/s)	Detachment diameter, $d_{b,d}$ (μm)	Bulk diameter, $d_{b,b}$ (μm)
0.00	15.4 (1.90 ¹)	30.63 (4.53)
1.56	12.94 (2.68)	24.57 (5.74)
3.38	10.18 (2.08)	17.63 (5.00)
7.02	7.57 (2.23)	13.51 (4.58)

¹ Standard deviation shown as bracketed values

Table F.8: Bubbles experiencing external upward liquid flow (platinum wire: 190 μm diameter; Current density: 354 A/m^2)

Upward liquid velocity (mm/s)	Detachment diameter, $d_{b,d}$ (μm)	Bulk diameter, $d_{b,b}$ (μm)
0.00	21.79 (3.35 ¹)	43.27 (8.89)
2.48	19.22 (3.72)	38.96 (7.61)
4.00	17.34 (4.59)	34.09 (9.06)
7.09	14.67 (2.72)	29.55 (5.64)

¹ Standard deviation shown as bracketed values

Appendix G

GAS COLLECTION DATA

In this appendix hydrogen gas rate captured from an electrochemical cell are presented. The hydrogen gas generation rate was measured as a function of solids concentration, mechanical agitation and presence of pre-existing dissolved gases.

Table G.1: Gas generation rate as a function of solids concentration (normal and stirred solution)

Experimental condition

Current density: 129 A/m²

Gas collection time: 24 min

Solids concentration (%)	Run No.	Gas generation rate (mL/min)	Average gas generation rate (mL/min)	Difference with mean (%)
0	1	1.60	1.56	2.56
	2	1.52		-2.56
	3	1.56		0.00
1.5	1	1.52	1.555	-2.25
	2	1.59		2.25
3	1	1.63	1.595	2.19
	2	1.56		-2.19
6	1	1.54	1.52	1.31
	2	1.50		-1.31
12	1	1.54	1.52	1.31
	2	1.50		-1.31
16	1	1.52	1.495	1.67
	2	1.47		-1.67
20	1	1.56	1.525	2.30
	2	1.49		-2.30

Table G.2: Gas generation rate as a function of solids concentration (degassed and stirred solution)

Experimental condition

Current density: 129 A/m²

Gas collection time: 24 min

Solids concentration (%)	Run No.	Gas generation rate (mL/min)	Average gas generation rate (mL/min)	Difference with mean (%)
0	1	1.48	1.51	-1.99
	2	1.55		2.64
	3	1.50		-0.67
1	1	1.47	1.51	-2.97
	2	1.56		2.97
2	1	1.44	1.48	-2.70
	2	1.52		2.70
4.00	1	1.47	1.49	-1.67
	2	1.52		1.67
8	1	1.52	1.49	1.67
	2	1.47		-1.67
12	1	1.50	1.46	2.74
	2	1.42		-2.74
16	1	1.45	1.49	-2.36
	2	1.52		2.36
20	1	1.44	1.48	-2.70
	2	1.52		2.70

Table G.3: Gas collection as a function of electrolysis time (degassed and stirred solution)

Experimental condition

Solution type: Degassed and stirred

Current density: 258 A/m²

Gas collection time: 12 min

Time (min)	Set #1		Set #2		Set #3	
	Burette reading (ml)	Cumulative gas vol (ml)	Burette reading (ml)	Cumulative gas vol (ml)	Burette reading (ml)	Cumulative gas vol (ml)
0	49.35	0	49.35	0	49.35	0
0.25	49.35	0	49.35	0	49.35	0
0.5	49.35	0	49.35	0	49.35	0
0.75	49.35	0	49.35	0	49.35	0
1	48.5	0.85	48.5	0.85	48.5	0.85
1.25	47.85	1.5	47.8	1.55	47.85	1.5
1.5	47	2.35	46.95	2.4	47	2.35
1.75	46.15	3.2	46.05	3.3	46.1	3.25
2	45.45	3.9	45.35	4	45.45	3.9
2.25	44.55	4.8	44.35	5	44.5	4.85
2.5	43.75	5.6	43.6	5.75	43.7	5.65
2.75	43	6.35	42.75	6.6	42.95	6.4
3	42.25	7.1	41.95	7.4	42.15	7.2
3.25	41.3	8.05	41	8.35	41.2	8.15
3.5	40.4	8.95	40.1	9.25	40.35	9
3.75	39.65	9.7	39.3	10.05	39.55	9.8
4	38.75	10.6	38.4	10.95	38.65	10.7
4.25	38	11.35	37.6	11.75	37.9	11.45
4.5	37.15	12.2	36.75	12.6	37.05	12.3
4.75	36.3	13.05	35.8	13.55	36.15	13.2

	Set #1		Set #2		Set #3	
Time (min)	Burette reading (ml)	Cumulative gas vol (ml)	Burette reading (ml)	Cumulative gas vol (ml)	Burette reading (ml)	Cumulative gas vol (ml)
5	35.5	13.85	35	14.35	35.4	13.95
5.25	34.75	14.6	34.2	15.15	34.6	14.75
5.5	34	15.35	33.45	15.9	33.85	15.5
5.75	33.15	16.2	32.55	16.8	33	16.35
6	32.35	17	31.75	17.6	32.2	17.15
6.25	31.6	17.75	30.95	18.4	31.4	17.95
6.5	30.8	18.55	30.15	19.2	30.6	18.75
6.75	30.05	19.3	29.35	20	29.85	19.5
7	29.1	20.25	28.4	20.95	28.9	20.45
7.25	28.35	21	27.6	21.75	28.15	21.2
7.5	27.55	21.8	26.75	22.6	27.35	22
7.75	26.75	22.6	25.95	23.4	26.55	22.8
8	25.95	23.4	25.1	24.25	25.75	23.6
8.25	25.2	24.15	24.3	25.05	24.95	24.4
8.5	24.4	24.95	23.5	25.85	24.15	25.2
8.75	23.75	25.6	22.8	26.55	23.45	25.9
9	23.1	26.25	22.15	27.2	22.85	26.5
9.25	22.05	27.3	21.05	28.3	21.75	27.6
9.5	21.25	28.1	20.25	29.1	20.95	28.4
9.75	20.5	28.85	19.45	29.9	20.2	29.15
10	19.85	29.5	18.75	30.6	19.55	29.8
10.25	18.9	30.45	17.75	31.6	18.55	30.8
10.5	18	31.35	16.85	32.5	17.7	31.65
10.75	17.35	32	16.15	33.2	17	32.35
11	16.65	32.7	15.45	33.9	16.3	33.05
11.25	15.7	33.65	14.5	34.85	15.4	33.95
11.5	15.05	34.3	13.8	35.55	14.7	34.65
11.75	14.25	35.1	13	36.35	13.9	35.45
12	13.45	35.9	12.15	37.2	13.1	36.25

Table G.4: Gas collection as a function of electrolysis time (degassed and non-stirred solution)

Experimental condition

Current density: 258 A/m²

Gas collection time: 12 min

Time (min)	Set #1		Set #2		Set #3	
	Burette reading (ml)	Cumulative gas vol (ml)	Burette reading (ml)	Cumulative gas vol (ml)	Burette reading (ml)	Cumulative gas vol (ml)
0	49.35	0	49.35	0	49.35	0
0.25	49.35	0	49.35	0	49.35	0
0.5	49.35	0	49.35	0	49.35	0
0.75	49.35	0	49.35	0	49.35	0
1	48.5	0.85	48.5	0.85	48.5	0.85
1.25	47.8	1.55	47.85	1.5	47.8	1.55
1.5	46.95	2.4	47.05	2.3	47	2.35
1.75	46.05	3.3	46.15	3.2	46.1	3.25
2	45.35	4	45.5	3.85	45.4	3.95
2.25	44.4	4.95	44.6	4.75	44.5	4.85
2.5	43.6	5.75	43.8	5.55	43.7	5.65
2.75	42.8	6.55	43.05	6.3	42.9	6.45
3	42	7.35	42.25	7.1	42.1	7.25
3.25	41.05	8.3	41.35	8	41.2	8.15
3.5	40.15	9.2	40.5	8.85	40.3	9.05
3.75	39.35	10	39.7	9.65	39.5	9.85
4	38.45	10.9	38.8	10.55	38.6	10.75
4.25	37.65	11.7	38	11.35	37.8	11.55
4.5	36.8	12.55	37.25	12.1	37	12.35
4.75	35.9	13.45	36.35	13	36.1	13.25
5	35.1	14.25	35.55	13.8	35.3	14.05
5.25	34.3	15.05	34.75	14.6	34.5	14.85
5.5	33.55	15.8	34.1	15.25	33.8	15.55

Time (min)	Set #1		Set #2		Set #3	
	Burette reading (ml)	Cumulative gas vol (ml)	Burette reading (ml)	Cumulative gas vol (ml)	Burette reading (ml)	Cumulative gas vol (ml)
5.75	32.65	16.7	33.2	16.15	32.9	16.45
6	31.85	17.5	32.4	16.95	32.1	17.25
6.25	31.05	18.3	31.65	17.7	31.3	18.05
6.5	30.25	19.1	30.85	18.5	30.5	18.85
6.75	29.45	19.9	30.05	19.3	29.7	19.65
7	28.5	20.85	29.2	20.15	28.8	20.55
7.25	27.7	21.65	28.4	20.95	28	21.35
7.5	26.9	22.45	27.6	21.75	27.2	22.15
7.75	26.1	23.25	26.8	22.55	26.4	22.95
8	25.25	24.1	26.05	23.3	25.6	23.75
8.25	24.45	24.9	25.25	24.1	24.8	24.55
8.5	23.65	25.7	24.5	24.85	24	25.35
8.75	22.95	26.4	23.8	25.55	23.3	26.05
9	22.3	27.05	23.2	26.15	22.7	26.65
9.25	21.2	28.15	22.1	27.25	21.6	27.75
9.5	20.4	28.95	21.35	28	20.8	28.55
9.75	19.6	29.75	20.55	28.8	20	29.35
10	18.95	30.4	19.95	29.4	19.4	29.95
10.25	17.95	31.4	18.95	30.4	18.4	30.95
10.5	17.05	32.3	18.1	31.25	17.5	31.85
10.75	16.35	33	17.4	31.95	16.8	32.55
11	15.65	33.7	16.7	32.65	16.1	33.25
11.25	14.7	34.65	15.8	33.55	15.2	34.15
11.5	14	35.35	15.15	34.2	14.5	34.85
11.75	13.2	36.15	14.35	35	13.7	35.65
12	12.35	37	13.55	35.8	12.85	36.5

For other gas collection data please see the excel file in the attached CD (see folder titled as Appendix G).

Appendix H

FLOTATION RECOVERY IN ELECTROFLOTATION CELL

In this appendix recovery of silica as a function of solids concentration, gas flow rate, and particle size using an electrochemical cell are presented. All the flotation experiments were performed for a constant time of two minutes.

Table H.1: Flotation recovery as a function of solids concentration

Experimental condition:

Current density:	775 A/m ²
Gas flow:	9.12 mL/min
Na ₂ SO ₄ :	0.2 M
CTAB:	4.46×10 ⁻⁵ M
MIBC:	30 ppm
Flotation time:	2 min
Bubble diameter:	41 μm
Particle diameter:	15 μm

Solids (%)	Run No.	Experimental recovery (%)	Average recovery (%)	Non-floatable fraction of silica, K4	Recovery based on floatable fraction of silica (%)
2	1	94.8	92.5	0.006	93.06
	2	90.2			
3.5	1	88.88	86.77	0.006	87.29
	2	84.65			
5	1	76.25	78.5	0.006	78.97
	2	80.75			
7.6	1	69.25	67.33	0.006	67.74
	2	65.41			
10	1	53.19	55.22	0.005	55.50
	2	57.25			
15	1	31.8	33.29	0.004	33.42
	2	34.77			
20	1	26.05	24.14	0.004	24.24
	2	22.23			

Experimental conditions for all experiments (Table H.2-H.5):

Gas type: Electrolytic Hydrogen
 Na₂SO₄: 0.2 M
 CTAB: 4.46×10⁻⁵ M
 MIBC: 30 ppm
 Bubble diameter: 30 μm
 Flotation time: 2 min
 Solids concentration: 2.0 %

Table H.2: Flotation recovery as a function of gas flow rate (d_p: 3.1 μm)

Experimental condition:

Non-floatable fraction of silica: 0.00

Current Density (A/m ²)	Hydrogen gas rate (mL/min)	Run No.	Experimental Recovery (%)	Average Recovery (%)	Difference from average (%)
122	0.380	1	39.76	38.90	-2.22
		2	38.04		2.22
196	0.608	1	49.81	48.78	-2.12
		2	47.75		2.12
269	0.836	1	63.65	65.01	2.08
		2	66.36		-2.08
342	1.064	1	76.53	77.84	1.68
		2	79.15		-1.68
416	1.293	1	79.68	81.36	2.06
		2	81.36		0.00
		3	83.03		-2.06
489	1.521	1	80.86	82.31	2.06
		2	83.77		0.00
587	1.825	1	83.90	82.23	1.77
		2	80.56		-1.77

Table H.3: Flotation recovery as a function of gas flow rate (d_p : 5.3 μm)

Experimental condition:

Non-floatable fraction of silica: 0.00

Current Density (A/m^2)	Hydrogen gas rate (mL/min)	Run No.	Experimental Recovery (%)	Average Recovery (%)	Difference from average (%)
122	0.380	1	50.12	49.07	-2.14
		2	48.02		2.14
196	0.608	1	63.31	64.63	2.04
		2	65.95		-2.04
269	0.836	1	75.96	77.30	1.73
		2	78.95		-2.13
		3	76.99		0.40
342	1.064	1	86.74	88.13	1.57
		2	89.51		-1.57
416	1.293	1	91.18	89.20	-2.22
		2	87.85		1.51
		3	88.57		0.71
489	1.521	1	92.48	91.25	-1.35
		2	90.02		1.35
587	1.825	1	88.32	89.62	1.45
		2	90.91		-1.45

Table H.4: Flotation recovery as a function of gas flow rate (d_p : 12.3 μm)

Current Density (A/m^2)	Hydrogen gas rate (mL/min)	Run No.	Experimental Recovery (%)	Average Recovery (%)	Difference from average (%)
122	0.380	1	41.51	42.31	1.91
		2	43.12		-1.91
196	0.608	1	59.95	58.90	-1.78
		2	57.86		1.78
269	0.836	1	75.32	76.51	1.55
		2	77.70		-1.55
342	1.064	1	82.25	83.50	1.50
		2	84.76		-1.50
416	1.293	1	85.39	87.12	1.99
		2	88.86		-1.99
489	1.521	1	85.85	87.21	1.55
		2	88.56		-1.55
587	1.825	1	84.92	86.52	1.85
		2	88.12		-1.85

Table H.5: Flotation recovery as a function of gas flow rate (d_p : 14.7 μm)

Current Density (A/m^2)	Hydrogen gas rate (mL/min)	Run No.	Experimental Recovery (%)	Average Recovery (%)	Difference from average (%)
122	0.380	1	34.95	34.20	-2.19
		2	33.45		2.19
196	0.608	1	43.98	43.10	-2.03
		2	42.23		2.03
269	0.836	1	55.84	54.84	-1.82
		2	53.84		1.82
342	1.064	1	67.86	66.51	-2.03
		2	65.16		2.03
416	1.293	1	79.24	77.80	-1.86
		2	76.35		1.86
489	1.521	1	81.15	79.49	-2.09
		2	77.82		2.09
587	1.825	1	76.66	78.11	1.85
		2	79.56		-1.85

Recovery by model prediction using Equation 3.84

Table H.6: Predicted recovery as a function of solids concentration

Diameter of particle: 15 μm
 Diameter of bubble: 41 μm
 Gas flow rate: 9.12 mL/min

Bubble surface coverage, φ	Solids Concentration (%)						
	2	3.5	5	7.6	10	15	20
	0.09	0.14	0.18	0.21	0.23	0.23	0.23

Time (s)	Solids Concentration (%)						
	2	3.5	5	7.6	10	15	20
0	0	0	0	0	0	0	0
1	0.70	0.71	0.69	0.54	0.42	0.27	0.20
2	1.53	1.46	1.38	1.09	0.85	0.55	0.40
3	2.39	2.22	2.07	1.63	1.27	0.82	0.59
4	3.24	2.98	2.76	2.17	1.69	1.10	0.79
5	4.10	3.74	3.45	2.71	2.12	1.37	0.99
6	4.96	4.51	4.14	3.26	2.54	1.64	1.19
7	5.82	5.27	4.83	3.80	2.96	1.92	1.39
8	6.68	6.03	5.51	4.34	3.39	2.19	1.59
9	7.54	6.79	6.20	4.88	3.81	2.47	1.78
10	8.39	7.55	6.88	5.43	4.23	2.74	1.98
11	9.25	8.31	7.57	5.97	4.66	3.01	2.18
12	10.11	9.07	8.25	6.51	5.08	3.29	2.38
13	10.97	9.83	8.94	7.05	5.50	3.56	2.58
14	11.83	10.59	9.62	7.60	5.93	3.83	2.78
15	12.68	11.35	10.31	8.14	6.35	4.11	2.97
16	13.54	12.11	10.99	8.68	6.77	4.38	3.17
17	14.40	12.86	11.68	9.22	7.20	4.66	3.37
18	15.25	13.62	12.36	9.77	7.62	4.93	3.57
19	16.11	14.38	13.05	10.31	8.04	5.20	3.77
20	16.96	15.14	13.73	10.85	8.47	5.48	3.97
21	17.82	15.90	14.42	11.40	8.89	5.75	4.16
22	18.68	16.66	15.10	11.94	9.31	6.03	4.36
23	19.53	17.42	15.79	12.48	9.74	6.30	4.56
24	20.39	18.18	16.47	13.02	10.16	6.57	4.76
25	21.24	18.93	17.16	13.57	10.58	6.85	4.96
26	22.09	19.69	17.84	14.11	11.01	7.12	5.16
27	22.95	20.45	18.52	14.65	11.43	7.40	5.35
28	23.80	21.21	19.21	15.19	11.85	7.67	5.55
29	24.65	21.96	19.89	15.74	12.27	7.94	5.75
30	25.51	22.72	20.57	16.28	12.70	8.22	5.95
31	26.36	23.48	21.26	16.82	13.12	8.49	6.15

Time (s)	Solids Concentration (%)						
	2	3.5	5	7.6	10	15	20
32	27.21	24.24	21.94	17.36	13.54	8.77	6.35
33	28.06	24.99	22.62	17.91	13.97	9.04	6.54
34	28.92	25.75	23.31	18.45	14.39	9.31	6.74
35	29.77	26.50	23.99	18.99	14.81	9.59	6.94
36	30.62	27.26	24.67	19.53	15.24	9.86	7.14
37	31.47	28.02	25.36	20.08	15.66	10.13	7.34
38	32.32	28.77	26.04	20.62	16.08	10.41	7.54
39	33.17	29.53	26.72	21.16	16.51	10.68	7.73
40	34.02	30.28	27.40	21.70	16.93	10.96	7.93
41	34.86	31.04	28.08	22.25	17.35	11.23	8.13
42	35.71	31.79	28.77	22.79	17.78	11.50	8.33
43	36.56	32.54	29.45	23.33	18.20	11.78	8.53
44	37.41	33.30	30.13	23.88	18.62	12.05	8.73
45	38.25	34.05	30.81	24.42	19.05	12.33	8.92
46	39.10	34.81	31.49	24.96	19.47	12.60	9.12
47	39.94	35.56	32.17	25.49	19.89	12.87	9.32
48	40.79	36.31	32.85	26.03	20.32	13.15	9.52
49	41.63	37.06	33.54	26.57	20.74	13.42	9.72
50	42.48	37.81	34.22	27.11	21.16	13.70	9.92
51	43.32	38.57	34.90	27.65	21.59	13.97	10.11
52	44.16	39.32	35.58	28.19	22.01	14.24	10.31
53	45.00	40.07	36.26	28.73	22.43	14.52	10.51
54	45.84	40.82	36.94	29.26	22.86	14.79	10.71
55	46.68	41.57	37.61	29.80	23.28	15.07	10.91
56	47.52	42.32	38.29	30.34	23.70	15.34	11.11
57	48.36	43.07	38.97	30.88	24.13	15.61	11.30
58	49.19	43.82	39.65	31.42	24.55	15.89	11.50
59	50.03	44.56	40.33	31.95	24.97	16.16	11.70
60	50.86	45.31	41.01	32.49	25.40	16.43	11.90
61	51.70	46.06	41.69	33.03	25.82	16.71	12.10
62	52.53	46.81	42.36	33.57	26.24	16.98	12.30
63	53.36	47.55	43.04	34.10	26.67	17.26	12.49
64	54.19	48.30	43.72	34.64	27.09	17.53	12.69
65	55.02	49.04	44.39	35.18	27.51	17.80	12.89
66	55.85	49.79	45.07	35.72	27.94	18.08	13.09
67	56.67	50.53	45.75	36.25	28.36	18.35	13.29
68	57.50	51.27	46.42	36.79	28.78	18.63	13.49
69	58.32	52.02	47.10	37.33	29.21	18.90	13.68
70	59.14	52.76	47.77	37.86	29.63	19.17	13.88
71	59.96	53.50	48.45	38.40	30.05	19.45	14.08
72	60.78	54.24	49.12	38.94	30.48	19.72	14.28
73	61.60	54.98	49.79	39.48	30.90	20.00	14.48
74	62.41	55.72	50.47	40.01	31.32	20.27	14.68
75	63.22	56.45	51.14	40.55	31.75	20.54	14.87
76	64.03	57.19	51.81	41.08	32.17	20.82	15.07
77	64.84	57.93	52.48	41.62	32.59	21.09	15.27
78	65.64	58.66	53.16	42.16	33.02	21.37	15.47
79	66.45	59.39	53.83	42.69	33.44	21.64	15.67

Time (s)	Solids Concentration (%)						
	2	3.5	5	7.6	10	15	20
80	67.25	60.13	54.50	43.23	33.86	21.91	15.87
81	68.04	60.86	55.17	43.76	34.29	22.19	16.06
82	68.84	61.59	55.84	44.30	34.71	22.46	16.26
83	69.63	62.32	56.50	44.84	35.13	22.73	16.46
84	70.41	63.04	57.17	45.37	35.55	23.01	16.66
85	71.20	63.77	57.84	45.91	35.98	23.28	16.86
86	71.98	64.49	58.51	46.44	36.40	23.56	17.06
87	72.75	65.22	59.17	46.98	36.82	23.83	17.25
88	73.52	65.94	59.84	47.51	37.25	24.10	17.45
89	74.29	66.66	60.50	48.05	37.67	24.38	17.65
90	75.05	67.38	61.16	48.58	38.09	24.65	17.85
91	75.80	68.09	61.83	49.11	38.52	24.93	18.05
92	76.55	68.81	62.49	49.65	38.94	25.20	18.25
93	77.29	69.52	63.15	50.18	39.36	25.47	18.44
94	78.03	70.23	63.81	50.72	39.79	25.75	18.64
95	78.76	70.93	64.47	51.25	40.21	26.02	18.84
96	79.48	71.64	65.13	51.78	40.63	26.30	19.04
97	80.20	72.34	65.78	52.32	41.05	26.57	19.24
98	80.90	73.04	66.44	52.85	41.47	26.84	19.44
99	81.60	73.73	67.09	53.38	41.89	27.12	19.63
100	82.29	74.42	67.74	53.91	42.31	27.39	19.83
101	82.97	75.11	68.40	54.45	42.73	27.67	20.03
102	83.64	75.80	69.05	54.98	43.15	27.94	20.23
103	84.30	76.48	69.69	55.51	43.57	28.21	20.43
104	84.94	77.16	70.34	56.04	43.99	28.49	20.63
105	85.58	77.83	70.99	56.57	44.41	28.76	20.82
106	86.20	78.50	71.63	57.10	44.83	29.03	21.02
107	86.81	79.16	72.27	57.64	45.25	29.31	21.22
108	87.41	79.82	72.91	58.17	45.67	29.58	21.42
109	87.99	80.47	73.55	58.70	46.09	29.86	21.62
110	88.56	81.11	74.18	59.23	46.51	30.13	21.81
111	89.11	81.75	74.82	59.76	46.93	30.40	22.01
112	89.64	82.39	75.45	60.29	47.35	30.68	22.21
113	90.16	83.01	76.07	60.81	47.77	30.95	22.41
114	90.67	83.63	76.70	61.34	48.19	31.23	22.61
115	91.15	84.24	77.32	61.87	48.61	31.50	22.81
116	91.62	84.84	77.94	62.40	49.03	31.77	23.00
117	92.07	85.43	78.55	62.93	49.45	32.05	23.20
118	92.50	86.02	79.16	63.45	49.87	32.32	23.40
119	92.91	86.59	79.77	63.98	50.29	32.60	23.60
120	93.31	87.15	80.37	64.51	50.71	32.87	23.80

Table H.7: Predicted recovery as a function of gas flow rate ($d_p = 3.1 \mu\text{m}$)Diameter of bubble: 30 μm

Solids Concentration: 2.0%

Bubble surface coverage, ϕ	Gas flow rate (mL/min)						
	0.38	0.608	0.836	1.064	1.293	1.521	1.825
	0.35	0.35	0.35	0.35	0.35	0.3	0.2

Time (s)	Gas flow rate (mL/min)						
	0.38	0.608	0.836	1.064	1.293	1.521	1.825
0	0	0	0	1	0	0	0
1	0.01	0.02	0.03	0.03	0.04	0.05	0.05
2	0.04	0.06	0.08	0.10	0.12	0.14	0.15
3	0.08	0.12	0.16	0.20	0.24	0.27	0.30
4	0.13	0.20	0.27	0.33	0.39	0.44	0.49
5	0.19	0.30	0.40	0.49	0.58	0.66	0.73
6	0.26	0.41	0.55	0.69	0.81	0.92	1.01
7	0.35	0.54	0.73	0.91	1.07	1.21	1.33
8	0.44	0.69	0.93	1.16	1.37	1.54	1.69
9	0.55	0.86	1.15	1.43	1.69	1.90	2.08
10	0.66	1.04	1.40	1.73	2.05	2.30	2.51
11	0.79	1.23	1.66	2.06	2.44	2.74	2.97
12	0.92	1.45	1.95	2.41	2.85	3.20	3.46
13	1.07	1.67	2.25	2.79	3.30	3.70	3.98
14	1.22	1.91	2.57	3.19	3.77	4.22	4.53
15	1.38	2.16	2.91	3.61	4.27	4.77	5.11
16	1.55	2.43	3.27	4.05	4.79	5.35	5.71
17	1.73	2.71	3.65	4.52	5.33	5.96	6.34
18	1.92	3.00	4.04	5.00	5.90	6.58	6.99
19	2.11	3.31	4.44	5.50	6.50	7.24	7.66
20	2.31	3.62	4.87	6.03	7.11	7.91	8.35
21	2.52	3.95	5.30	6.56	7.74	8.61	9.06
22	2.74	4.28	5.75	7.12	8.39	9.32	9.79
23	2.96	4.63	6.22	7.69	9.07	10.05	10.53
24	3.19	4.99	6.69	8.28	9.75	10.81	11.29
25	3.43	5.36	7.18	8.88	10.46	11.58	12.06
26	3.67	5.73	7.69	9.50	11.18	12.36	12.85
27	3.92	6.12	8.20	10.13	11.92	13.16	13.65
28	4.17	6.51	8.72	10.77	12.67	13.98	14.46
29	4.43	6.91	9.26	11.42	13.43	14.81	15.29
30	4.70	7.32	9.80	12.09	14.21	15.65	16.12
31	4.97	7.74	10.35	12.77	15.00	16.50	16.96
32	5.25	8.17	10.92	13.45	15.80	17.37	17.81
33	5.53	8.60	11.49	14.15	16.62	18.24	18.67
34	5.81	9.04	12.07	14.86	17.44	19.13	19.54
35	6.10	9.48	12.66	15.58	18.27	20.02	20.42
36	6.40	9.94	13.25	16.30	19.11	20.92	21.29
37	6.70	10.39	13.86	17.03	19.96	21.83	22.18
38	7.00	10.86	14.47	17.77	20.82	22.75	23.07

Time (s)	Gas flow rate (mL/min)						
	0.38	0.608	0.836	1.064	1.293	1.521	1.825
39	7.31	11.33	15.08	18.52	21.68	23.67	23.97
40	7.62	11.80	15.71	19.28	22.55	24.60	24.86
41	7.93	12.28	16.33	20.04	23.43	25.53	25.77
42	8.25	12.77	16.97	20.80	24.31	26.47	26.67
43	8.57	13.26	17.61	21.57	25.20	27.41	27.58
44	8.90	13.75	18.25	22.35	26.09	28.36	28.49
45	9.22	14.25	18.90	23.13	26.98	29.30	29.40
46	9.56	14.75	19.56	23.92	27.88	30.25	30.31
47	9.89	15.26	20.21	24.70	28.79	31.21	31.23
48	10.23	15.77	20.87	25.50	29.69	32.16	32.14
49	10.57	16.28	21.54	26.29	30.60	33.12	33.06
50	10.91	16.80	22.21	27.09	31.51	34.07	33.97
51	11.26	17.32	22.88	27.89	32.42	35.03	34.88
52	11.60	17.84	23.55	28.69	33.33	35.98	35.80
53	11.95	18.36	24.23	29.50	34.24	36.94	36.71
54	12.31	18.89	24.91	30.30	35.15	37.89	37.62
55	12.66	19.42	25.59	31.11	36.06	38.84	38.53
56	13.02	19.96	26.27	31.92	36.97	39.80	39.43
57	13.37	20.49	26.96	32.73	37.88	40.74	40.34
58	13.74	21.03	27.65	33.54	38.79	41.69	41.24
59	14.10	21.57	28.33	34.35	39.70	42.63	42.14
60	14.46	22.11	29.02	35.16	40.61	43.58	43.03
61	14.83	22.65	29.71	35.97	41.50	44.51	43.92
62	15.20	23.20	30.41	36.78	42.39	45.43	44.80
63	15.57	23.74	31.10	37.58	43.27	46.33	45.68
64	15.93	24.29	31.79	38.39	44.14	47.23	46.54
65	16.30	24.83	32.47	39.18	45.00	48.12	47.40
66	16.67	25.37	33.15	39.97	45.85	49.00	48.25
67	17.03	25.91	33.82	40.75	46.69	49.87	49.09
68	17.40	26.44	34.49	41.52	47.52	50.73	49.92
69	17.76	26.97	35.16	42.29	48.34	51.58	50.75
70	18.12	27.50	35.82	43.05	49.16	52.42	51.56
71	18.49	28.03	36.48	43.81	49.96	53.25	52.37
72	18.85	28.56	37.13	44.55	50.76	54.07	53.18
73	19.21	29.08	37.78	45.30	51.55	54.88	53.97
74	19.57	29.60	38.43	46.03	52.33	55.68	54.76
75	19.93	30.12	39.07	46.76	53.10	56.47	55.54
76	20.28	30.64	39.70	47.48	53.86	57.25	56.31
77	20.64	31.15	40.34	48.19	54.61	58.02	57.07
78	21.00	31.66	40.96	48.90	55.35	58.78	57.82
79	21.35	32.17	41.59	49.61	56.09	59.54	58.57
80	21.71	32.68	42.21	50.30	56.82	60.28	59.31
81	22.06	33.19	42.83	50.99	57.54	61.01	60.04
82	22.41	33.69	43.44	51.67	58.24	61.73	60.76
83	22.77	34.19	44.05	52.35	58.95	62.45	61.47
84	23.12	34.69	44.65	53.02	59.64	63.15	62.18
85	23.47	35.19	45.25	53.68	60.32	63.85	62.88
86	23.82	35.68	45.84	54.34	61.00	64.53	63.57
87	24.16	36.17	46.44	54.99	61.67	65.21	64.25
88	24.51	36.66	47.02	55.64	62.33	65.88	64.93

Time (s)	Gas flow rate (mL/min)						
	0.38	0.608	0.836	1.064	1.293	1.521	1.825
89	24.86	37.15	47.61	56.28	62.98	66.53	65.59
90	25.20	37.64	48.18	56.91	63.62	67.18	66.25
91	25.55	38.12	48.76	57.53	64.25	67.82	66.90
92	25.89	38.60	49.33	58.15	64.88	68.45	67.54
93	26.24	39.08	49.90	58.77	65.50	69.07	68.17
94	26.58	39.56	50.46	59.37	66.11	69.69	68.80
95	26.92	40.03	51.02	59.97	66.71	70.29	69.42
96	27.26	40.51	51.57	60.57	67.30	70.88	70.02
97	27.60	40.98	52.12	61.16	67.89	71.47	70.62
98	27.94	41.44	52.67	61.74	68.47	72.05	71.22
99	28.28	41.91	53.21	62.32	69.04	72.61	71.80
100	28.62	42.37	53.75	62.89	69.60	73.17	72.38
101	28.96	42.83	54.28	63.45	70.16	73.72	72.95
102	29.29	43.29	54.81	64.01	70.70	74.26	73.51
103	29.63	43.75	55.34	64.56	71.24	74.80	74.06
104	29.96	44.20	55.86	65.10	71.77	75.32	74.60
105	30.29	44.66	56.38	65.64	72.30	75.84	75.14
106	30.63	45.11	56.89	66.17	72.81	76.35	75.67
107	30.96	45.55	57.40	66.70	73.32	76.85	76.19
108	31.29	46.00	57.90	67.22	73.82	77.34	76.70
109	31.62	46.44	58.41	67.74	74.32	77.82	77.20
110	31.95	46.88	58.90	68.25	74.80	78.29	77.70
111	32.27	47.32	59.39	68.75	75.28	78.76	78.18
112	32.60	47.76	59.88	69.25	75.75	79.22	78.66
113	32.93	48.19	60.37	69.74	76.22	79.67	79.14
114	33.25	48.62	60.85	70.22	76.67	80.11	79.60
115	33.58	49.05	61.32	70.70	77.12	80.55	80.06
116	33.90	49.48	61.80	71.17	77.57	80.97	80.51
117	34.22	49.91	62.26	71.64	78.00	81.39	80.95
118	34.55	50.33	62.73	72.10	78.43	81.80	81.38
119	34.87	50.75	63.19	72.56	78.85	82.21	81.81
120	35.19	51.17	63.64	73.01	79.27	82.61	82.23

Table H.8: Predicted recovery as a function of gas flow rate ($d_p = 5.3 \mu\text{m}$)Diameter of bubble: 30 μm

Solids Concentration: 2.0%

Bubble surface coverage, ϕ	Gas flow rate (mL/min)						
	0.38	0.608	0.836	1.064	1.293	1.521	1.825
	0.19	0.16	0.15	0.15	0.12	0.1	0.08

Time (s)	Gas flow rate (mL/min)						
	0.38	0.608	0.836	1.064	1.293	1.521	1.825
0	0	0	0	0	0	0	0
1	0.04	0.07	0.09	0.12	0.14	0.16	0.18
2	0.13	0.20	0.27	0.34	0.40	0.45	0.50
3	0.25	0.39	0.52	0.65	0.76	0.85	0.94
4	0.41	0.63	0.84	1.05	1.21	1.34	1.47
5	0.59	0.91	1.21	1.51	1.73	1.91	2.08
6	0.80	1.22	1.64	2.04	2.32	2.55	2.75
7	1.03	1.58	2.10	2.62	2.96	3.23	3.46
8	1.29	1.96	2.61	3.25	3.64	3.96	4.22
9	1.57	2.37	3.14	3.92	4.37	4.73	5.00
10	1.86	2.80	3.71	4.63	5.13	5.52	5.81
11	2.17	3.25	4.30	5.36	5.92	6.34	6.64
12	2.50	3.72	4.92	6.13	6.73	7.18	7.49
13	2.83	4.20	5.55	6.92	7.55	8.03	8.34
14	3.18	4.70	6.20	7.73	8.40	8.90	9.21
15	3.54	5.21	6.86	8.55	9.26	9.78	10.08
16	3.91	5.73	7.54	9.40	10.13	10.66	10.96
17	4.28	6.26	8.22	10.25	11.01	11.56	11.85
18	4.67	6.80	8.92	11.12	11.90	12.46	12.74
19	5.06	7.35	9.63	12.00	12.80	13.36	13.63
20	5.45	7.90	10.34	12.88	13.70	14.27	14.52
21	5.85	8.46	11.05	13.78	14.61	15.18	15.41
22	6.26	9.02	11.78	14.67	15.52	16.10	16.31
23	6.67	9.59	12.51	15.58	16.43	17.01	17.21
24	7.08	10.16	13.24	16.49	17.35	17.93	18.10
25	7.50	10.74	13.97	17.40	18.27	18.85	19.00
26	7.92	11.31	14.71	18.31	19.18	19.76	19.89
27	8.35	11.89	15.45	19.23	20.10	20.68	20.79
28	8.77	12.47	16.19	20.15	21.02	21.60	21.69
29	9.20	13.06	16.93	21.07	21.94	22.52	22.58
30	9.63	13.64	17.68	21.99	22.86	23.43	23.47
31	10.06	14.23	18.42	22.91	23.78	24.35	24.37
32	10.50	14.82	19.17	23.83	24.70	25.27	25.26
33	10.93	15.40	19.91	24.75	25.62	26.18	26.15
34	11.37	15.99	20.66	25.67	26.54	27.09	27.04
35	11.81	16.58	21.41	26.59	27.46	28.00	27.93
36	12.24	17.17	22.15	27.51	28.37	28.91	28.82
37	12.68	17.76	22.90	28.43	29.29	29.82	29.70
38	13.12	18.35	23.65	29.35	30.20	30.73	30.59
39	13.56	18.94	24.39	30.27	31.11	31.64	31.47
40	14.00	19.53	25.14	31.18	32.02	32.54	32.35

Time (s)	Gas flow rate (mL/min)						
	0.38	0.608	0.836	1.064	1.293	1.521	1.825
41	14.45	20.13	25.88	32.10	32.93	33.44	33.23
42	14.89	20.72	26.63	33.01	33.83	34.34	34.11
43	15.33	21.31	27.37	33.92	34.74	35.24	34.99
44	15.77	21.90	28.12	34.82	35.64	36.14	35.86
45	16.22	22.49	28.86	35.73	36.54	37.04	36.74
46	16.66	23.08	29.60	36.63	37.43	37.93	37.61
47	17.10	23.67	30.34	37.53	38.33	38.82	38.48
48	17.55	24.26	31.08	38.43	39.22	39.71	39.35
49	17.99	24.85	31.82	39.33	40.11	40.59	40.21
50	18.43	25.44	32.56	40.22	41.00	41.48	41.08
51	18.88	26.03	33.29	41.11	41.89	42.36	41.94
52	19.32	26.61	34.03	42.00	42.77	43.24	42.80
53	19.76	27.20	34.76	42.89	43.65	44.12	43.66
54	20.21	27.79	35.49	43.77	44.53	44.99	44.52
55	20.65	28.37	36.22	44.65	45.40	45.86	45.37
56	21.09	28.96	36.95	45.53	46.27	46.73	46.22
57	21.54	29.55	37.68	46.40	47.14	47.59	47.07
58	21.98	30.13	38.41	47.27	48.01	48.46	47.92
59	22.42	30.71	39.13	48.13	48.87	49.32	48.76
60	22.87	31.30	39.86	49.00	49.73	50.17	49.60
61	23.31	31.88	40.58	49.85	50.59	51.03	50.44
62	23.75	32.46	41.30	50.71	51.44	51.88	51.28
63	24.19	33.04	42.02	51.56	52.29	52.72	52.11
64	24.63	33.62	42.73	52.41	53.13	53.57	52.94
65	25.07	34.20	43.45	53.25	53.97	54.41	53.77
66	25.52	34.78	44.16	54.09	54.81	55.24	54.59
67	25.96	35.36	44.87	54.92	55.64	56.08	55.41
68	26.40	35.94	45.58	55.75	56.47	56.90	56.23
69	26.84	36.51	46.28	56.57	57.29	57.73	57.04
70	27.27	37.09	46.99	57.39	58.11	58.55	57.85
71	27.71	37.66	47.69	58.21	58.93	59.36	58.66
72	28.15	38.24	48.39	59.02	59.74	60.18	59.46
73	28.59	38.81	49.09	59.82	60.54	60.98	60.26
74	29.03	39.38	49.79	60.62	61.35	61.79	61.06
75	29.46	39.95	50.48	61.41	62.14	62.58	61.85
76	29.90	40.52	51.17	62.20	62.93	63.38	62.64
77	30.34	41.09	51.86	62.99	63.72	64.17	63.42
78	30.77	41.66	52.54	63.76	64.50	64.95	64.20
79	31.21	42.22	53.23	64.53	65.28	65.73	64.97
80	31.64	42.79	53.91	65.30	66.04	66.50	65.74
81	32.08	43.35	54.59	66.06	66.81	67.27	66.50
82	32.51	43.92	55.26	66.81	67.57	68.03	67.26
83	32.95	44.48	55.94	67.56	68.32	68.78	68.02
84	33.38	45.04	56.61	68.30	69.06	69.53	68.77
85	33.81	45.60	57.27	69.03	69.80	70.28	69.51
86	34.24	46.16	57.94	69.76	70.54	71.01	70.25
87	34.68	46.71	58.60	70.48	71.26	71.75	70.98
88	35.11	47.27	59.26	71.19	71.98	72.47	71.71
89	35.54	47.82	59.91	71.90	72.69	73.19	72.43
90	35.97	48.38	60.56	72.60	73.40	73.90	73.14

Time (s)	Gas flow rate (mL/min)						
	0.38	0.608	0.836	1.064	1.293	1.521	1.825
91	36.40	48.93	61.21	73.29	74.10	74.60	73.85
92	36.83	49.48	61.86	73.97	74.79	75.30	74.55
93	37.26	50.03	62.50	74.65	75.47	75.99	75.25
94	37.69	50.58	63.14	75.32	76.15	76.67	75.94
95	38.11	51.13	63.77	75.98	76.81	77.34	76.62
96	38.54	51.67	64.40	76.63	77.47	78.00	77.29
97	38.97	52.22	65.03	77.27	78.12	78.66	77.96
98	39.39	52.76	65.66	77.90	78.76	79.31	78.61
99	39.82	53.30	66.28	78.53	79.40	79.95	79.26
100	40.24	53.84	66.89	79.15	80.02	80.58	79.91
101	40.67	54.38	67.50	79.76	80.64	81.20	80.54
102	41.09	54.91	68.11	80.36	81.25	81.81	81.17
103	41.52	55.45	68.71	80.95	81.84	82.42	81.78
104	41.94	55.98	69.31	81.53	82.43	83.01	82.39
105	42.36	56.51	69.91	82.10	83.01	83.59	82.99
106	42.78	57.04	70.50	82.66	83.58	84.17	83.58
107	43.20	57.57	71.09	83.21	84.14	84.73	84.16
108	43.62	58.09	71.67	83.76	84.69	85.29	84.73
109	44.04	58.62	72.24	84.29	85.23	85.83	85.29
110	44.46	59.14	72.82	84.81	85.75	86.36	85.84
111	44.88	59.66	73.38	85.33	86.27	86.89	86.38
112	45.30	60.18	73.95	85.83	86.78	87.40	86.91
113	45.72	60.70	74.50	86.32	87.28	87.90	87.43
114	46.13	61.21	75.06	86.81	87.76	88.39	87.94
115	46.55	61.72	75.60	87.28	88.24	88.86	88.43
116	46.96	62.23	76.14	87.74	88.70	89.33	88.92
117	47.38	62.74	76.68	88.19	89.16	89.79	89.39
118	47.79	63.25	77.21	88.63	89.60	90.23	89.86
119	48.20	63.75	77.74	89.06	90.03	90.66	90.31
120	48.61	64.25	78.26	89.48	90.45	91.08	90.75

Table H.9: Predicted recovery as a function of gas flow rate ($d_p = 12.3 \mu\text{m}$)Diameter of bubble: 30 μm

Solids Concentration: 2.0%

Bubble surface coverage, ϕ	Gas flow rate (mL/min)						
	0.38	0.608	0.836	1.064	1.293	1.521	1.825
	0.06	0.05	0.05	0.05	0.04	0.04	0.03

Time (s)	Gas flow rate (mL/min)						
	0.38	0.608	0.836	1.064	1.293	1.521	1.825
0	0	0	0	1	0	0	0
1	0.37	0.50	0.69	0.88	0.86	1.02	0.94
2	0.75	1.00	1.38	1.77	1.73	2.05	1.88
3	1.12	1.50	2.08	2.65	2.59	3.07	2.82
4	1.50	2.00	2.77	3.54	3.46	4.10	3.76
5	1.87	2.50	3.46	4.42	4.32	5.12	4.69
6	2.25	3.00	4.15	5.31	5.18	6.15	5.63
7	2.62	3.51	4.84	6.19	6.05	7.17	6.57
8	3.00	4.01	5.53	7.07	6.91	8.20	7.51
9	3.37	4.51	6.23	7.96	7.78	9.22	8.45
10	3.75	5.01	6.92	8.84	8.64	10.25	9.39
11	4.12	5.51	7.61	9.73	9.51	11.27	10.33
12	4.49	6.01	8.30	10.61	10.37	12.30	11.27
13	4.87	6.51	8.99	11.50	11.23	13.32	12.21
14	5.24	7.01	9.68	12.38	12.10	14.35	13.14
15	5.62	7.51	10.38	13.26	12.96	15.37	14.08
16	5.99	8.01	11.07	14.15	13.83	16.40	15.02
17	6.37	8.51	11.76	15.03	14.69	17.42	15.96
18	6.74	9.01	12.45	15.92	15.55	18.45	16.90
19	7.12	9.52	13.14	16.80	16.42	19.47	17.84
20	7.49	10.02	13.83	17.69	17.28	20.50	18.78
21	7.86	10.52	14.53	18.57	18.15	21.52	19.72
22	8.24	11.02	15.22	19.45	19.01	22.55	20.66
23	8.61	11.52	15.91	20.34	19.88	23.57	21.59
24	8.99	12.02	16.60	21.22	20.74	24.60	22.53
25	9.36	12.52	17.29	22.10	21.60	25.62	23.47
26	9.74	13.02	17.98	22.98	22.47	26.65	24.41
27	10.11	13.52	18.68	23.85	23.33	27.67	25.35
28	10.49	14.02	19.37	24.73	24.20	28.70	26.29
29	10.86	14.52	20.06	25.60	25.06	29.72	27.23
30	11.23	15.02	20.75	26.47	25.92	30.75	28.17
31	11.61	15.53	21.44	27.35	26.79	31.77	29.11
32	11.98	16.03	22.13	28.22	27.65	32.80	30.04
33	12.35	16.53	22.83	29.09	28.52	33.82	30.98
34	12.72	17.03	23.52	29.97	29.38	34.84	31.92
35	13.10	17.53	24.20	30.84	30.25	35.85	32.86
36	13.47	18.03	24.89	31.71	31.11	36.86	33.80
37	13.84	18.53	25.57	32.58	31.97	37.87	34.74
38	14.22	19.03	26.26	33.45	32.84	38.87	35.68
39	14.59	19.53	26.94	34.32	33.70	39.88	36.62
40	14.96	20.03	27.63	35.19	34.57	40.89	37.56

Time (s)	Gas flow rate (mL/min)						
	0.38	0.608	0.836	1.064	1.293	1.521	1.825
41	15.33	20.53	28.31	36.07	35.43	41.89	38.49
42	15.71	21.03	29.00	36.93	36.29	42.90	39.43
43	16.08	21.54	29.68	37.80	37.15	43.90	40.37
44	16.45	22.04	30.37	38.67	38.00	44.91	41.31
45	16.83	22.54	31.05	39.54	38.85	45.91	42.25
46	17.20	23.04	31.74	40.41	39.70	46.91	43.19
47	17.57	23.54	32.42	41.28	40.55	47.91	44.13
48	17.94	24.04	33.10	42.15	41.40	48.92	45.07
49	18.32	24.54	33.79	43.01	42.25	49.92	46.01
50	18.69	25.04	34.47	43.88	43.11	50.91	46.94
51	19.06	25.54	35.15	44.75	43.96	51.91	47.88
52	19.43	26.03	35.84	45.61	44.80	52.91	48.80
53	19.81	26.53	36.52	46.48	45.65	53.91	49.73
54	20.18	27.03	37.20	47.34	46.50	54.90	50.65
55	20.55	27.53	37.89	48.20	47.35	55.89	51.57
56	20.92	28.02	38.57	49.07	48.20	56.89	52.49
57	21.30	28.52	39.25	49.93	49.05	57.88	53.41
58	21.67	29.02	39.93	50.79	49.89	58.87	54.33
59	22.04	29.51	40.61	51.65	50.74	59.86	55.25
60	22.41	30.01	41.30	52.51	51.58	60.84	56.16
61	22.79	30.51	41.98	53.37	52.43	61.83	57.08
62	23.16	31.01	42.66	54.23	53.27	62.81	57.99
63	23.53	31.50	43.34	55.09	54.12	63.79	58.91
64	23.90	32.00	44.02	55.94	54.96	64.77	59.82
65	24.28	32.50	44.70	56.80	55.80	65.75	60.73
66	24.65	32.99	45.38	57.65	56.64	66.72	61.65
67	25.02	33.49	46.06	58.51	57.48	67.69	62.56
68	25.39	33.99	46.74	59.36	58.32	68.66	63.46
69	25.77	34.48	47.42	60.21	59.16	69.63	64.37
70	26.14	34.98	48.10	61.06	60.00	70.59	65.28
71	26.51	35.48	48.78	61.91	60.84	71.55	66.18
72	26.88	35.97	49.46	62.76	61.67	72.51	67.09
73	27.26	36.47	50.13	63.60	62.51	73.46	67.99
74	27.63	36.96	50.81	64.45	63.34	74.41	68.89
75	28.00	37.46	51.49	65.29	64.17	75.35	69.78
76	28.37	37.96	52.17	66.13	65.01	76.29	70.68
77	28.74	38.45	52.84	66.97	65.84	77.23	71.57
78	29.12	38.95	53.52	67.81	66.66	78.15	72.46
79	29.49	39.44	54.20	68.64	67.49	79.08	73.35
80	29.86	39.94	54.87	69.48	68.32	79.99	74.23
81	30.23	40.44	55.55	70.31	69.14	80.90	75.11
82	30.60	40.93	56.22	71.14	69.96	81.80	75.99
83	30.98	41.43	56.89	71.96	70.78	82.69	76.87
84	31.35	41.92	57.57	72.78	71.60	83.57	77.74
85	31.72	42.42	58.24	73.60	72.41	84.44	78.61
86	32.09	42.91	58.91	74.42	73.22	85.31	79.47
87	32.46	43.41	59.59	75.23	74.03	86.15	80.32
88	32.84	43.90	60.26	76.04	74.84	86.99	81.18
89	33.21	44.40	60.93	76.85	75.65	87.81	82.02
90	33.58	44.89	61.60	77.65	76.45	88.62	82.86

Time (s)	Gas flow rate (mL/min)						
	0.38	0.608	0.836	1.064	1.293	1.521	1.825
91	33.95	45.39	62.27	78.45	77.24	89.41	83.69
92	34.32	45.88	62.94	79.24	78.04	90.17	84.52
93	34.69	46.38	63.60	80.03	78.83	90.92	85.33
94	35.07	46.87	64.27	80.81	79.61	91.65	86.14
95	35.44	47.37	64.94	81.58	80.40	92.35	86.94
96	35.81	47.86	65.60	82.35	81.17	93.03	87.72
97	36.18	48.35	66.27	83.11	81.94	93.68	88.50
98	36.55	48.85	66.93	83.87	82.71	94.30	89.26
99	36.92	49.34	67.59	84.61	83.47	94.89	90.00
100	37.29	49.84	68.25	85.35	84.22	95.45	90.73
101	37.67	50.33	68.91	86.08	84.96	95.97	91.44
102	38.04	50.82	69.57	86.79	85.70	96.46	92.14
103	38.41	51.32	70.23	87.50	86.43	96.90	92.81
104	38.78	51.81	70.89	88.19	87.15	97.32	93.46
105	39.15	52.30	71.54	88.87	87.86	97.69	94.08
106	39.52	52.80	72.20	89.54	88.55	98.03	94.68
107	39.89	53.29	72.85	90.19	89.24	98.33	95.25
108	40.26	53.78	73.50	90.83	89.91	98.60	95.78
109	40.64	54.27	74.15	91.45	90.57	98.83	96.29
110	41.01	54.77	74.80	92.05	91.21	99.03	96.76
111	41.38	55.26	75.44	92.63	91.84	99.20	97.19
112	41.75	55.75	76.09	93.19	92.45	99.35	97.59
113	42.12	56.24	76.73	93.73	93.04	99.47	97.95
114	42.49	56.73	77.37	94.25	93.61	99.58	98.28
115	42.86	57.22	78.00	94.74	94.16	99.66	98.56
116	43.23	57.72	78.64	95.21	94.68	99.73	98.81
117	43.60	58.21	79.27	95.66	95.18	99.79	99.03
118	43.97	58.70	79.90	96.08	95.66	99.83	99.22
119	44.34	59.19	80.52	96.47	96.10	99.87	99.37
120	44.71	59.68	81.14	96.84	96.52	99.90	99.50

Table H.10: Predicted recovery as a function of gas flow rate ($d_p = 14.7 \mu\text{m}$)Diameter of bubble: 30 μm

Solids Concentration: 2.0%

Bubble surface coverage, ϕ	Gas flow rate (mL/min)						
	0.38	0.608	0.836	1.064	1.293	1.521	1.825
	0.05	0.04	0.03	0.03	0.03	0.03	0.02

Time (s)	Gas flow rate (mL/min)						
	0.38	0.608	0.836	1.064	1.293	1.521	1.825
0	0	0	0	0	0	0	0
1	0.38	0.48	0.50	0.64	0.78	0.93	0.76
2	0.75	0.97	1.00	1.28	1.57	1.87	1.53
3	1.13	1.45	1.50	1.92	2.35	2.80	2.29
4	1.51	1.93	2.00	2.57	3.14	3.73	3.06
5	1.88	2.42	2.51	3.21	3.92	4.66	3.82
6	2.26	2.90	3.01	3.85	4.71	5.60	4.59
7	2.63	3.38	3.51	4.49	5.49	6.53	5.35
8	3.01	3.87	4.01	5.13	6.28	7.46	6.11
9	3.39	4.35	4.51	5.77	7.06	8.40	6.88
10	3.76	4.83	5.01	6.41	7.84	9.33	7.64
11	4.14	5.32	5.51	7.05	8.63	10.26	8.41
12	4.52	5.80	6.01	7.70	9.41	11.19	9.17
13	4.89	6.28	6.51	8.34	10.20	12.13	9.94
14	5.27	6.77	7.02	8.98	10.98	13.06	10.70
15	5.64	7.25	7.52	9.62	11.77	13.99	11.46
16	6.02	7.73	8.02	10.26	12.55	14.93	12.23
17	6.40	8.22	8.52	10.90	13.34	15.86	12.99
18	6.77	8.70	9.02	11.54	14.12	16.79	13.76
19	7.15	9.18	9.52	12.18	14.90	17.72	14.52
20	7.53	9.67	10.02	12.83	15.69	18.66	15.29
21	7.90	10.15	10.52	13.47	16.47	19.59	16.05
22	8.28	10.63	11.03	14.11	17.26	20.52	16.82
23	8.65	11.12	11.53	14.75	18.04	21.46	17.58
24	9.03	11.60	12.03	15.39	18.83	22.39	18.34
25	9.41	12.08	12.53	16.03	19.61	23.32	19.11
26	9.78	12.57	13.03	16.67	20.40	24.25	19.87
27	10.16	13.05	13.53	17.32	21.18	25.19	20.64
28	10.54	13.53	14.03	17.96	21.96	26.12	21.40
29	10.91	14.02	14.53	18.60	22.75	27.05	22.17
30	11.29	14.50	15.03	19.24	23.53	27.99	22.93
31	11.66	14.98	15.54	19.88	24.32	28.92	23.69
32	12.04	15.47	16.04	20.52	25.10	29.85	24.46
33	12.42	15.95	16.54	21.16	25.89	30.78	25.22
34	12.79	16.43	17.04	21.80	26.67	31.72	25.99
35	13.17	16.92	17.54	22.45	27.46	32.65	26.75
36	13.55	17.40	18.04	23.09	28.24	33.58	27.52
37	13.92	17.88	18.54	23.73	29.02	34.52	28.28
38	14.30	18.37	19.04	24.37	29.81	35.45	29.04
39	14.67	18.85	19.54	25.01	30.59	36.38	29.81
40	15.05	19.33	20.05	25.65	31.38	37.31	30.57

Time (s)	Gas flow rate (mL/min)						
	0.38	0.608	0.836	1.064	1.293	1.521	1.825
41	15.43	19.82	20.55	26.29	32.16	38.25	31.34
42	15.80	20.30	21.05	26.93	32.95	39.18	32.10
43	16.18	20.78	21.55	27.58	33.73	40.11	32.87
44	16.56	21.27	22.05	28.22	34.51	41.05	33.63
45	16.93	21.75	22.55	28.86	35.30	41.98	34.39
46	17.31	22.23	23.05	29.50	36.08	42.91	35.16
47	17.68	22.72	23.55	30.14	36.87	43.84	35.92
48	18.06	23.20	24.06	30.78	37.65	44.78	36.69
49	18.44	23.68	24.56	31.42	38.44	45.71	37.45
50	18.81	24.17	25.06	32.07	39.22	46.64	38.22
51	19.19	24.65	25.56	32.71	40.01	47.57	38.98
52	19.57	25.13	26.06	33.35	40.79	48.51	39.75
53	19.94	25.62	26.56	33.99	41.57	49.44	40.51
54	20.32	26.10	27.06	34.63	42.36	50.37	41.27
55	20.69	26.58	27.56	35.27	43.14	51.31	42.04
56	21.07	27.07	28.06	35.91	43.93	52.24	42.80
57	21.45	27.55	28.57	36.55	44.71	53.17	43.57
58	21.82	28.03	29.07	37.20	45.50	54.10	44.33
59	22.20	28.52	29.57	37.84	46.28	55.04	45.10
60	22.58	29.00	30.07	38.48	47.07	55.97	45.86
61	22.95	29.48	30.57	39.12	47.85	56.90	46.62
62	23.33	29.97	31.07	39.76	48.63	57.84	47.39
63	23.70	30.45	31.57	40.40	49.42	58.77	48.15
64	24.08	30.93	32.07	41.04	50.20	59.70	48.92
65	24.46	31.42	32.57	41.68	50.99	60.63	49.68
66	24.83	31.90	33.08	42.33	51.77	61.57	50.45
67	25.21	32.38	33.58	42.97	52.56	62.50	51.21
68	25.59	32.87	34.08	43.61	53.34	63.43	51.97
69	25.96	33.35	34.58	44.25	54.13	64.37	52.74
70	26.34	33.83	35.08	44.89	54.91	65.30	53.50
71	26.71	34.32	35.58	45.53	55.69	66.23	54.27
72	27.09	34.80	36.08	46.17	56.48	67.15	55.03
73	27.47	35.28	36.58	46.82	57.26	68.06	55.80
74	27.84	35.77	37.09	47.46	58.05	68.96	56.56
75	28.22	36.25	37.59	48.10	58.83	69.87	57.32
76	28.60	36.73	38.09	48.74	59.62	70.77	58.09
77	28.97	37.22	38.59	49.38	60.40	71.67	58.85
78	29.35	37.70	39.09	50.02	61.19	72.57	59.62
79	29.72	38.18	39.59	50.66	61.97	73.47	60.38
80	30.10	38.67	40.09	51.30	62.75	74.36	61.15
81	30.48	39.15	40.59	51.95	63.54	75.26	61.91
82	30.85	39.63	41.09	52.59	64.32	76.15	62.68
83	31.23	40.12	41.60	53.23	65.11	77.03	63.44
84	31.61	40.60	42.10	53.87	65.89	77.92	64.20
85	31.98	41.08	42.60	54.51	66.68	78.80	64.97
86	32.36	41.57	43.10	55.15	67.46	79.68	65.73
87	32.73	42.05	43.60	55.79	68.23	80.55	66.50
88	33.11	42.53	44.10	56.44	68.99	81.42	67.26
89	33.49	43.02	44.60	57.08	69.76	82.29	68.03
90	33.86	43.50	45.10	57.72	70.52	83.15	68.79

Time (s)	Gas flow rate (mL/min)						
	0.38	0.608	0.836	1.064	1.293	1.521	1.825
91	34.24	43.98	45.60	58.36	71.28	84.00	69.55
92	34.62	44.47	46.11	59.00	72.04	84.85	70.32
93	34.99	44.95	46.61	59.64	72.80	85.69	71.08
94	35.37	45.43	47.11	60.28	73.56	86.52	71.85
95	35.74	45.92	47.61	60.92	74.32	87.34	72.61
96	36.12	46.40	48.11	61.57	75.08	88.16	73.38
97	36.50	46.88	48.61	62.21	75.83	88.96	74.13
98	36.87	47.37	49.11	62.85	76.59	89.75	74.87
99	37.25	47.85	49.61	63.49	77.34	90.53	75.61
100	37.63	48.33	50.12	64.13	78.09	91.29	76.35
101	38.00	48.82	50.62	64.77	78.84	92.03	77.09
102	38.38	49.30	51.12	65.41	79.58	92.75	77.83
103	38.75	49.78	51.62	66.05	80.32	93.45	78.56
104	39.13	50.27	52.12	66.70	81.07	94.13	79.30
105	39.51	50.75	52.62	67.34	81.80	94.78	80.03
106	39.88	51.23	53.12	67.98	82.54	95.40	80.76
107	40.26	51.72	53.62	68.61	83.27	95.99	81.49
108	40.64	52.20	54.12	69.24	84.00	96.55	82.21
109	41.01	52.68	54.63	69.86	84.72	97.06	82.93
110	41.39	53.17	55.13	70.49	85.44	97.53	83.65
111	41.76	53.65	55.63	71.12	86.15	97.96	84.37
112	42.14	54.13	56.13	71.74	86.86	98.34	85.08
113	42.52	54.62	56.63	72.37	87.56	98.68	85.79
114	42.89	55.10	57.13	73.00	88.26	98.96	86.49
115	43.27	55.58	57.63	73.62	88.94	99.21	87.19
116	43.65	56.07	58.13	74.24	89.62	99.40	87.89
117	44.02	56.55	58.63	74.87	90.29	99.56	88.57
118	44.40	57.03	59.14	75.49	90.95	99.69	89.26
119	44.78	57.52	59.64	76.11	91.60	99.78	89.93
120	45.15	58.00	60.14	76.73	92.24	99.85	90.59